Summer 8-2013

# Relation Between the Adsorption Behavior and Bulk Complexation in Oppositely Charged Polyelectrolyte-Surfactant Systems: Effect of Polyelectrolyte Concentration, Molecular Weight, Charge Localization and Backbone Rigidity/Hydrophobicity

Vipul Suhas Padman
*University of Southern Mississippi*

The University of Southern Mississippi

# RELATION BETWEEN THE ADSORPTION BEHAVIOR AND BULK COMPLEXATION IN OPPOSITELY CHARGED POLYELECTROLYTE-SURFACTANT SYSTEMS: EFFECT OF POLYELECTROLYTE CONCENTRATION, MOLECULAR WEIGHT, CHARGE LOCALIZATION AND BACKBONE RIGIDITY/HYDROPHOBICITY

by

Vipul Suhas Padman

Abstract of a Dissertation
Submitted to the Graduate School
of The University of Southern Mississippi
in Partial Fulfillment of the Requirements
for the Degree of Doctor of Philosophy

August 2013

ABSTRACT

RELATION BETWEEN THE ADSORPTION BEHAVIOR AND BULK COMPLEXATION IN OPPOSITELY CHARGED POLYELECTROLYTE-SURFACTANT SYSTEMS: EFFECT OF POLYELECTROLYTE CONCENTRATION, MOLECULAR WEIGHT, CHARGE LOCALIZATION AND BACKBONE RIGIDITY/HYDROPHOBICITY

by Vipul Suhas Padman

August 2013

Due to a wide range of applications, much emphasis has been placed on understanding the physicochemical behavior of polyelectrolyte/surfactant complexes, both at air-water interface and in the bulk. However, the correlation between the adsorption behavior and complexation in the bulk is less explored. In this research, this correlation is investigated and its dependence on polyelectrolyte concentration, molecular weight, charge localization and backbone rigidity and hydrophobicity is studied. The polyelectrolyte concentration is normalized with respect to it critical overlap concentration in order to compare the polymer in same concentration regime.

Different polyelectrolyte systems were used to analyze the polyelectrolyte structural effect:

- The molecular weight effect was studied between low molecular weight cationic hydroxyethylcellulose (JR400)/SDS and high molecular weight hydroxyethylcellulose (JR30M)/SDS system
- The charge localization effect was studied between the linearly charged poly(methacrylamidopropyltrimethylammonium chloride) (MAPTAC) and

locally charged poly(methacrylamide propyl (methoxy-carbonyl-methyl) dimethyl ammonium chloride) (AMT)

- The effect of rigidity and hydrophilicity/hydrophobicity of the polyelectrolyte backbone was studied by comparing and contrasting flexible/hydrophobic MAPTAC and semi rigid/hydrophilic JR30M

All of these polyelectrolytes were interacted with sodium dodecyl sulfate (SDS) surfactant. The concentration of these polyelectrolytes was varied over a sufficient range to analyze the polyelectrolyte-surfactant interaction in different concentration regimes. The adsorption behavior was analyzed by surface tension measurements, while, the complexation in the bulk was examined by rheological measurements. Fluorescence measurement techniques were additionally used to analyze the effect of charge localization on the structure of the polyelectrolyte/surfactant complexes.

In the molecular weight study, as a function of surfactant concentration, the surface tension at the interface varied in the one phase region above the surfactant's critical aggregation concentration (CAC). The surface tension increased with increase in the SDS concentration and this became more pronounced with increase in polyelectrolyte molecular weight. This is counterintuitive. This increase can be explained by intermolecular association taking place in the bulk between the polymer and surfactant through hydrophobic association of the bound surfactants. This bulk intermolecular association was favored by the interfacial complex over the surface adsorption, thereby increasing desorption of the polyelectrolyte-surfactant complex from the surface. Increase in molecular weight increased this intermolecular association and the surface tension increased with increase in the molecular weight.

Charge localization on the polyelectrolyte chain increased the surface tension in the two phase region. From fluorescence measurements it was observed that the charge localization enhances SDS aggregation. The charge localization of AMT causes an observed increase in the surface tension above the surfactant CAC and this can be interpreted as desorption of the surface complex as the bulk complex phase-separates. On the other hand, in the linearly charged MAPTAC/SDS complex the surface tension stays constant as SDS concentration is increased, signifying that the surface adsorbed complex cannot be desorbed by the formation of the MAPTAC/SDS complex in the bulk.

Unlike the polyelectrolytes which have flexible hydrophobic backbones, the stiff, hydrophilic polymers were observed to increase the surface tension even while they remained in the one phase region. The association between the rigid and hydrophilic JR30M polymer and surfactant is higher than MAPTAC. For JR30M, pronounced desorption of the surface active species is observed in the one phase region above the CAC. On the other hand, in the case of flexible and hydrophobic MAPTAC, the association with SDS at the surfactant CAC causes the viscosity of the MAPTAC/SDS system reduces by addition of SDS. We deduce from this that the MAPTAC collapses with addition on surfactant in the one phase region. Thus, the surface tension stays constant.

In all the studied polymer/surfactant systems, the adsorption behavior of the complex at the interface was linked to the changes taking place in the bulk complexation.

The University of Southern Mississippi

# RELATION BETWEEN THE ADSORPTION BEHAVIOR AND BULK COMPLEXATION IN OPPOSITELY CHARGED POLYELECTROLYTE-SURFACTANT SYSTEMS: EFFECT OF POLYELECTROLYTE CONCENTRATION, MOLECULAR WEIGHT, CHARGE LOCALIZATION AND BACKBONE RIGIDITY/HYDROPHOBICITY

by

Vipul Suhas Padman

A Dissertation
Submitted to the Graduate School
of The University of Southern Mississippi
in Partial Fulfillment of the Requirements
for the Degree of Doctor of Philosophy

Approved:

Dr. Robert Y. Lochhead_____
Director

Dr. Sarah E. Morgan_____

Dr. Sergei I. Nazarenko_____

Dr. Derek L. Patton_____

Dr. Shelby F. Thames_____

Dr. Susan A. Siltanen_____
Dean of the Graduate School

August 2013

ACKNOWLEDGMENTS

I would like to thank my research advisor, Dr. Robert Y. Lochhead, for his guidance, support, suggestions and encouragement throughout my graduate years. He has been instrumental in developing my scientific research skills. I express my appreciation to him for giving me the independence to manage my work and provide me with the internship opportunities at Procter and Gamble.

I would like to thank Dr. William Jarrett for his advice and assistance in NMR measurements. I would like to thank my graduate committee members: Dr. Sarah E. Morgan, Dr. Sergei I. Nazarenko, Dr. Derek L. Patton and Dr. Shelby F. Thames for their support.

I am also thankful to Dr. Daniel A. Savin, Dr. James W. Rawlins and Dr. Faqing Huang for providing access to their lab instruments.

I would like to thank all the faculty and staff members of polymer science department and all my friends, who helped me throughout my graduate years. I would also like to thank a special person who was always with me during my graduate years.

Finally, I would like to dedicate this document to my parents, Swati and Suhas Padman, for their love and support.

TABLE OF CONTENTS

LIST OF TABLES

Table

LIST OF ILLUSTRATIONS

Figure

LIST OF ABBREVIATIONS

| | |
|---|---|
| 12-6-2012 | Hexylene-1,6-bis(dodecyldimethylammonium bromide) |
| AAm | Acrylamide |
| AMPS | Acrylamidomethylpropane sulfonate |
| AMT | Poly(methacrylamide propyl (methoxy-carbonyl-methyl)dimethyl ammonium chloride) |
| C* | Critical overlap concentration |
| $C_{12}E_5$ | Penta-ethyleneglycol mono n-dodecylether |
| $C_{12}E_n$ | Oligoethylene glycol monododecyl ether |
| $C_{14}$TAB | Tetradecyltrimethylammonium bromide |
| CAC | Critical aggregation concentration |
| CCC | Critical condensation concentration |
| $C_e$ | Critical entanglement concentration |
| CEC | Critical electrolyte concentrations |
| CMC | Critical micelle concentration |
| CMC | Carboxy-methylcellulose |
| $C_n$PC | Alkylpyridinium chloride |
| $C_n$PyBr | Alkylpyridinium bromide |
| $C_n$PyX | Alkylpyridinium halides |
| $C_n$TAB | Alkyltrimethylammonium bromide |
| CPyC | Cetylpyridinium chloride |
| DLS | Dynamic light scattering |
| DPyC | Dodecylpyridinium chloride |
| DTABr/$C_{12}$TAB | Dodecyltrimethylammonium bromide |
| EA | Ethyl acrylate |
| HASE | Hydrophobically modified alkali-soluble emulsion |
| ITC | Isothermal titration calorimetry |
| L | Contour length |
| $L_p$ | Persistence length |
| $L_{p,e}$ | Electrostatic persistence length |

| | |
|---|---|
| $L_{p,o}$ | Intrinsic persistence length |
| LPEI | Linear poly(ethyleneimine) |
| MA | Methacrylic acid |
| MAPTAC | Poly(methacrylamidopropyltrimethylammonium chloride) |
| NaAl | Sodium alginate |
| NaCMC | Carboxymethylcellulose |
| NaDxS | Sodium dextran sulfate |
| NaDxS | Sodium dextran sulfate |
| NaHy | Sodium hyaluronan |
| NaPAA | Sodium polyacrylate |
| NaPSS | Sodium poly(styrene sulfonate) |
| P(DADMAC-stat-NMVA) | Poly(diallyldimethylammoniumchloride-stat-N-methyl-N-vinylacetamide) |
| PAA | Poly(acrylic acid) |
| PDADMAC | Poly(diallyldimethylammonium chloride) |
| PEO | Polyethylene oxide |
| PMAA | Poly(sodium methacrylate) |
| PMAOVE | Poly(maleic acid/octyl vinyl ether) |
| PVAm | Poly(vinylamine) |
| SCnS | Sodium alkyl sulfate |
| SDS | Sodium dodecyl sulfate |
| SDS | Sodium dodecyl sulfate |
| SLS | Sodium lauryl sulfate |
| TTABr | Tetradecyltrimethylammonium bromide |
| TX100 | Triton X-100 |
| $\beta$ | Degree of binding |
| $\mu$ | Chemical potential |
| $\xi$ | Charge density |
| $\epsilon$ | Electrochemical potential |

# CHAPTER I

# INTRODUCTION

For the last half century, the interactions between polyelectrolyte and oppositely charged surfactant systems have been explored. However, a detailed understanding of the correlation between the adsorption behavior and bulk complexation have only been performed in recent years. This correlation with respect to polyelectrolyte concentration, molecular weight, charge localization and backbone rigidity/hydrophobicity remained relatively unexplored and yet it is important for both fundamental understanding and also for the improvement of the articles of commerce. The need to better understand this important area provided the impetus for the research presented in this dissertation.

## Polyelectrolytes

A polyelectrolyte is a polymer having ionizable groups on its monomeric units (Figure 1). Based on the chemical nature of these ionic groups, a polyelectrolyte can be categorized as a weak (Figure 1a) or strong (Figure 1b) polyelectrolyte.[1,2] In the former polyelectrolyte category, the ionic groups show high degrees of dissociation at extreme pH conditions: either acidic or basic depending upon whether the polyelectrolyte is a poly(acid) or a polybase. However, these polyelectrolytes can show low dissociation at intermediate pH conditions. In the latter polyelectrolyte category, by contrast, the ionic groups dissociate over a broad range of pH conditions.[2,3]

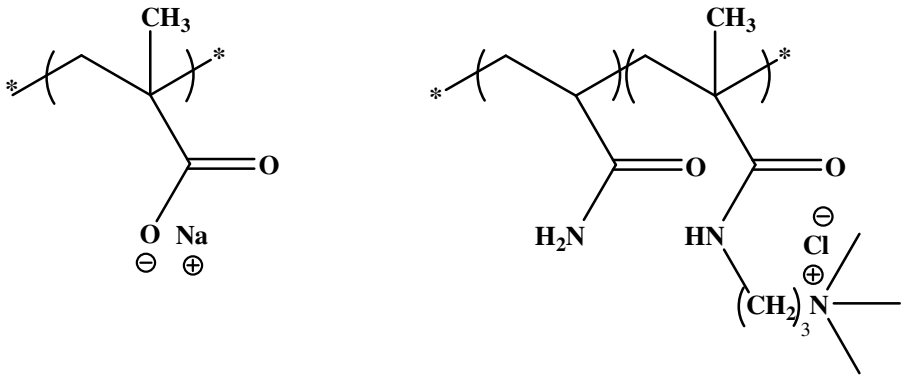


(a) (b)

*Figure 1.* (a) Weak Polyelectrolyte: Sodium polyacrylate (b) Strong Polyelectrolyte: (3-(methacryloylamino)propyl) trimethylammonium chloride (MAPTMAC).

The linear charge density ($\xi$) of the polyelectrolyte can be expressed as:[3-6]

$$\xi = {e^2}/{4\pi\epsilon_0\epsilon bkT} \qquad \text{Equation 1}$$

where, $e$ = the magnitude of the electrostatic charge, $\epsilon_0$ = the permittivity of vacuum, $\epsilon$ = the dielectric constant of the solvent, $b$= the average linear distance between the ionic groups on the polyelectrolyte (Figure 2) and $k$ = the Boltzmann constant, $T$ = the temperature.

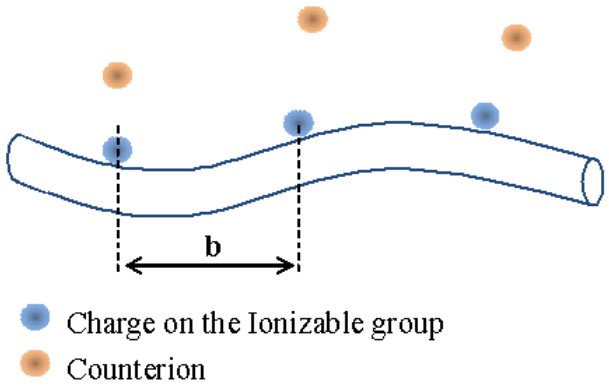


*Figure 2.* Representation of a polyelectrolyte with the average linear distance between the ionic groups as 'b'.

The electrostatic interactions arising from the charges present on the polyelectrolyte affect intramolecular as well as intermolecular interactions. These intramolecular interactions result in short and long range interactions. The former influences the local flexibility of the polyelectrolyte, whereas, the latter affects the excluded volume effects and intermolecular interactions.[5]

The electric potential developed by the charges on the polyelectrolyte attracts oppositely charged counterions. The distribution of these counterions around the polyelectrolyte depends on the equilibrium between electrochemical potential and chemical potential. The electrochemical potential (ϵ) drives the counterions towards the polyelectrolyte, whereas, the chemical potential (μ)drives the counterions away from the polyelectrolyte in a Donnan equilibrium (Figure 3).[4]

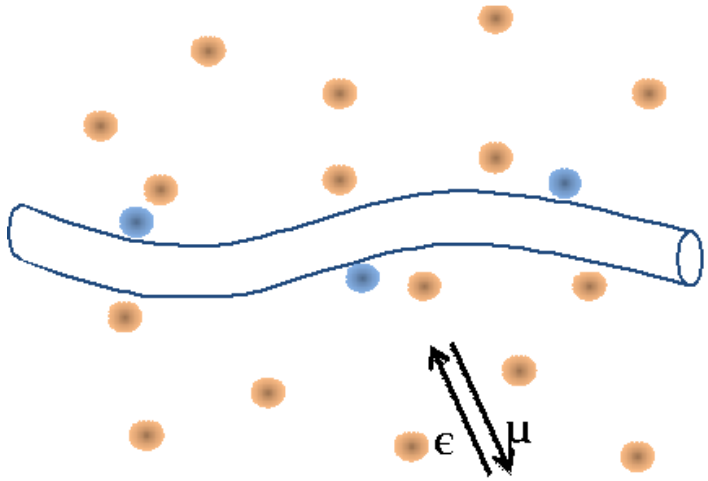


*Figure 3.* Distribution of counterions around the polyelectrolyte.

The distribution of the counterions around the polyelectrolyte is described by the Gouy-Chapman-Stern model of the electric double layer: Stern layer and diffuse layer (Figure 4).[4,7,8] The Stern layer consists of counterions that are condensed on the polyelectrolyte because of attraction between the charges on the ionizable groups and the

counterions. This layer is in the immediate vicinity of the polyelectrolyte charged groups. The diffuse layer arises because the chemical potential of binding is disfavored relative to the chemical potential of dissociation, but the electrostatic potential is sufficient to keep the counterions in a diffuse cloud around the polyion. Binding of multivalent counterions or amphiphilic counterions can sometimes cause reversal of the charge on the polyelectrolyte chain. In this case, the diffuse layer consists of counterions which would remain attracted to the polyelectrolyte but are repelled by the counterions in the Stern layer. The concentration of the counterions in the diffuse layer decreases exponentially with increase in the distance away from the polyelectrolyte.[4,9-11]

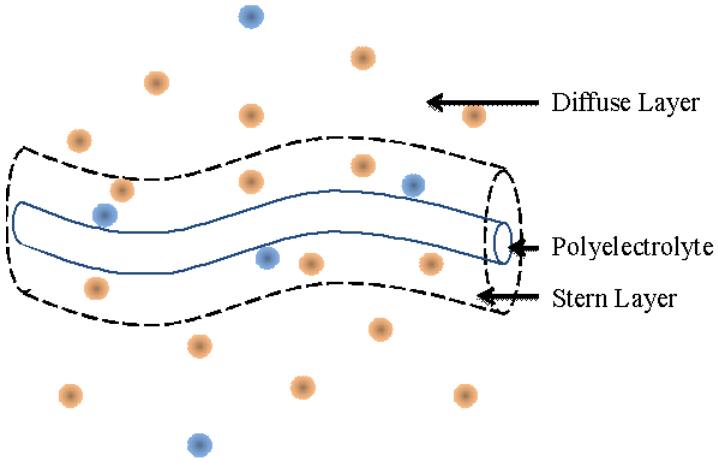


*Figure 4.* Representation of the Gouy-Chapman-Stern model.

Increase in the charge density of the polyelectrolyte causes condensation of the counterions on the polyelectrolyte. According to Manning's counterion condensation theory, in dilute polyelectrolyte solution, the counterions condense on the polyelectrolyte when the charge density ($\xi$) $\geq 1$.[3,4,6]

The charge density ($\xi$) of the polyelectrolyte can also be expressed as:

$$\xi = {e^2}/{\epsilon bkT} = {l_B}/{b} \qquad \text{Equation 2}$$

where, $l_B$= the Bjerrum length. At the counterion condensation condition ($\xi = 1$), $l_B$= b. Using these criteria, the distance 'b' in water at 25°C is 7.1 Å.[12] Therefore, if the distance 'b' between the ionic sites is below 7.1 Å, counterion condensation occurs.

The effective charge density of the polyelectrolyte becomes constant above $\xi = 1$ due to the condensation of the counterions. Hence, the critical condensation concentration (CCC) becomes independent of the charge density above $\xi = 1$. However, below $\xi = 1$, the CCC increases with increase in the charge density.[12-14]

The stiffness of the polyelectrolyte chain is affected by intrachain steric hindrance and electrostatic repulsion.[15] Steric hindrance depends on the structural features of the polyelectrolyte, such as bond length, bond angle and the presence of bulky groups.[5,16] Chain stiffness due to electrostatic repulsion arises as a result of repulsion between ionic groups present on the polyelectrolyte. These repulsive forces cause short range interaction, thereby, affecting the local flexibility of the polyelectrolyte.[17]

The stiffness of the chain is measured in terms of persistence length ($L_p$). This length describes the length scale over which the polymer maintains its tangent orientation.[18] In monodispersed systems of unperturbed wormlike chains, the persistence length is expressed in terms of radius of gyration ($R^2_{G,\theta}$) and contour length (L):[15,19,20]

$$R^2_{G,\theta} = \frac{LL_p}{3} - L_p^2 + \frac{2L_p^3}{L} - \frac{2L_p^4}{L^2}\left(1 - e^{-L/L_p}\right) \qquad \text{Equation 3}$$

The contour length (L) is defined as:[4,21]

$$L = Nb$$

where, N = number of segments in the polymer chain of length 'b'.


*Figure 5.* Schematic representation of the correlation between (L) the contour length and the persistence length ($L_p$): (a) flexible (b) semi-flexible and (c) rigid polyelectrolyte.[21]

The persistence length, according to the Odijk-Skolnick-Fixman (OSF) theory[22-25], is the sum of the intrinsic ($L_{p,o}$) and the electrostatic ($L_{p,e}$) persistence length.

Therefore, the persistence length of the polyelectrolyte is given as;

$$L_p = L_{p,o} + L_{p,e} \qquad \text{Equation 4}$$

$$L_{p,e} = {\xi^2}/{(4\kappa^2 l_B)} \text{ for } \xi < 1$$

where, $l_B$ = Bjerrum length = $e^2/\epsilon kT$

$\kappa^{-1}$ = Debye- Hückel screening length = $8\pi l_B c_S$

$c_S$ = concentration of monovalent salt

$\xi$ = accounts for counterion condensation and falls between 0 and 1.

In the case of a neutral polymer, $l_{p,e} = 0$.

## Surfactants

Surfactants comprise molecules that contain two parts: a hydrophobic segment that is expelled by water and a hydrophilic segment that interacts strongly with water.

Such molecules are said to be amphipathic (amphi meaning 'dual' and 'pathic' from the same root as pathos can be interpreted as 'suffering'). Thus, a surfactant molecule 'suffers' both oil and water. This dual nature confers interesting properties on surfactants in aqueous solution. At very low concentrations the surfactant is expelled to the surface; a process called adsorption. This adsorption causes the surfactant concentration at the surface to be much higher than the surfactant concentration in the bulk of the solution. At extremely low concentrations Traube's rule applies. Traube's Rule states that the ratio of the concentration of surfactant at the surface to the bulk concentration increases threefold for each $CH_2$ group of an alkyl chain.[26] The effective concentration at the surface in excess of the bulk concentration is called the 'surface excessconcentration'.[27] According to this rule, soap with a dodecyl chain should have a surface excess concentration that is more than half a million times its concentration in the bulk solution. At extremely low concentrations the surfactant molecules on the surface act as a 2-dimensional gas. As the concentration increases, the surfactant molecules begin to interact, but they are still mobile within the plane; they behave as 2-dimensional liquids. At even higher concentrations, as the surfactant saturates the surface, the chains orient out of the surface plane and the chain-chain interactions cause the surfactant to behave as a 2-dimensional solid. Irving Langmuir was awarded the 1932 Nobel Prize in Chemistry for measuring this effect and explaining it on a molecular basis.[28] When a surfactant adsorbs to saturate an aqueous surface, the surface is largely composed of the surfactant's hydrophobic groups, and this means that the surface essentially has low surface energy.

Relatively large aggregates form within solution just beyond the concentration at which the surface becomes essentially saturated with surfactant.[29] 'Saturation' in this

respect is denoted as the surfactant concentration at which the chemical potential for adsorption at the air/water interface becomes equal to the chemical potential for formation of the large aggregates in the bulk. Beyond this critical concentration the chemical potential favors large aggregates over adsorption. These aggregates are surfactant micelles in which the hydrophobes are segregated within the core of the aggregate and the hydrophilic groups are located on the surface where they interact strongly with water.[30] To re-iterate, for a given system, micelles initially form at the precise concentration at which the driving force for surface adsorption becomes equal to the driving force for aggregate formation. This driving force is the chemical potential of the surfactant species. The lowest concentration at which micelles form is named the critical micelle concentration (cmc). The aggregates are large; for example, micelles of sodium dodecyl sulfate at the CMC contain about 100 molecules and the thickness of the head group layer is about 0.4 nm.[31]

Surfactant micelles have liquid centers. They effectively solubilize hydrophobic substances only when the temperature of the system is above the Krafft point. Krafft found this phenomenon in 1895 and 68 years later Shinoda explained that the Krafft point corresponds to the melting point of the hydrated solid surfactant.[32] Micelles have different shapes. The simplest shape is the spherical micelle that was postulated by Hartley in 1936. The shape of a micelle can be explained on the basis of the ‘principle of opposing forces’. Two or three amphipathic molecules alone cannot form a stable micelle because micellization is essentially a cooperative process that requires the participation of many amphipathic molecules bound together by hydrophobic interaction. However, if hydrophobic interaction accounted solely for the formation of micelles, then the

association would continue until phase separation occurred, as in oil separating from water. Therefore, there must be a force that opposes the hydrophobic association and controls the size of the micelles. This force is the repulsion between the head groups that could arise from ion-ion repulsion and/or hydration of the head groups.[31] Theoretically the repulsive surface terms are difficult to handle from a thermodynamic perspective but the presence of micelles has been extensively validated experimentally.

## Coacervate

The interaction between oppositely charged species such as, polyelectrolyte-polyelectrolyte, polyelectrolyte-protein, polyelectrolyte-surfactant and polyelectrolyte-micelle, may either result in a soluble complex or a coacervate or a precipitate.[33,34] Coacervation is characterized by liquid-liquid phase separation, while precipitation is characterized by liquid-solid phase separation. Coacervate is also defined as a fluid phase that is water-immiscible despite being water-rich.[35]

Initially, complex coacervation between oppositely charged proteins and polysaccharides was revealed by Tiebackx.[36] Later, Bungenberg de Jong and co-workers studied this behavior comprehensively, and named this phenomenon as ‘coacervation’.[37] This word is drawn from Latin; “co” (together) and “acerv” (a heap).[38] Coacervates can be further divided into simple and complex coacervates.[39] Simple coacervation can be achieved by reducing the polymer-solvent interaction by adding salt and/or changing temperature and/or changing solvent, while complex coacervation is achieved via electrostatic interactions between oppositely charged species.[39,40] Formation of a complex coacervate can be summarized as a building up of soluble complex due to primary columbic forces between oppositely charged species, which then interact electro-

statically to form a neutral insoluble complex i.e. coacervate.[38] These systems contain an equilibrium phase (poor in polymer concentration) and a coacervate phase (rich in polymer concentration).[40,41]

Complex coacervate formation in polyelectrolyte-surfactant systems is described as an anion-exchange process. In this process, polyelectrolyte ions displace surfactant counterions resulting in a gain in entropy, which drives the interaction.[42] Coacervate formation can be a result of associative or segregative phase separation. In an associative phase separation, the effective attraction between the polyelectrolyte and surfactant is strong. As a result, the coacervate phase contains high concentrations of polyelectrolyte and surfactant, whereas, the equilibrium phase contains poor concentration of polyelectrolyte and surfactant. Conversely, in segregative phase separation, an effective thermodynamic repulsion between the polyelectrolyte and surfactant causes two distinct phases. One phase contains high concentration of polyelectrolyte, while, the other phase contains high concentration of surfactant.[43] Coacervate formation depends of the structural properties of polyelectrolyte and surfactant as well as external parameters, such as, ionic strength, temperature and pH. The possibility of formation of the coacervate can be conceptualized somewhat by considering by Flory-Huggins theory.

Flory-Huggins theory is based on a statistical approach on a regular lattice to determine the free energy of the mixing of polymer solutions. This theory was independently developed by Paul Flory[44,45] and Maurice Huggins[46,47] in the early 1940s, to describe the criteria for phase stability and construct phase diagrams for polymer blends and solutions. According to this theory, the free energy of mixing ($\Delta G_{\mathrm{mix}}$) is expressed as:[48-50]

$$\Delta G_{\mathrm{mix}} = RT[n_1 ln\phi_1 + n_2 ln\phi_2 + n_1\phi_1 \mathrm{X}_{12}] \quad \text{Equation 5}$$

where, $R$ = gas constant, $T$ = absolute temperature, $n_1$ = number of moles of solvent, $\phi_1$ = volume fraction of solvent, $\mathrm{n}_2$ = number of moles of polymer, $\phi_2$ = number of moles of polymer and $\mathrm{X}_{12}$ is the Flory-Huggins interaction parameter and can be calculated from the Equation 5.

$$\mathrm{X} = {V_S(\delta_1 - \delta_2)^2}/{RT} \quad \text{Equation 6}$$

where, $V_S$ = volume of polymer, $\delta_1$ & $\delta_2$ = the Hildebrand solubility parameter of solvent and polymer. In effect, the expression is valid only for amorphous and non-polar systems. A positive value of 'X' suggests that polymer-solvent interactions are less favorable as compared to polymer-polymer and solvent-solvent interactions. On the other hand, a negative value of 'X' suggests that polymer-solvent interactions are more favorable as compared to interactions within individual components and results in solvation of the polymer.[49] The first two terms in the Equation 6 denote the combinatorial entropy of mixing ($\mathrm{T\Delta S_{mix}}$), while the third term denotes the enthalpy of mixing ($\Delta H_{\mathrm{mix}}$).[50-52]

Just as for regular solutions, $\Delta H_{\mathrm{mix}} < 0$ and $\mathrm{T\Delta S_{mix}} > 0$, then $\Delta G_{\mathrm{mix}} < 0$. Thus for all compositions of $\phi_2$ the system is homogenous (Figure 6a). In this system, the energy of miscibility is more favorable that energy of phase separation.[50-52]

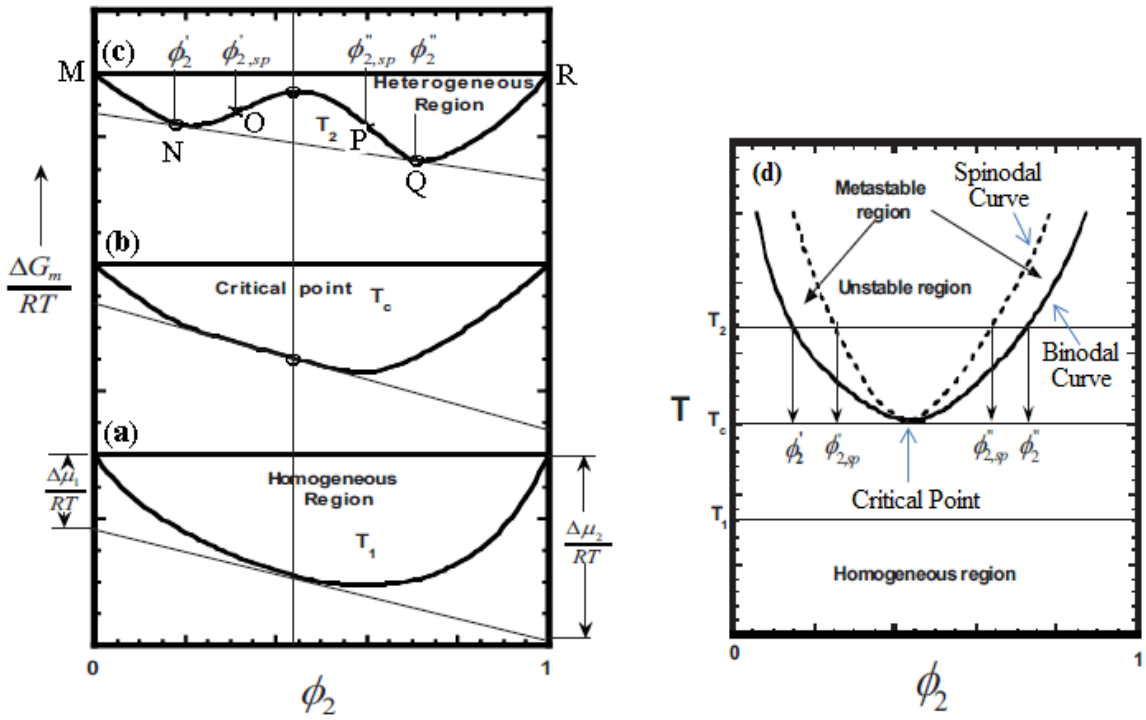


*Figure 6*. Free energy curve of the polymer system as a function of volume fraction of polymer, at a particular temperature: (a) stable phase (b) meta-stable phase and (c) unstable phase. (d) represents phase diagram of the polymer as a different temperatures.[48]

When $\Delta H_{mix} > 0$ and $T\Delta S_{mix} > 0$, phase separation will occur for a particular $\phi_2$composition range in which $\Delta G_{mix} > 0$ (Figure 6c). In Figure 6c, the regions M-N and Q-R represent stable single phase regions.[50-53] In these regions,

$$\frac{\partial^2 \Delta G_{mix}}{\partial \phi_2^2} > 0 \qquad \text{Equation 7}$$

The minima exhibited by the free energy on the curve (points N and Q) represent binodal points. The points where the slope changes from positive to negative or vice versa on the curve (points O and P) represent spinodal points.[50-53] At these points,

$$\frac{\partial^2 \Delta G_{mix}}{\partial \phi_2^2} = 0 \qquad \text{Equation 8}$$

The regions N-O and P-Q defines the meta-stable phase, whereas, the region O-P defines the unstable phase,[50-53] where,

$$\frac{\partial^2 \Delta G_{\mathrm{mix}}}{\partial \phi_2^2} < 0 \qquad \text{Equation 9}$$

The locus of spinodal points (points O and P) as a function of temperature represents a spinodal curve (Figure 6d).The locus of binodal points (points N and Q) as a function of temperature represents a binodal curve (Figure 6d). The point at which the two curves overlap is termed as a critical point.[50-53] At this point,

$$\frac{\partial^3 \Delta G_{\mathrm{mix}}}{\partial \phi_2^3} = 0 \qquad \text{Equation 10}$$

The Flory Huggins theory for binary systems: polymer blends or polymer solutions, have been extended to ternary systems: polymer, surfactant and solvent, by Lindman and coworkers. In these ternary systems, the entropy of mixing ($\mathrm{S_{mix}}$) and internal energy (U) of the system is described as:[43,54,55]

$$\mathrm{S_{mix}} = -\mathrm{RM_o}\left\{\emptyset_1 \ln\emptyset_1 + \left(\emptyset_2/\mathrm{L_2}\right)\ln\emptyset_2 + \left(\emptyset_3/\mathrm{L_3}\right)\ln\emptyset_3\right\} \qquad \text{Equation 11}$$

$$\mathrm{U} = \mathrm{RTM_o}\{\mathrm{X_{12}}\emptyset_1\emptyset_2 + \mathrm{X_{23}}\emptyset_2\emptyset_3 + \mathrm{X_{31}}\emptyset_3\emptyset_1\} \qquad \text{Equation 12}$$

where, $R$ = gas constant, $T$ = absolute temperature, $M_o$ = total number of cells, $\phi_1, \phi_2 \& \phi_3$ = volume fraction of solvent, polymer and surfactant, $\mathrm{L_2}$ = polymerization number of the polymer, $\mathrm{L_3}$ = fitting parameter for surfactant and depends on aggregation number of the surfactant, and $\mathrm{X_{12}}$, $\mathrm{X_{23}}$ & $\mathrm{X_{31}}$ is the Flory-Huggins interaction parameter solvent-polymer, polymer-surfactant and surfactant-water systems, respectively.[54]

The ternary phase diagrams produced by Flory Huggins theory are a reasonable fit to the experimental phase diagrams. However, Lindman and coworkers found some limitations of the model:[54]

- The strength of interaction between different components cannot be determined.
- This model considers the aggregation number of the free micelle only. However, the aggregation number of the surfactants is different for a free micelle and a polymer bound micelle.
- The mean field approximation theory, which assumes even distribution of polymer and solvent molecules in the system, is not correct. This is because the concentration of the polymer varies in the system; it is higher close to the surfactant micelle surface due to electrostatic interaction.
- Lindman's phase diagram shows the change from associative interaction to segregative phase separation as salt concentration increases.

Addition of salt in the polyelectrolyte/surfactant system has a complex behavior on the polyelectrolyte and surfactant interaction. In some systems, the interaction is weakened or suppressed while in others it is enhanced depending on the concentration of the salt.[56,57]

*The Two phase region:* Thalberg and coworkers noticed that the area of the two phase region increased with increase in the alkyl chain length of the surfactant, in the anionic polysaccharide hyaluronan (NaHy) and cationicalkyltrimethylammonium bromide ($C_n$TAB, n = 10, 12 and 14) systems (Figure 7).[55] They attributed this increase to the stronger interaction between the surfactant micelles and the polyelectrolyte chains with increase in the alkyl chain length.

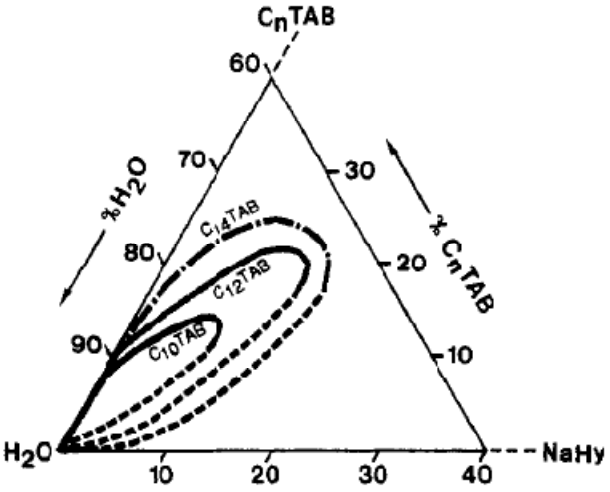


*Figure 7.* Phase diagram for NaHy, $H_20$, and $C_nTAB$ (n = 10, 12 and 14) system.[55]

*Weakening of the interaction*: Introduction of salt to the polyelectrolyte/surfactant system causes electrostatic shielding between the polyelectrolyte charged sites and the surfactant head groups.[17] Therefore, the interaction between the polyelectrolyte and surfactant is weakened.[58-61] The weakening of the polyelectrolyte and surfactant interaction was observed in the sodium dextran sulfate (NaDxS)/ dodecyltrimethylammonium bromide (DTABr) and sodium poly(styrene sulfonate) (NaPS)/dodecyltrimethylammonium bromide (DTABr) system.[58] Kwak and coworkers studied the interaction in these systems by producing binding isotherms, using a potentiometric technique at different NaCl concentration (Figure 8 and 9). Here, the degree of binding is defined as the amount of bound surfactant per ionic site on the polyelectrolyte.[61] From the binding isotherm curves, they observed that on increasing the NaCl concentration the degree of binding (β) commences at higher $m_D^f$ values, suggesting weakening of the interaction.

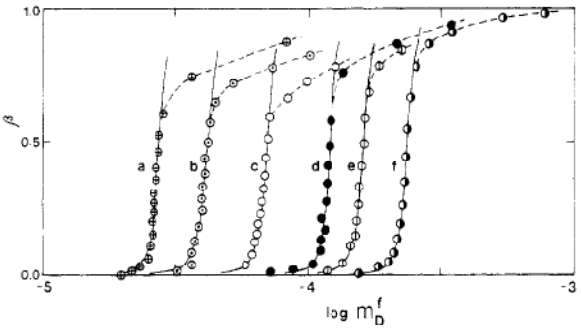


*Figure 8.* Binding isotherm curves for NaDxS/DTABr system. (a) 0.006, (b) 0.010, (c) 0.020, (d) 0.040, (e) 0.062, (f) 0.106 mol/kg of NaCl.[58]

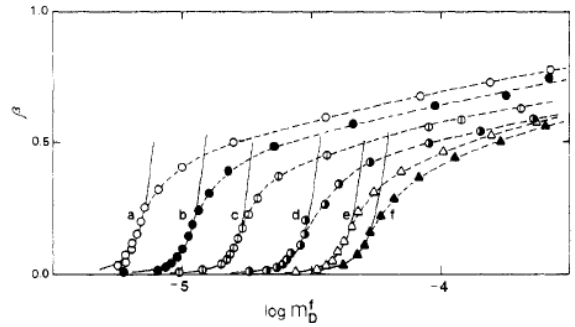


*Figure 9.* Binding isotherm curves for NaPS/DTABr system. (a) 0.021, (b) 0.041, (c) 0.082, (d) 0.176, (e) 0.444, (f) 1.12 mol/kg of NaCl.[58]

*Two opposite effects on the Interaction:* Addition of salt showed two opposite effects: at lower salt concentration, the interaction between the polyelectrolyte and surfactant was enhanced, while at higher salt concentration, the interaction was suppressed.[56,57,62-66] The nature of the interaction is governed by the dominance of compression of electric diffusive layer effect or the screening of the electrostatic interaction effect. In the salt enhancing effect, addition of salt compresses the diffusive layer and therefore, increases the interaction between the surfactant head groups and polymer charged sites. On the other hand, in the salt suppressing effect, addition of salt screens the electrostatic interaction between the surfactant head groups and polymer charged sites.[64,66]

The enhancement or suppression of the interaction was illustrated by measuring the critical aggregation concentration (CAC) of the cationic hexylene-1,6-bis(dodecyldimethylammoniumbromide) (12-6-12) and anionic sodium polyacrylate (NaPAA) system, with fluorescence spectroscopy as a function of NaBr concentration (Figure 10).[64] At low levels of NaBr (0.002 and 0.02 M), the salt enhancing effect decreased the CAC value of the NaPAA/12-6-12 system. However, high salt levels (0.1 M) increased the CAC.

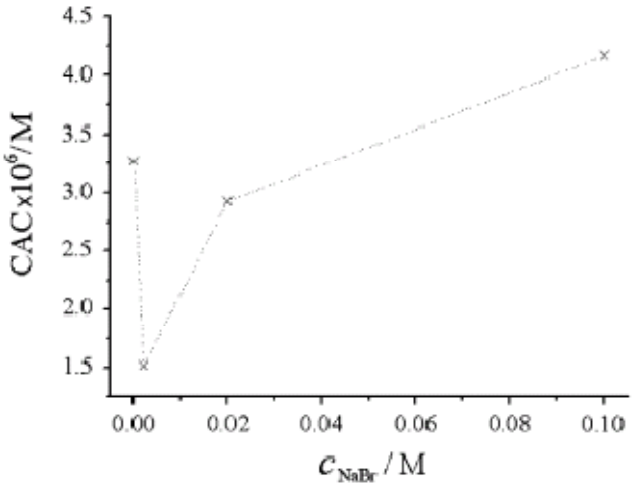


*Figure 10.* Effect of NaBr concentration on the CAC of the NaPAA/12-6-12 system.[64]

The enhancement or suppression of the interaction was also studied by measuring the critical surfactant concentration ($C_1$), which defines the onset of the complex formation. In the sodium carboxymethylcellulose (NaCMC) and dodecyltrimethylammoniumbromide (DTAB) system, addition of NaBr decreased the $C_1$value to 0.20 mM of NaBr concentration. Above this NaBr concentration, the $C_1$ value increased (Figure 11).[63]

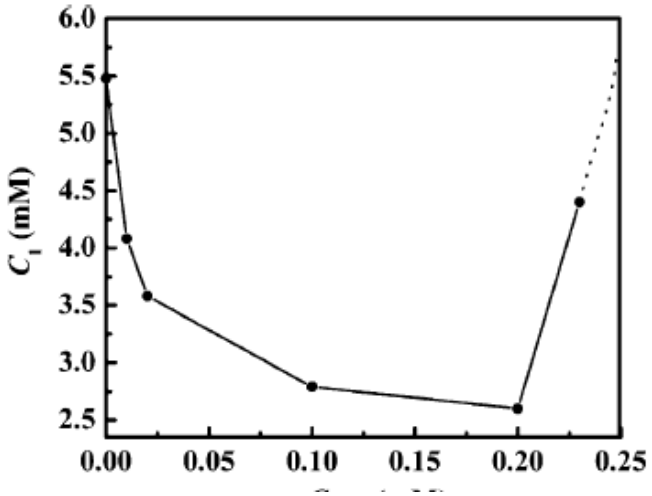


*Figure 11.* Critical surfactant concentration ($C_1$) of the NaCMC and DTAB system as a function of NaBr concentration.[63]

*Suppression of the phase separated region:*

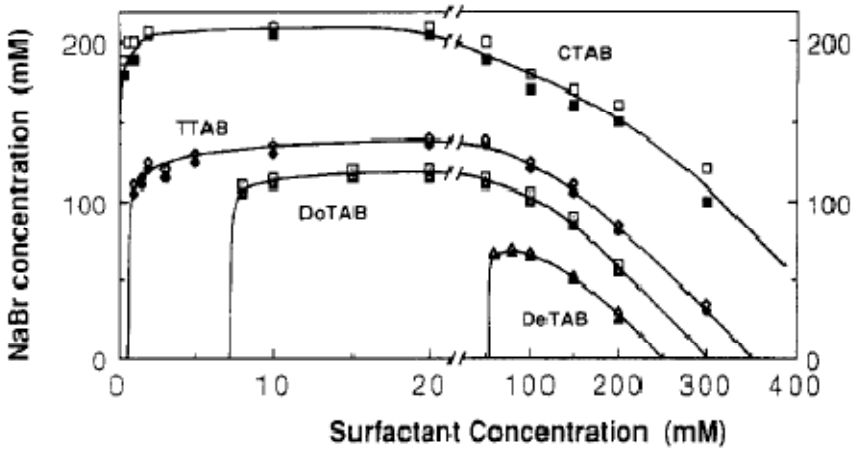


*Figure 12.* Critical electrolyte concentrations (CEC) for NaBr/1.0mMNaHy/ alkyltrimethylammonium bromide system, as a function of the surfactant concentration.One-phase is represented by open symbols and two phase is represented by filled symbols.[67]

At high salt concentration and surfactant concentration, in addition to the shielding of the electrostatic interaction, the salt also stabilizes the micelle. The stabilization occurs through a decrease of the CMC of the surfactant with increase in salt concentration. Thus, free micelles exist in the two phase region. The micelles reduce the

activity of the free surfactant and this adversely affects the polyelectrolyte and surfactant interaction. Therefore, the polyelectrolyte and surfactant phase separation is suppressed at higher salt and surfactant concentration. This suppression is analyzed by measuring the critical electrolyte concentration (CEC). This concentration is defined as the amount of salt required to redissolve the phase separated polyelectrolyte/surfactant complex. In NaBr/sodium hyaluronan (NaHy) and alkyltrimethylammonium bromide system, the CEC values start to decrease significantly above 80 mM of CTAB suggesting suppression in the two phase region (Figure 12).[67]

*Associative and segregative phase separation:* Interesting behavior was observed in the anionic polysaccharide sodium hyaluronate (NaHy) and cationic surfactant tetradecyltrimethylammonium bromide ($C_{14}$TAB) system in presence of NaBr (Figure 13).[68] At 0 mM of salt, the system showed associative phase separation i.e., the phase separated volume contained high amounts of polyelectrolyte and surfactant concentration compared to the other phase. As the salt level increased (75 mM of NaBr), the area of the phase separated region was suppressed. Moreover, at intermediate salt level, 250 mM of NaBr, a complete suppression of the phase separated region was observed. The phase separated region occurred at 75 mM and 250 mM of NaBr due to screening of the electrostatic interactions. In this system, the screening was not only due to NaBr but also due to sodium counterions in the NaHy. The total ionic strength of the system is referred as effective ionic strength. The effective ionic strength increases with increase in the NaHy concentration. Therefore, at a higher NaHy concentration larger electrostatic screening is experienced. Above 500 mM of salt the system showed segregative phase separation. At this NaBr concentration, the analysis of the regions showed that

supernatant had high amounts of surfactant, while phase separated region had high amounts of polymer.

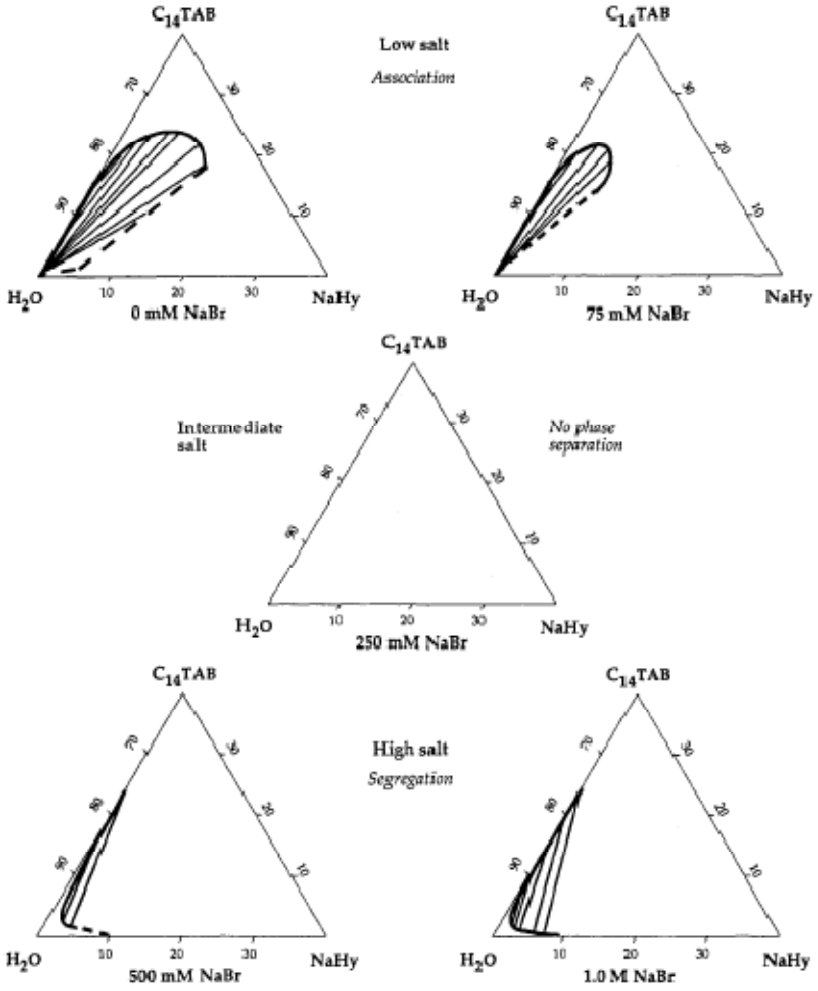


*Figure 13.* Phase diagrams for NaHy, $C_{14}TAB$ and water at different concentrations of NaBr.[69]

## Polymer-Surfactant Interactions

There is enduring interest to understand the interaction mechanism of the water soluble polymers with surfactants due to the importance of these systems in applications ranging from laundry, personal care, coating, electronics to pharmaceutics.[70-72] Extensive studies have been performed to understand the interaction mechanism between polymer and surfactant systems.[60,73-79] These systems can broadly be divided into three different

categories: nonionic water-soluble polymer/surfactant systems, polyelectrolyte/surfactant systems and hydrophobically modified polyelectrolyte/surfactant systems. The nature of the interaction mechanism and the way polymer and surfactant interact, depends on the physical properties of the polymer. For example, in the first and sometimes in the last of these three categories the interaction is weak and mainly driven by hydrophobic interaction between the polymer and surfactant. On the other hand, in the polyelectrolyte/surfactant systems, the interaction is dominated by strong electrostatic interaction between the polyelectrolyte and surfactant.

The interaction between nonionic polymer and surfactant was studied and explained by Jones for the polyethylene oxide (PEO) and sodium dodecyl sulfate (SDS) system, based on transition points observed by conductance and surface tension measurements.[17,70,80] These measurements revealed that at SDS concentrations lower than the cmc of the SDS, the data points for the PEO/SDS system overlapped with the data points for the SDS system alone. The specific conductance of the PEO/SDS system linearly increased (Figure 16) while the surface tension of the PEO/SDS system decreased (Figure 17) as in the case of SDS system. Therefore, it was inferred that at these SDS concentrations, the interaction between the polymer and surfactant was absent.

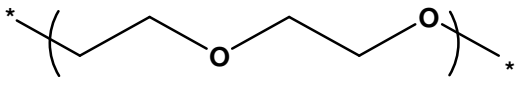


*Figure 14.* Chemical structure of polyethylene oxide.

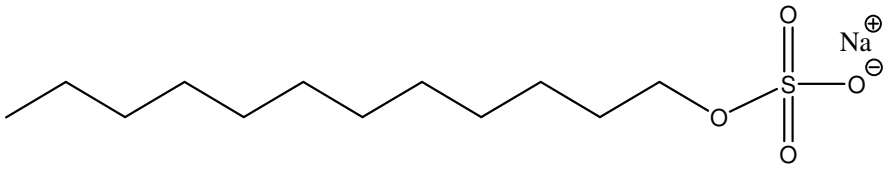


*Figure 15.* Chemical structure of SDS.

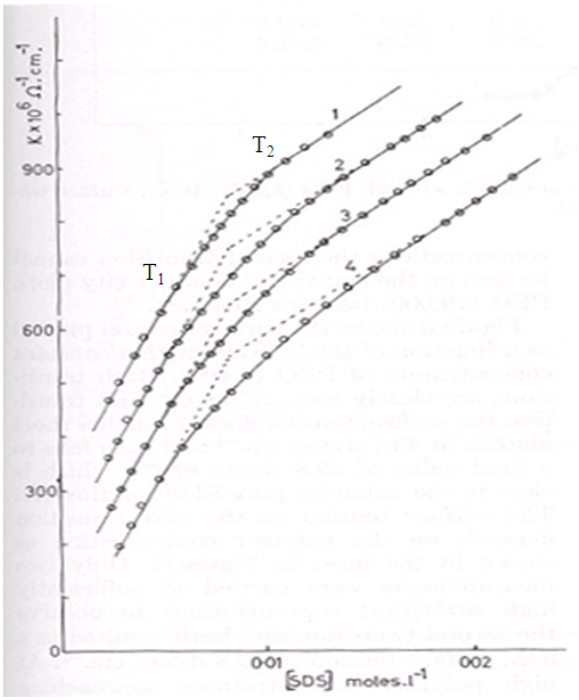


*Figure 16.* Specific conductance curve for PEO/SDS system, at different PEO concentrations. Dotted line represents surfactant specific conductance curve.[80]

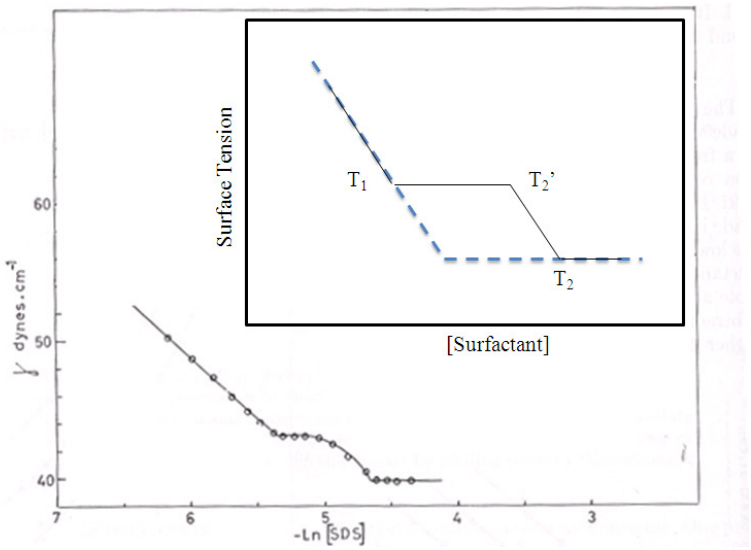


*Figure 17.* The surface tension curve for 0.025 % PEO/SDS system. Insert: Schematic surface tension plot pointing transition points. Dotted line: surfactant surface tension curve; solid line: polymer/surfactant surface tension curve.[80]

With addition of SDS, the data points for PEO/SDS systems deviate from the data points for SDS system. In conductance measurements (Figure 16), the PEO/SDS system follows a curve instead of linear fit as in case of SDS system (dotted line). Similarly, in surface tension measurements (Figure 17), deviation occurred as the PEO/SDS surface tension was higher than the surface tension of SDS, remained constant over a period of SDS concentration that ranged from below the SDS CMC to above that CMC. The onset of this deviation of the data points was referred as first transition ($T_1$) which existed at SDS concentration just above the CMC of SDS. However, further with addition of SDS, the data points for PEO/SDS approached those of SDS-alone system at a concentration that was above the CMC. This point was referred as second transition ($T_2$) and it occurred above the CMC of SDS. The deviation of the data points in between $T_1$and $T_2$ suggested interaction between PEO and SDS which occurs through interaction between polymer and surfactant that competed for adsorption of the surfactant at the interface, comparable

to micellization. This interaction was also observed through viscosity studies, which showed steady increase between $T_1$ and $T_2$ suggesting the formation of complexes. Above $T_2$, Jones opined that free SDS micelles coexisted with the PEO and SDS complex. Between the transition points $T_1$ and $T_2$, the interaction of the polymer with the surfactant occurs as a consequence of the chemical potential of polymer surfactant interaction being favored over surfactant adsorption at the interface. At surfactant concentrations greater than $T_2$, the chemical potential favors surfactant micelles.[80]

In contrast, for polyelectrolytes interacting with surfactants of opposite charge, a strong interaction takes place at extremely low surfactant concentration below $T_1$. The interaction mechanism between oppositely charged polyelectrolyte/surfactant systems was explained by Goddard and coworkers, based on surface tension measurements.[17,70,81] For this study, the surface tension data for cationic hydroxyethylcellulose (JR400) and nonionic surfactant-C11-15 Pareth-9 (Tergitol 15-S-9) (Figure 19) was compared with JR400 and the anionic surfactant- sodium lauryl sulfate (SLS) (Figure 15).

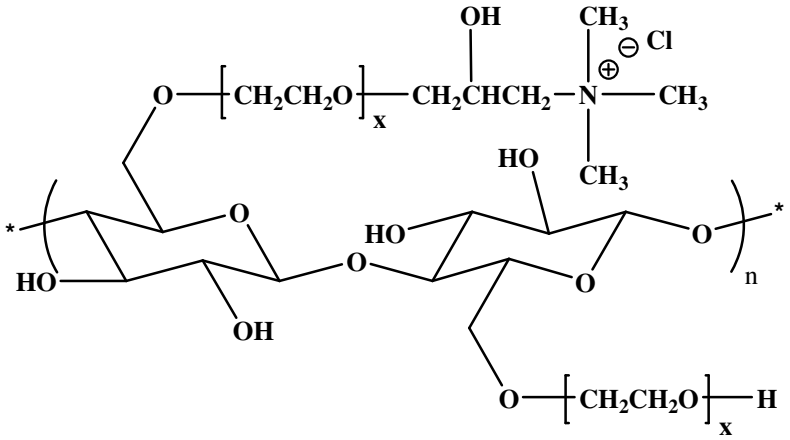


*Figure 18.* Chemical structure of Polyquaternium-10 (JR400). Chemical name: Cationic hydroxyethyl cellulose polymer.

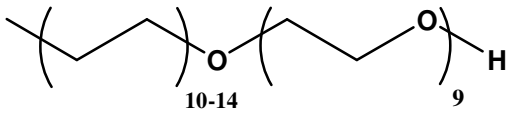


*Figure 19.* Chemical structure of TERGITOL™ 15-S-9. Chemical name: Secondary alcohol ethoxylate.

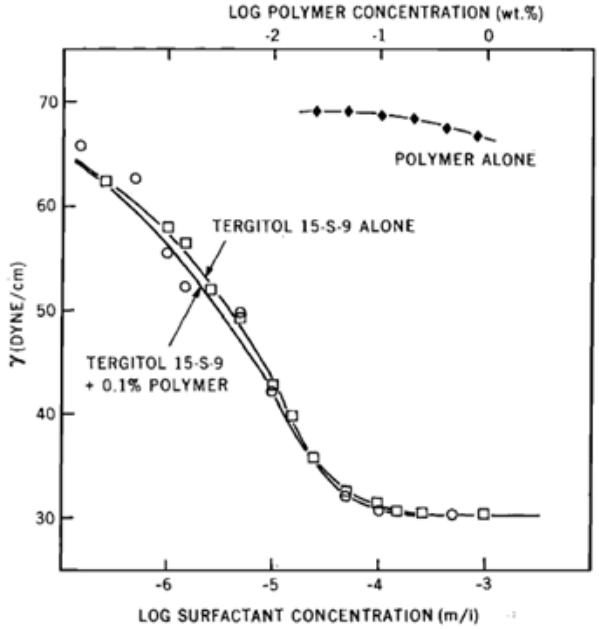


*Figure 20.* Surface tension data for Tergitol 15-S-9 with and without 0.1 % JR400.[81]

The surface tension curve of the nonionic surfactants is shown in Figure 20. 0.1% JR400 had no significant effect on the surface tension of nonionic surfactant. This suggested that there is minimal interaction between JR400 and nonionic surfactants. In the JR400 system alone (Figure 20), the surface tension of the system varies less as a function of the concentration.

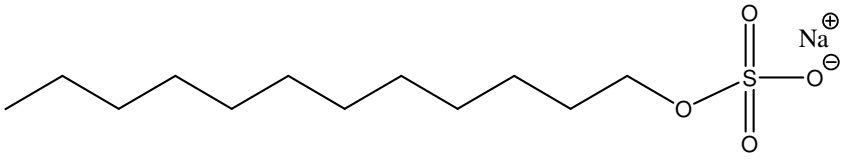


*Figure 21.* Chemical structure of SLS. Chemical name: Sodium dodecyl sulfate.

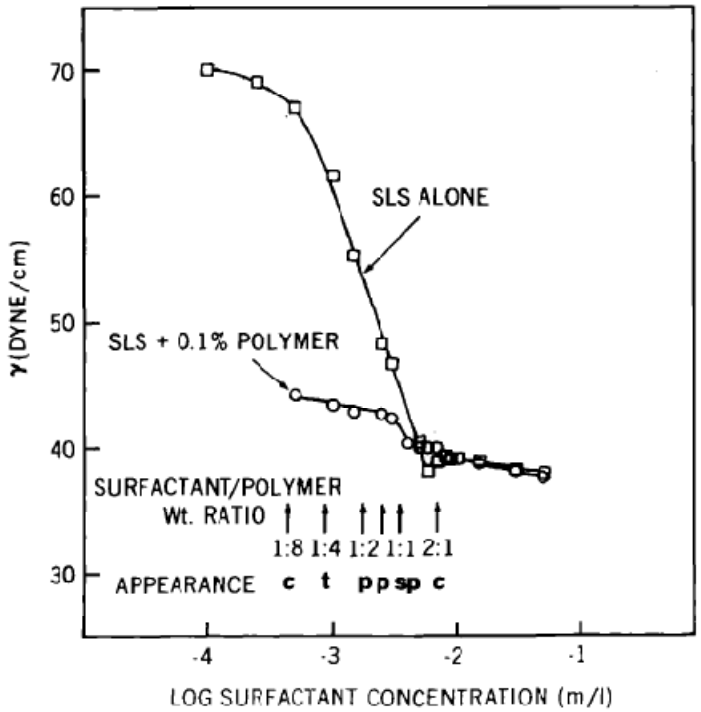


*Figure 22.* Surface tension data for sodium lauryl sulfate (SLS) with and without 0.1 % JR400.[81]

In contract to the JR400/nonionic surfactant systems, the JR400/anionic surfactant systems showed a strong interaction even for concentrations of surfactant that were two decades below cmc. In the presence of 0.1 % JR400 the surface tension values of anionic surfactants drop significantly compared to the surface tension values of the anionic surfactants alone (Figure 22). Therefore, for the JR400/anionic surfactant system, it was inferred that JR400 interacted with anionic surfactants to form a surface active complex. The surface activity of JR400/anionic surfactant complex was attributed to 'head-to-head' site-specific ion-ion interaction between the cationic sites of JR400 and the anionic surfactant head groups (Figure 23a). The association between JR400 and anionic surfactant was also shown by the presence of phase separation and increase in the viscosity. Besides this, maximum precipitation was observed at the charge neutralization point between the anionic surfactant and JR400. This observation is also consistent with

site specific ion-ion interaction. To verify the contribution of the JR400 cationic charges towards interaction, a surface tension plot for Cellosize® QP-300, a parent polymer of JR400 without cationic substitution, and anionic surfactant was produced. The surface tension curve for the Cellosize® QP-300/anionic surfactant system overlapped with the surface tension curve for anionic surfactant and also, precipitation was absent in this system. These observations led to the conclusion that the cationic charges on JR400 and the anionic charges on the surfactants were involved in the interaction.[81]

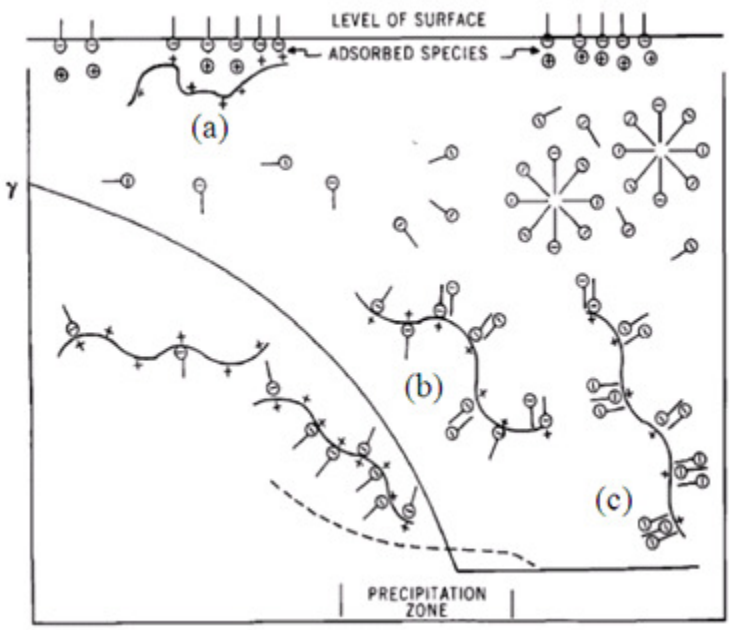


*Figure 23.* Schematic representation of the JR400/anionic surfactant system in bulk and air-water interface. The solid and dotted line marks hypothetical surface tension curve of anionic surfactant and JR400/anionic surfactant system. The formation of the (a), (b) and (c) systems are described in the text.[81]

According to Goddard, further increase in the anionic surfactant concentration causes adsorption of the surfactant on to the first layer of adsorbed, ion exchanged anionic surfactant on the polyelectrolyte.[81] This confers a negative potential to the polyelectrolyte anionic surfactant complex and it solublizes the complex (Figure 23c).

In contrast to the site specific ion-ion interactions proposed by Goddard, Dubin has hypothesized a polyelectrolyte-macroion interaction model[82] based on studies of the interactions between cationic poly(diallyldimethylammonium chloride) (PDADMAC) /nonionic Triton X-100(TX100) –anionic sodium dodecyl sulfate (SDS).[83-98] In this model, the macroion is made up of mixed micelles of TX100 and SDS in which the ratio of the two surfactant species is varied to change the effective charge density of the micelle surface.

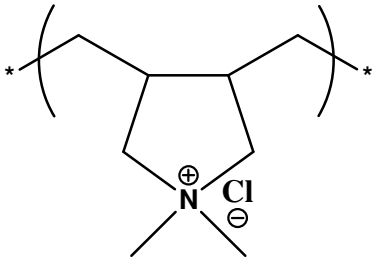


*Figure 24.* Chemical Structure of poly(diallyldimethylammonium chloride).

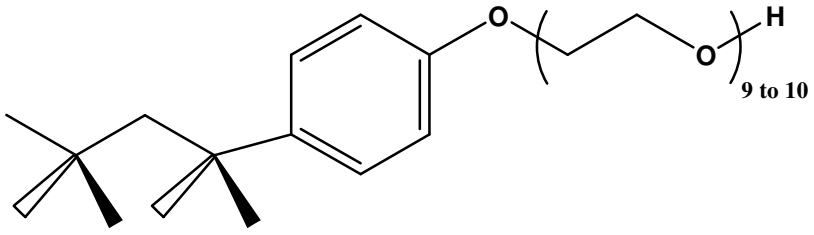


*Figure 25.* Chemical Structure of Triton X-100.

The advantage of using the mixed micelle is that it offers the prospect of examining the effect of micelle charge density on the interactions between the polyelectrolyte and surfactant system above the CMC of the surfactant where the

complex would be predicted to be soluble according to Goddard; except in the immediate region of 1:1 charge neutralization. Elucidation of the molecular mechanisms that underpin the interactions between the oppositely charged polyelectrolyte and surfactant system above the CMC, are complicated by phase separation of the complex. Such complexation can render the system 'opaque' to many common analytical methods. Therefore, most of the Dubin's interaction studies for these systems were performed below or much higher than the CMC of the surfactant, or a polyelectrolyte with low charge density was used, to avoid phase separation. In order to study the interactions above the CMC of the surfactant, Dubin and coworkers used mixed micelles. In mixed micelles, the surface charge density can be controlled by controlling the mole fraction of anionic surfactant in the micelle. Therefore, by adjusting the surface charge density, they attempted to avoid phase separation of the system.[83,85,94] For these systems, the ion-ion attractive forces are mainly responsible for driving the polyelectrolyte-micelle interaction as well as controlling the coacervate region.

In the PDADMAC/TX100-SDS system, the high charge density PDADMAC and SDS exist in one phase above the CMC of the surfactant in the presence of a simple electrolyte and TX100. The phase boundary for this system is highly dependent on the electrolyte concentration and the mole fraction of the SDS (Y) in the mixed micelle, and is independent of PDADMAC and total TX100-SDS concentration.[85] Y is related to the surface charge density of the mixed micelle. Here, Y is expressed as:

$$Y = \frac{[SDS]}{[SDS] + [TX100]} \qquad \text{Equation 13}$$

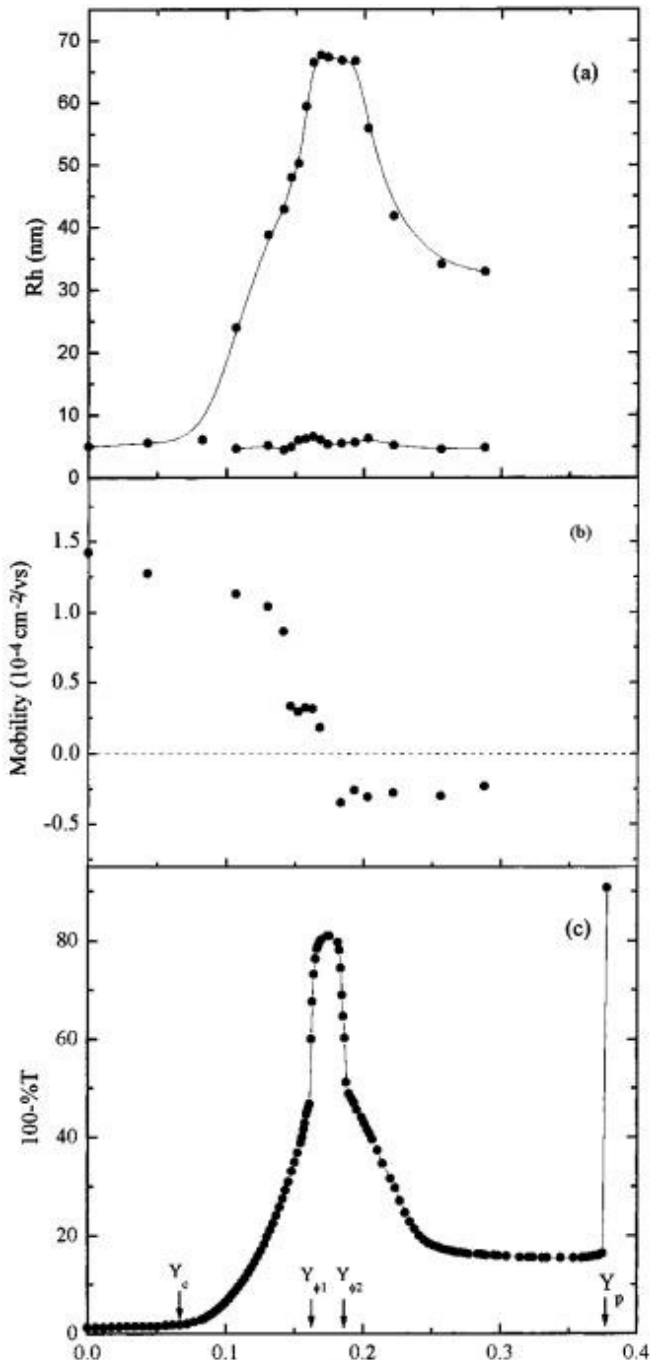


*Figure 26.* (a) Hydrodynamic radius, (b) mobility and (c) turbidity of the PDADMAC /TX100–SDS system in 0.10 M NaCl with increase in Y.[99]

The phase behavior of the PDADMAC/TX100-SDS system in 0.10 M NaCl was monitored using turbidity measurements (Figure 26c), whereas the structural behavior of this system was explored by dynamic light scattering (DLS) (Figure 26a) and electrophoretic mobility measurements (Figure 26b), as a function of Y. Turbidity was measured for PDADMAC/TX100 solutions in 0.10 M NaCl to which equal volumes of SDS and PDADMAC/TX100 solutions in 0.10 M NaCl were added. The SDS solution was added to vary Y i.e. vary the charge density of the mixed micelle. On the other hand, PDADMAC/TX100 solution was added to keep the PDADMAC and TX100 concentration constant through the measurements.

For initial values of Y, the turbidity of the system was low and constant. In this region, the hydrodynamic size of the system was small and constant. This size corresponded to the mixed micelles and not the polymer, as the polymer concentration was low compared to the mixed micelles. The mobility exhibited high positive values, due to the presence of a highly charged PDADMAC. A slight decrease in mobility was observed with increase in Y because the concentration of SDS in the mixed micelle is very low. Above a certain critical value of $Y = Y_c$, the turbidity of the system increased until the coacervate was formed at $Y=Y_{\Phi 1}$. In the $Y_c< Y < Y_{\Phi 1}$ region, the size of the complex increased while the mobility decreased with increase in Y. These changes suggested formation of a complex between PDADMAC and TX100-SDSmicelles. The unbound TX100-SDS micelles also coexisted with the complex which were observed using DLS (lower curve). Beyond $Y = Y_{\Phi 1}$, the turbidity increased markedly due to formation of coacervate in the system. With further increase in Y, the system was single phase and above $Y = Y_{\Phi 2}$ phase-separated coacervate was absent in the system leading to

decrease in the turbidity. The region in between $Y_{\Phi 1}$ and $Y_{\Phi 2}$ is defined as a coacervate region where the large complexes were present and the mobility approached zero. Beyond $Y_{\Phi 2}$, the turbidity decreased and then, remained constant. In the $Y_{\Phi 2} < Y < Y_p$ region, the complex size decreased while the mobility became negative. However, a drastic increase in the turbidity was observed at $Y = Y_p$ which suggested formation of a precipitate. In the Y > Yp region, it was difficult to monitor the size and mobility as large particles existed in the system.

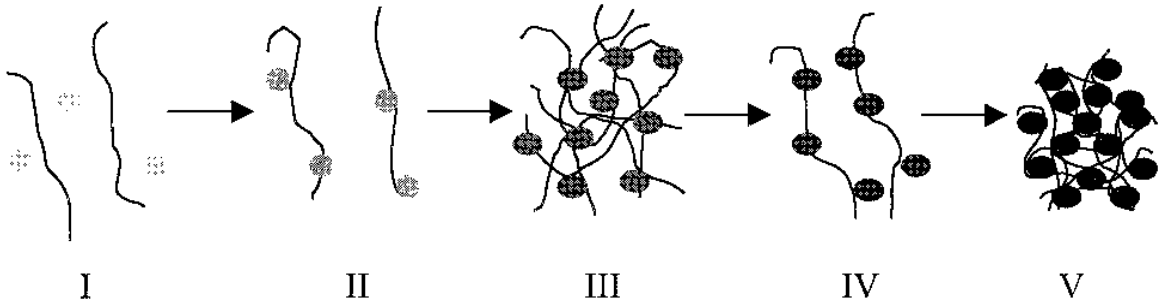


*Figure 27.* Schematic representation of Dubin's model for polyelectrolyte-macroion interaction. Dark shades of micelle indicate increase in surface charge density.[99]

Dubin's explanation for the turbidity changes observed as a function of Y for PDADMAC/TX100–SDS is shown schematically in Figure 26. In the $Y < Y_c$ region, the charge density of the TX100-SDS micelle is lower than the minimum surface charge density ($m_{scd}$) required for interaction. Therefore, no interaction occurred between the PDADMAC and TX100-SDS micelle. As a result, the turbidity, size and mobility of the system remained unchanged (Figure 27I). In the $Y_c < Y < Y_{\Phi 1}$ region, the charge density of the micelle is greater than $m_{scd}$. As a consequence, the PDADMAC and TX100-SDS micelle interact. This led to increase in turbidity and complex size, while decrease in mobility (Figure 27II). In the $Y_c < Y < Y_{\Phi 1}$ region, the charge density of the micelle is high enough to neutralize the PDADMAC /TX100-SDS complex. Therefore, mobility

approached zero. These neutralized complexes aggregate into interpolymer complexes forming a coacervate. The coacervate formation resulted in maximum turbidity and size (Figure 27III). In the $Y_{\Phi 2} < Y < Y_p$ region, the negative mobility values implied that inter-micellar and inter-complex repulsion occurred. Therefore, the complex was solubilized and hence, the turbidity and size decreased (Figure 27VI). In the Y >Yp region, the highly charged TX100-SDS micelle interacted strongly with PDADMAC, resulting in precipitation (Figure 27V). In short, according to Dubin's interaction model, the average charge density of the mixed micelle is a critical factor in controlling the coacervate formation, but Goddard postulates that coacervate formation is driven by site-specific interaction between the oppositely charged polymer functional group and surfactant head group.[99]

Dubin's interaction model emphasizes that the coacervate formation is controlled by the average charge density of the mixed micelle. However, this model ignores the effect of salt on the TX 100-SDS system. It has been reported in the literature that the size and shape of the TX 100-SDS mixed micelles is dependent on the salt and SDS concentration.[100] Increase in these two factors changes the shape from a spherical to rod-like or worm-like micelle. Therefore, these factors also may aid coacervation or precipitation other than the average charge density of the mixed micelle.

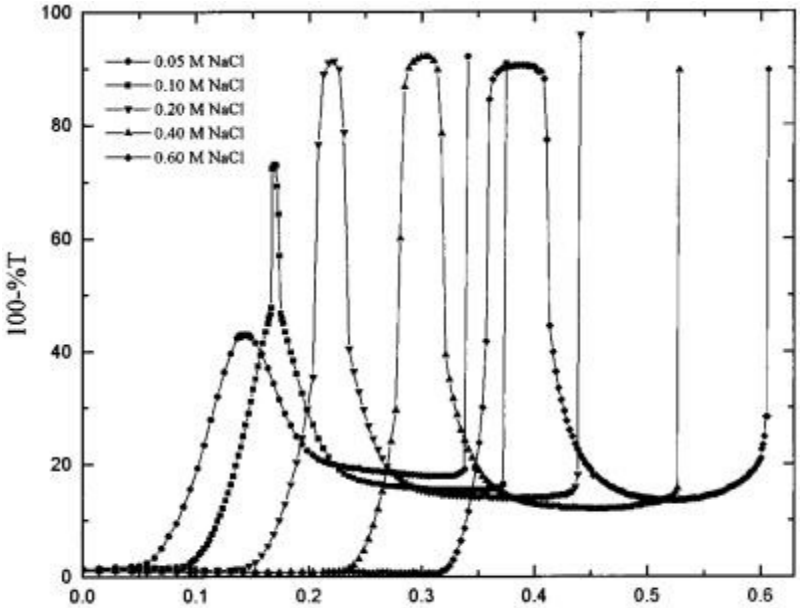


*Figure 28.* Turbidity curves of the PDADMAC/ TX 100-SDS system at different NaCl and Y values.[99]

Figure 28 represents the turbidity curves for the PDADMAC/ TX 100-SDS system at different NaCl concentration, as a function of Y. The presence and extent of the coacervate region depends on the salt and SDS concentration (Figure 28). At lower NaCl and SDS concentration coacervate region is absent. On the other hand, the extent of the coacervate region increases with increase in NaCl and SDS concentration. Dubin has explained the difference in the occurrence in the coacervate region as a function of micelle size. At low NaCl and SDS concentration, the hydrodynamic radius of the micelle is small compared to the hydrodynamic radius at higher NaCl and SDS concentration.

However, Dubin ignored the effect of NaCl and SDS concentration on the shape of the micelle. Increase in these concentrations may change the shape of the micelle from spherical to elliptical which may further increase the ion-ion binding between the polymer and micelle thereby increasing the coacervate region.

In the precipitation region, the NaCl and SDS concentration is higher than in the coacervate region. Therefore, the shape of the micelle in the precipitate region may further elongate. The effect of salt on micelle shape for SDS/TX100, according to Mata is shown in Table 1.

Table 1

*Physical parameters of the TX 100/SDS micelle.*[100]

| | NaCl concentration (M) | | | | | | | |
|---|---|---|---|---|---|---|---|---|
| SDS | 0 | | 0.3 | | 0.4 | | 0.5 | |
| (mM) | L | $N_{agg}$ | L | $N_{agg}$ | L | $N_{agg}$ | L | $N_{agg}$ |
| 0 | S | 72 | - | - | | - | S | 72 |
| 10 | S | 72 | S | 72 | S | 72 | 11.8 | 307 |
| 15 | S | 72 | 12.2 | 344 | 16.7 | 472 | 24.9 | 705 |
| 40 | S | 72 | S | 72 | 9.7 | 273 | 11.5 | 297 |
| SDS | 0.6 | | 0.8 | | 1.0 | | 1.5 | |
| (mM) | L | $N_{agg}$ | L | $N_{agg}$ | L | $N_{agg}$ | L | $N_{agg}$ |
| 0 | - | - | - | - | S | 72 | S | 72 |
| 10 | 15.3 | 439 | 21.3 | 604 | 15.6 | 441 | - | - |
| 15 | 35.7 | 1012 | 39.4 | 1116 | 40.7 | 1151 | - | - |
| 40 | 13.5 | 382 | 10.1 | 286 | 9.7 | 239 | - | - |

S = Sphere, L = length of the rod (nm), $N_{agg}$ = aggregation number.

In one of the TX 100/SDS system studies, the shape of the TX 100/SDS micelle was analyzed as a function of NaCl and SDS concentration (Table 1). From Table 1, it is seen that the spherical micelles changed to rod-like micelle with increase in NaCl and SDS concentration. Moreover, the length of the rod-like micelle also increased with increase in these concentrations. If the concentration of the SDS, which is expressed in mM in Table 1, is converted to the mole fraction of SDS i.e. Y, then the value of Y at which rod-like micelles were formed lies close to the precipitation of the PDADMAC/ TX 100-SDS system. It is plausible that the transition of the spherical micelle to the rod-like micelle may influence the ion-ion interaction and the decrease the entropy of the micelle/polymer mixture and this could lead to stronger phase separation.

Goddard's interaction model has put forth a simple representation of the polyelectrolyte and surfactant interaction mechanism in different zones[81] from his results of a surface tension study. However, this model does not take into account the complexities involved in the interaction. These complexities are dependent on the physical properties of both the polyelectrolyte and surfactant. For polyelectrolytes, some of these complexities are backbone flexibility, charge density and hydrophobic modification. Therefore, recent studies on interaction have been directed to explore these complexities.

The adsorption profile of the polyelectrolyte and surfactant systems depend on the electrostatic and hydrophobic interaction between the two species. Therefore, the Gibbs Equation cannot be applied to these systems to analyze the surface composition. In order to gather information about the surface composition, neutron reflectivity studies were conducted.[101] This technique not only determines the amount of polyelectrolyte and

surfactant at the surface but also measures the thickness of the absorbed layer. With the help of this technique, Taylor and coworkers investigated the polyelectrolyte and surfactant systems displaying two distinct adsorption profiles observed by surface tension measurements. In one of the absorption profiles, the polyelectrolyte and surfactant complexes showed a strong absorption at the interface, resulting in a constant surface tension.[102] Whereas, in another absorption profile, the polyelectrolyte and surfactant complexes exhibited partial desorption from the interface, thereby, increasing the surface tension.[103] These two adsorption profiles are discussed below in detail.

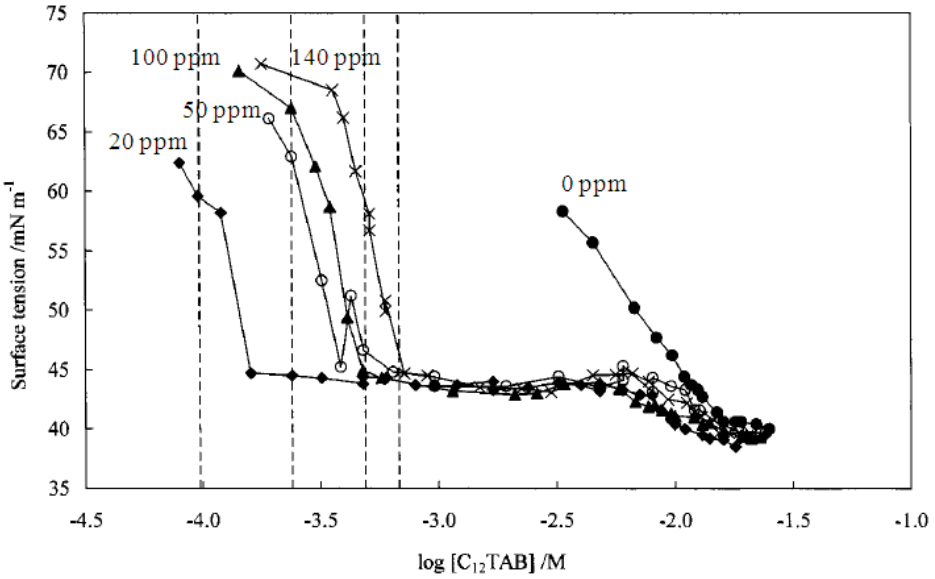


*Figure 29.* The surface tension profile of NaPSS/SDS system at different NaPSS, as a function of SDS concentration.[102]

A strong absorption profile was observed for the system comprising polymer sodium poly(styrene sulfonate) (NaPSS) and dodecyl trimethylammonium bromide ($C_{12}$TAB) system. The surface tension plot for this system is shown in Figure 29 at different NaPSS concentration. The plot showed strong adsorption of NaPSS/$C_{12}$TABcomplexes (~ 45 mN/m of surface tension) over a broad $C_{12}$TAB

concentration range. The cause behind the strong adsorption was probed by neutron reflectivity.

Table 2

*Layer parameters obtained from neutron scattering experiment.*[102]

| Layer | No. of surfactants | No. of segments | Hydration no. |
|---|---|---|---|
| 1+2 | 1 | 0.50 | 3.5 |
| 3 | 0.64 | .36 | 14 |
| 4 | 1.08 | .21 | 9 |
| 5 | 0.14 | .26 | 12.5 |
| Total | 2.86 | 1.33 | 39 |

Neutron reflectivity studies revealed formation of a thick absorbed layer comprising of polymer and surfactant. Based on these results, it was concluded that in this thicker layer is a sandwich of outer surfactant layer and inside polymer-micellar or bilayer complex (Table 2).[102]

Compared to the NaPSS/$C_{12}$TABsystem, the surface tension plot of the poly(dimethyldiallylammonium chloride) (PDMDAAC)/SDS system showed different adsorption profiles. The PDMDAAC/SDS system displayed a sudden increase in the surface tension in the two phase region (Figure 30). To better understand this behavior, further neutron scattering measurements were performed.

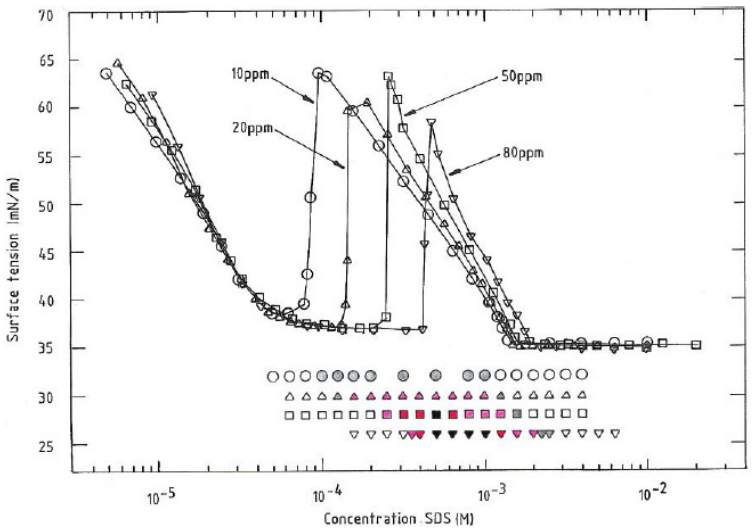


*Figure 30.* The surface tension profile of PDMDAAC/SDS system at different PDMDAAC, as a function of SDS concentration. Phase details: clear, white; almost clear, gray; cloudy, pink; visible aggregates, red and precipitates, black.[103]

In this system, neutron reflectivity was used to measure the SDS adsorption, polymer volume fraction, SDS thickness and polymer thickness at the interface as a function of SDS concentration (Figure 31). Compared to pure SDS, the adsorption of SDS in presence of PDMDAAC occurred at a lower SDS concentration (Figure 31a). This indicated co-adsorption of PDMDAAC/SDS complex at the interface. However, a small drop in the SDS adsorption was observed for the SDS concentration corresponding to the increase in the surface tension. In the same SDS concentration range, the polymer volume fraction (Figure 31b) and polymer thickness (Figure 31d) decreased. Therefore, the increase in the surface tension was due to the loss of the PDMDAAC/SDS complex from the interface. On the other hand, the SDS thickness over the entire SDS concentration stayed around 20 Å (Figure 31b), indicating absence of thick polymer/surfactant complex at the interface.[103]

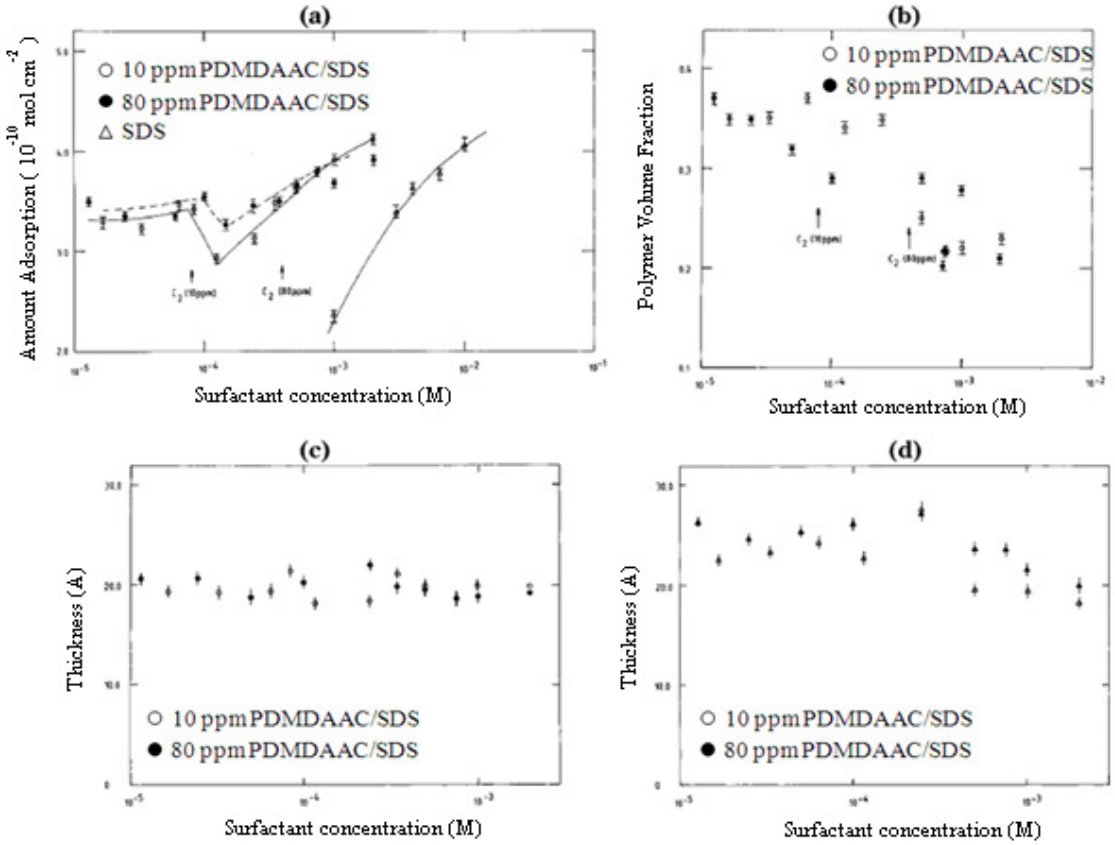


*Figure 31.* Neutron reflectivity data for the PDMDAAC/SDS system. (a) SDS adsorption (b) Polymer volume fraction (c) SDS thickness and (d) Polymer thickness at the interface as a function of SDS concentration.[103]

Taylor and coworkers explained these surface tension profiles based on the formation of three different polymer-surfactant complexes: $P_S$, a surface active polymer/surfactant complex which forms a monolayer at the interface; $P_S'$, a surface active polymer/surfactant complex which is absorbed below $P_S$ and contains surfactant micellar/bilayer aggregates; $P_{SM}$, a bulk polymer/surfactant complex comprising surfactant aggregates. The surface active complex $P_S$ is formed at lower surfactant concentration due to electrostatic interaction between the polymer and surfactant. Adsorption of this complex at the interface results in decrease in the surface tension. The other surface active complex ($P_S'$) and bulk complex ($P_{SM}$) is formed at a relatively higher

surfactant concentration compared to the surfactant concentration. The formation of $P_S'$ depends on the relative stability of the surface active or bulk complex. If the formation of surface active complex is preferred, the added surfactant will form $P_S'$, whereas, if the formation of bulk complex is preferred, the added surfactant will form $P_{SM}$.[101]

In the NAPSS/$C_{12}$TAB system, a thick interface layer is formed due the formation of $P_S'$ below $P_S$. On the other hand, in the PDMDAAC/SDS system, the formation of the $P_{SM}$ complex is preferred and adsorption of $P_S$' below $P_S$ does not take place. The increase in the surface tension occurs due to variation in the $P_S$ composition.

Taylor and coworkers were able to gain some insightful understanding of adsorption of the polymer and surfactant complexes from the neutron reflectivity measurements. However, this understanding did not relate the changes taking place in the bulk with the surface adsorption as it was solely based on analysis of the surface. Furthermore, the difference in the adsorption profile based on the polymer structural properties was not explored.

Campbell and coworkers further studied the kinetic behavior of the PDADMAC/SDS system. They found that the surface tension of this system is controlled by precipitation/suspension of the phase separated colloidal bulk complexes.[104,105]

Figure 32 shows that the turbidity and the surface tension of the freshly prepared and aged (3 days) PDADMAC/SDS system. According to the turbidity data, the suspended phase-separated colloidal complexes precipitate after 3 days. In the same region, the surface tension of the system increased significantly with precipitation. The loss of the complexes in the precipitate region is also supported by recording the dry weight of the supernatant (Figure 33). Moreover, the neutron scattering measurements

indicated desorption of polymer and surfactant from the interface in the precipitation region with time (Figure 34). They further studied the aged PDADMAC/SDS system by re-dispersing the system using mechanical stress. The turbidity of the system showed a slight change which was attributed to the flocculation of the phase separated particles (Figure 32). However, the surface tension of the system decreased drastically (Figure 32). Furthermore, the adsorption of polymer and surfactant also increased at the interface (Figure 33). Based on these experiments, Campbell and coworkers concluded that precipitation caused desorption of the surface active PDADMAC/SDS complexes resulting in the increase in surface tension, rather than just an interplay between the complexes at interface and in bulk as explained by Staples and coworkers.[105]

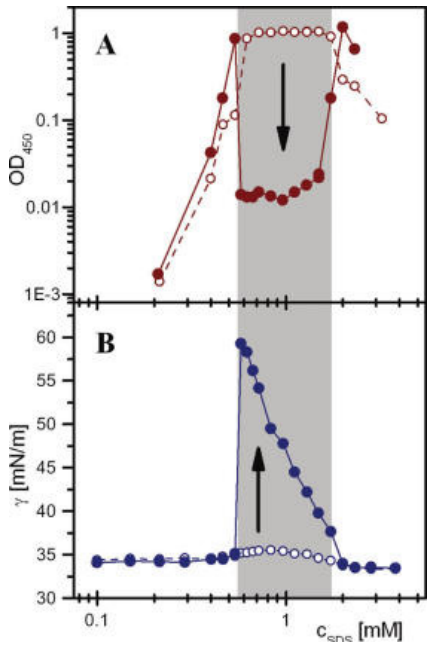


*Figure 32.* (a) Turbidity and (b) surface tension surface of PDADMAC/SDS solutions. Open symbols: fresh mixed and closed symbols: aged settled samples. Precipitation region is indicated by gray shaded area.[105]

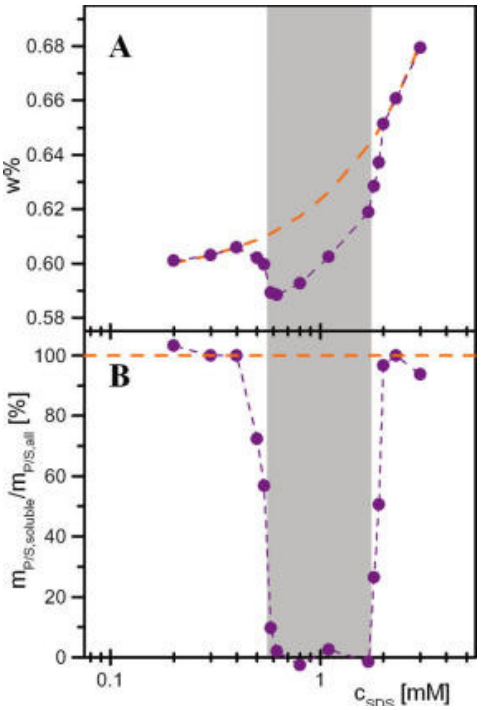


*Figure 33.* (a) Percentage dry mass of 100 ppm PDADMAC/0.1 M NaCl at different SDS concentrations (b) same data represented as into the percentage. Orange line: Expected amount of dissolved or suspended material. Precipitation region is indicated by gray shaded area.[105]

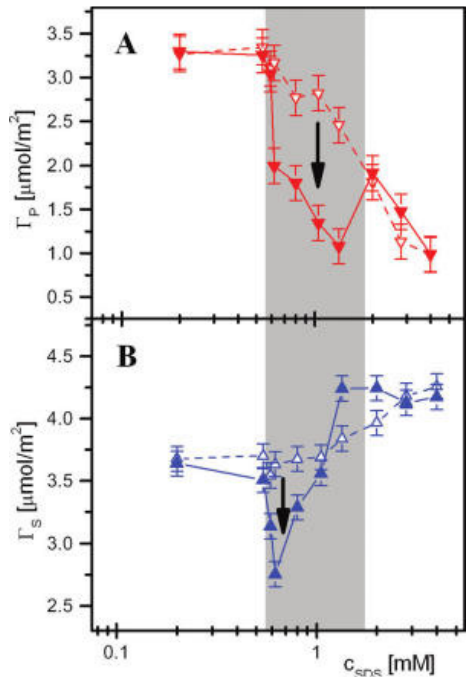


*Figure 34.* Neutron reflectivity data: (a) PDADMAC and (b) SDS surface excesses in PDADMAC /SDS solutions. Open symbols: fresh mixed and closed symbols: aged settled samples. Precipitation region is indicated by gray shaded area.[105]

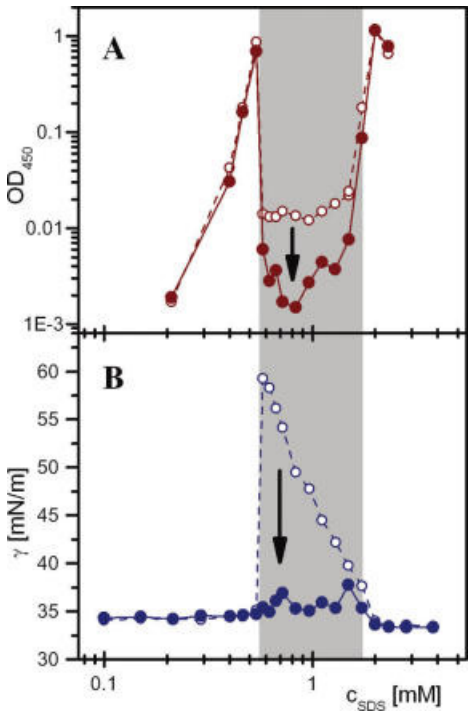


*Figure 35.* (a) Turbidity and (b) surface tension surface of PDADMAC/SDS solutions. Open symbols: aged settled and closed symbols: aged redispersed samples. Precipitation region is indicated by gray shaded area.[105]

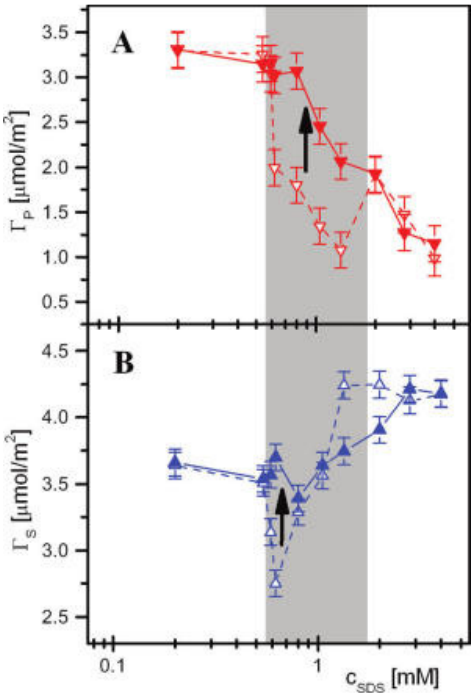


*Figure 36.* Neutron reflectivity data: (a) PDADMAC and (b) SDS surface excesses in PDADMAC /SDS solutions. Open symbols: aged settled and closed symbols: aged redispersed samples. Precipitation region is indicated by gray shaded area.[105]

Mészáros and coworkers found that the sample preparation method did not affect the surface tension of the poly(vinylamine) (PVAm)/ SDS system. However, they found that the preparation method influenced the physical properties of the PVAm/SDS complex size in bulk, which ultimately produced the same surface tension curve. They implemented gentle mixing and stop-flow mixing methods. In the former method, the PVAm/SDS system is simply mixed by turning the test tube, while, in the latter system, the system is mixed in a few milliseconds.[56]

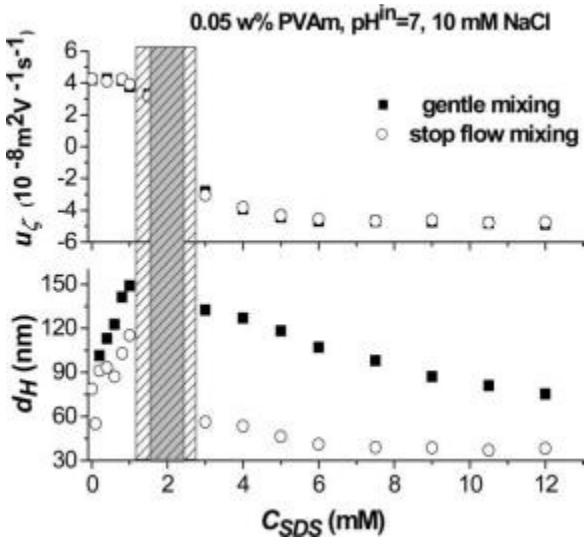


*Figure 37.* Electrophoretic mobility and hydrodynamic diameter of the PVAm/SDS complexes at [PVAm] = 0.05 wt %, [NaCl] = 10 mM and pH = 7, as a function of the SDS concentration for the two mixing methods. Gray area: two phase region for the stop flow method, gray + sparse areas: two phase region for gentle mixing methods.[56]

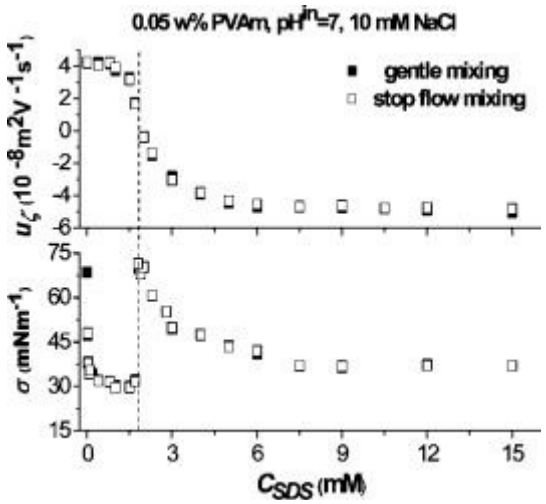


*Figure 38.* Electrophoretic mobility and surface tension of the PVAm/SDS systems at [PVAm] = 0.05 wt %, [NaCl] = 10 mM and pH = 7, as a function of the SDS concentration for the two mixing methods.[56]

The bulk and surface behavior of the PVAm/SDS system is represented in Figure 37 and 38, respectively. The electrophoretic mobility and the surface tension of the system were independent of mixing methods. However, the size of the system was dependent on the mixing method. They suggested that may be due to large size or electrostatic replusion between the complexes in the bulk which could hinder the adsorption of the complex in the gentle mixing method.

Zhou and coworkers studied the interaction between a semi-rigid cationic hydroxyethyl cellulose (cHEC) polymer and sodium dodecyl sulfate (SDS)[76] by characterizing their mixtures using rheological, dynamic light scattering (DLS), and small angle X-ray scattering (SAXS) measurements.

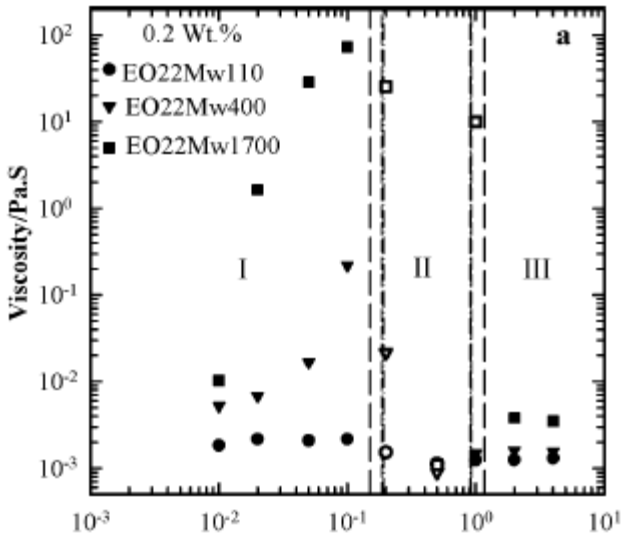


*Figure 39.* Viscosity of the cHEC-SDS system as a function of SDS concentration. In the two phase region the measurements were performed on the supernatant.[76]

The viscosity was measured for different polymer molecular weights in the one phase (I), two phase[106] and 'redissolved' phase (III) regions of the phase diagram (Figure 39). They observed that in the one phase region, the viscosity of the solutions of highest molecular weight polymers increased with increase in the SDS concentration. In this phase, the maximum viscosity value was recorded near the two phase boundary. In the two phase region, the system was centrifuged and the supernatant was analyzed. The viscosity in the initial part of the two phase region was high, but lower than the maximum value recorded in the one phase region. Zhou postulated that at the initial point of phase separation, the polymer still contains an excess of cationic charge and this is offered as an explanation for the high viscosity of the supernatant under these conditions being due to expanded polyelectrolyte chains. Of course, with addition of more (charge-neutralizing) anionic surfactant, the viscosity decreases dramatically. However, in the latter part of the two phase region the viscosity of the system approached the viscosity of water. Here, the cHEC-SDS complexes are separated, especially at the 1:1 neutralization point. In the

redissolved phase, the viscosity of the cHEC-SDS system remains low. However, Zhou does not seem to have determined whether the solutions were in the dilute or semi-dilute regions, with respect to polyelectrolyte concentration. We note, however, that the viscosity of the lowest molecular weight polymer does not increase as SDS is increased in region I and the viscosity of the surfactant decreases exactly at the phase boundary. This behavior is consistent with the EO22Mw110 polymer solution being below its critical overlap concentration and the other polymers being above their critical overlap concentrations in Zhou's experiments. Opposite ion attraction between the polymer and surfactant combined with hydrophobic association of surfactant tail groups would be expected to result in a reduction in isolated chain dimensions below the C*. Conversely, these same interactions might be expected to enhance polymer networks above C*.

These authors measured the size of the low molecular weight cHEC/SDS complex and its distribution in different phases using DLS, as a function of SDS concentration (Figure 40). In the absence of SDS and salt, bimodal distribution was observed. They inferred that the fast mode at smaller size was due to the diffusional fluctuations of the counterion cloud. On the other hand, slow mode at bigger size was due to the collective diffusion of the polyelectrolyte domain as the relaxation rates showed $q^3$ dependence (Figure 40a). With addition of 0.25 M NaCl to the cHEC solution the fast and the slow mode peaks merge to form a uni-modal peak due to screening of charges at lower $R_h$ (Figure 40b). My results support the importance of analyzing the data consistent with an understanding of the system relative to the critical overlap concentration, C*. I observed that below C* the viscosity of JR400 decreases with increase in the salt concentration. Whereas, above C*, the viscosity of increases with increase in the salt concentration.

Therefore, decrease in the $R_h$ on adding salt suggests that, in the Zhou study, the concentration of low molecular weight cHEC was below C*.

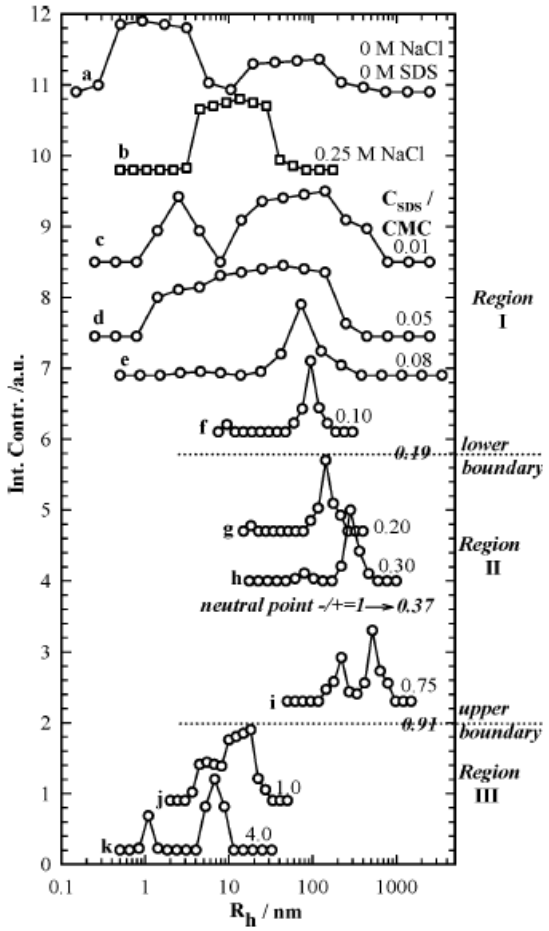


*Figure 40.* Distribution curves of the hydrodynamic radius ($R_h$) of (a) 0.2 wt % cHEC solution (b) 0.2 wt % cHEC solution in 0.25 M NaCl and (c-k) 0.2 wt % cHEC/SDS solutions as a function of SDS concentration. The measurements were performed at T = 25°C and θ=60°. Phase separation was observed between 0.19 cmc and 0.91 cmc of SDS.[76]

With addition of 0.01 CMC of SDS to the cHEC, the fast mode distribution sharpened, and it is apparent that the fastest fluctuations in the distribution were lost. This would be consistent with a redistribution of the counterion fluctuations upon addition of SDS. The broader distribution for the slow mode was attributed to presence of a network formed between cHEC and SDS micellar aggregates (Figure 40c). Further increase in the

concentration of SDS caused the fast mode and slow mode distributions to merge and then the slow mode sharpened and the diffusional times increased. Zhou suggests that this may be due to growth of the surfactant micelles to rods and even lamellae. Alternatively, the observation would be consistent with an increase in flock size.

Based on the above structural insights, Zhou and coworkers projected the interaction mechanism between the semi-rigid cHEC and SDS (Figure 41).

*Region I:* Region I represents one phase of the low molecular weight cHEC and SDS system at lower SDS concentration. According to Zhou and coworkers, the observed increase in viscosity was attributed to enhancement of the cHEC network in this phase due to the association of the cHEC polymer chains via hydrophobic tail-tail interaction between the SDS molecules. Zhou suggested that this structure was stabilized by the excess of cationic charge of the cHEC/SDS complex. With addition of SDS, this network condensed due to the neutralization of cHEC polymer chains with SDS molecules as well as due to increase in the SDS tail-tail interaction (Figure 41a). Further addition of SDS reduced of the overall size of the complex. Therefore, they suggested that the SDS molecules in the complex reorganized themselves from a lamellar to a micelle or vesicle, producing a compact complex (Figure 41b). However, they offered no evidence to support the presence of lamellar or vesicle structure. This led to pronounced increase in the viscosity. However, from Zhou's work, it can be noted that the high molecular weight cHEC showed an increase in viscosity but the low molecular weight cHEC did not. The viscosity increase for the high molecular weight cHEC may be because the concentration is above C* that could form an entangled network which could be enhanced by hydrophobic interaction between the bound SDS alkyl groups.

*Region II:* Region II represents two phase of the cHEC and SDS system, where macroscopic phase separation occurred close to the charge neutralization point. From SAXS measurements, it was concluded that the average inter-distance of the SDS domain in the phase separated complex is about 3.6 nm (Figure 41). This correlation length is much smaller than the polymer hydrodynamic dimensions. Therefore, they surmised that the SDS aggregates present in the complex are spherical or elongated micelles (Figure 41c), but again they offered no conclusive evidence for the presence of such elongated micelle. As a result of phase separation, a significant amount of cHEC is lost from the supernatant, thereby decreasing the viscosity.

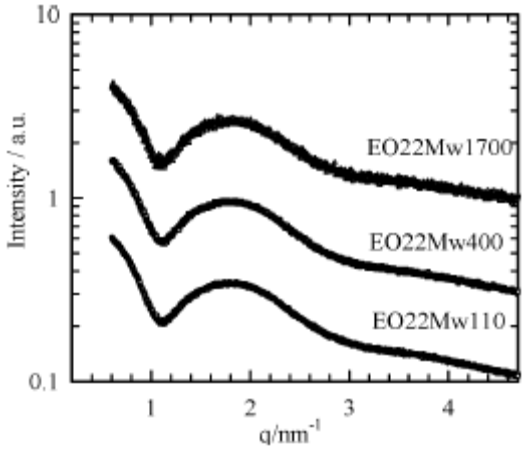


*Figure 41.* SAXS profiles of the phase separated cationic cHEC-SDS complexes formed at 1.5 (-/+)charge ratio with different molecular weights of polymers.[76]

*Region III:* Beyond the neutralization point, the phase separated complexes were solubilized in the presence of an excess of SDS molecules above the critical micelle concentration. Zhou asserted that the re-solubilization occurred through hydrophobic association of the added SDS micellar aggregates within the complex. As a consequence, the complex was believed to be stabilized by excess negative charge (Figure 41d).

Region III represents a solubilized one phase cHEC and SDS system. At higher SDS concentration, Zhou postulated that the large cHEC/SDS complexes disintegrated into smaller complexes as a result of the repulsion of same charges of SDS micelles. Therefore, the viscosity remained low (Figure 41e).

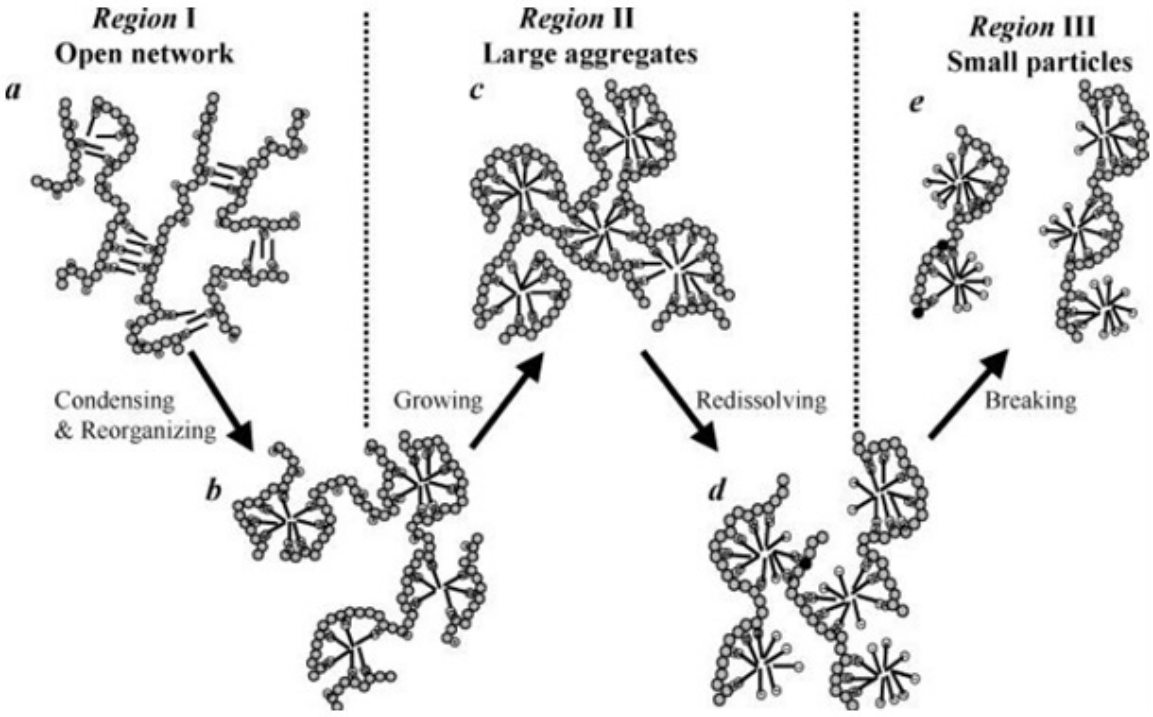


*Figure 42.* Interaction mechanism for a semi-rigid cationic hydroxyethyl cellulose (cHEC) polymer with sodium dodecyl sulfate (SDS) in different regions: Region I- one phase, Region II- phase separated phase, and Region III- resolubilized one phase.[76]

Tam and coworkers[60] studied the interactions between methacrylic acid/ethyl acrylate (EA) copolymers[107] and dodecyltrimethylammonium bromide (DoTab), using isothermal titration calorimetry[1] and laser light scattering[108] studies. This copolymer was referred as HASEx-y, where 'x' is the MAA mole % and 'y' is EA mol %. In this ITC study, they found that the width of one peak which they denoted peak 'A' was proportional to the MAA mol % (Figure 43). Therefore, they concluded that peak 'A' denoted the electrostatic interaction between HASE and DoTab. According to our

calculations, above 60 mol % of EA in the polymer, the width of peak 'A' does not increase proportionally (Figure 43). Therefore, I believe that at higher MAA mol % some of the anionic charges of the polymer are not available to the DoTab ions. I surmise that they may be are trapped in the hydrophobic part.

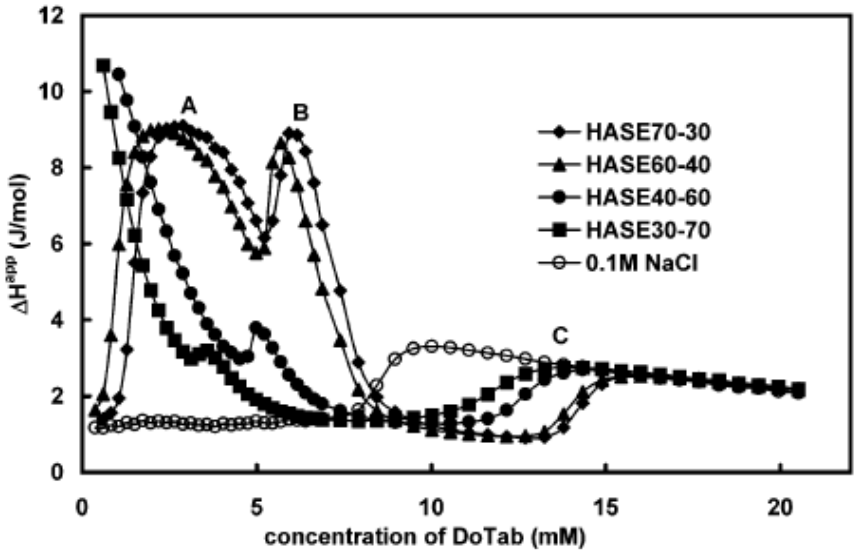


*Figure 43.* ITC curves for 0.05 wt % HASE and DoTab in 0.1 M NaCl solution at different copolymer ratios.[60]

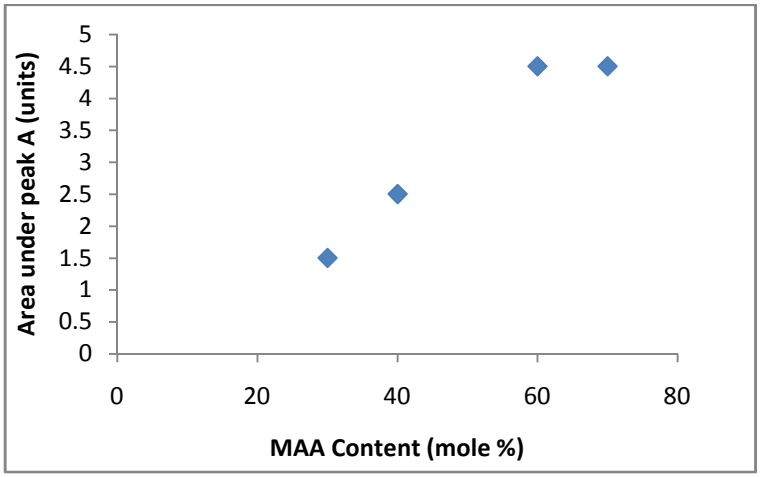


*Figure 44.* Relation between the area under the peak 'A' and the MAA mol % content.

On the other hand, they found that the onset of the peak 'B' decreased with increase in the carbon atoms in the alkyl chains (Figure 44). Therefore, they suggested that the peak 'B' denoted hydrophobic interaction between polymer bound surfactants and EA segments. I noted that the decrease of peak B is sharper and occurred at earlier surfactant concentrations for higher alkyl chain lengths. This indicates more or tighter binding for higher alkyl chain lengths followed by a rapid decrease in the ability to bind – the decrease is steeper for higher alkyl chain lengths. I ask, "does this mean the chain collapses and leaves fewer binding sites available on the downside of curve A?"

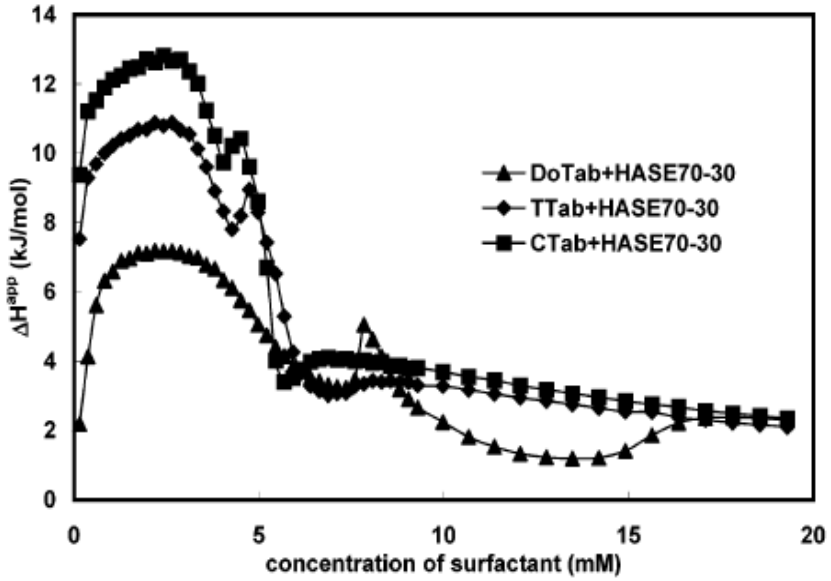


*Figure 45.* ITC curves for 0.05 wt % HASE 70-30 and alkyltrimethylammonium bromide ($C_n$TAB, n = 12, 14 and 16) in 0.1 M NaCl solution.[60]

Tam defined critical interaction points on the isothermal titration calorimetry[1] curves: onset of electrostatic binding ($C_1$), micellization of the polymer bound surfactants (C'), saturation with the bound surfactant micelles ($C_2$), and formation of free micelles ($C_M$) (Figure 45). The difference between the C2 and $C_M$ concentration denotes the amount of surfactant absorbed on the HASE chain. Based on this concept, our

calculations showed that the absorption DoTab molecules, with respect to available MAA on the HASE chain, decreased with increase in the MAA content (Table 3). Therefore, it is reasonable to presume that the anionic charges get buried in the hydrophobic cluster with increasing MAA mol %.

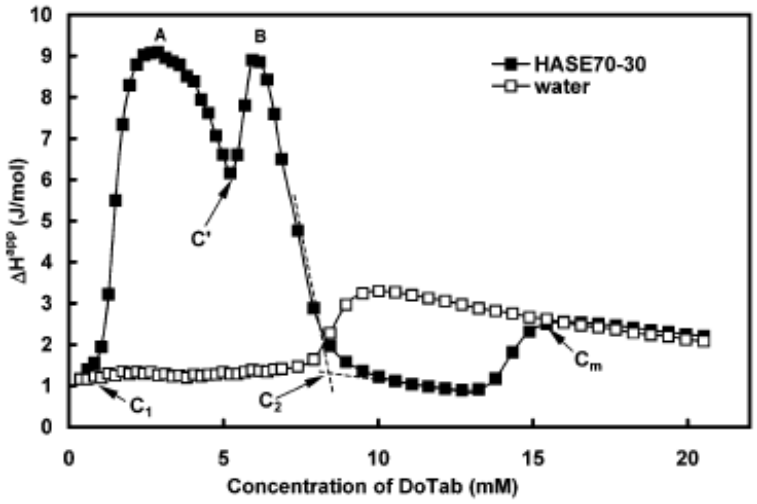


*Figure 46.* Critical interaction points on the 0.05 wt % HASE 70-30/DTAB ITC curve.[60]

Table 3

*Relation between MAA mol % and amount of DOTAB absorbed.*

| **MAA Mol%** | **$C_m$-$C_2$** | **[DoTab]/[MAA]** |
|---|---|---|
| 30 | 7 | 4.083 |
| 40 | 7 | 3.06 |
| 60 | 6.5 | 1.89 |
| 70 | 6 | 1.5 |

In this study, Tam and coworkers produced ITC curves at 0.05 % and 0.1% of HASE 70 -30/DoTab system (Figure 46 and 47). If the two curves are compared, we observe that by doubling the concentration of HASE, the saturation concentration (C')

decreased by half. Instead this C' should proportionally increase. Moreover, the enthalpy of binding doubled with the concentration. This is consistent with an equilibrium binding that depends upon both [DoTAB] and [COO-]. Therefore, this may indicate that this is equilibrium binding and may be consistent with the polymer being a network throughout the solution. This is not even mentioned by the authors.

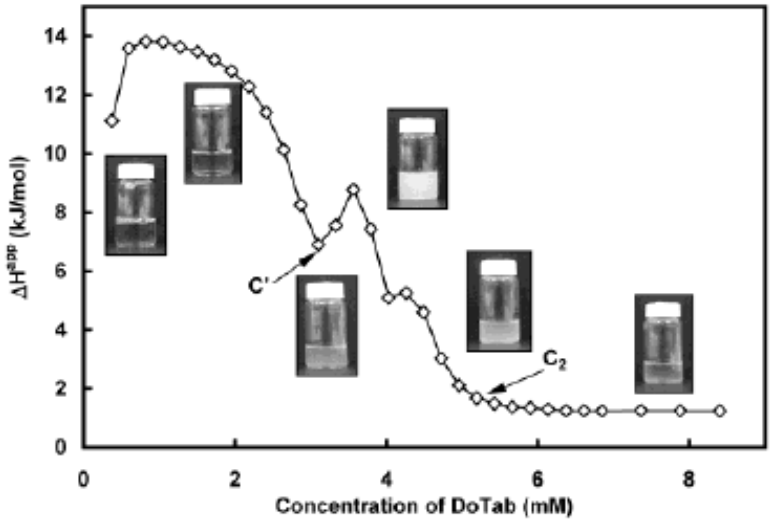


*Figure 47.* ITC curves for 0.1 wt % HASE 70-30 and DoTab in 0.1 M NaCl solution.[60]

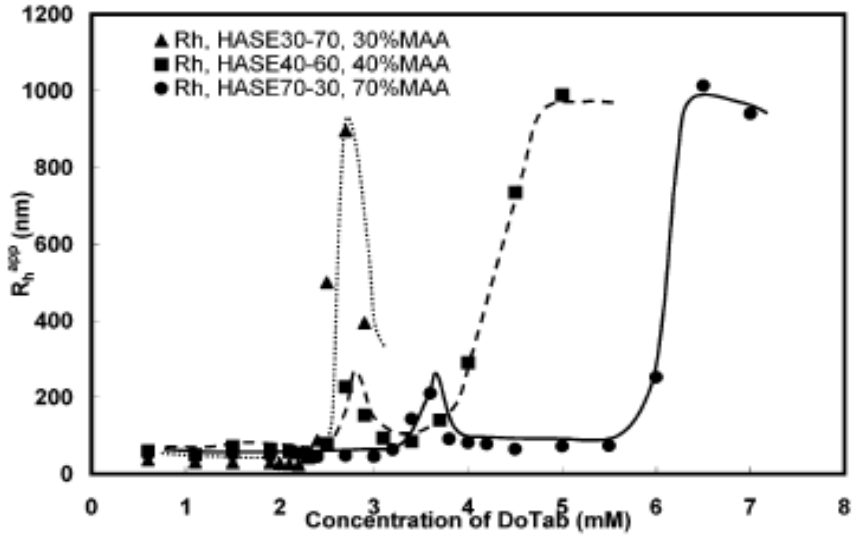


*Figure 48.* Hydrodynamic radius of the 0.1 wt % HASE/ DoTab complex as a function of surfactant concentration.[60]

Based on the isothermal titration calorimetry[1] and laser light scattering[108] studies, Tam and coworkers proposed the interaction mechanism between HASE and DoTab. They suggested that at low DoTab concentration, the polymer formed a cluster with the DoTab hydrophobic tail protruding into water (Figure 49a). However, free suspension the DoTab hydrophobic tail in water is thermodynamically unfavorable. With further addition of DoTab, the system experienced precipitation. They attributed the precipitation formation to the reorganization of the DoTab molecules in the HASE/DoTab complex (Figure 49b & 49c). However, no evidence for reorganization of the DoTab molecules in the complex was provided. Moreover, the precipitation region of the HASE30-70/DoTab system was narrow and the complex size in this region suddenly increased (Figure 49). Based upon the experimental evidence, we postulate that the sudden increase in the complex size of the HASE30-70/DoTab system was due to flocculation of the HASE30-70/DoTab complexes rather than reorganization. On the other hand, the precipitate region of HASE70-30/DoTab system showed gelation (Figure 49e). In HASE 70-30/DoTab system, the gelation may be induced in the system as the concentration of HASE 70-30 may be above C*.

As an extension of Tam's work, I have studied the interaction between the flexible polymer- MAPTAC and SDS to attempt to understand the interaction mechanism. This system was studied with broad characterization techniques, below and above the CMC so as to explore solution and phase-separated coacervates.

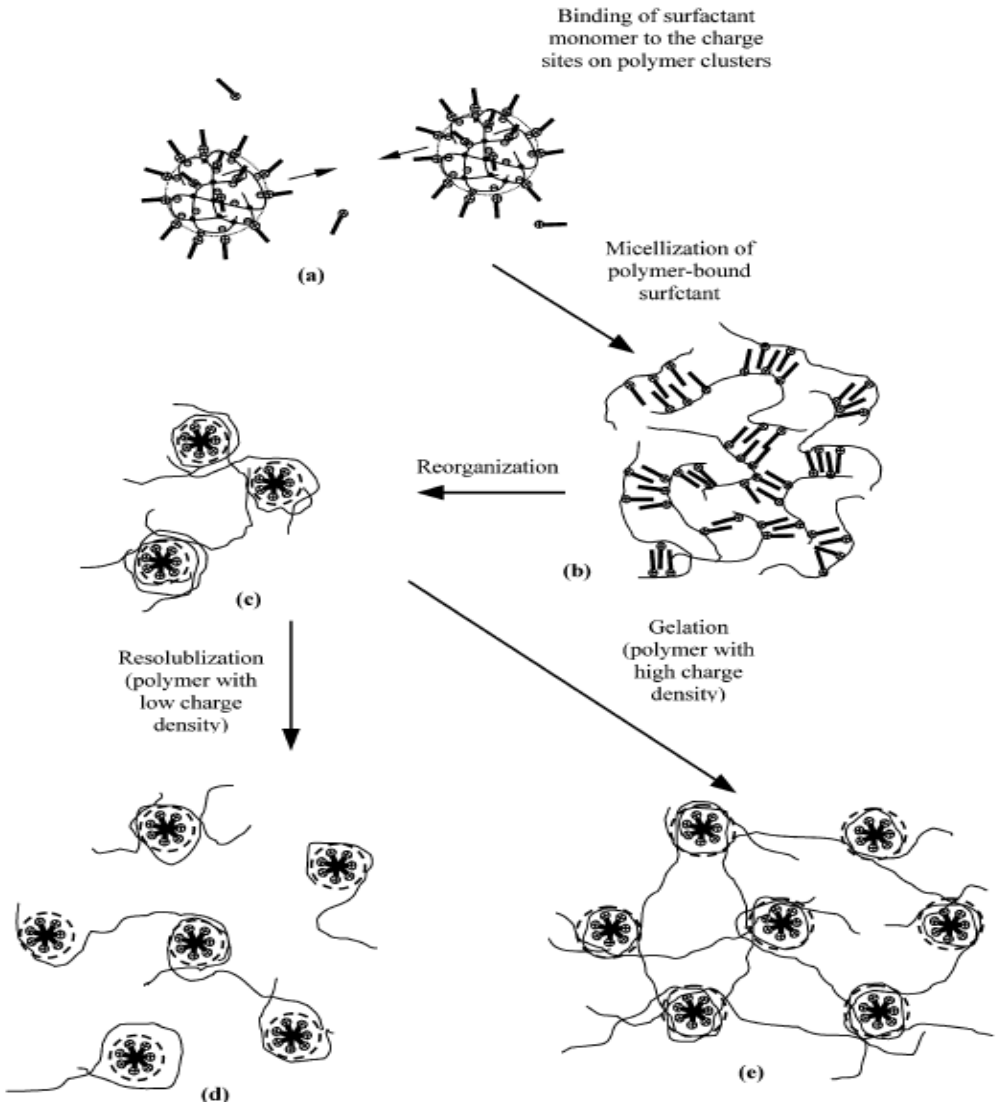


*Figure 49*. Schematic representation of the mechanism of interaction between HASE and DoTab.[60]

## Hydrophobically modified polyelectrolytes

Hydrophobically modified polyelectrolytes (HMP)contain a small fraction of hydrophobic groups either attached to the polyelectrolyte backbone[109,110] (Figure 50a) or as terminal groups[111-113] (Figure 50b).[1,114-116] These hydrophobic groups may be separated from the HMP backbone via a spacer. For example, in HASE (Figure 50a), poly(ethylene oxide) (PEO) acts as a spacer for the hydrophobic substituents (R). The molecular

dimensions of the hydrophobes[117-122] and the length of the spacers[109,123-125] control the aqueous solution rheological properties as well as the microstructure of the HMP aggregates.[123] It seems reasonable to assume that the distribution of the hydrophobes along the chain will also affect the solution the solution rheology and microstructure aggregates.

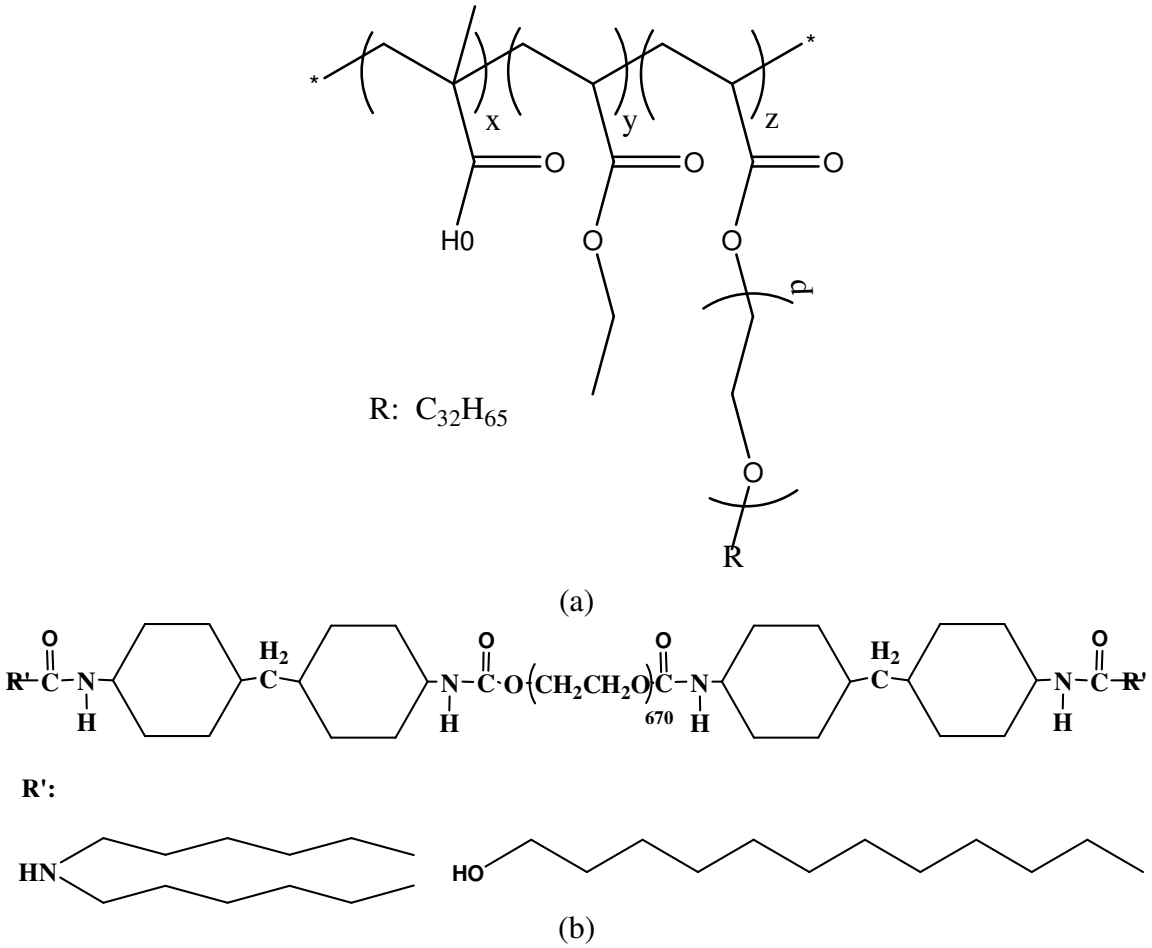


*Figure 50.* (a) Hydrophobic (R) modification of the alkali soluble polymers (HASE) on the backbone[109] (b) Hydrophobic(R') modification of the ethoxylated urethane (HEUR) on the terminal groups.[113]

The hydrophobes present on the polyelectrolyte undergo hydrophobic interactions.[126] These interactions lead to intramolecular and/or intermolecular association of the polymers (Figure 51).[118,127-129] The nature of the association depends on

the concentration of the polyelectrolyte. In the dilute regime, the polymer chains are isolated and therefore, the hydrophobes interact to form intramolecular associations (Figure 51a). Due to these associations, in the dilute regime the viscosity of the hydrophobically modified polyelectrolytes is similar or lower than unmodified polyelectrolyte. In the semi-dilute regime, the polyelectrolyte chains overlap and intermolecular interactions dominate. Hence, the viscosity and the elastic modulus increase considerably with the polymer concentration (Figure 51b). In the concentrated regime, the hydrophobes are engaged in intermolecular interaction and a weaker dependence of viscosity with polymer concentration is observed (Figure 51c).[130]

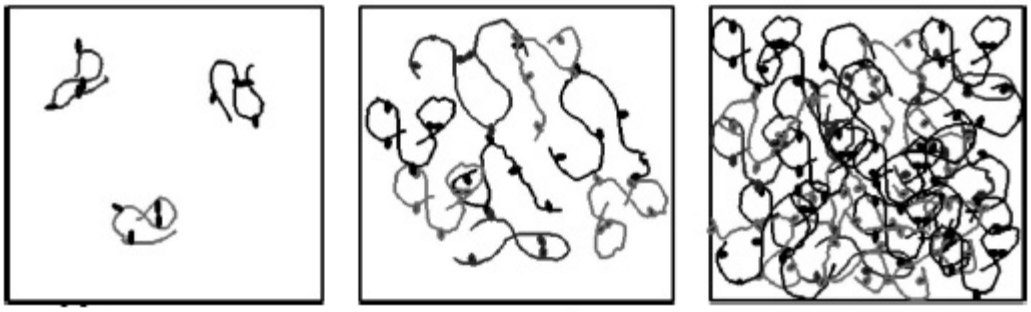

(a) (b) (c)

*Figure 51.* Schematic representation of the concentration regimes: (a) dilute regime (b) intermediate regime (c) concentrated regime.[130]

*The effect of hydrophobe chain length on polymer association:*

The extent of individual hydrophobic association depends on: (1) the chemical potential of the hydrophobe compared to its (aqueous) environment and (2) steric factors. According to Jenkins, the chemical potential of the hydrophobe ($\Delta\mu$) can be calculated by the following Equation:[131]

$$\Delta\mu = 2RT - \frac{V_s + V_p}{2}\left(\delta_s - \delta_p\right)^2\chi^2 \qquad \text{Equation 14}$$

where, R is the universal gas constant; T is the temperature in degrees Kelvin; $V_s$ and $V_p$ are the molar volumes of the solvent (water) and hydrophobe respectively; $\delta_s$ and

$\delta_p$ are the solubility parameters of the solvent (water) and hydrophobe respectively; and x is the volume fraction concentration of hydrophobe. We note that in this case, Hildebrand Solubility parameters are used instead of Hansen-Hoy solubility parameters. This essentially restricts the use of this Equation to non-polar media and certainly not to water. Moreover, only enthalpic factors are considered. In polymer solutions and in self-assmbled associations, the entropic contribution to the chemical potential should be considered. I bear these constraints in mind when evaluating Wang and Tam's contributions[59] to this field of endeavor.

When the chemical potential value becomes more negative, the hydrophobic associations are highly-favored and stable. Therefore, from the Equation 14it can be concluded that a large difference between the molar volumes and the solubility parameters favors the hydrophobic associations. The hydrophobe molar volume increases with alkyl chain length (Figure 52) and the Hildebrand solubility parameter decreases slightly with increase in alkyl chain length. When the chemical potential is zero or positive, aggregation by hydrophobic association is not expected.[131]

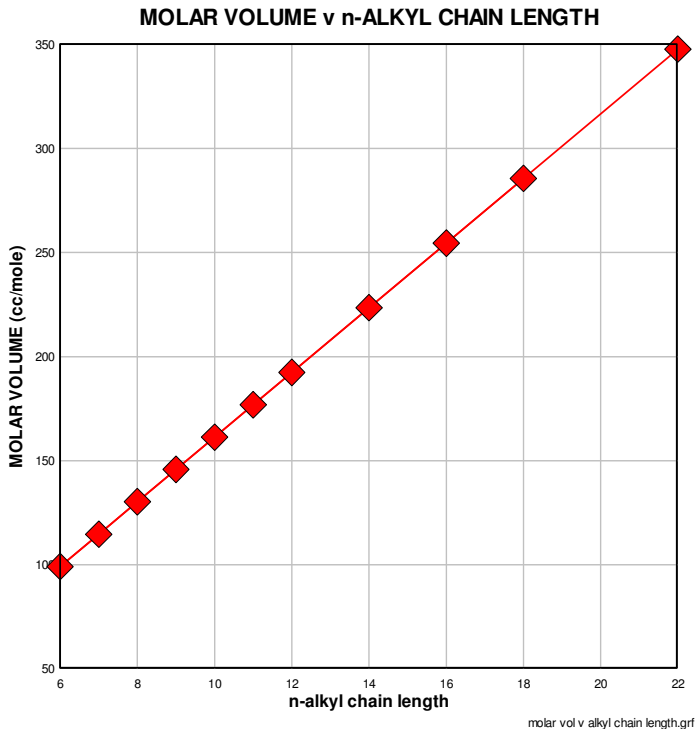


*Figure 52.* Molar volumes of hydrophobes as a function of alkyl chain length.[131]

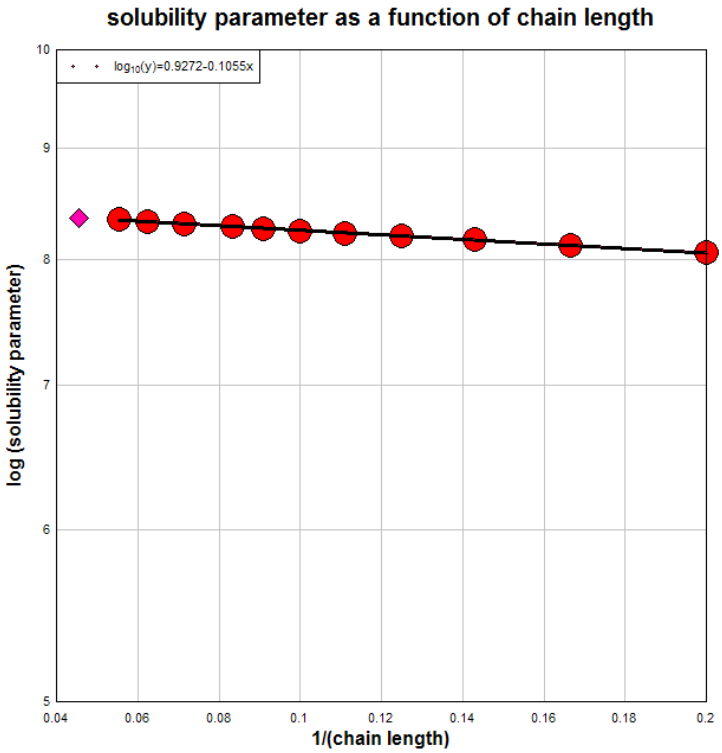


*Figure 53.* Solubility parameter of hydrophobes as a function of alkyl chain length.[131,132]

By substituting the values of molar volume and solubility parameter obtained from the plots above into the Equation $\Delta\mu = 2\mathrm{RT} - \frac{\mathrm{V_s} + \mathrm{V_p}}{2}\left(\delta_s - \delta_p\right)^2 x^2$, the trend of chemical potential with n-alkyl chain length was investigated (Figure 54) according to Wang and Tam. However, it is difficult to calculate the value of $x^2$ due to steric hindrances of the polymer chain preventing association of the hydrophobes. However, for a same class of hydrophobically modified polyelectrolyte value of $x^2$ would not vary significantly. Therefore, based on this assumption and as 2RT term is constant, a plot the value of the term, $\frac{\mathrm{V_s} + \mathrm{V_p}}{2}\left(\delta_s - \delta_p\right)^2$, against n-alkyl chain length. This plot shows a linear upward trend as a function of alkyl chain length.

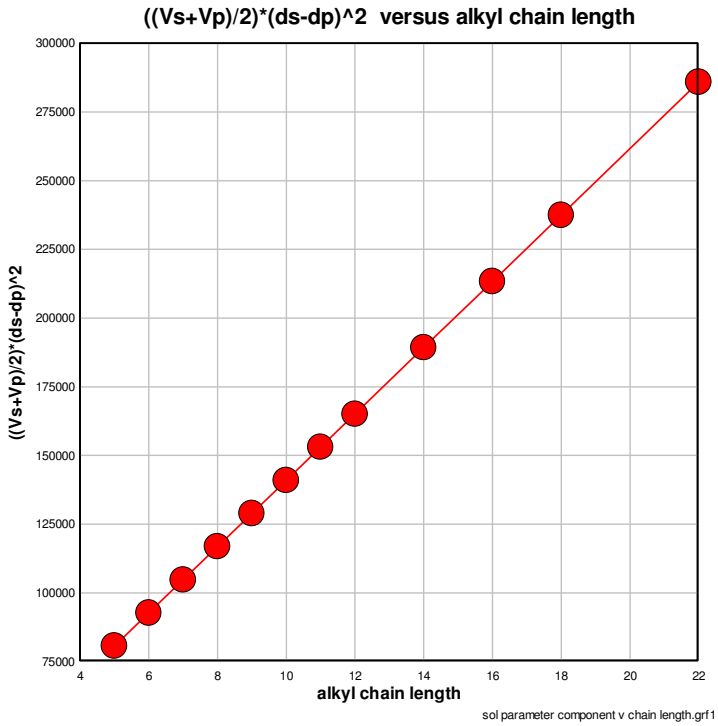


*Figure 54.* $\frac{\mathrm{V_s} + \mathrm{V_p}}{2}\left(\delta_s - \delta_p\right)^2$ of hydrophobes as a function of alkyl chain length.[131]

The length of the hydrophobes also affects the modulus of the polymer solution. Increase in the length of the hydrophobes increases the elastic modulus (G') and causes it to surpass the loss modulus (G"). The HASE shows power law relationship of the form $G' \sim c^n$ (Figure 55). The power law exponent 'n' increases with the hydrophobe size.

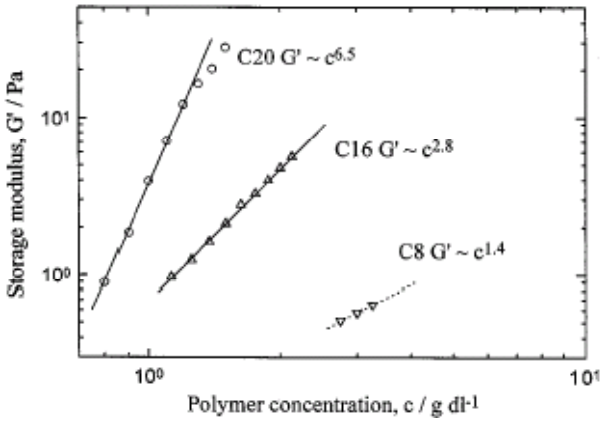


*Figure 55.* Storage modulus of HASE at 1 rad/s as a function of polymer concentration for different *n*-alkyl modified HASE polymers.[131]

*The effect of spacer group length on polymer association*

Jenkins and coworkers probed the effect of the poly(ethylene oxide) spacer chain length on hydrophobically modified alkali-soluble emulsion polymer (HASE) by rheological measurements (Figure 56 a) and dynamic light scattering techniques (Figure 56b).[124] With zero spacer length, the HASE chains associate through the blocky polymeric backbones. At this spacer length, the hydrophobic modification only slightly strengthens the backbone association. As spacer chain length is increased to 5 or 10 ethylene oxide units, the viscosity and apparent size of the aggregation decreased. Jenkins suggested that these changes were manifested by hydrophobes undergoing intramolecular association instead of intermolecular association at such short spacer lengths. However, the viscosity and apparent size significantly increased for PEO length of between 15 and

32 ethylene oxide units. At this spacer length, the hydrophobes are a sufficient distance from the backbone to form intermolecular associations and therefore, HASE forms a network. On the other hand, the viscosity and apparent size decreased as the PEO spacer chain lengthsurpassed32 ethylene oxide units. Jenkins suggested that this decrease was due to structural reorganization of the aggregates and it makes sense that poly(ethylene oxide) changes the hydrophilic/lipophilic balance to favor hydrophilicity (Figure 57).

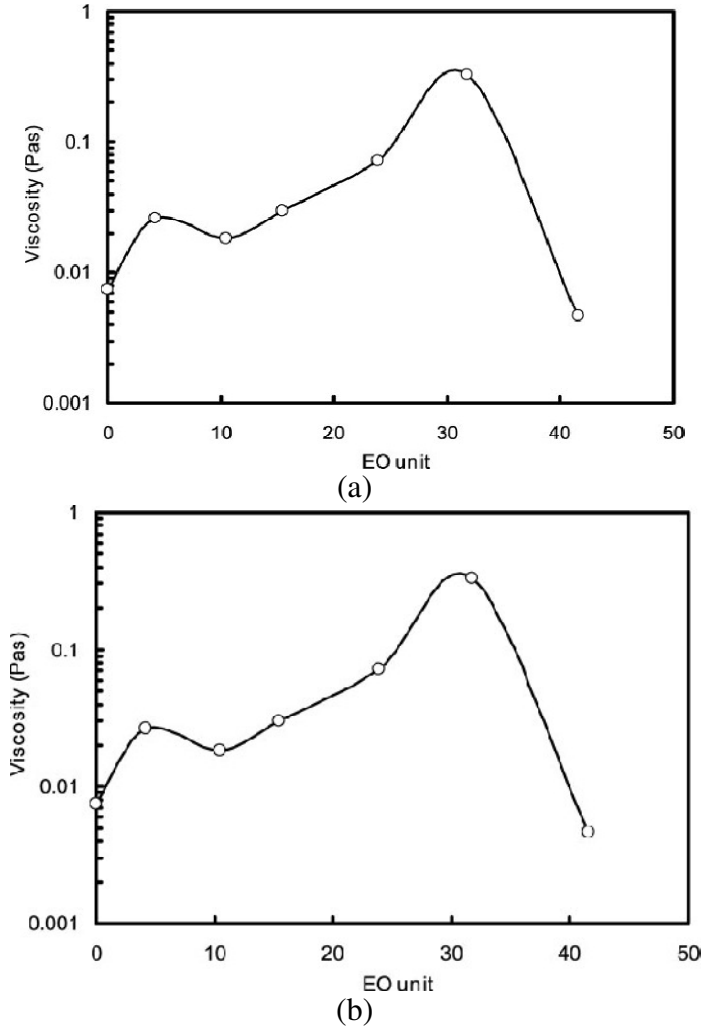


*Figure 56.* (a) Zero shear viscosity (b) diffusion coefficients (open circles) and apparent hydrodynamic radii (filled circles) of 1 wt % of HASE as a function of degree of ethoxylation, at pH 9.[124]

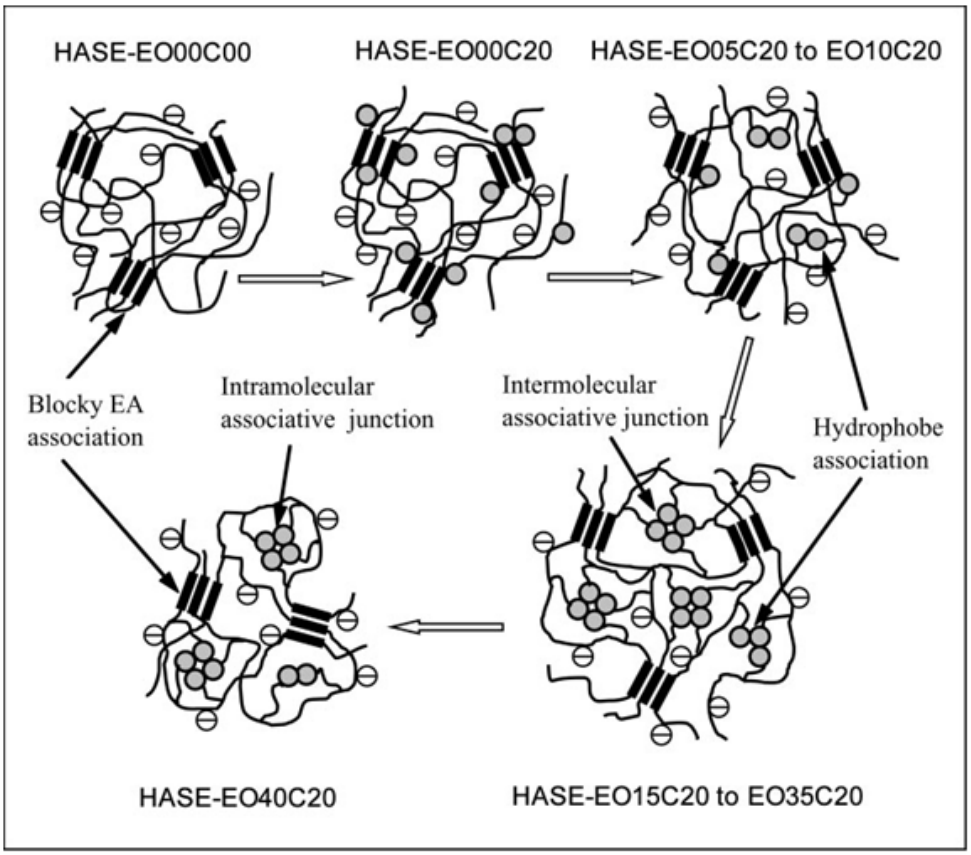


*Figure 57*. Schematic representation of the association mechanisms of HASE in semidilute region. The length of the hydrophobes is fixed, whereas, lengths of PEO spacer chains varies on the HASE.[124]

## Hydrophobically modified polyelectrolyte-Surfactant Interactions

Hydrophobically modified polyelectrolytes (HMP) undergo co-micellization in the presence of the surfactant molecules. This co-micellization is strongly driven by the hydrophobic interactions between the polymers' alkyl groups and the surfactant tail groups. These interactions can overwhelm the electrostatic repulsion in similarly charged polyelectrolyte/surfactant systems. Therefore, the overall interaction depends on the degree of modification,[133-135] length,[133-137] and branching[113,138] of the hydrophobic alkyl group on the HMP. Other than the alkyl groups, the nature and extent of interaction is also affected by the degree ionization[79] of the HMP backbone as well as on the length of

the surfactant tail group,[139-141] the charge[77-79,116,133] and the size[74] of the surfactant head group. Physically, the HMP/surfactant systems have shown a pronounced increase in viscosity by several orders of magnitude in presence of surfactants in the vicinity of the CMC. This behavior is the opposite to that observed for polyelectrolytes that have not been hydrophobically modified.[77,142] The hydrophobic interactions between chains lead to extended network structures that render HMP useful as emulsion stabilizers and rheology modifiers in coatings formulations. They have also found applications in food industry as gelling agents, pharmaceutical industry as drug delivery system, cosmetics as thickening agents and heavy duty liquid detergents as stain remover.[17,143,144] Owing to these wide ranges of applications, the understanding of the interaction mechanism between the HMP and surfactant systems has been important. Therefore, the interaction mechanism of the HMP with neutrally,[73,74,77] similarly[78] and oppositely[79,145] charged surfactants have been explored.

The interaction between HMP and a neutral surfactant was reported by Iliopoulos[145] and Somasundaran.[79] Iliopoulos used hydrophobically modified anionic poly(sodium acrylate) (HMPA) with a degree of hydrophobic substitution of 3 mole % and with 12 carbon atoms in the alkyl chain. On the other hand, Somasundaran[79] used anionic poly(maleic acid/octyl vinyl ether) (PMAOVE) with a high degree of substitution (50 mole %) and with 8 carbon atoms in the alkyl chain. Therefore, it is interesting to compare both of these systems with different hydrophobic characters.

In Iliopoulos's work,[145] HMPA (Figure 58) was interacted with nonionic surfactants- oligoethylene glycol monododecyl ether ($C_{12}E_n$, with $n$ = 4, 5, and 8) (Figure 59) and was characterized using viscosity measurements.[74] HMPA polymer was

synthesized by randomly attaching alkyl chains to poly(sodium acrylate). They designated this polymer as 3C12, where, the numerical number on the left side of 'C' denoted the degree of substitution is mole percent, while the number on the right side denoted the number of carbon atoms of the alkyl groups.

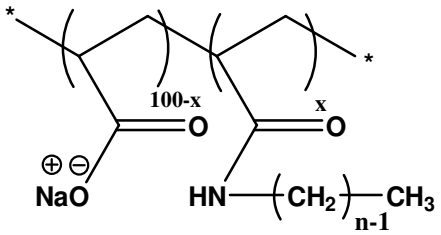


*Figure 58.* Chemical structure of hydrophobically modified anionic poly(sodium acrylate) (HMPA) (x = 3 and n = 12).

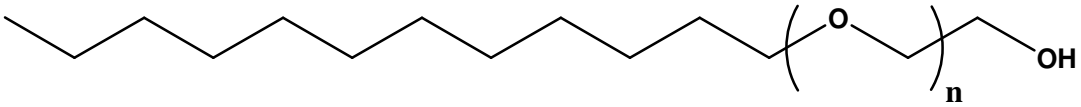


*Figure 59.* Chemical structure of oligoethylene glycol monododecyl ether surfactants ($C_{12}E_n$, with n = 4, 5, and 8).

From viscosity ($\eta$) measurements, they concluded that the viscosity of the system significantly increased with increase in the hydrophobic character of the nonionic surfactant (Figure 60). Here, the viscosity of the HMPA/$C_{12}E_8$ system showed a slight increase, whereas, the viscosity of the HMPA/$C_{12}E_5$ and HMPA/$C_{12}E_4$ system showed pronounced increase in the order: $\eta_{HMPA/C_{12}E_5} < \eta_{HMPA/C_{12}E_4}$.

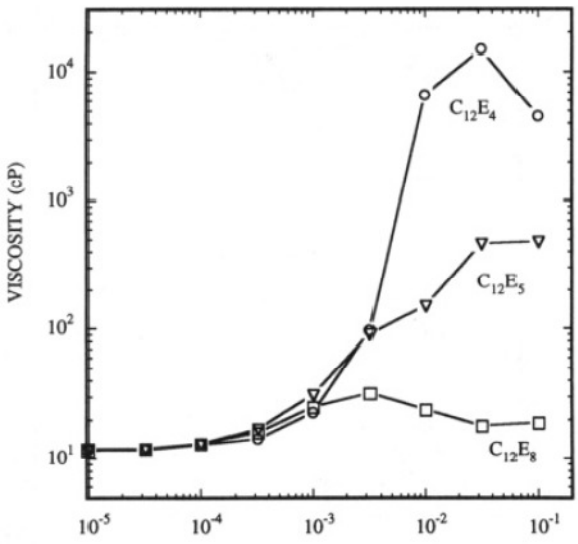


*Figure 60.* Effect of viscosity on the hydrophobically modified anionic poly(sodium acrylate) (3C12) and nonionic surfactant ($C_{12}E_n$, with n = 4,5, and 8) solutions as a function of surfactant concentration.[145]

Iliopoulos also verified the role of micellar growth of the nonionic surfactant in the viscosity increment by measuring the viscosity of the unmodified anionic poly(sodium acrylate) (PA) and nonionic surfactants ($C_{12}E_n$) system as a function of $C_{12}E_n$concentration (Figure 61). This system was selected as the nonionic surfactants do not interact with PA. Therefore, any increase in the viscosity of the system can solely be due to the micellar growth. In the PA/$C_{12}E_8$ system, a small increase in the viscosity was observed around $10^{-1}$ mole/L. However, in PA/$C_{12}E_5$ system, a considerable increase the viscosity of the system was observed above $10^{-2}$ mole/L. Based on these observations, they concluded that micellar growth affects the viscosity of the system.

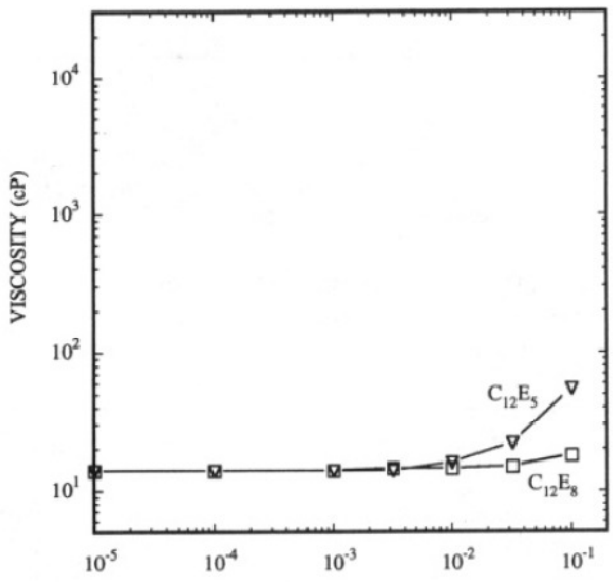


*Figure 61.* Effect of viscosity on the unmodified anionic poly(sodium acrylate) and nonionic surfactant ($C_{12}E_n$, with n = 5, and 8) solutions as a function of surfactant concentration.[145]

In absence of the nonionic surfactant, the viscosity of the HMPA (Figure 60) and PA (Figure 61) system was lower. However, by examining Ilioupolis' published results[145], and, thereby, comparing the viscosities reported of HMPA and PA at $10^{-5}$ mole/L of surfactant, we found that the viscosity of HMPA was slightly lower than PA. As the surfactant concentration is very low, this may be due to intra-molecular association of the HMPA chains which results in collapse of the chain. With addition of the surfactant, the viscosity of the HMPA/$C_{12}E_n$ system increased by few orders of magnitude than the PA/$C_{12}E_n$ system. Moreover, in case of HMPA/$C_{12}E_5$ system, the maximum viscosity was achieved in the same surfactant concentration region (above $10^{-2}$ mole/L) where $C_{12}E_5$ micelle growth was detected. Therefore, Iliopoulos and coworkers postulated that the viscosity increment was due to formation of HMPA/$C_{12}E_n$ network via mixed micelle (Figure 62B). These mixed micelles consisted of alkyl groups from different HMPA polymer chains and nonionic surfactants micelle forming a network. In

the HMPA/$C_{12}E_8$ system, at higher $C_{12}E_8$ concentration ($10^{-1}$ mole/L) the viscosity of decreased. Therefore, they suggested that the network disintegrated and the mixed micelles consisted of alkyl chains from an individual HMPA polymer chain and nonionic surfactant micelle.[145]

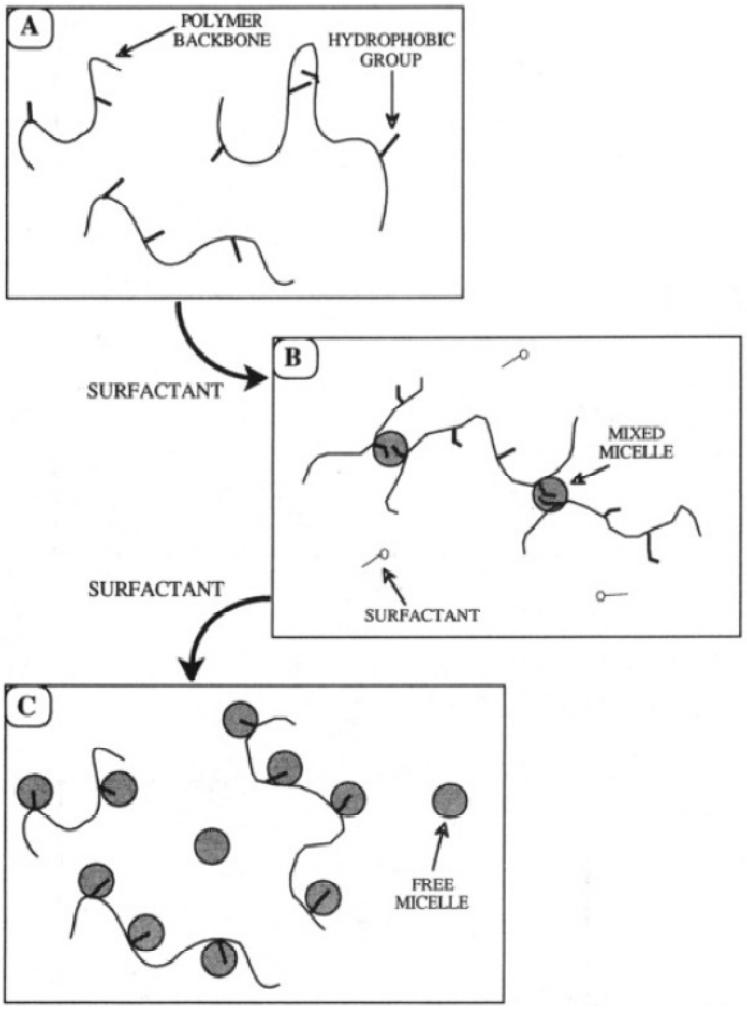


*Figure 62.* Interaction mechanism between the HMPA and $C_{12}E_n$ system as a function of $C_{12}E_n$ concentration.[145]

In Somasundaran's work,[79] PMAOVE (Figure 63a) was interacted with nonionic surfactant - penta-ethyleneglycol mono *n*-dodecylether ($C_{12}E_5$) (Figure 63b). This interaction was characterized by surface tension, viscosity, electron paramagnetic resonance (EPR) spectroscopy, light scattering, and fluorescence spectroscopic

techniques.[77] PMAOVE was an alternating polymer, synthesized by free-radical polymerization of a 1:1 moleratio of maleic anhydride and octyl vinyl ether.

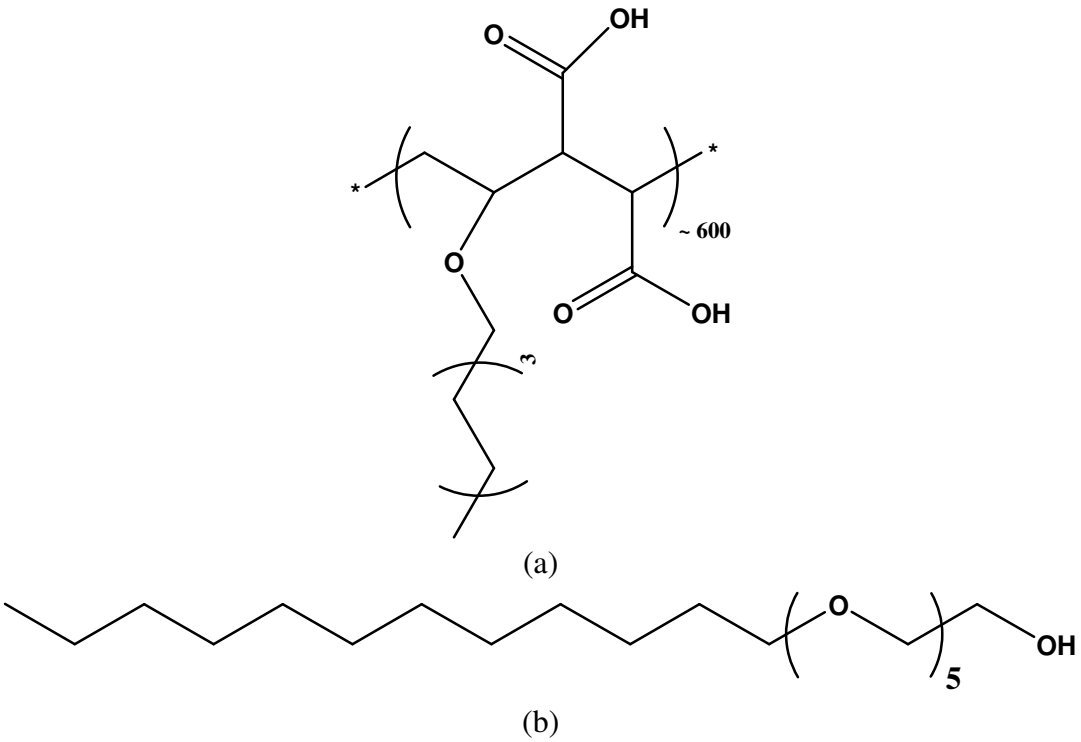


*Figure 63.* Chemical structure of (a) poly(maleic acid/octyl vinyl ether) (PMAOVE) (b) penta-ethyleneglycol mono n-dodecylether ($C_{12}E_5$).

From the surface tension measurements, the critical micelle concentration of $C_{12}EO_5$ was found to be 0.06 mM (Figure 64b). In the PMAOVE/$C_{12}EO_5$ system, the surface tension increased in the 0.0075 mM < [$C_{12}EO_5$] < 0.075 mM zone, due to decreased in the PMAOVE and $C_{12}EO_5$ concentration at the surface (Figure 64a). According to Somasundaran, this occurred due to adsorption of the $C_{12}EO_5$ molecules in the PMAOVE hydrophobic domains. Further increase in the surfactant, reduced the surface tension due to adsorption of $C_{12}EO_5$ molecules at the surface. Finally, above 1 mM of $C_{12}EO_5$, free $C_{12}EO_5$ micelles were formed in the PMAOVE/$C_{12}EO_5$ system. The relative viscosity of the $C_{12}EO_5$ system increased beyond 0.06 mM of $C_{12}EO_5$ due to

formation of the micelles (Figure 65). In the PMAOVE/$C_{12}EO_5$ system, the relative viscosity increased above 0.01 mM of $C_{12}EO_5$. Similar to the surface tension study, Somasundaran[79] suggested that the increase was due to continuous adsorption of $C_{12}EO_5$ on the PMAOVE hydrophobic domain, thereby, increasing the size of the domain.

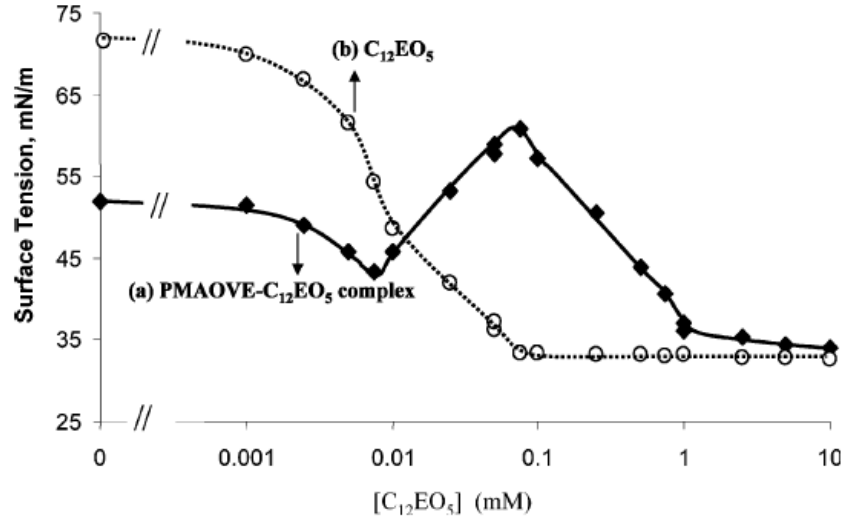


*Figure 64.* Surface tension curves of (a) 0.1 wt. % PMAOVE/$C_{12}EO_5$ system and (b) $C_{12}EO_5$ system as a function of $C_{12}EO_5$.[79]

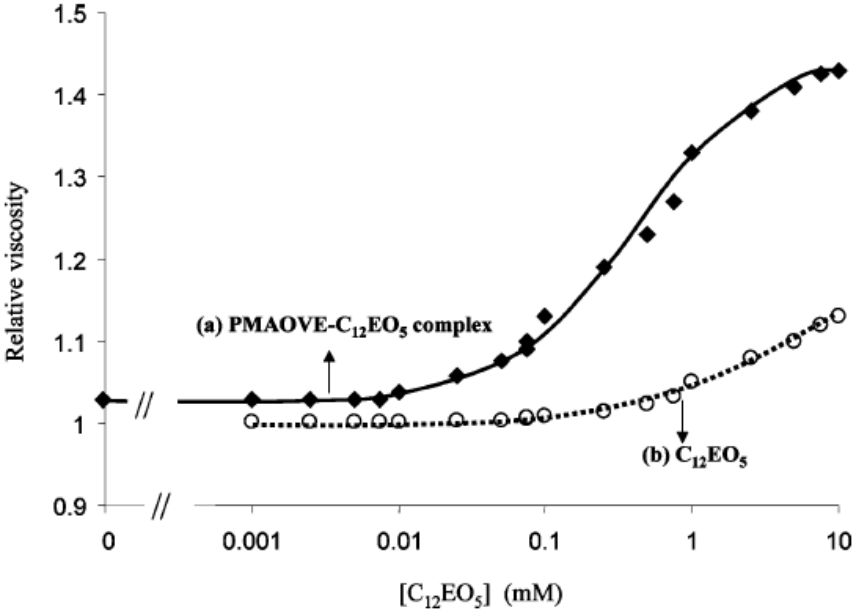


*Figure 65.* Relative viscosity of (a) 0.1 wt. % PMAOVE/$C_{12}EO_5$ system and (b) $C_{12}EO_5$ system as a function of $C_{12}EO_5$.[79]

The molecular level interactions between PMAOVE and $C_{12}EO_5$ were studied by EPR which measured the rotational correlation time (Figure 66) and the hyperfine splitting constant (Figure 67) of 5-doxyl stearic acid spin probe. The former parameter measured the microviscosity, while the latter parameter measured the micropolarity of the PMAOVE and $C_{12}EO_5$ system.

In presence of PMAOVE alone, the spin probe exhibits low rotational mobility and a less polar environment than the $C_{12}EO_5$ micelles. This suggests that the hydrophobes on the PMAOVE form a tighter hydrophobic domain (Figure 70). Above 0.01 mM of $C_{12}EO_5$, the microviscosity decreased, while, the polarity increased. Therefore, Somasundaran concluded that the $C_{12}EO_5$ molecules get incorporated in the hydrophobic domain. As a result, the PMAOVE chains became more hydrophilic, thereby, increasing the surface tension. With further addition of $C_{12}EO_5$, more $C_{12}EO_5$ molecules get absorbed in the hydrophobic domain. However, above 1 mM of $C_{12}EO_5$, the PMAOVE chains get saturated with the $C_{12}EO_5$ molecules and thereafter; free $C_{12}EO_5$ micelles exists in the system as the polarity of the PMAOVE/$C_{12}EO_5$ system is close to $C_{12}EO_5$ system. The EPR polarity measurements were also confirmed by fluorescence spectroscopy with a pyrene probe (Figure 68).

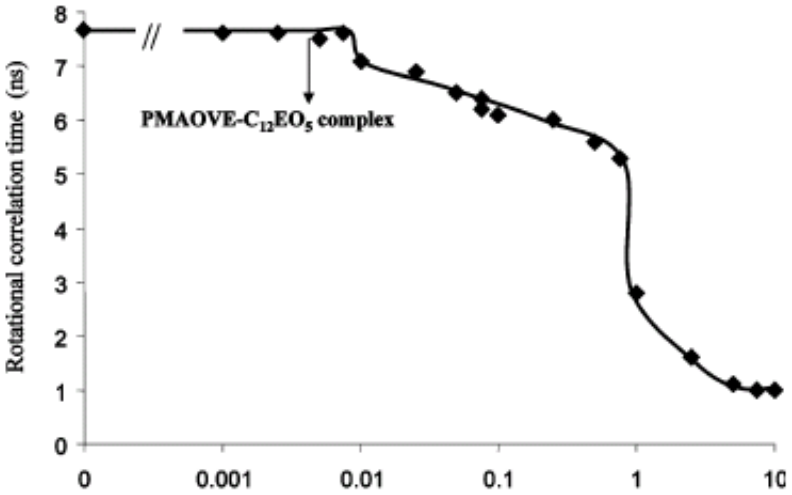


*Figure 66.* Rotational correlation time of the 5-doxyl stearic acid (0.1mM) in (a) 0.1 wt. % PMAOVE/$C_{12}EO_5$ system and (b) $C_{12}EO_5$ system as a function of $C_{12}EO_5$.[79]

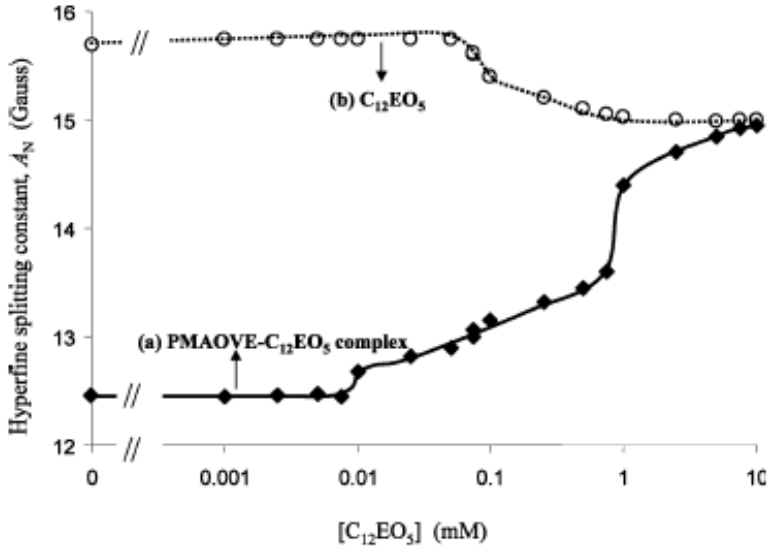


*Figure 67.* Hyperfine splitting constant ($A_N$) of 5-doxyl stearic acid (0.1 mM) in (a) 0.1 wt. % PMAOVE/$C_{12}EO_5$ system and (b) $C_{12}EO_5$ system as a function of $C_{12}EO_5$.[79]

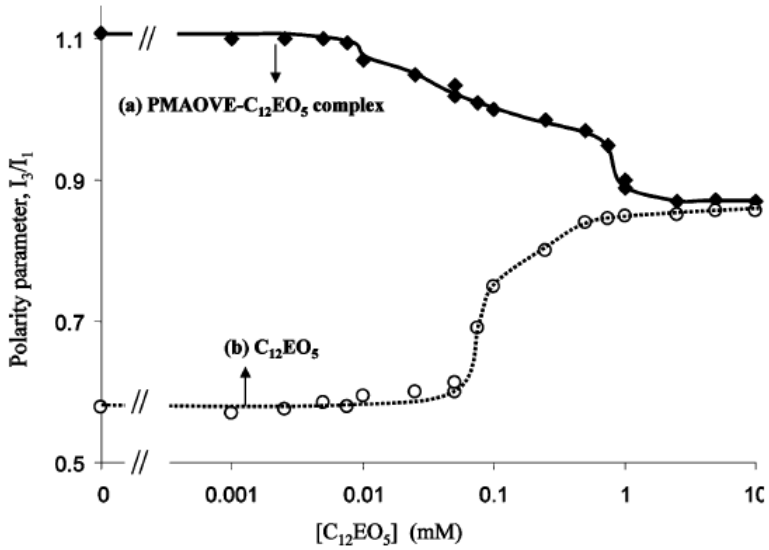


*Figure 68.* Intensity ratio of (a) 0.1 wt. % PMAOVE/$C_{12}EO_5$ system and (b) $C_{12}EO_5$ system as a function of $C_{12}EO_5$.[79]

The hydrodynamic diameter of the PMAOVE/$C_{12}EO_5$ complex increased in the 0.01 mM < $[C_{12}EO_5]$ < 1 mM zone. The change in the size was situated in the same $C_{12}EO_5$concentration region as observed by the other techniques.

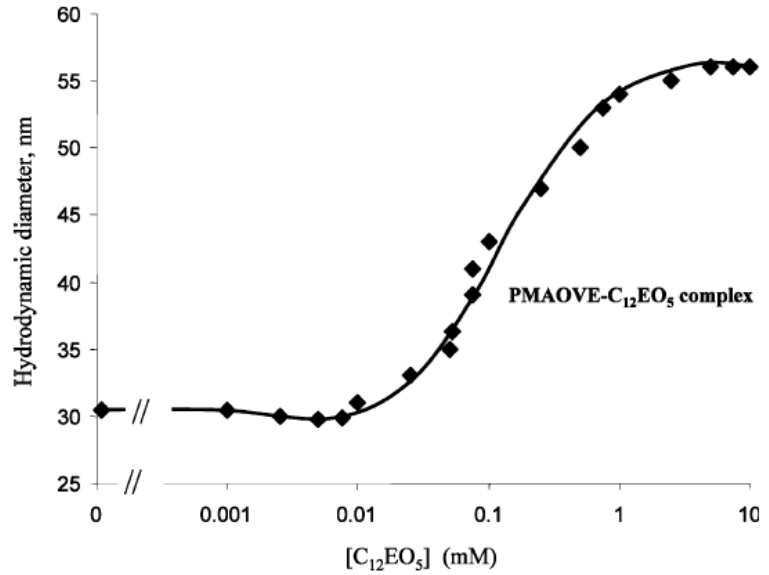


*Figure 69.* Hydrodynamic radius of the 0.1 wt % PMAOVE/$C_{12}EO_5$ system as a function of $C_{12}EO_5$.[79]

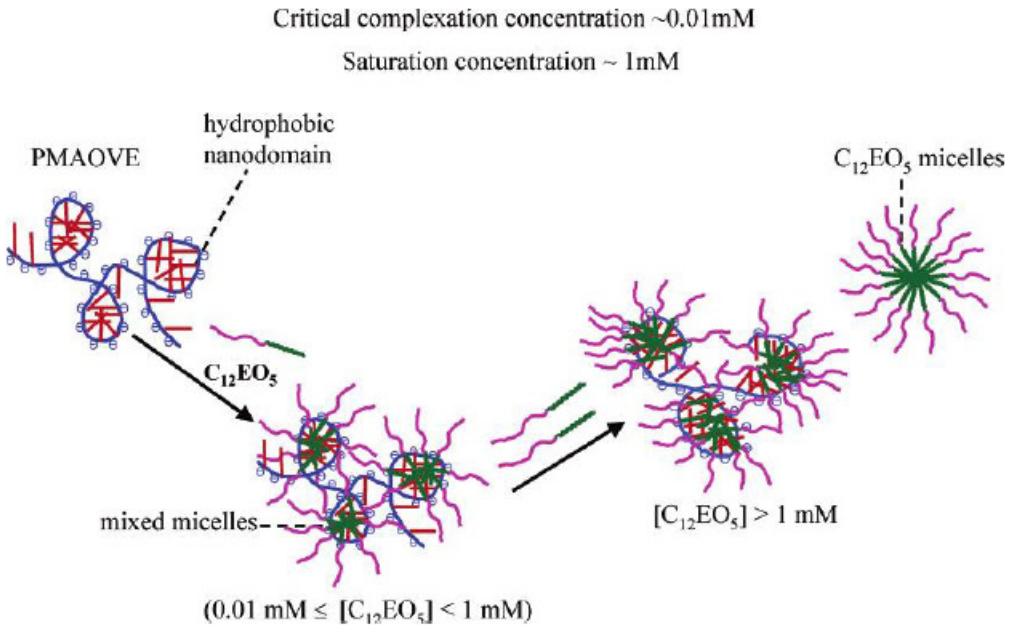


*Figure 70.* Schematic representation of the interaction mechanism between PMAOVE and $C_{12}EO_5$.[79]

Iliopoulos and coworkers reported the mechanism of interaction between hydrophobically modified anionic poly(sodium acrylate) (HMPA) and cationic dodecyltrimethylammonium chloride (DTAC) surfactant in one phase, using rheological and fluorescence analysis.[145] HMPA polymers were synthesized by randomly attaching alkyl chains with different chain lengths and degree of modification to poly(sodium acrylate). These polymers were designated as 1C12, 3C12 and 1C18, where the numerical number on the left side of 'C' denoted the mole percent degree of substitution, while the number on the right side denoted the number of carbon atoms of the alkyl groups.

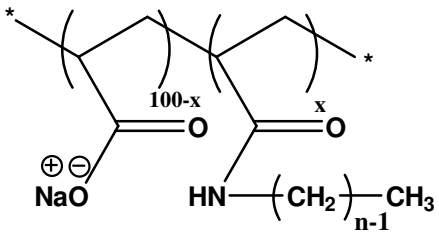


*Figure 71.* Chemical structure of hydrophobically modified anionic poly(sodium acrylate) (HMPA) (x = 1 or 3 and n = 12 or 18).

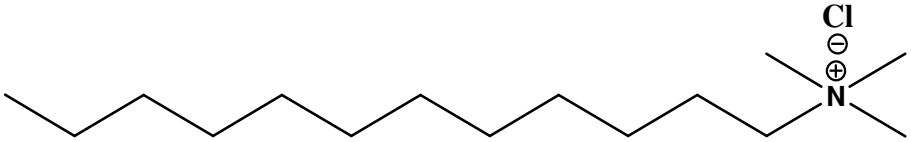


*Figure 72.* Chemical structure of dodecyltrimethylammonium chloride (DTAC).

Figure 73 shows the viscosity of the PA polymer and HMPA polymers as a function of DTAC in one phase. In the absence of the DTAC, the viscosities of the HMPA polymers and the PA polymer were comparable (Figure 76a). The viscosity of the PA polymers almost remained constant with increase in the DTAC concentration. However, the viscosity of the HMPA polymers showed a pronounced increase, followed by a decrease just before the phase separation. For the HMPA polymers, the viscosity increased with increase in the degree of modification and the length of the alkyl chain.

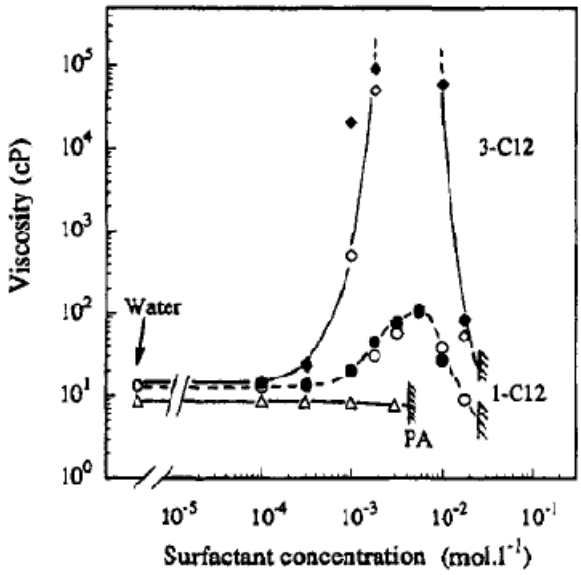


*Figure 73.* Viscosity of the 1% aqueous solution of PA polymer and HMPA polymers as a function of DTAC concentration. The hatch symbol represents phase separation.[145]

The fluorescence intensity ratio (I1/I3) of pyrene in DTAC/0.1 M NaCl solution with and without 1% PA polymer and HMPA polymers in water as a function of DTAC concentration was obtained from steady-state fluorescence spectroscopy (Figure 74). On addition of the DTAC molecules, the cac of the HMPA polymers was found to be lower than the PA polymer and within the HMPA polymers, the cac decreased with increase in the hydrophobic modification or chain length of the alkyl group. As the cac was dependent on the hydrophobic modification, Iliopoupos et al. suggested that the DTAC molecules favored binding near the hydrophobic alkyl chains of the HMPA polymers and formed hydrophobic domains. The favored binding also resulted in the phase separation of the HMPA polymers, and this occurred at higher DTAC concentration than it did in the presence of an equivalent concentration of the PA polymer (Figure 73). Iliopoupos et al. concluded that the hydrophobic domains were hydrophobically associated with other domains formed on other chains to form a HMPA cross-linked network (Figure 76b).[145]

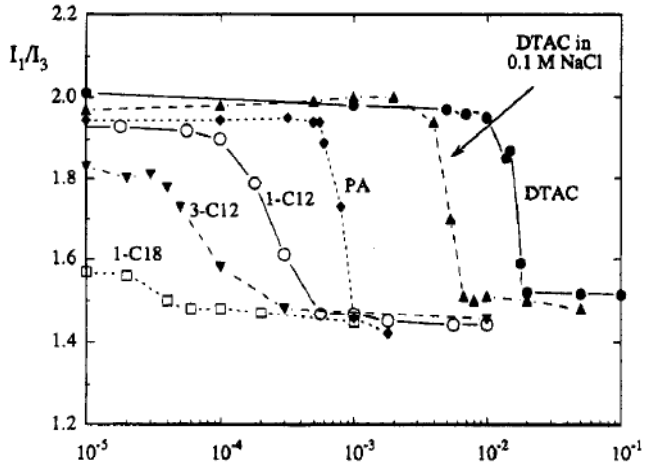


*Figure 74.* Intensity ratio as a function of DTAC concentration for pure DTAC in water and 0.1 M NaCl, and 1% PA polymer and HMPA polymers in water.[145]

The DTAC aggregation number and the number of alkyl groups in the micelle were calculated for the HMPA polymers at different DTAC concentrations using the fluorescence quenching technique. In this technique, pyrene and dodecylpyridinium chloride (DPC) were used as fluorescence probe and quencher, respectively. At different DTAC concentrations, the variation in the aggregation number for the HMPA polymers/DTAC system was small, whereas the number of alkyl groups in the micelle showed a noticeable difference. Figure 75 shows the relation between the number of alkyl groups in the micelle ($N_a$) and the viscosity of the HMPA polymers/DTAC as a function DTAC concentration. The number of alkyl groups in the micelle increased as the viscosity increased, while the number of alkyl groups in the micelle decreased as the viscosity decreased. Also, the $N_a$ at maximum viscosity is about 2 times the $N_a$ at viscosity before the phase separation.

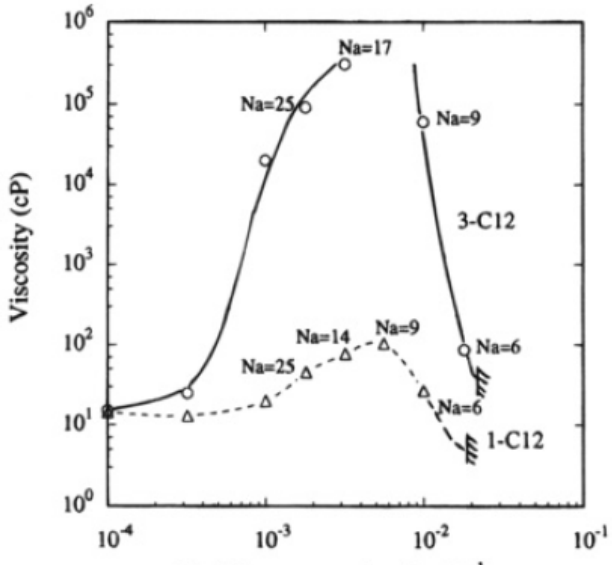


*Figure 75.* Relationship between the number of alkyl groups in the micelle ($N_a$) and the viscosity of the HMPA polymers/DTAC as a function DTAC concentration.[145]

Iliopoulos et al suggested that the low viscosity values just before the phase separation indicate that the HMPA polymer chains are no longer networked.[145] Therefore, the $N_a$ involved in the aggregate formation belongs to one polymer hydrophobic group. This is characterized by intrachain aggregates (Figure 76d). At maximum viscosity, the $N_a$ is about twice the $N_a$ at lowest viscosity at the point of phase separation. Hence, at this stage, the intrachain aggregates would initially be merged together to form interchain aggregates (Figure 76c). The formed aggregates induce crosslinking in between the chain, thereby increasing the viscosity in this region. The interaction mechanism proposed by Iliopoulos and coworkers has revealed the organizational behavior between the hydrophobically modified polyelectrolytes and the surfactant molecules, which causes increase in the viscosity.

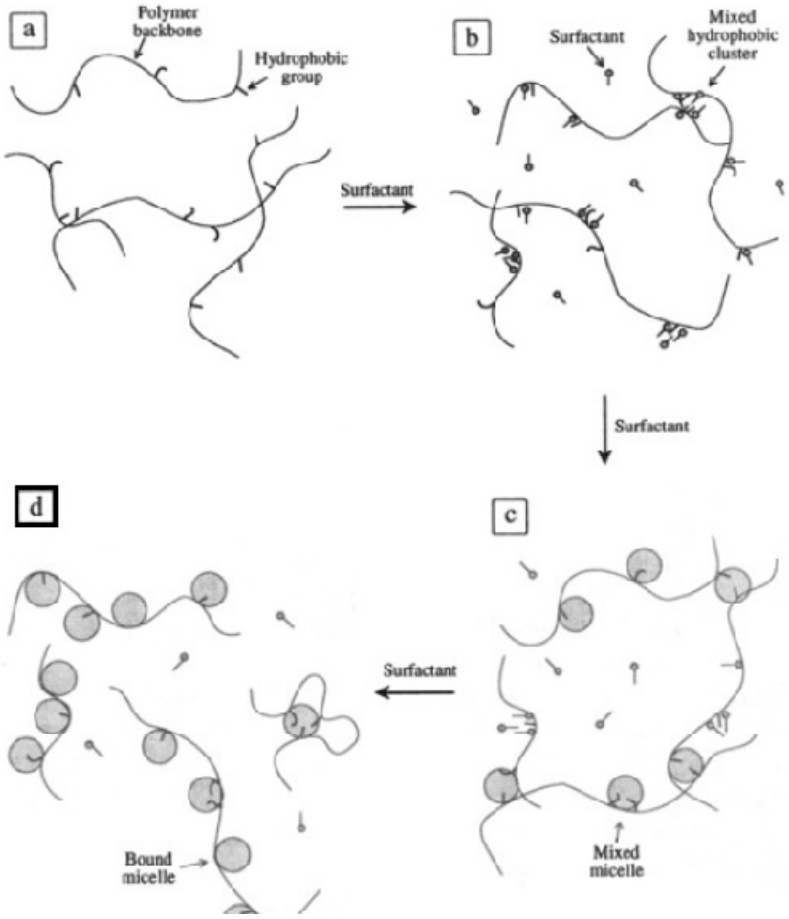


*Figure 76.* The interaction mechanism between HMPA and DTAB according to Iliopoulos and coworkers[145]: (a) HMPA solution (b) HPMA solution with DTAB (C < cac) (c) HPMA solution with DTAB (C > cac) (d) HPMA solution with higher DTAB concentration.

Effect of polyelectrolyte properties on the interaction

*Molecular Weight*

*Surface Absorption:* The molecular weight of the polymer affects the adsorption behavior of the polymer-surfactant complex at the interface. In the linear poly(ethyleneimine) (LPEI)/SDS system, with increase in the polymer molecular weight, the adsorption changed from monolayer to multilayer.[146] However, at higher polymer molecular weight, the adsorption again changed to monolayer from multilayer. This

behavior was also found to be strongly dependent on the pH of the system. At a low pH, LPEI is highly charged, whereas, at a high pH it is a neutral polymer. Penfold and coworkers studied this molecular weight dependence using surface tension and neutron reflectivity.

Figure 77 shows surface tension curves for the LPEI/SDS system at different molecular weight and pH. The LPEI molecular weight of 320, 640 and 2000 Da are represented as $LPEI_6$, $LPEI_{12}$ and $LPEI_{40}$. For all molecular weight and pH 3 and 7, the surface tension decreased due to co-adsorption of the PEI/SDS complexes at the interface, at low SDS concentration. However, for $LPEI_6$/SDS system and pH 10, the surface tension curve is similar to the surface tension curve of SDS. This indicated low interaction between LPEI and SDS as LPEI is neutral at pH 10. However, with increase in the molecular weight, the surface tension became similar to that of SDS. This suggested increase in the LPEI/SDS interaction at pH 10. This increase in the interaction was also confirmed as the system turned cloudy with increase in the molecular weight. At pH 3, the surface tension showed increase in the surface tension with increase in the molecular weight.

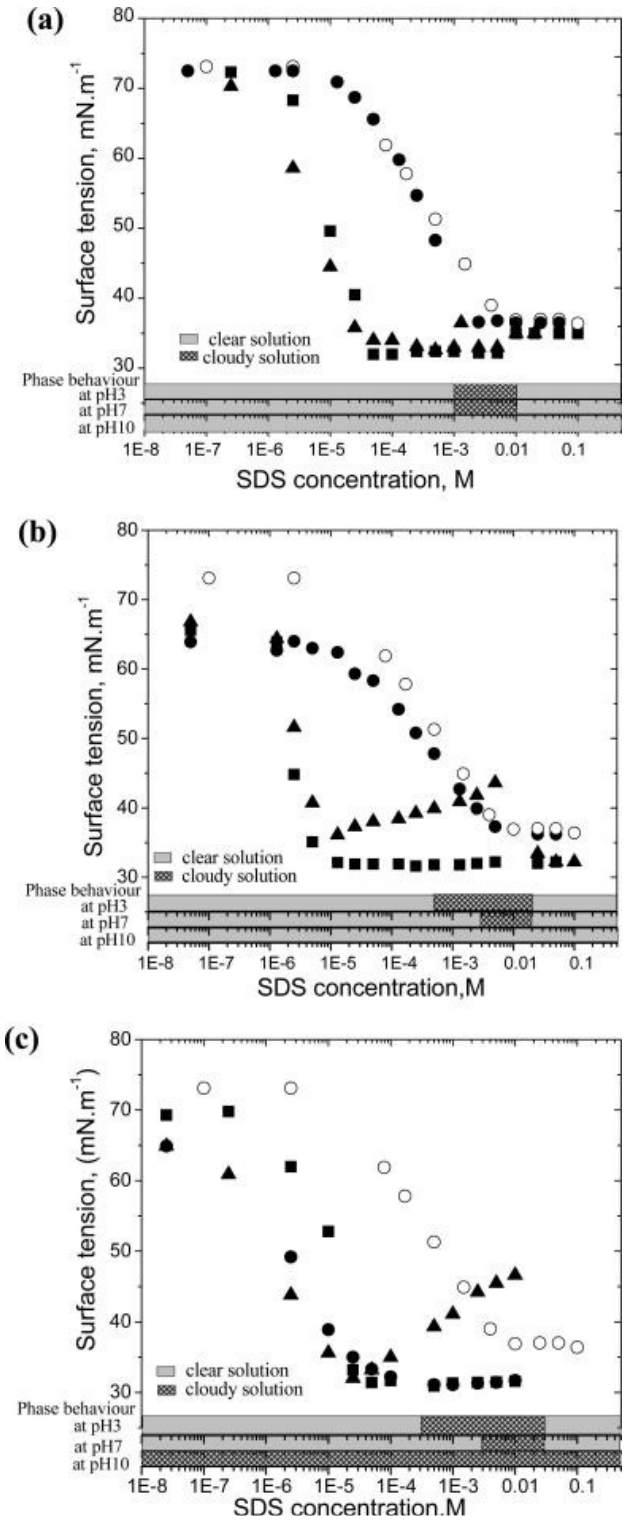


*Figure 77.* Surface tension and phase behavior of the (a) $LPEI_6$/SDS (b) $LPEI_{12}$/SDS and (c) $LPEI_{40}$/SDS system at different molecular weight and pH.[146]

Neutron scattering measurements were performed to measure the thickness of the absorbed layer at the interface. When the absorbed layer was thin (~ 20 Å), the layer was considered as monolayer as this thickness is close to $C_{12}$ alkyl chain of the surfactant. Therefore, it represented monolayer adsorption of surfactant on the polymer chain. Whereas, if the absorbed layer was thick (~35 to 39 Å), multilayers of LPEI and SDS were inferred. It was found that depending on the molecular weight and pH of the system, the absorbed layer showed mono to multi-layer formation. Findings for $LPEI_6$ and $LPEI_{12}$ are summarized in the surface phase diagram (Figure 78).

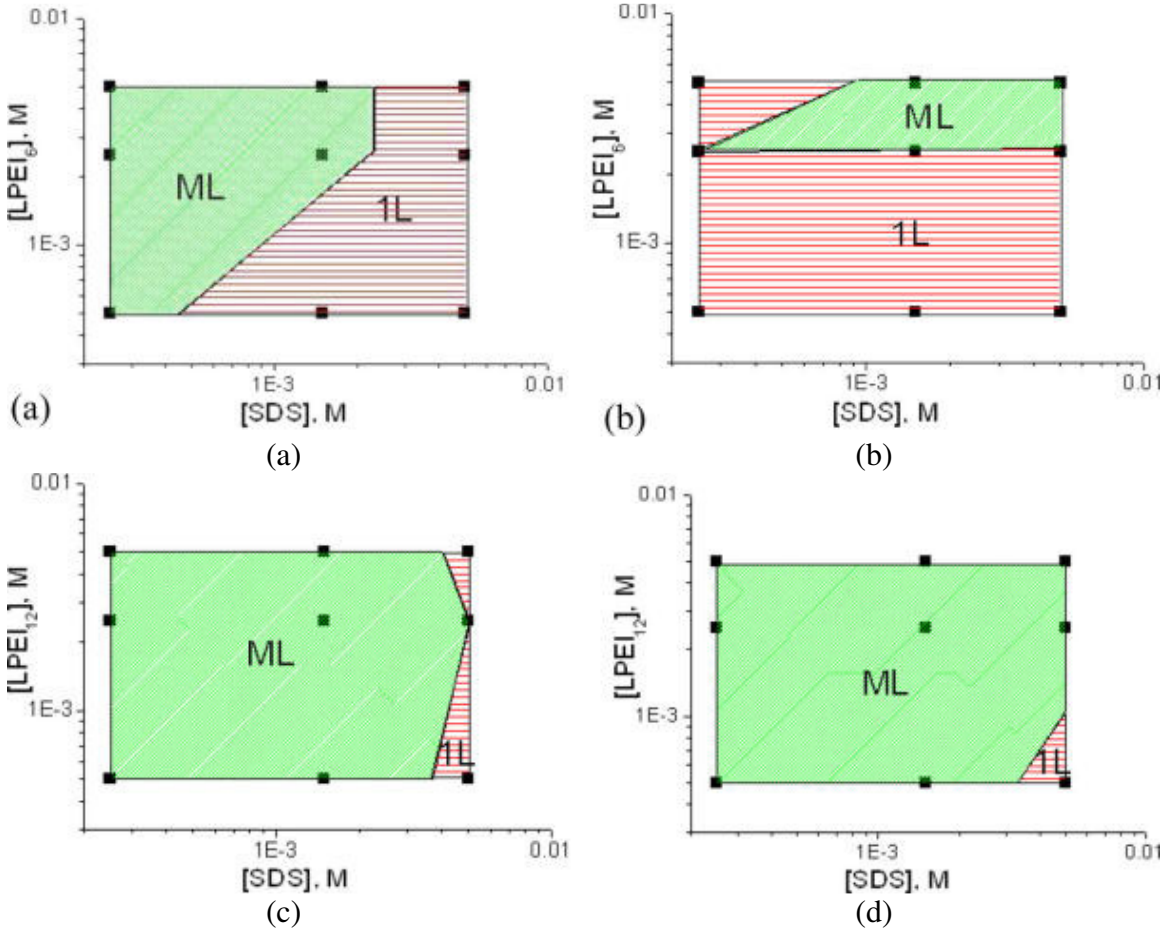


*Figure 78.* Surface phase diagram for (a) $LPEI_6$/SDS at pH 7 (b) $LPEI_6$/SDS at pH 10 (c) $LPEI_{12}$/SDS at pH 7 and (d) $LPEI_{12}$/SDS at pH 10 (1L: monolayer, ML: multilayer).[146]

At pH 3, the LPEI/SDS system formed monolayers at the interface for all the studied molecular weights (not shown in the Figure). At pH 10 $LPEI_6$ showed multilayer formation above a critical value of polymer concentration. At pH 7, LPEI6 showed multilayer formation at lower levels of SDS. For this system, the concentration of SDS required to cause the transition from multilayer to monolayer showed a linear dependence with polymer concentration. This could be attributed to either solubilization of the complex multilayer or the transition from surface complexes to complexes in the bulk of the solution. However, above a critical concentration of polymer, which seemed to coincide with the critical polymer concentration at pH 10, the transition from multilayer to monolayer became independent of SDS concentration. This is clear indication of a stoichiometric interaction below a critical surfactant concentration and critical concentrations of both surfactant and polymer above this region. With the higher molecular weight PEI, multilayer formation was dominant at both pH 7 and pH 10 (Figure 78). It was found that the layer formation in the $LPEI_{40}$/SDS system was similar to the $LPEI_{12}$/SDS system. However, in the former system, the multi-layers were weakly formed. At higher molecular weight 25,000 Da, monolayer adsorption was once more observed.[146]

*Intrapolymer and interpolymer associations:* The polymer molecular weight greatly influences the intrapolymer and interpolymer associations in polymer/surfactant systems. In the former association, the micellar bridging occurs in between the surfactants present on the same polymer chain, while in the latter association, the micellar bridging occurs in between the surfactants present on the different polymer chains.

In the poly(dimethyldiallylammonium chloride) (PDMDAAC) / Triton X-100 (TX100) / sodium dodecyl sulfate (SDS) system, Dubin and coworkers studied the effect of PDMDAAC concentration and molecular weight on the association.[94] They concluded that, the PDMDAAC concentration at which the switch from intrapolymer to interpolymer association occurs is found to decrease with increase in the PDMDAAC molecular weight. Here, the PDMDAAC concentration was expressed in terms of PDMDAAC/TX100-SDS weight ratio ($C_p$).The switch in the association was observed by monitoring the excess scattering intensity ($I_q$) of the complex as a function of polymer/surfactant ratio, using a static light scattering (SLS) study. Mathematically, the $I_q$ of the complex is directly related to the weight-average molecular weight of the complex and difference in the refractive index between the solute/complex and the solvent in the system. Whenever the intrapolymer association switches to interpolymer association, the complex becomes bigger and therefore, the weight-average molecular weight of the complex increases. Consequently, the scattering intensity of the complex increases ($I_{qmax}$) (Figure 79). These interpolymer complexes are unstable and so, they show associative phase separation. Therefore, the high molecular weight PDMDAAC showed an increase in the extent of the phase separated region. In contrast, for the low molecular weight PDMDAAC, the scattering intensity of the complex linearly increased suggesting the absence of the interpolymer complexes (Figure 79). Therefore, associative phase separation is absent. In simple terms, we believe that increase in the molecular weight decreases the critical overlap concentration (C*) of PDMDAAC. Therefore, the switch in the association occurs at lower PDMDAAC concentration as molecular weight increased.

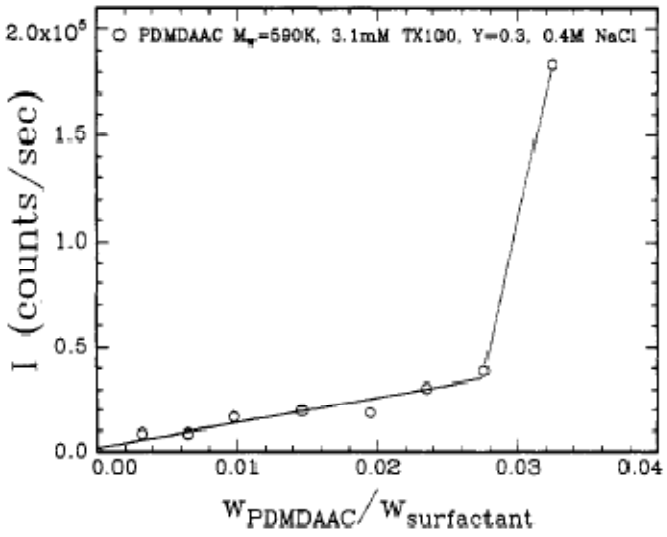


(a)

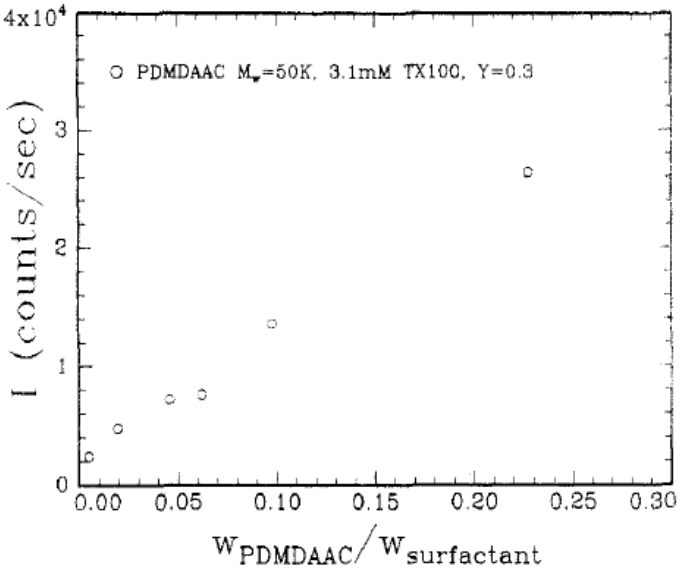


(b)

*Figure 79.* Excess light scattering intensity of PDMDAAC/TX-100/SDS system different $M_w$ of PDMDAAC: (a) 500K and (b) 50k.[94]

Below the critical overlap concentration dissolved polymers are considered to exist as isolated macromolecules dispersed throughout the solvent. These isolated polymers can be considered to be discrete reservoirs for interaction with surfactant. If this is the case, then one would expect to observe the interaction to be enhanced by molecular weight of the polymer. This molecular weight dependence should be especially

noticeable for the interaction of ionic surfactants with polyelectrolytes of opposite charge. In this case the isolated polyelectrolyte molecules could be considered to be finite regions of high charge density with localized counterions within the effective electrohydrodynamic volume of each coil.

Evidence for this concept came from the poly(acrylic acid) (PAA)/ dodecyl trimethylammonium bromide ($C_{12}$TMAB) system, Kim and coworkers inferred that the high molecular weight PAA favored intrapolymer association than the low molecular weightPAA.[147] This association was detected by a fluorescence study using a pyrene probe, which showed a lower critical aggregation concentration (CAC) value for the high molecular weight PAA (Figure 80). Since, the high molecular weight PAA contains more binding sites per unit volume (in isolated molecules) than the low molecular weight PAA, cooperative binding is promoted in the high molecular weight PAA. This is consistent with Kim's reported results; intrapolymer association occurred and the cac was lower for higher molecular weight PAA. A similar conclusion was reached by Shirahama and coworkers for a sodium poly(aspartate) and alkylpyridinium (C12 and C14) chloride system.[148] Since, the high molecular weight PAA undergoes intrapolymer association, we conclude that the concentration of the PAA is far below C* compared to Dubin's system where the studies embrace concentrations that include the C* of PDMDAAC.

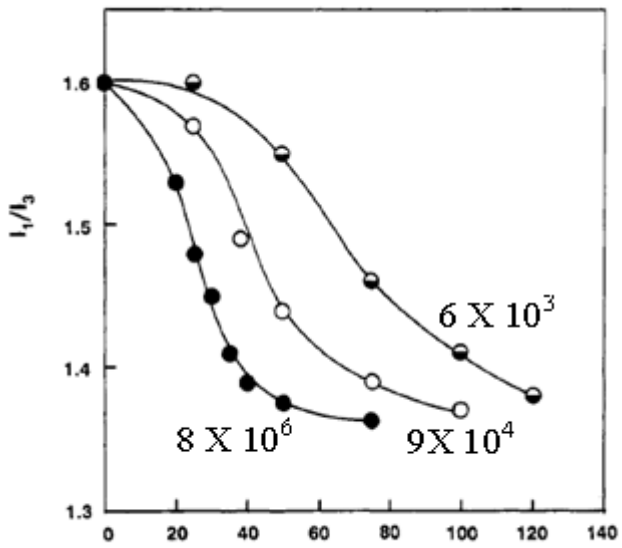


*Figure 80.* Intensity ratio of the PAA/$C_{12}$TMAB system as a function of $C_{12}$TMAB, at different PAA molecular weight.[147]

*Effect on the structure of the complex:* Dubin and coworkers also observed that, at a particular PDMDAAC molecular weight, the radius of gyration of the pure PDMDAAC was not affected by addition of Triton X-100 / SDS. This observation was valid for all the studied molecular weights (Figure 81a). Therefore, they suggested that, on addition of Triton X-100 / SDS, the polymer conformation did not change considerably, as the mobile solvent molecules within the polymer were replaced by the immobile micelles. As a result, the hydrodynamic radius increased but the radius of gyration was unaffected as it is dependent on the topological condition of the complex (Figure 81b). Therefore, the complex structure in the intrapolymer region was unaltered due to molecular weight.

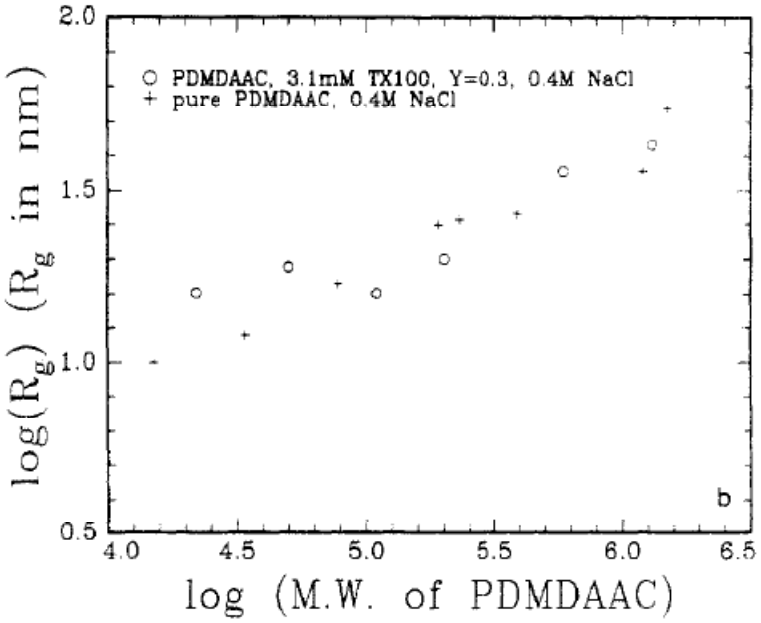


(a)

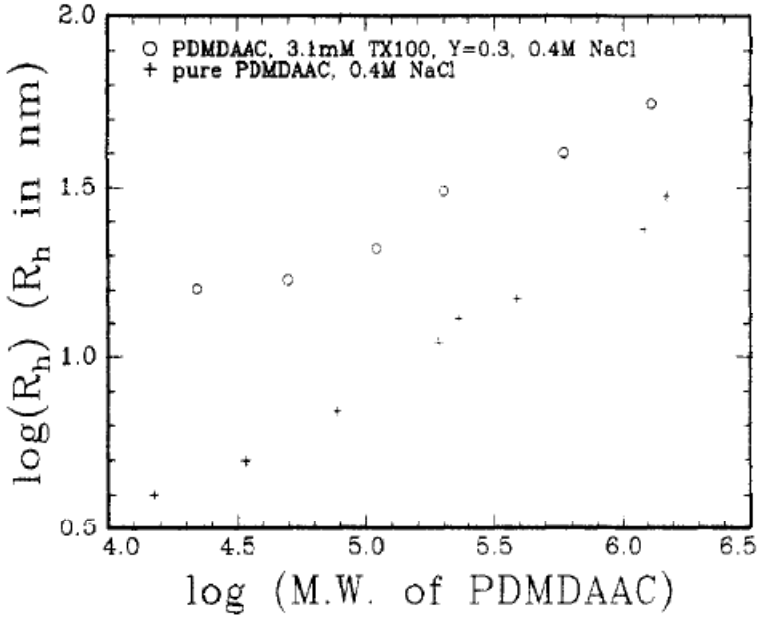


(b)

*Figure 81.* (a) Radius of gyration and (b) hydrodynamic radius of pure PDMDAAC and PDMDAAC/TX-100/SDS complexes as a function of PDMDAAC molecular weight.[94]

*Strength of Association and the influence of concentration relative to C*:*

In the high (JR30M) molecular weight polymers/surfactant systems, Chronakis and Alexandridis found that the strength of association in between polymer chains was higher than the lower (JR400) molecular weight polymers/surfactant systems.[149] They studied the association using rheological measurements on the gels formed in one phase by interacting polymers with different surfactants, at different surfactant concentrations (Figure 82 and 83). At constant frequency, the elastic modulus of the JR30M/surfactant gels was higher that the JR400/surfactant gels. Although the crosslink density for the two systems is the same, since the concentration and charge density of the polymers is same, a difference in modulus value was observed. Therefore, they attributed this difference to the stronger association between the JR30M polymer chains than JR400 polymer chains because the high molecular weight polymer contains more crosslinks per chain. In this work, it is notable that all the polymer/surfactant gels contained 1.0 wt. % polymer. However, according to our experimental work, C* for JR400 is at 0.9 wt. %, whereas, for JR30M it is 0.4 wt. %. Therefore, higher G' in JR30M/surfactant gels may result from higher intermolecular association in a network since the JR30M was studied well beyond C* whereas JR 400 was studied at a concentration in the vicinity of C*.

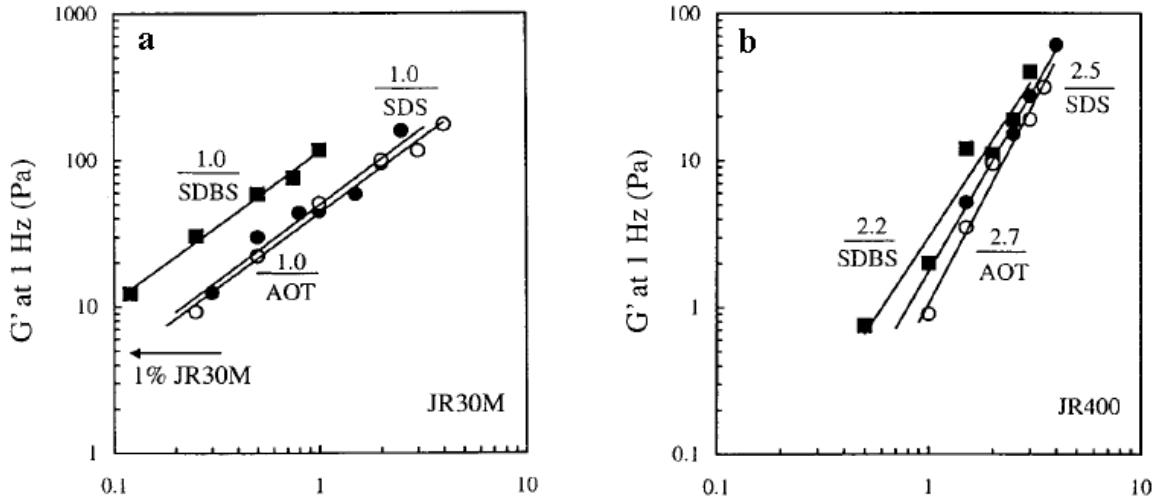


*Figure 82.* Elastic modulus (G') of the (a) 1 wt. % JR30M and (b) 1 wt. % JR400 with different surfactants, as a function of surfactant concentration.[150]

Additionally, Chronakis and Alexandridis observed that the complex viscosity of the JR30M/surfactant gels measured at different surfactant concentration was higher and less dependent on the surfactant concentration than the JR400/surfactant gels.[149] They used the slope, obtained from a log-log plot of the complex viscosity of the gels against the SDS concentration to compare the systems. The slope of the JR400/surfactant system was about 2.5 times higher than the slope of the JR30M/surfactant system (Figure 82 and 83). Therefore, the complex viscosity of JR30M/surfactant gels is less dependent on the surfactant concentration that the JR400/surfactant gels. Based on the two traits, higher complex viscosity and lower surfactant dependence, of the JR30M/surfactant gels they suggested that the polymer dependent crosslinks and chain entanglement occur in high molecular weight polymers. In JR400/surfactant gels, the crosslinking is more surfactant controlled as the complex viscosity is dependent on the surfactant concentration. It certainly is plausible, and I consider that the difference in the complex viscosity may arise due to the difference in concentrations relative to C* in this study.

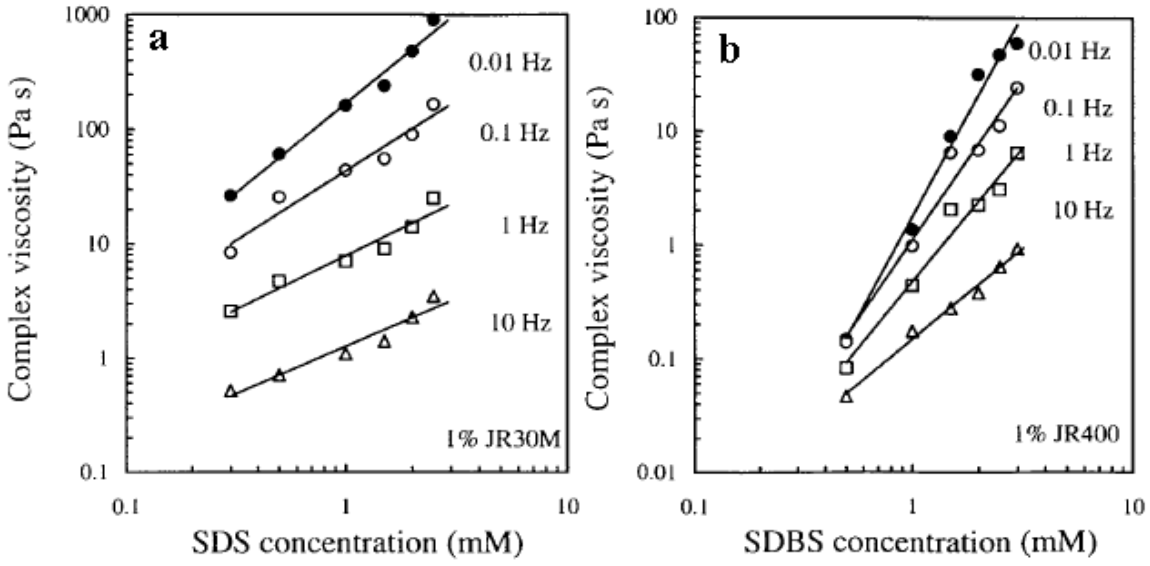


*Figure 83.* Complex viscosity of the (a) 1 wt. % JR30M and (b) 1 wt. % JR400 at different frequencies, as a function of surfactant concentration.[150]

*Backbone Flexibility*

During the last few decades, a considerable amount of research has been done to study the effect of polyelectrolyte backbone flexibility on the interaction between polyelectrolyte and oppositely charged species. Much of the literature available on the polyelectrolyte backbone rigidity focuses on polyelectrolyte and macroion interaction is based on theoretical studies. Some attempts have been made to study the interaction on an experimental basis. Much of the reported work is directed to polyelectrolyte and macroion interaction and is less concerned with polyelectrolyte and surfactant molecular interaction. However, in these studies the conclusions are not clear because the flexible and rigid polymers were not compared on the same grounds. The polyelectrolyte parameters, such as molecular weight and charge density, and experimental conditions varied from study to study. Moreover, these studies were restricted to one/soluble phase of the system. As a consequence, our work is an effort to understand the effect of

polyelectrolyte backbone flexibility on the polyelectrolyte-surfactant interaction based on experimental study. In our study, the polyelectrolyte parameters were comparable, and along with one/soluble phase, the two phase region was also explored.

*Theoretical studies on the effect of chain flexibility on the binding of oppositely charged polyelectrolytes and macro-ions:* Based on Monte Carlo (MC) simulation and thermodynamic parameters, Wallin and Linse[151] explored the effect of polyelectrolyte backbone flexibility on the interaction between a polyelectrolyte and an oppositely charged micelle. They concluded that the more flexible the polymer, the more was the association with micelle. The extent of association decreased with increasing polymer rigidity. This decrease in association was attributed to a decrease in conformational entropy. In another study, Jonsson and Linse[152] interacted a linear polyelectrolyte of varying flexibility with an oppositely charged macroion. They also found that the interaction increased with polyelectrolyte flexibility. Indeed, they concluded that polyelectrolyte would wrap around the macroion. As the backbone flexibility of the polyelectrolyte decreased, the amount of wrapping on the macroion surface decreased. They extended their study to the interaction with four macroions. In this system, the flexible polyelectrolyte formed a condensed structure. As the flexibility decreased, the complex became unraveled. Skepo and Linse[153] studied a more complex system containing a polyelectrolyte in presence of numerous macroions and at different salt concentrations using MC simulation. They concluded that, for a flexible polyelectrolyte, the interaction decreased with increasing salt concentration. In contrast, for the rigid polyelectrolyte, the interaction stayed the same but was lower compared to flexible polyelectrolyte. Besides the interaction, Stoll and Chodanowski[154] found that

polyelectrolyte backbone flexibility affected the adsorption and spreading of the polyelectrolyte on the oppositely charged spherical particle, using MC simulations. Therefore, they suggested that the adsorption of the polyelectrolyte could be increased by increasing the chain flexibility, and also by decreasing the ionic concentration of the medium. Furthermore, in another system, Stoll and coworkers[155] calculated, by MC simulation, that the adsorbed polyelectrolyte displayed different conformations on interaction with a micelle. The adsorption/desorption limits of the polyelectrolyte calculated by this simulation was in good agreement with the experimental study.

*Experimental studies on the effect of chain flexibility on the binding of oppositely charged polyelectrolytes and macro-ions:* Dubin and coworkers have experimentally studied the interaction between different polyelectrolyte and macroion systems: (1) hyaluronic acid and acrylamidomethylpropanesulfonate/acrylamide copolymers with cationic surfactant micelles and protein serum albumin[156] (2) polydimethyldiallyl ammonium chloride and chitosan with oppositely charged micelles[157] (3) different polyelectrolytes with bovine serum albumin and micelles.[158] They measured the interaction in terms of the onset of the polyelectrolyte and micelle binding (Yc). The critical surface charge density of the colloid ($\sigma_{\mathrm{crit}}$) required for the polyelectrolyte and colloid binding is defined as:[157,158]

$$\sigma_{crit}\xi^{a}\sim\kappa^{b} \qquad \text{Equation 15}$$

where, $\xi$ is the polyelectrolyte charge density, $\kappa$ is the Debye-Huckel parameter, *a* and *b* are empirical scaling parameters. In this study, a flexible copolymer composed of acrylamidomethylpropane sulfonate (AMPS) (20 mol %)/acrylamide and a rigid hyaluronic acid polymer were independently interacted with mixed cationic/nonionic

micelles (DTAB/TX100).[156] They measured the turbidity of the polyelectrolyte and micelle systems as a function of ionic strength, using turbidity measurements (Figure 85). The onset of the polyelectrolyte and micelle binding (Yc) corresponded to sudden increase in the turbidity values represented by intersection of two lines on the turbidity plots.

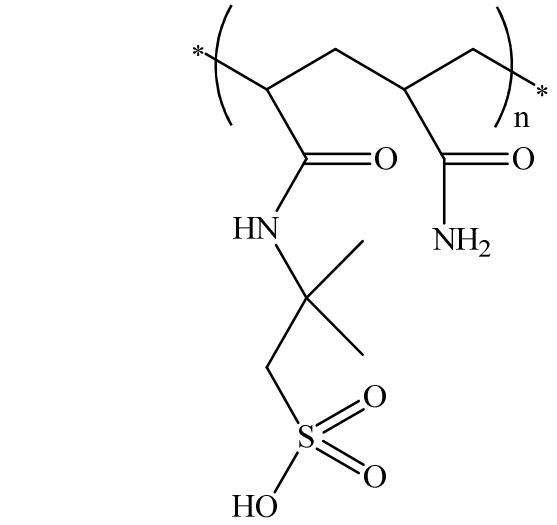


(a)

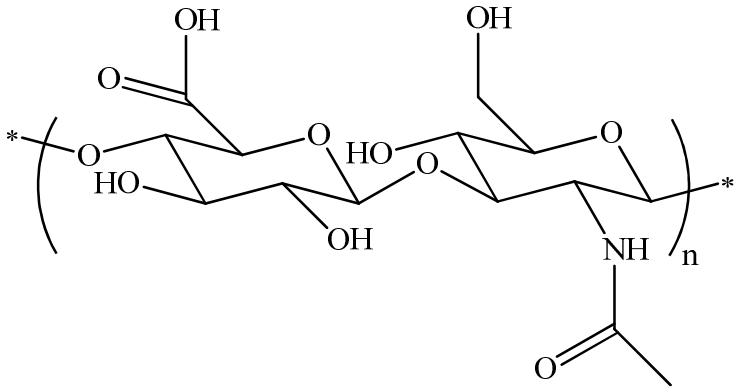


(b)

*Figure 84.* Chemical structure of (a) flexible copolymer of acrylamidomethylpropane sulfonate (AMPS) (20 mol %) and acrylamide (AAm); Persistence length lies between 2 and 3 nm, Mol. Wt. = 200K g/mol, (b) rigid hyaluronic acid (HA); Persistence length lies between 4 and 9 nm, Mol. Wt. = 900K g/mol. Charge density of both the polymers are comparable ($\xi = 0.6$).

They observed that at ionic strength I> 75 mM, the Yc values for the two polymers differed (Figure 86). However, at I< 75 mM, the Yc values for these two polymers were indistinguishable. They argued that if the polymer stiffness was solely based on the bare persistence length ($l_{po}$), the Yc values at lower I would be the different. They considered the effect of electrostatic persistence length ($l_{pe}$), which affected the local stiffness of the chain. The effective persistence length ($l_{eff}$),which accounts for the bare and the electrostatic persistence length, was plotted as a function of ionic strength.

$$l_{eff} = l_{po} + (1/4)l_{pe}$$

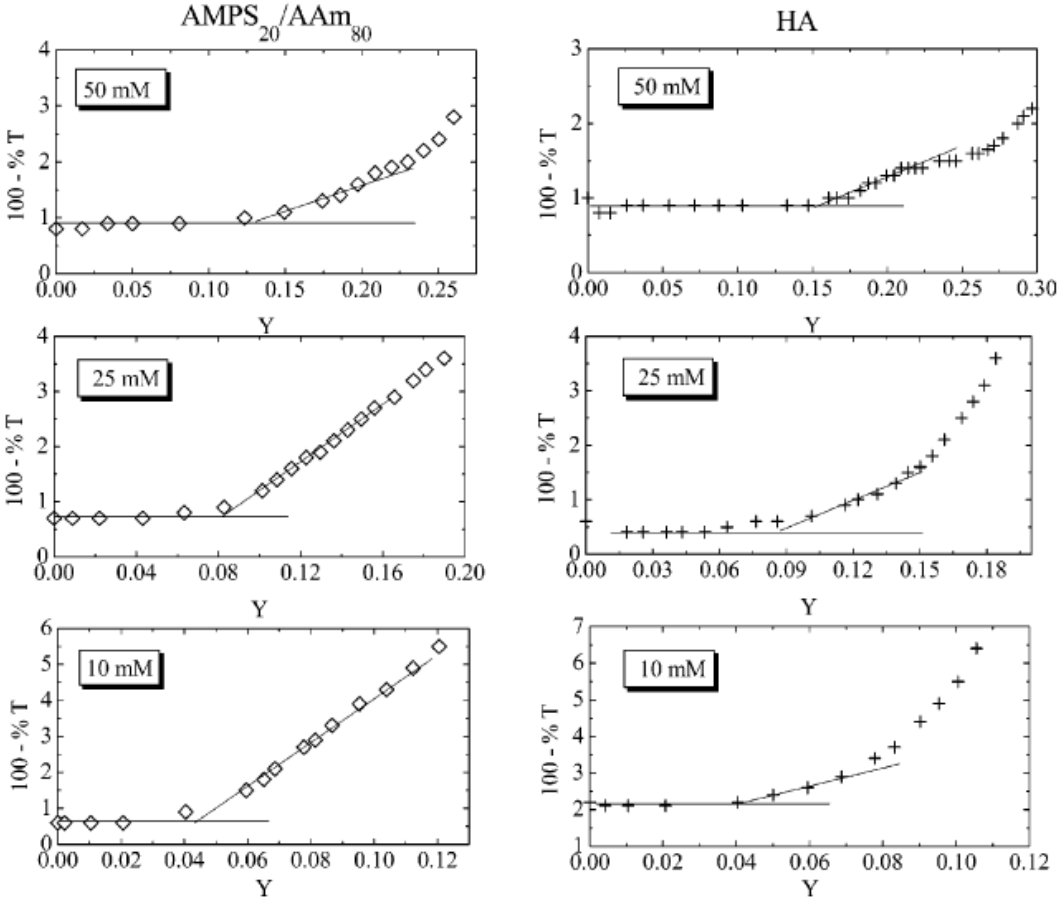


*Figure 85.* Turbidity plots for AMPS/AAm and HA with anionic micelles in the presence of NaCl.[156]

At lower I, the relation between the Yc and the effective persistence length was the same, while, at higher I, it differed. They concluded that at lower I, the polymer chains became stiffer due to the electrostatic contributions. However, at higher I, these contributions are reduced due to higher salt concentration. Hence, at higher I, the Yc values differed as the bare persistence length of HA is higher than AMPS/AAm. Therefore, the flexible AMPS/AAm showed strong binding towards oppositely charged micelles than HA. Upon inspection of these results, I note that the molecular weight of the two polymers differed significantly. The molecular weight of the rigid HA was 4.5 times greater that the flexible AMPS/AAm. Thus, the difference in the interaction of the flexible AMPS/AAm and rigid HA polymer cannot be solely be attributed to the difference in the backbone flexibility.

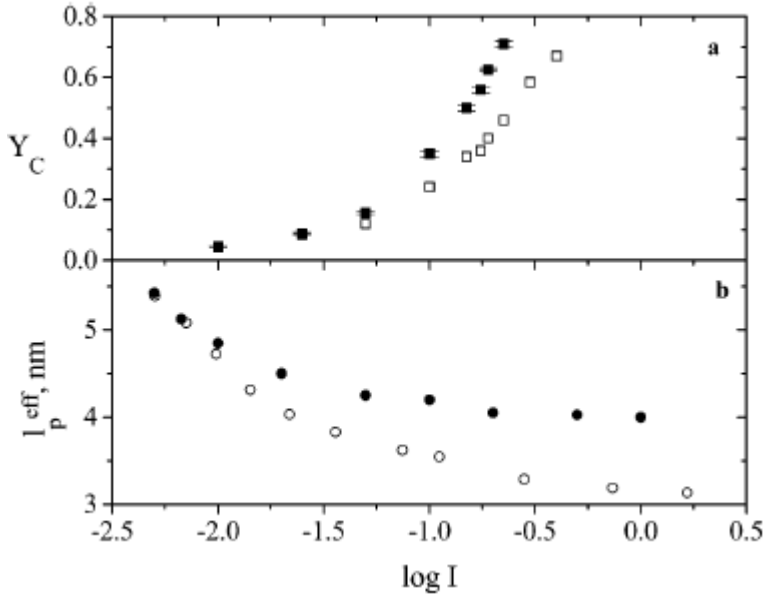


*Figure 86*. (a) The onset of AMPS/AAm and HA with anionic micelle binding (Yc) and (b) the effective persistence length as a function of NaCl. Open symbols for AMPS/AAm and filled for HA.[156]

In the above study, a precise relation between the bare persistence length and the polyelectrolyte/micelle binding was difficult to determine, as the binding of the oppositely charged species influenced the electrostatic persistence length. Therefore, in order to gain better understanding of the relation between the bare persistence length and binding, Dubin conducted another study using flexible PDADMAC and rigid chitosan with SDS/TX100 micelles. These polymers had a considerable difference in the bare persistence length.[157]

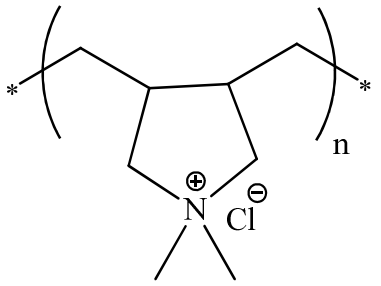


(a)

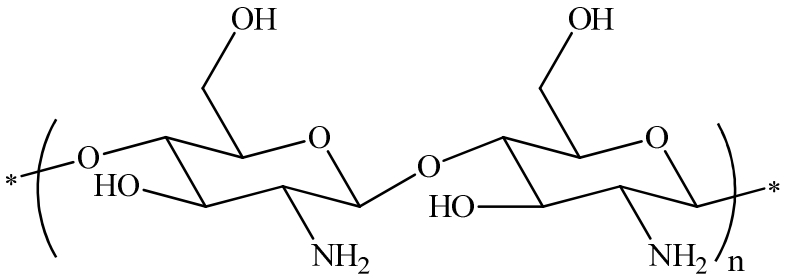


(b)

*Figure 87.* Chemical structure of (a) flexible poly(dimethyldiallyammonium chloride) (PDADMAC); Persistence length = 2.5 nm, Mol. Wt. = 219K g/mol; Charge density (ξ) = 1.15 (b) rigid chitosan (degree of acetylation = 12 %); Persistence length = 6nm, Mol. Wt. = 193K g/mol; Charge density (ξ) = 1.2.

In this study, they analyzed the binding behavior by producing titration curves and recording the onset of the binding (Yc) (Figure 88), similar to the previous study (Figure 85). They found that the flexible PDADMAC showed weak binding (high Yc)

compared to the rigid chitosan (DA = 12%), at both low and high ionic strengths. This observation was consistent even when these polymers were interacted with other different micelles. However, comparable Yc values were obtained for both polymers for smaller micellar systems (Table 4).

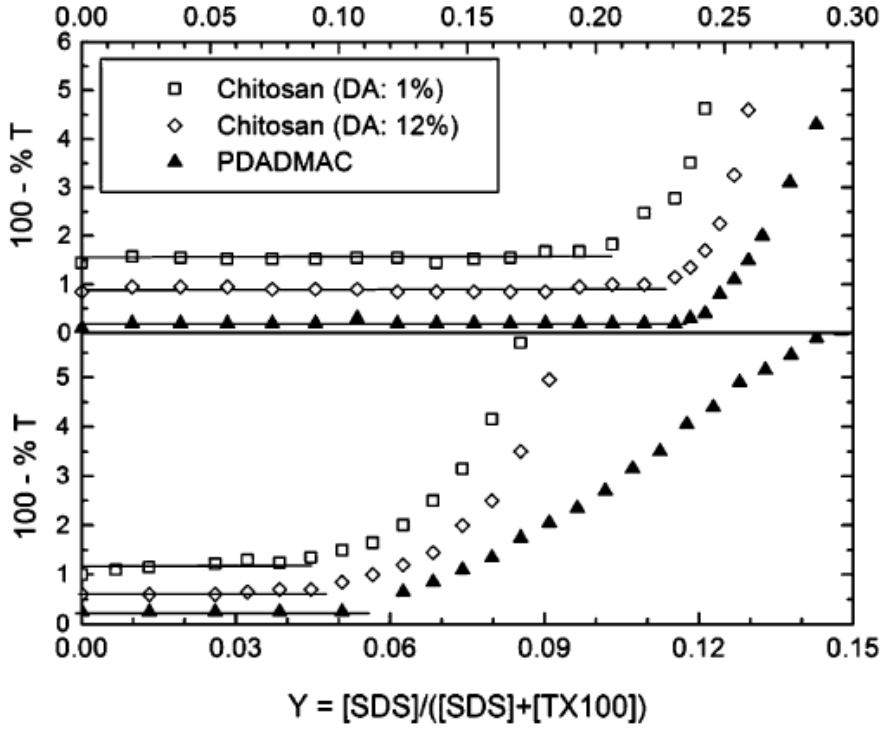


*Figure 88.* Turbidity plots for PDADMAC and chitosan with SDS/TX100 micelle in presence of NaCl (a) I = 0.4 M (b) I = 0.05 M.[157]

In the systems (AMPS/AAm and HA), the onset of the binding at low ionic strength converged, but on the other hand, at high ionic strength it diverged. However, in the system (PDADMAC and chitosan), the onset of the binding was lower for the rigid chitosan compared to the flexible PDADMAC throughout the range of the ionic concentration. Therefore, Dubin and coworkers[157] concluded that the chain flexibility affected the polyelectrolyte and colloid binding, but persistence length is not true measure of the chain flexibility.

Table 4

*Size of different micellar systems and the onset of binding (Yc).*[157]

| Surfactant System | I (M) | Y | Micelle Radius (nm) | Yc | | |
|---|---|---|---|---|---|---|
| | | | | PDADMAC | Chitosan DA = 12% | Chitosan DA = 1% |
| $C_{12}E_6$ | In D20 | 0 | 6.5 ± 0.2 | 0.038 ± 0.001 | 0.029 ± 0.002 | 0.026 ± 0.002 |
| TX100-SDS | 0.40 | 0.30 | 9.0 | 0.235 ± 0.005 | 0.227 ± 0.005 | 0.205 ± 0.005 |
| TX100-SDS | 0.05 | 0.05 | 4.5 | 0.056 ±0.005 | 0.048 ± 0.002 | 0.045 ± 0.003 |
| OP10-SDS | 0.05 | 0.07 | 4.2 ± 0.1 | 0.065 ±0.002 | 0.062 ± 0.002 | 0.037 ± 0.003 |
| TX102-SDS | 0.05 | 0.07 | 3.7 ± 0.1 | 0.075 ±0.004 | 0.072 ± 0.002 | 0.080 ± 0.005 |

Although the molecular weights of the two polymers in the current system were comparable, the pH of the polyelectrolyte solution varied. The pH of the chitosan solution was kept below 3 in order to dissolve chitosan in water. Introduction of anionic surfactants in this extreme acidic condition will either lower the surfactant activity or hydrolytically degrade the surfactant. On the other hand, pH of the PDADMAC solution was not altered compared to other polymer/surfactant system. Thus, these polymers were not tested under the same experimental conditions and therefore, it is difficult to rely on these observations. Moreover, Dubin's work[157] on the polyelectrolyte backbone flexibility only considered interaction between polyelectrolyte and macroion, neglecting interaction between polyelectrolyte and small molecules such as surfactants.

*Experimental studies on the effect of chain flexibility on the binding of oppositely charged polyelectrolytes and surfactant:* Early work was performed by Kwak and coworkers to understand the backbone flexibility effects on the polyelectrolytes and

surfactant interactions, by evaluating the binding constants using potentiometric studies (Figure 89).[159] They studied the interaction between anionic polyelectrolytes and cationic tetradecyltrimethylammonium bromide (TTABr). The flexible polyelectrolytes included polyacrylate (PA), while, the rigid polyelectrolytes included alginate, pectate, and carboxy-methylcellulose (CMC). They found that flexible polyelectrolytes had higher overall binding constant than rigid polyelectrolytes. Therefore, they concluded that polyelectrolyte rigidity is one of the important factors in polyelectrolyte and surfactant interaction.

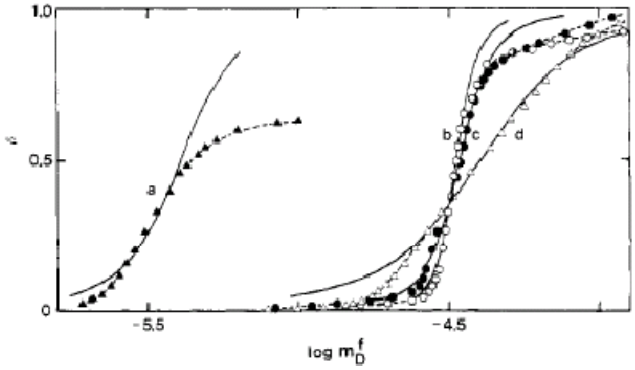


*Figure 89.* Binding isotherm curves for (a) PA (b) alginate (c) pectate (d) CMC with $TTA^+$, as a function of free surfactant concentration ($m_D^f$).[159]

Wang and coworkers studied the effect of molecular weight, surfactant architecture along with backbone rigidity on the interaction of flexible poly(sodium acrylate) (PAA) and more rigid poly(sodium styrene sulfonate) (PSS) with oppositely charged surfactants.[160] They found few differences in their interactions by characterizing these polyelectrolyte/surfactant mixtures using isothermal titration microcaloirmetry, turbidity and fluorescence measurements.

According to the ITC studies, the interaction in the PAA-surfactant system was endothermic, while, in the PSS-surfactant system it was exothermic (Figure 90). The

endothermic behavior of the PAA-surfactant system as attributed to the dehydration of the PAA chains. In PSS/DTAB, the surfactant alkyl groups are in close vicinity of the PSS benzene ring. This suggested that the benzene rings are incorporated in the micelle surface. However, in this study, the role of the polymer backbone flexibility was really not highlighted. Moreover, the difference in the persistence length of PAA and PSS is small[161] compared to the polymer systems used in Dubin's and Kwak's work.

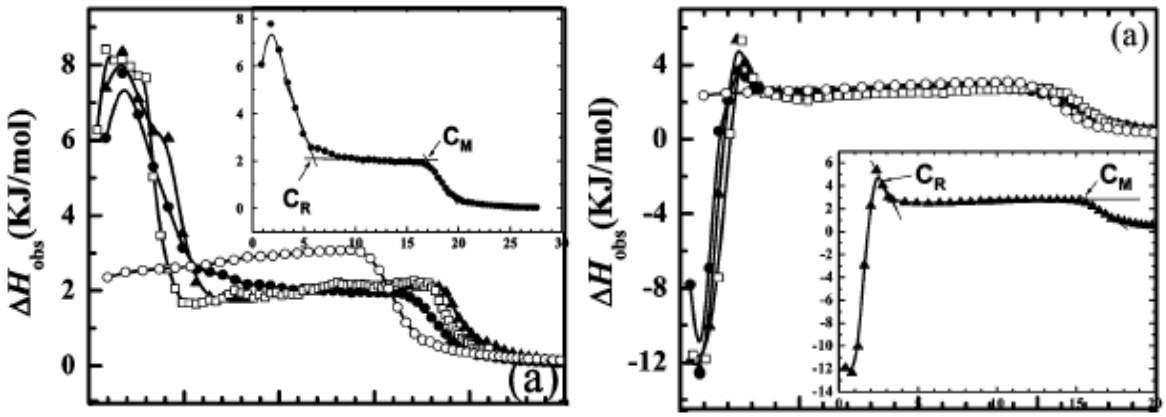


*Figure 90.* ITC curves for the PAA/DTAB and PSS/DTAB system.[160]

Polyelectrolytes with substantial difference in the persistence length were used by Langevin and coworkers to study the interaction polyelectrolytes and surfactants. They interacted flexible polyacrylamidopropanesulfonate (PAMPS) and rigid sodium carboxymethylcellulose (CMC) with cationic alkyltrimethylammonium bromide ($C_nTAB$, n = 12, 14 and 16).[162] In this study, along with the backbone flexibility, effects of other structural parameters were also studied. The emphasis was not on the effect of backbone flexibility. Besides that, the interaction was evaluated by simply comparing the critical aggregation concentration of the systems. They found that the cac of the systems was almost the same. This study was not conclusive and was restricted only to the soluble phase of the system.

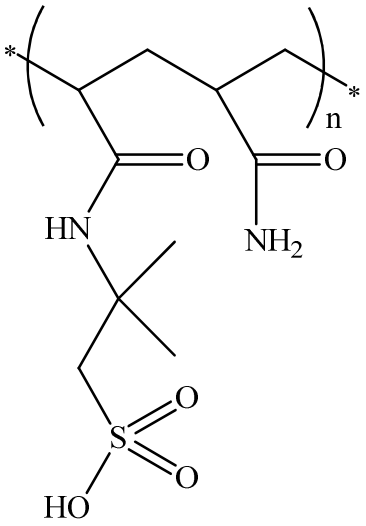

(a)

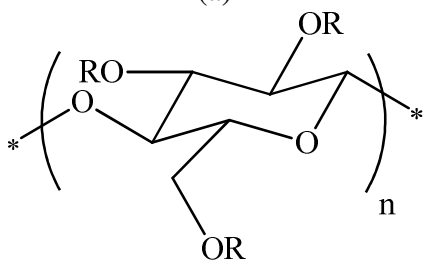

R = H or $CH_2CO_2Na$

(b)

*Figure 91.* Chemical structure of (a) flexible polyacrylamide sulfonate (PAMPS); Persistence length ≈ 1 nm, Mol. Wt. = 400K g/mol, distance between the charges = 5 Å (b) rigid carboxymethyl cellulose (CMC); Persistence length = 10 nm, distance between the charges = 4.2 Å.

In some studies, a rigid DNA is used as comparison. For example, Langevin and coworkers measured the CAC of the polyelectrolyte/surfactant interaction.[163] The precept here is that the lower the CAC, the higher would be the interaction strength between the polymer and surfactants. In semi flexible CMC/DTAB, the cac is 0.2 mM while, for rigid DNA/DTAB, the cac is 0.9 mM. They attributed this difference to the wrapping of the flexible chains around surfactant micellar aggregates than the rigid chains. However, the molecular weight of DNA was lower than CMC and the charge density and HLB of these two macromolecules is different.

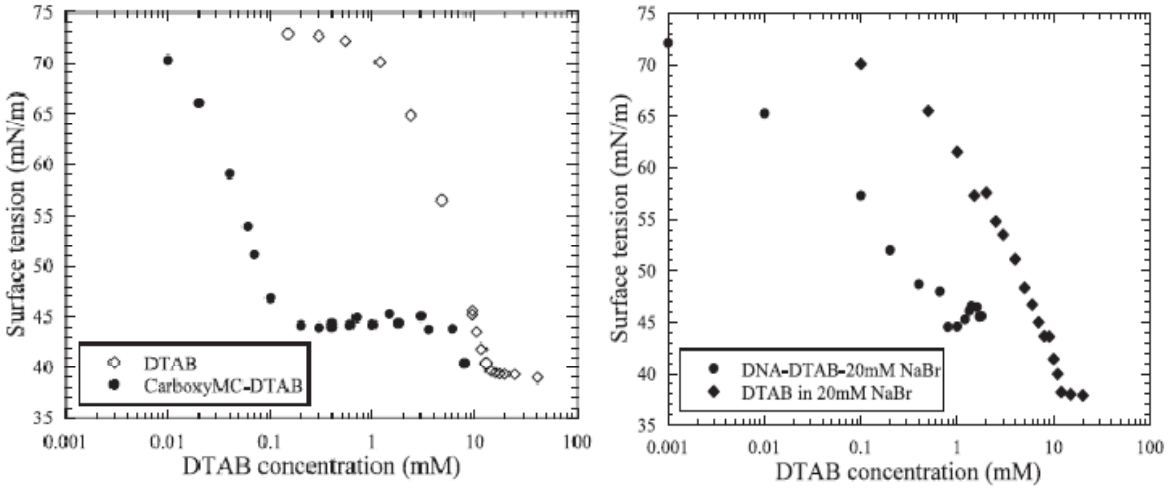


*Figure 92.* Surface tension curves for (a) CMC/DTAB and (b) DNA/DTAB systems.[163]

Thus, it can be seen that, there is a real need for a systematic study of the polyelectrolyte and surfactant interaction to extend our fundamental understanding based on the polyelectrolyte backbone flexibility. In my study I have attempted to glean more understanding of the role of chain flexibility by studying a comparison of a flexible MAPTAC and a rigid JR30M with comparable molecular weight and charge density. The interaction of each of these polymers with SDS was studied. We chose these polymers because there is already a rich literature based upon their commercial utility for the formation of coacervates. In my studies, I have included a broad range of surfactant concentrations, below and above the CMC and also inclusive of solution and phase-separated coacervates.

*Charge Density*

The linear charge density ($\xi$) of the polyelectrolyte is expressed as:

$$\xi = {e^2}/{4\pi\epsilon_0\epsilon bkT} \qquad \text{Equation 16}$$

where, $e$ = the magnitude of the electrostatic charge, $\epsilon_0$ = the permittivity of vacuum, $\epsilon$ = the dielectric constant of the solvent, $b$ = the average linear distance

between the ionic sites on the polyelectrolyte and $k$ = the Boltzmann constant, $T$ = the temperature.[17]

From this expression it can be seen that the charge density of the polyelectrolyte is inversely dependent on the distance 'b'. Therefore, increase in the distance 'b' decreases the charge density and vice versa. This distance is a vital parameter in polyelectrolyte/surfactant interaction as the distance 'b' affects the interaction and packing of the polyelectrolyte around surfactant molecules.

*Surface Absorption:* Klitzing studied the effect of poly(diallyldimethylammonium chloride-stat-N-methyl-N-vinylacetamide) (P(DADMAC-stat-NMVA)) charge density on the surface tension for the P(DADMAC-stat-NMVA)/SDS system (Figure 93).[164] Initially, the surface tension decreases with increase in the charge density. This was accredited to the formation of surface active complexes as a result of increase in hydrophobicity of the complex due to adsorption of surfactant molecules on the polymer. However, at higher charge density the surface tension increases with increase in charge density. This was attributed to conformational changes taking place in the polymer. Higher charge density increased electrostatic repulsion causing the polymer to stretch and therefore, favored adsorption in a flat conformation.

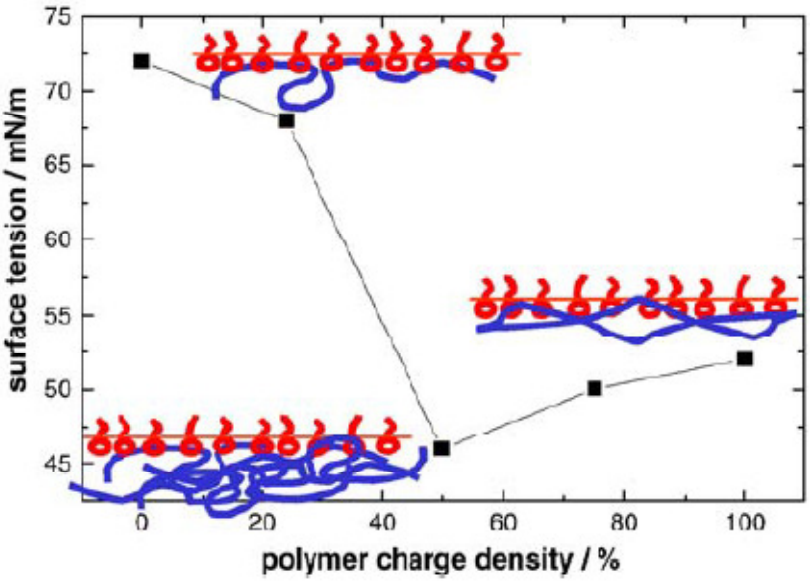


*Figure 93.* Effect of polymer charge density of the random copolymer P(DADMAC-stat-NMVA) on the surface tension. [P(DADMAC-stat-NMVA)] = $5*10^{-3}$monomol$^{-1}$and [SDS] = $10^{-5}$M.[164]

*Effect on Cooperative Parameter:* The cooperative parameter accounts for binding of the surfactant in the vicinity of the surfactant bound to the polyelectrolyte. Kwak and coworkers suggested that the distance between the polyelectrolyte ionic sites (b) may also influence the cooperative parameter.[159] Increase in the charge density may increase the cooperative parameter. However, Kwak's work, which included a wide set of anionic polyelectrolytes, did not support this postulate. He suggested that this may be because of difficulty in separating the charge density effect from the other polyelectrolyte structural parameters: molecular weight, chemical nature of the ionic groups and backbone flexibility, which should also influence the interaction.

In order to diminish the effect of the other structural parameters, the charge density of a polyelectrolyte was varied by adjusting the pH of the solution.[165] Using this approach, Hansson and Almgren studied the effect of the charge density on the cooperative parameter in the sodium (carboxymethyl) cellulose (NaCMC)/

dodecyltrimethylammonium bromide system, by producing binding isotherms.[14] They observed that with increase in the charge density of NaCMC, the cooperative parameter increased (Figure 94).[14] A similar conclusion was drawn in the poly(maleic acid-*co*-methyl vinyl ether)/ dodecyltrimethylammonium chloride)[13] and poly((3-(methacryloylamino)propyl) trimethylammonium chloride-co-acrylamide)/ sodium dodecyl sulfate[166] systems. From Figure 93, we see that, with increase in charge density the cooperative parameter increases. This could be attributed to enhancement of the hydrophobic interaction between bound surfactants. Thus, the probability of surfactant binding to the site 'a*', adjacent to already bound surfactant is higher than site 'a' in the Figure 95. Therefore, the cooperativity increases with decreases the distance 'b' i.e. with increase in the charge density.

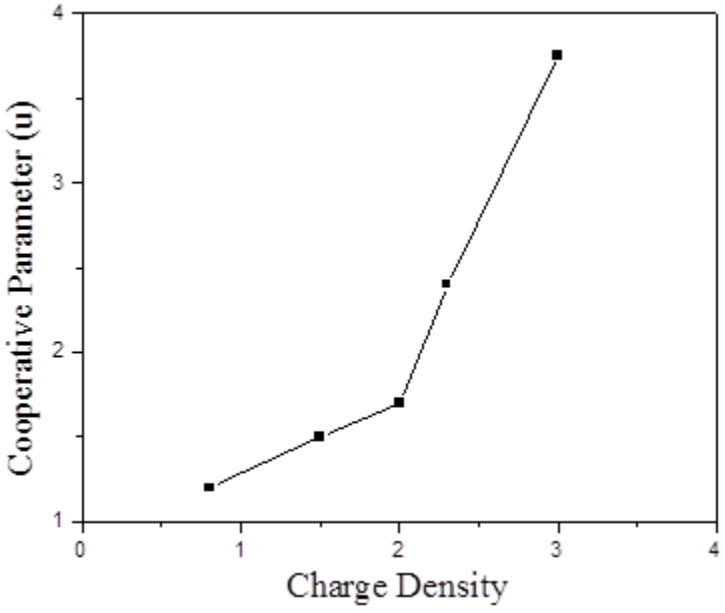


*Figure 94.* Effect of the charge density (ξ) on the cooperative parameter in the sodium (carboxymethyl) cellulose/ dodecyltrimethylammonium bromide system.[14]

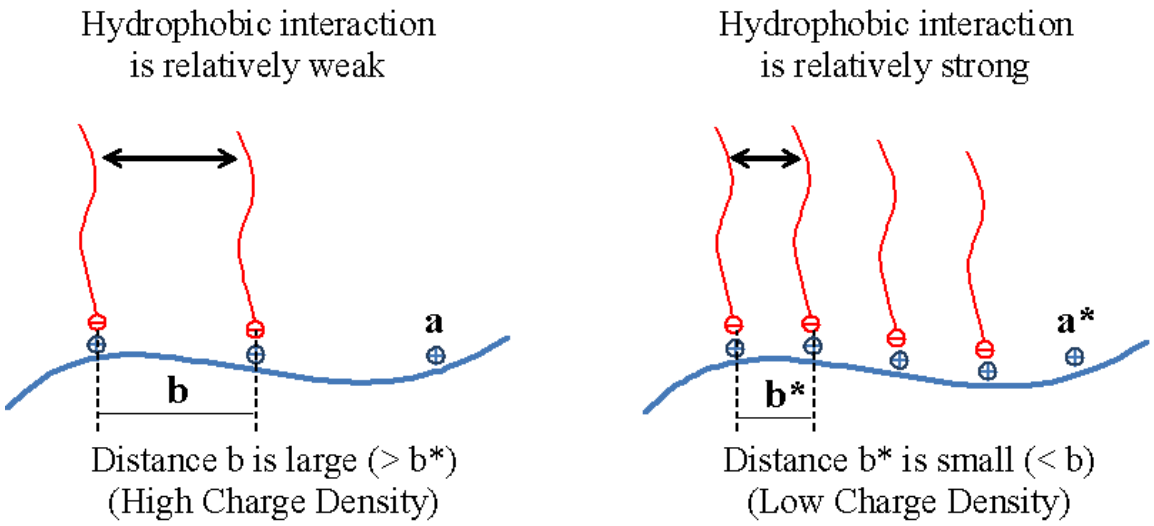


*Figure 95.* Schematic illustration representing the relation between the distance 'b' and cooperative parameter in the cationic polyelectrolyte/ anionic surfactant system.

*Effect on Critical Aggregation Concentration:* According to Manning's counterion condensation theory, in dilute polyelectrolyte solution, the counterions condense on the polyelectrolyte when the normalized charge density (ξ) is greater than unity.

The charge density ($\xi$) of the polyelectrolyte can also be expressed as:

$$\xi = {e^2}/{\epsilon bkT} = {l_{Bj}}/{b} \qquad \text{Equation 17}$$

where, $l_{Bj}$ = the Bjerrum length. The Bjerrum length is the distance between ionic charges at which the electrostatic interaction is comparable to the themal energy kT. According to Manning counterion condensation theory, counterion condensation occurs when the chain critical charge density $l_{Bj}/b$ exceeds unity.

At the counterion condensation condition ($\xi = 1$), $l_{Bj} = b$. The distance 'b' in water at 25 $^{o}$C is 7.1 Å.[12] If the effective distance 'b' between the ionic sites is less than 7.1 Å, counterion condensation occurs.

The effective charge density of the polyelectrolyte becomes constant above $\xi = 1$ due to the condensation of the counterions. Hence, the critical aggregation concentration (cac) becomes independent of the charge density above $\xi = 1$. However, below $\xi = 1$, the cac increases with increase in the charge density.[12-14]

Accordingly, in the poly(maleic acid-*co*-methyl vinyl ether) (PS1)/ dodecyltrimethylammonium chloride) (DoTac) system, Anthony and Zana[13] found that, below $\xi = 1$, the cac decreased with increase in the charge density. This was due to increase in the electrostatic interactions with increase in the charge density, thereby decreasing the cac. On the other hand, above $\xi = 1$, the cac remained constant due to the condensation of the counterions on PS1 (Figure 96). Analogous observations were made in the NaCMC-DoTab system (Figure 96).[14]

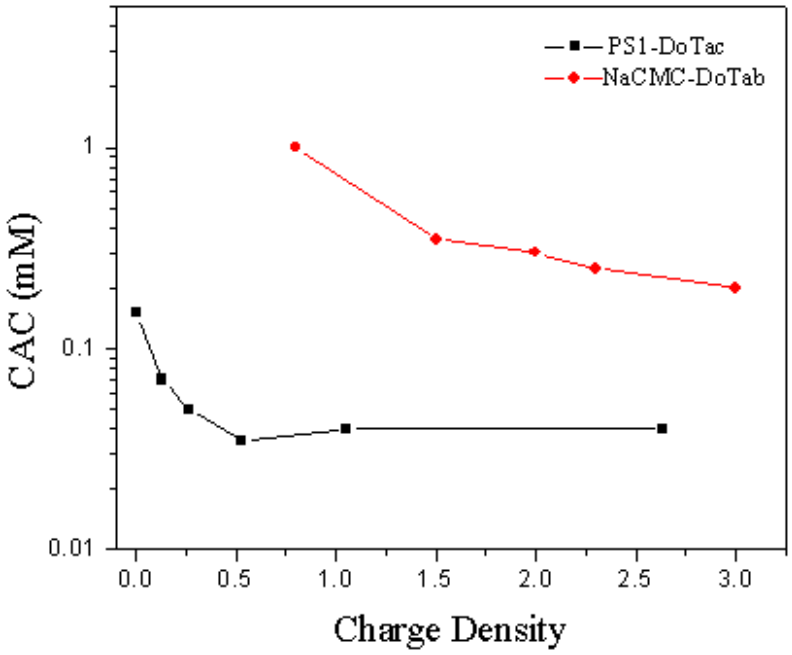


*Figure 96.* Effect of the charge density (ξ) on the critical aggregation concentration (cac).[13,14]

*Effect on Aggregation Number:* The aggregation number ($N_s$) in the polyelectrolyte/ surfactant complex depends on the repulsion between the surfactant head groups and the hydrophobic interaction between the surfactant tail groups. As the repulsion between the head group decreases, the aggregation number increases. With increase in the charge density, the screening of the charges on the surfactant head groups increases. Therefore, as repulsion between the head group decreases, the aggregation number increases. Thus, in the NaCMC-DoTab system, Hansson and coworkers found that the aggregation number of DoTab increased with increase in the NaCMC charge density (Figure 97).[14]

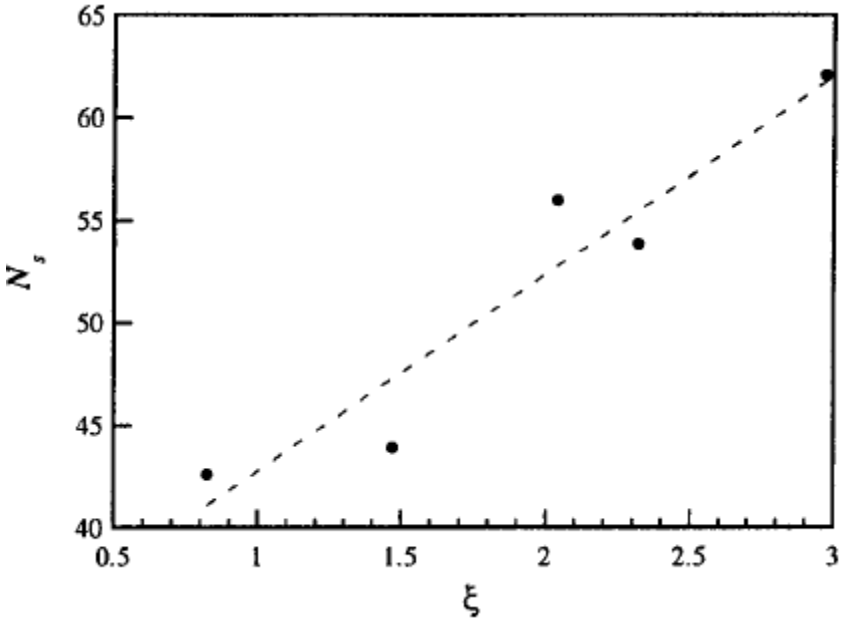


*Figure 97.* Effect of the charge density (ξ) on the aggregation number ($N_s$).[14]

*Effect on the Type of Interaction:* Tam and coworkers found that the charge density of the poly(acrylic acid) governs the type of interaction- hydrophobic or electrostatic, between poly(acrylic acid) (PAA) and dodecyltrimethylammonium bromide

(DoTab), using isothermal titration calorimetry[1] (Figure 98a) and laser light scattering[108] techniques (Figure 98b).[12]

Tam adjusted the charge density (α) of PAA by addition of sodium hydroxide. At lower charge density ($\alpha \leq 0.3$), the PAA-DoTab system exhibited an exothermic peak. However, as the charge density increased ($\alpha \geq 0.3$), the system exhibited an endothermic peak. Therefore, they attributed that, at $\alpha \leq 0.3$, the interaction was driven due to hydrophobic association between the nonpolar PAA segments and the DoTab tail groups. On the other hand, at $\alpha \geq 0.3$, the interaction took place due to electrostatic binding between the PAA ionic sites and the DoTab head groups. This conclusion was further strengthened by the LLS studies. At low charge density ($\alpha \leq 0.3$), they found that the apparent hydrodynamic radius ($R_h^{app}$) of the PAA-DoTab complex increased due to this separation. Compared to this system, at high charge density ($\alpha \geq 0.3$), the system experienced a phase separation due to electrostatic interaction, at relatively higher DoTab concentration. Therefore, they suggested that phase separation in the low charge density system occurred due to hydrophobic association, rather than electrostatic binding. Moreover, in the low charge density system, $R_h^{app}$ decreased with increase in DoTab concentration and the system turned clear. Hence, they suggested that the PAA-DoTab complex was solubilized due to the formation of micelles on the PAA chain.

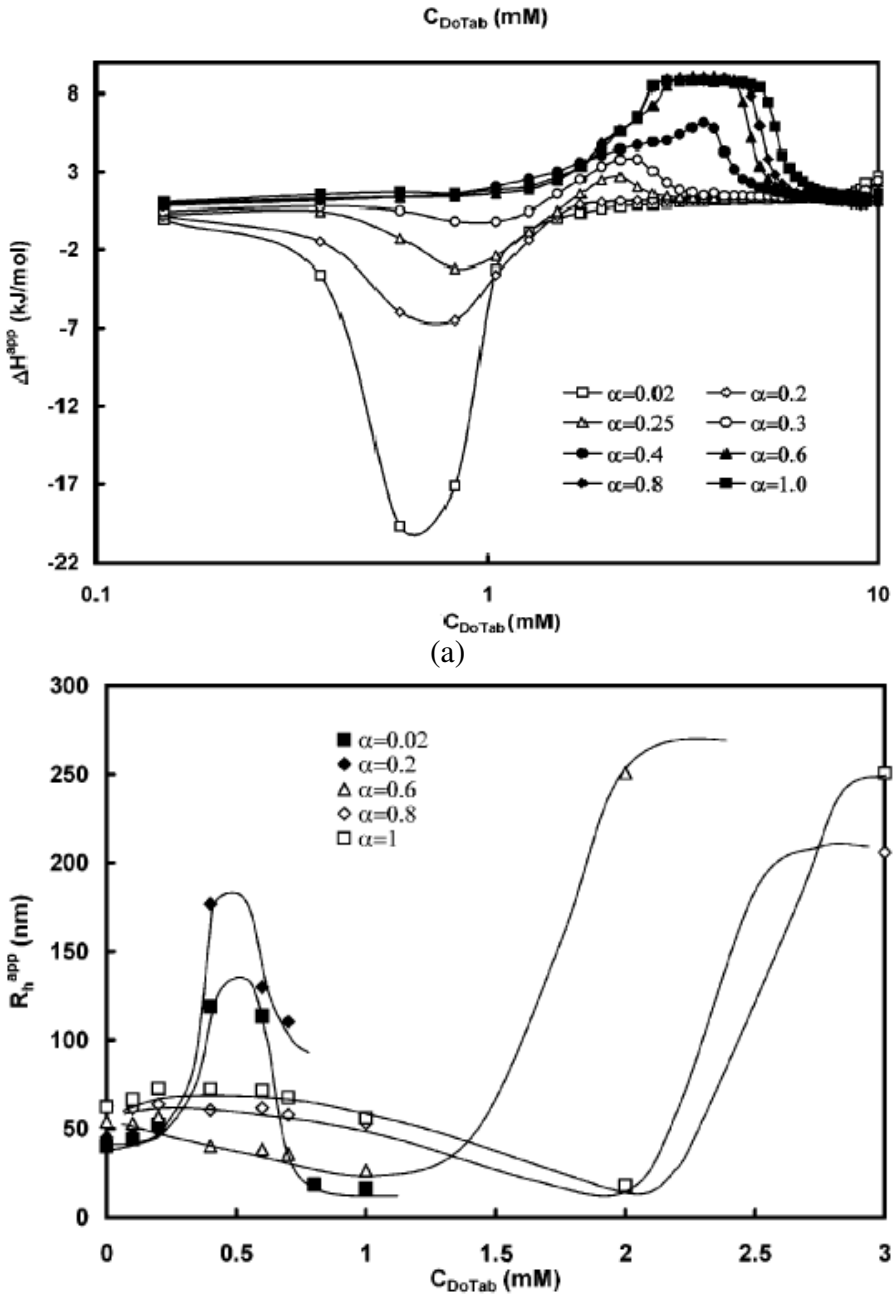


*Figure 98.* (a) Isothermal titration calorimetry[1] curves and (b) apparent hydrodynamic radius of the PAA-DoTab system at different charge densities (α), as a function of DoTab concentration.[12]

*Effect on the Polymer/Surfactant Structure:* Kogej and coworkers[167] studied the structural organization between sodium polyacrylate (PA) and the surfactants-dodecylpyridinium chloride (DPyC) and cetylpyridinium chloride (CPyC). Using small-angle X-ray technique (SAXS), they observed that by increasing the charge density, the surfactants are packed tightly resulting in the formation of highly ordered polyelectrolyte/surfactant structures. The characteristic distance (d) in the complex obtained from SAXS linearly increased with increase in the charge density, in the PA/DPyC and PA/DPyC systems (Figure 99). At lower charge density ($\alpha = 0$), the value of 'd' corresponded to the dimensions of a micelle. On the other hand, at higher charge density ($\alpha = 1$), the value of 'd' was higher than the dimensions of the micelle. Therefore, Kogej and coworkers suggested that, at $\alpha = 0$, hydrophobic interactions between the surfactant and polymer drives the micelles formation. Therefore, these systems showed poor surfactant packing. However, $\alpha = 1$, the increment in the 'd' value (6.4 Å) at $\alpha = 1$ was comparable to the radius of PA chain (5.5 Å). They suggested that due to strong electrostatic interaction between the polymer and surfactant the PA chain was incorporated in between the micelles. As a result, the surfactants were arranged in a definite pattern to form an ordered cubic structure in the complex.

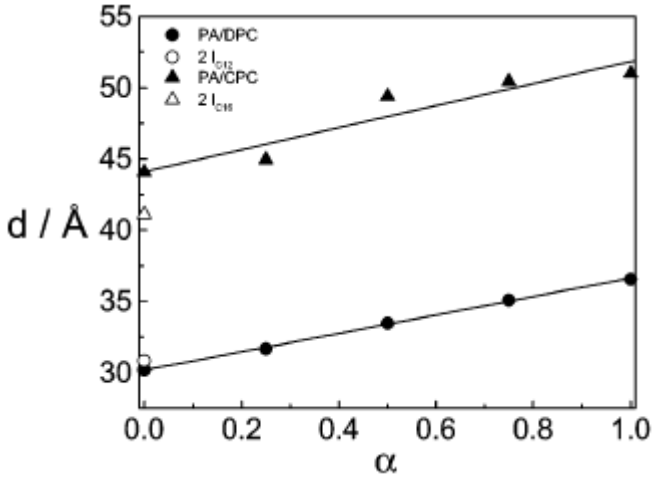


*Figure 99.* Relation between the PA charge density and the characteristic distance (d) of the PA/DPyC and PA/CPyC systems.[167]

Similarly in poly(styrenesulfonate)/N-alkylpyridinium chlorides system Osada and coworkers[168] found that surfactants are arranged in ordered structures at 1:1 surfactant / polyelectrolyte molar ratio (m), due to the tail-tail interaction. Above this ratio, the added surfactant molecules still get packed in the complex through hydrophobic binding with surfactant molecules in the complex, forming an insoluble complex. On the other hand, in the poly(styrenesulfonate-co-styrene)/N-alkylpyridinium chloride system, at 1:1 ratio, the complex is electrostatically neutralized to form an insoluble complex. With further addition of surfactant, the added surfactant molecules hydrophobically associate with the hydrophobic region-styrene of the polymer. These associated surfactant molecules provided cationic charge to the complex, thereby solubilizing the complex.

From the above two studies, we observe that the distance between the ionic sites (b) on the polyelectrolyte influence the surfactant-surfactant packing in the polyelectrolyte/surfactant systems. At low values of 'b', the surfactants were able to pack in systematically, thereby, forming order polyelectrolyte/surfactant structures.

In another study, Osada and coworkers[169] observed that increase in the distance 'b' also switched the surfactant-surfactant interaction to surfactant-polyelectrolyte interaction. Here, the structural organization between a *x*,*y*-ionene bromide polymer with charges on the backbone and anionic surfactant system was studied using SAXS. Osada and coworkers observed that the organization was influenced by the mole fraction of x and y i.e. the charge density of the polymer.

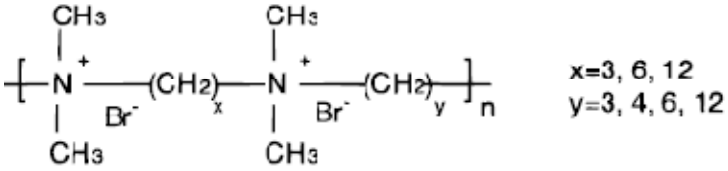


*Figure 100*. Structure of *x*,*y*-ionene bromide polymer.[169]

At low mole fractions of x and y (x = 3, y = 3) i.e. high charge density, the anionic surfactants bound to *x*,*y*-ionene bromide polymer were in close vicinity to each other and this favored side by side packing through tail-tail interaction, to form an ordered structure (Figure 101). Conversely, at lower charge density (x = 6, y = 12), the tail-tail interaction between anionic surfactants was inadequate to pack them in ordered structures. However, the surfactant tail hydrophobically interacted with the hydrophobic segments of *x*,*y*-ionene bromide polymer.

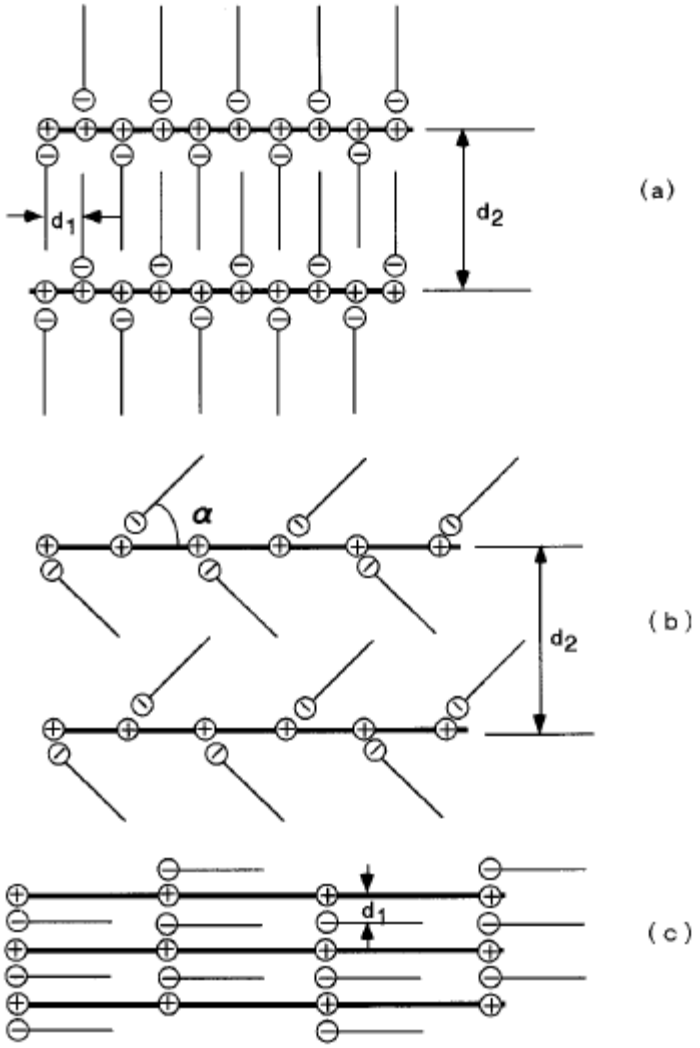


*Figure 101.* Schematic representation of the polymer-surfactant structure (a) x = 3, y = 3 (b) x = 6, y= 4 and x = 6, y= 6 (c) x = 6, y = 12.[169]

## Effect of surfactant properties on the interaction

### *Surfactant Tail Length*

*Surfactant Adsorption:* At low surfactant concentrations, surfactant molecules are preferentially adsorbed at the air/water or oil/water interfaces. Adsorption of amphiphiles at the air/water interface was formalized as Traube's Rule which states "For a homologous series of surfactants, the surface activity approximately triples for each additional $CH_2$ group in the hydrophobe".[26] That is, the surface activity increases geometrically as the number of carbon atoms in the hydrophobe increases arithmetically.

The adsorption of surfactant at an aqueous interface is expressed thermodynamically by the Gibbs' adsorption isotherm[27] (Equation 18) which allows the calculation of the surface excess concentration from the variation of surface tension with surfactant concentration.

For ionic surfactants with no electrolyte,

$$\Gamma_2 = -\frac{1}{4.606\mathrm{RT}}\left(\frac{\partial\gamma}{\partial\log C_2}\right)_T \qquad \text{Equation18}$$

Adsorption of surfactant at the interface reaches an effective limit at the critical micelle concentration. At this critical concentration the chemical potential of surfactant adsorption becomes equal to the chemical potential of micelle formation.

*Effect on the Air/Water Interface:* Surfactant alkyl chain length affects the adsorption of the polyelectrolyte/surfactant complex at the air-water interface.[102,103,170-174] This is because the alkyl chain length governs polyelectrolyte/surfactant interactions and the width of two phase region which affects the adsorption.

For example, in polystyrene sulfonate (PSS) and alkyltrimethylammonium bromide (CnTAB, n = 12 & 16) ellipsometry measurements, Monteux and coworkers

observed that the initial adsorption increased due to formation of surface active soluble complexes (Figure 102).[174] However, the adsorption of the complex further decreased due phase separation (macroscopic precipitation) of the complexes. The extent of desorption increased with increase in the width of two phase region. The adsorption increased again due to re-solubilization of the phase separated complexes. In contrast, they observed that the PSS/$C_{10}$TAB and PSS/$C_8$TAB systems showed one hump in the ellipsometry curve. The PSS/$C_{10}$TAB system experienced turbidity but not phase separation. This prevented significant loss of the PSS/$C_{10}$TAB complex from the surface. Therefore, this system displayed the highest adsorption values. The adsorption in the PSS/$C_8$TAB system was lowest as this system did not show precipitation or turbidity at any the $C_8$TAB concentration. Moreover, the PSS/$C_8$TAB complexes did not absorb at the interface as$C_8$TAB is not sufficiently hydrophobic due to short surfactant chain length.

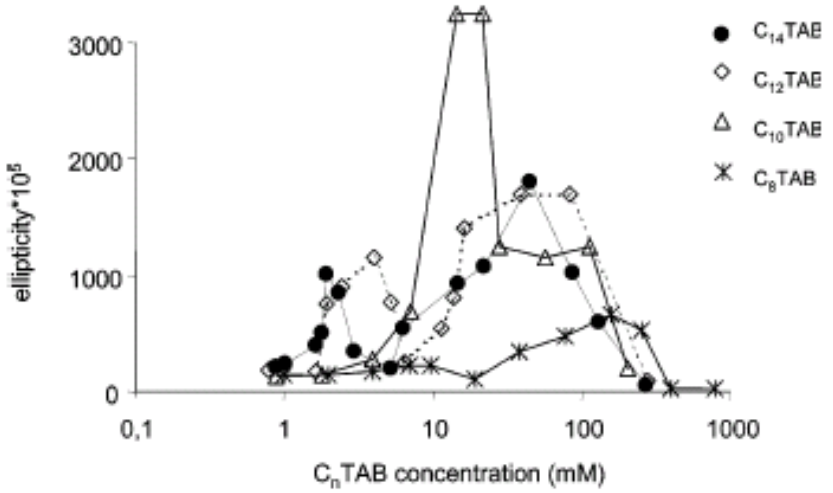


*Figure 102.* Ellipticity values of the 2.4 mM PSS and C*n*TAB (*n* = 8, 10, 12, 14) systems as a function of C*n*TAB.[174]

*Micelles*: The formation of surfactant micelles arises as a consequence of two opposing forces; namely hydrophobic interaction between the tail groups which drives aggregation of the surfactant molecules and repulsion between the hydrophilic head groups which imposes a curvature on the aggregate that limits the size of the aggregate. Tanford refers to this phenomenon as the Principle of Opposing Forces. For the same hydrophilic head group and for constant extrinsic factors increase in the alkyl chain length of the surfactant results in decrease in the cmc of the surfactant system (Figure 103).[133,139,162,175-178] This arises as a consequence of the concomitant increase in hydrophobic interaction as the molar volume of the alkyl group is increased and this in turn increases hydrophobic interaction.[175] However, above a certain chain length, the relation between cmc and the alkyl chain length is nonlinear and beyond a certain chain length complete phase separation will occur.[176]

At very long hydrophobic group molecular volume, or with very small hydrophilic groups, the repulsion between head groups is insufficient to induce curvature at the micelle surface and bulk phase separation occurs. Alternatively, at relatively high surfactant concentrations mesomorphic phases ranging from hexagonally close-packed cylindrical micelles, lamellar phases, and inverse micelles may form as the relative sizes of the hydrophile to the hydrophobic group is reduced.

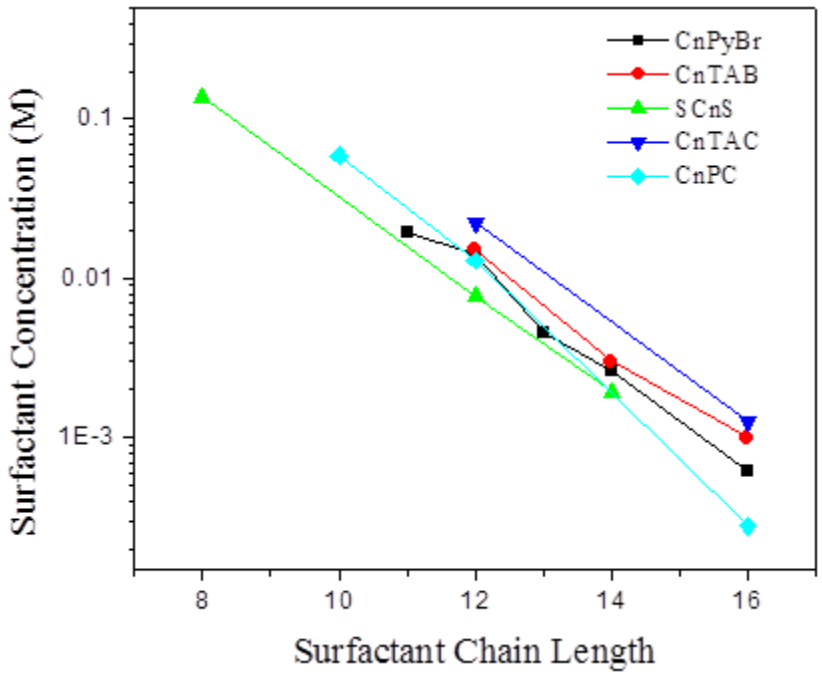


*Figure 103.* Critical micelle concentration (cmc) of the surfactants as a function of surfactant chain length. Plot was compiled from data obtained from: Alkylpyridinium bromide ($C_nPyBr$)[177], alkyltrimethylammonium bromide($C_nTAB$)[162], sodium alkyl sulfate (SC*n*S)[139], alkyltrimethylammonium chloride ($C_nTAC$)[133], and alkylpyridiniumchloride ($C_nPC$)[178].

*The Critical Aggregation Concentration (CAC):* When polymers are added to surfactant solution, polymer–surfactant interaction often causes surfactant molecules to aggregate at lower concentration than the CMC of the surfactant.

Oppositely-charge polyelectrolytes and ionic surfactants interact to form surface-active complexes at surfactant concentrations that are several decades lower than the surfactant CMC. Moreover, it has been suggested that that such interaction is cooperative with respect to surfactant. Increase in the alkyl chain length increases the cooperative interaction, which has been ascribed to hemi-micelle formation on the polyelectrolyte.[179] Increase in the alkyl chain length decreases the cac the polyelectrolyte-surfactant system (Figure 104).

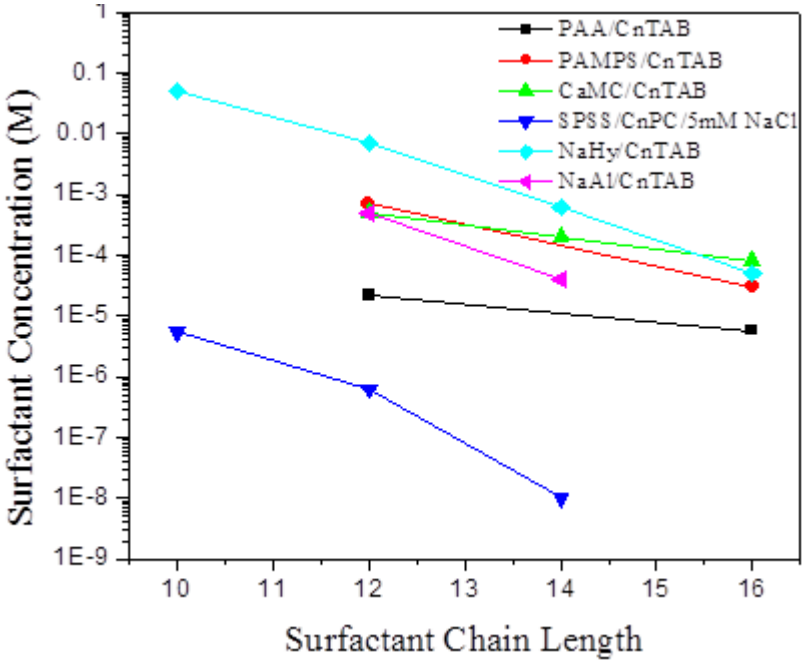


*Figure 104.* Critical aggregation concentration (cac) of the polelectrolyte/surfactant systems as a function of surfactant chain length. Data references: Poly(acry1ic acid)/ alkyltrimethylammonium bromide (PAA/$C_n$TAB)[147], poly(acrylamide sulfonate)/ alkyltrimethylammonium bromide (PAMPS /$C_n$TAB)[162], sodium carboxymethylcellulose/ alkyltrimethylammonium bromide (CaMC /$C_n$TAB)[162], sodium polystyrene sulfonate/ alkylpyridiniumchloride/5mM NaCl(SPSS/$C_n$PC/5mM NaCl)[178], sodium hyaluronate/ alkyltrimethylammonium bromide (NaHy /$C_n$TAB)[159]and sodium alginate/ alkyltrimethylammonium bromide (NaAl /$C_n$TAB)[159].

*The Binding Constant and Cooperative Parameter:* The degree of binding ($\beta$) for a polyelectrolyte surfactant system is defined as:

$$\beta = {(m_D - {m_D}^f)}/{m_p} \qquad \text{Equation 19}$$

where, $m_D$ = total surfactant concentration, ${m_D}^f$ = free surfactant concentration and $m_p$ = total polyelectrolyte concentration. A plot of degree of binding ($\beta$) vs. log ${m_D}^f$ is the called as binding isotherm (Figure 105).

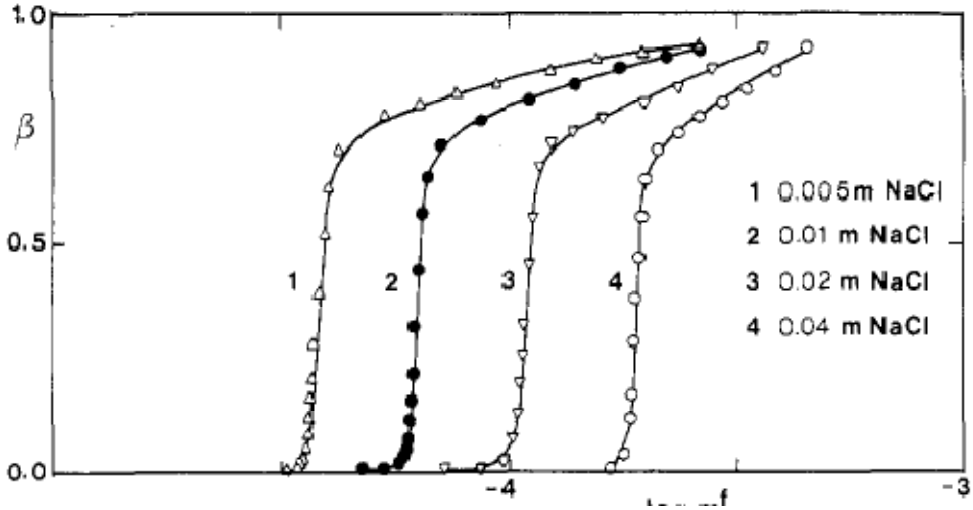


*Figure 105.* Binding isotherms for sodium dextran sulfate - undecyl-tetradecylpyridinium bromide - NaC1.[177]

The binding of a surfactant can occur at two different sites on the polyelectrolyte (Figure 106): an isolated site on the polyelectrolyte (site a*) or at a site where the neighboring site is already occupied by the surfactant (site b*).

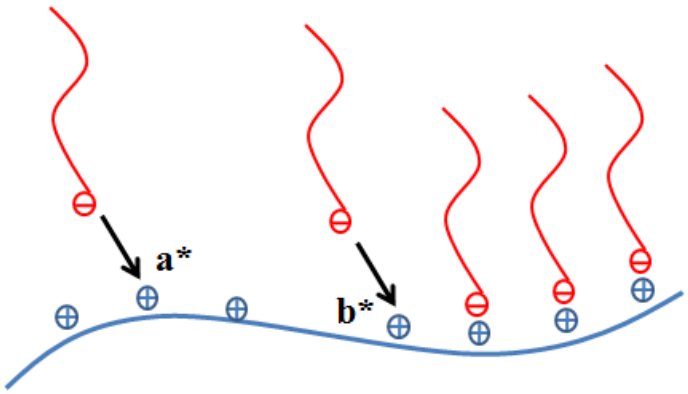


*Figure 106.* Schematic representation of binding of surfactant to a polyelectrolyte at isolated site (site a*) and occupied site (site b*).

The overall binding constant considers both situations and is expressed as[58,61,159,177];

$$Ku = (m_D{}^f)_{1/2}{}^{-1} \qquad \text{Equation 20}$$

where, K = binding constant of the surfactant at an isolated site on the polyelectrolyte

u = cooperative parameter which accounts for the binding of the surfactant neighboring the occupied site and is equal to slope of the binding isotherm at half bound point ($\beta = 0.5$). 'u' is expressed as:

$$\sqrt{u/4} = \left( d\beta / dInm_D{}^f \right)_{1/2} \quad \text{Equation 21}$$

Binding of an ionic surfactant to an oppositely charged polyelectrolyte reduces the ionic repulsion between the surfactant head groups. Once binding has occurred, hydrophobic chain-chain interaction drives cooperative binding of the free surfactant to the polyelectrolyte. This cooperativity is detected by an increase in the binding constant and cooperative parameter for these systems at concentrations in the vicinity of the CAC. The sodium dextran sulfate (NaDxS) and alkylpyridinium halides ($C_nPyX$) system, Kwak and coworkers found that the overall binding constant (Ku) and the cooperative parameter (u) increased with increase in the alkyl chain length (Figure 107).[177]

From the Figure 107, they observed that the increase in ln(Ku) is independent of the increase in the alkyl chain length and the salt concentration. This increase was found to grow with 1.29kT with each additional alkyl group in the chain when the free energy of binding at the half binding point, expressed as kTln(Ku). Furthermore, the cooperative parameter (u) increases with increase in the alkyl chain length: $u_{C_{11}Py^+} = 900 \pm 200$, $u_{C_{12}Py^+} = 1700 \pm 600$ and $u_{C_{13}Py^+}$ & $u_{C_{14}Py^+} = >2000$). This suggested that the cooperative binding increased with increase in the surfactants alkyl chain length.[177]

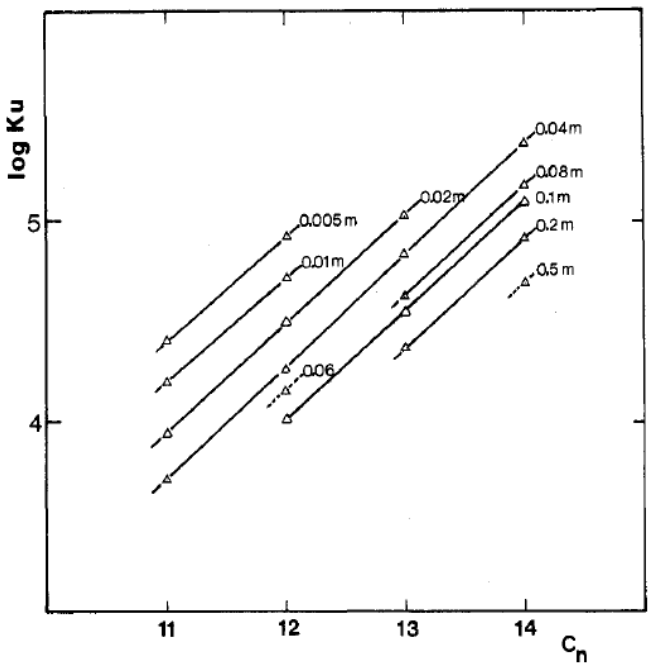


*Figure 107.* Binding constant (Ku) of the NaDxS/$C_n$PyX systems as a function of surfactant chain length, at different NaCl concentrations.[177]

*Coacervate Structure:* The organization of the surfactant molecule inside the polyelectrolyte/surfactant system results in highly ordered nanostructures.[106,180-188] The length of the surfactant tail is one of the important factors that differentiates between the possible internal structures. Increase in the surfactant tail length increases the hydrophobic interaction between the polyelectrolyte and surfactant, and it decreases the volume ratio of polar to non polar entities of the surfactant. These two effects favor nanostructure formation.[188]

The nanostructures formed by poly(sodium methacrylate) (PMAA) gel and alkyltrimethylammonium bromide ($C_n$TAB) (n = 8 to 18) have been studied by small angle X-ray scattering (SAXS) (Figure 108). It can be concluded from the above Figure that at n = 8, the complex shows a broad peak suggesting lack of orderliness in the structure. However, with increase in the carbon atoms in the alkyl chains (n = 10 to 16) sharp peaks were observed. According to the positioning of the peaks, it was inferred that

Pm3n cubic structure was formed. With increase in the surfactant tail length, the scattering peaks became sharper and stronger, suggesting increase in ordering of the nanostructure. This was a result of increase in the interaction between the surfactant-surfactant molecules and polymer-surfactant molecules through hydrophobic interaction. However, at n = 18, the sharp peaks disappeared. The gel lost ordered structure as the size of the gel mesh was too small to promote ordered structuring of the long alkyl chain. Thus, the fixed mesh size of the gel hindered the formation of the nanostructure.

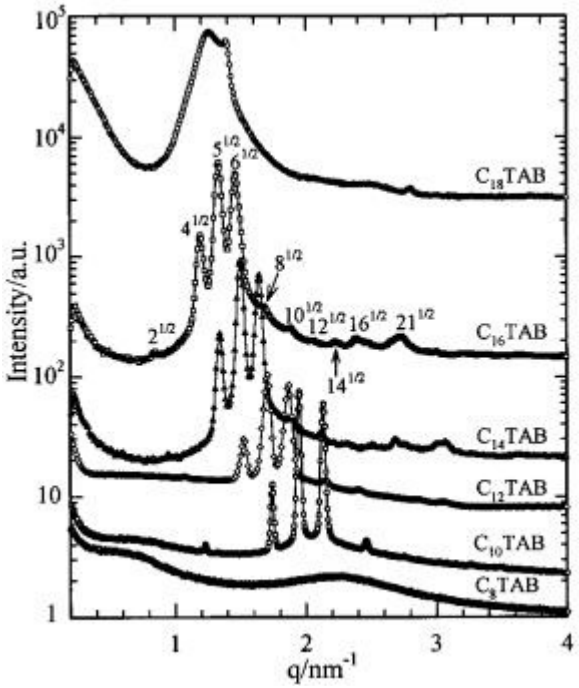


*Figure 108.* SAXS data of PMAA-$C_n$TAB complexes. 'n' denotes number of carbon atoms in the alkyl chain length.[188]

## Summary

Taylor and coworkers investigated the polyelectrolyte and surfactant systems displaying two distinct adsorption profiles observed on surface tension plot, using neutron reflectivity. One of the absorption profiles showed a strong absorption at the interface above $T_1$.[102,170] Whereas, the another absorption profile exhibited abrupt

increase the surface tension in the two phase region.[103] Taylor and coworkers were able to explain the adsorption behavior observed for these systems from the neutron reflectivity measurements. However, these studies were solely based on the surface analysis and therefore, did not relate the adsorption behavior to the bulk complexation.

Furthermore, Campbell and coworkers found that the extreme fluctuations in the surface tension in the PDMDAAC/SDS system, in the two phase region, was due to precipitation/suspension of the phase separated bulk complexes.[104,105] Mészáros and coworkers found that sample preparation method did not affect the surface tension of the poly(vinylamine) (PVAm)/ SDS system. They found that the preparation method influenced the physical properties of PVAm/SDS complex size in bulk, which ultimately produced same surface tension curve.[189] These studies concluded that the adsorption behavior is related to the bulk complexation in the system. However, this relation is not explained based on the polymer structural properties. Moreover, these studies are restricted to low polymer concentration.

Therefore, in this research, the relation between the adsorption behavior and bulk complexation has been explored over a wide polyelectrolyte concentration and analyzed with respect to polyelectrolyte structural properties such as molecular weight, charge localization, and backbone rigidity/hydrophobicity.

# CHAPTER II

# EXPERIMENTAL

## Materials

Cationically modified cellulosic polymers, JR400 & JR30M, with different molecular weight and charge density were supplied by Amerchol Corporation, a division of The Dow Chemical Company and were used as received. These polymers are synthesized by modification of hydroxyethylcellulose (HEC) via addition of trimethylammonium substituted epichlorohydrin to create quaternary ammonium salts with a chloride counterion. The average molar degree of ethoxylation of the unsubstituted HEC was 2.5. Synthetic polymers, poly(methacrylamidopropyltrimethylammonium chloride) (MAPTAC), and polyquaternium 76, were supplied by Rhodia, respectively and were used as received.

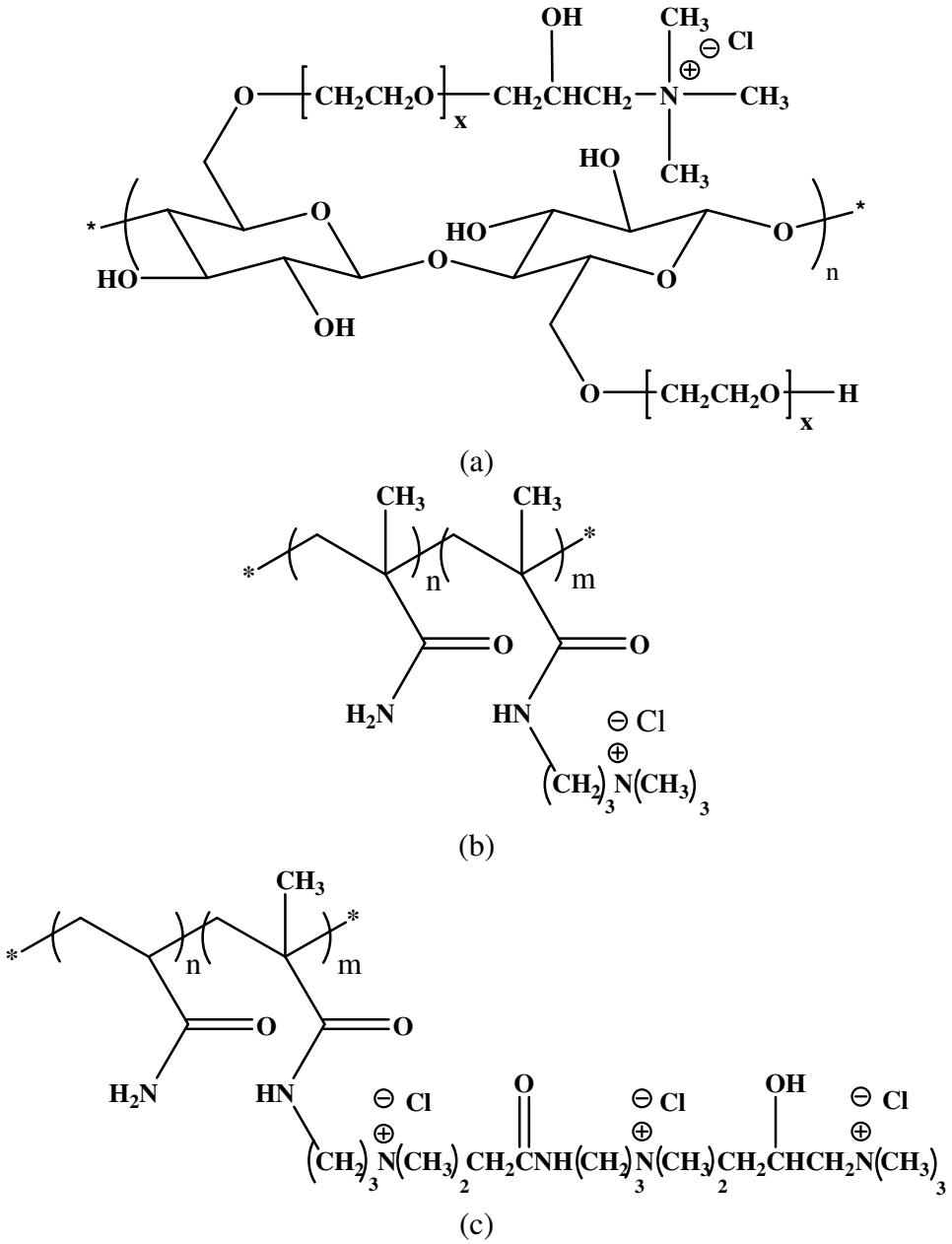

*Figure 109.* Chemical structure of cationic (a) quaternized hydroxyethylcellulose (JR400& JR30M) (b) methylene-*bis*-acrylamide methacrylamido propyltrimethyl ammonium chloride (MAPTAC) (c) polyquaternium 76 polymers.

Table 5

*Chemical composition and physical parameters of the cationic polymers.*

| Polymer | MW[a] ($10^3$ g/mol) | Rg[a] (nm) | C.D[b] (meq/g) |
|---|---|---|---|
| JR 400 | 568 ± 66 | 105.1 ± 9.9 | 1.33 |
| JR 30M | 1080± 130 | 142 ± 12 | 1.29 |
| MAPTAC | 1316 ± 45 | 67.1 ± 4.5 | 1.70 |
| AMT | 849 ± 42 | 87.4 ± 2.8 | 1.89 |

Data produced by [a] Zimm plot and [b] 13C NMR

Sodium dodecyl sulfate (SDS) was supplied by Sigma and was used as received. The chemical structure of the surfactant is shown in Figure 110.

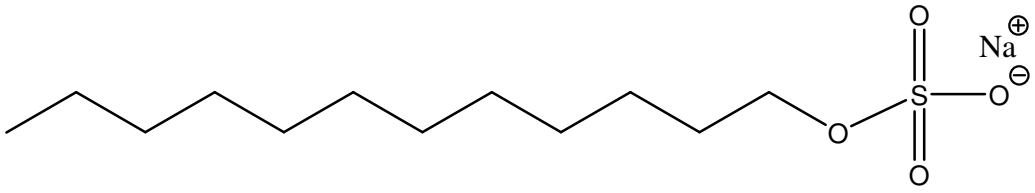


*Figure 110.* Chemical structure of SDS.

The critical micelle concentration (CMC) of SDS was determined in water at 25 $^{o}$C using surface tension measurements (Figure 111).

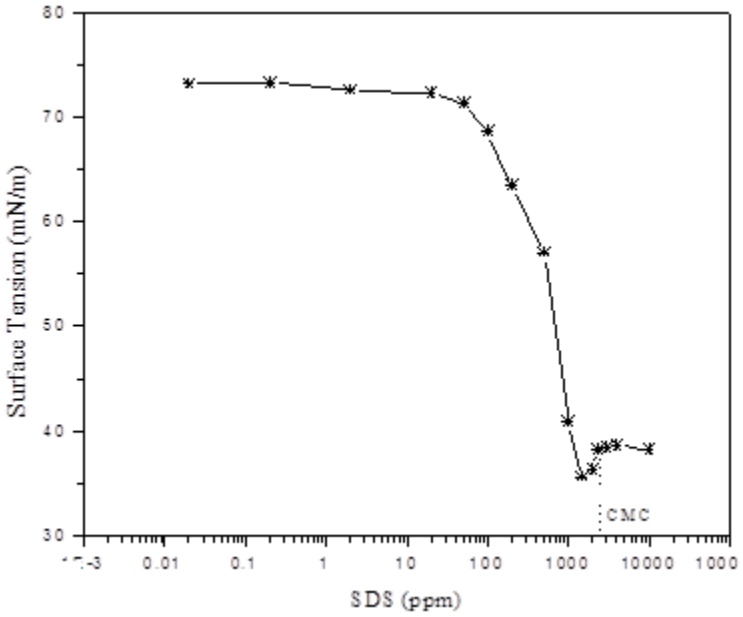


*Figure 111.* Surface tension curve of sodium dodecyl sulfate in water at 25°C.

The dip in the surface tension curve around 2000 ppm can be assigned to the impurities present in SDS. This is usually attributed to the long chain alkanols that are formed from the hydrolysis of SDS. The CMC of the SDS was found to be 2300 ppm i.e. 7.98 mM which is in good agreement with the reported value of 8.0 mM in the literature.[190]

Deionized water (resistivity = 18.0 MW) was obtained from Barnstead Nanopure reverse osmosis/filtration setup. Sodium chloride was purchased from Fisher Scientific and was used as received. Pyrene was purchased from Aldrich and was used as received. Cetylpyridinium bromide was purchased from Aldrich and was purified by ether extraction and four re-crystallizations from ethanol/ethyl acetate (v/v =1) mixture.

## Methods

*Sample Preparation*

The polymer and surfactant stock solutions were diluted to a concentration which was twice the required concentration in the mixture. To prepare all mixtures, the diluted polymer solution was added drop wise to a magnetically stirred diluted surfactant solution in equal amounts by weight, to form a polymer/surfactant mixture. These mixtures were mixed for 24 hours with a magnetic stirrer (at 500 rpm), and then were set aside undisturbed to achieve equilibrium for 48 hr. These mixtures were examined visually to determine the phase behavior.

*Zimm plot*

The weight average molecular weight of the polymers was measured by light scattering by plotting a Zimm plot (Figure 112 to 115). Incident light at 633 nm from a Spectra Physics Model 127 HeNe laser operating at 40 mW was used to perform static light scattering measurements on the polymer/surfactant mixtures. These mixtures were placed in a temperature controlled bath at 25 ± 0.1$^{o}$C, mounted on a Brookhaven Instruments BI-200SM goniometer with an avalanche photodiode detector and a TurboCorr correlator. The data was recorded over a wide angular range, 40$^{o}$ to 145$^{o}$ in steps of 5$^{o}$, and varying polymer concentration. The ionic strength of the polymer solution was adjusted to 0.5 wt. % of NaCl for each polymer. The dn/dc value was calculated for each polymer using a reflectometer. The measured molecular weights and radius of gyration are listed in Table 5.

$$\frac{K_c}{R_\theta} = \frac{1}{M_w} + \frac{2B(k_c)}{k} \quad \text{Equation 22}$$

where, $M_w$ = weight average molecular weight

B = second virial coefficient

k = arbitrary constant

c = concentration of the polymer

K is defined as

$$K = \frac{2\pi^2 n^2}{N_0 \lambda^4}\left(\frac{dn}{dc}\right)^2 \quad \text{Equation 23}$$

n = refractive index

$N_0$ = Avogadro's number

$\lambda$ = wavelength of light

$R_\theta$ = Raleigh ratio, defined as

$$R_\theta = \frac{r^2 i_\theta}{I_o(1 + \cos^2\theta)} \quad \text{Equation 24}$$

r = distance between the detector and the oscillating dipole

$i_\theta$ = intensity at angle $\theta$

$I_o$ = incident intensity

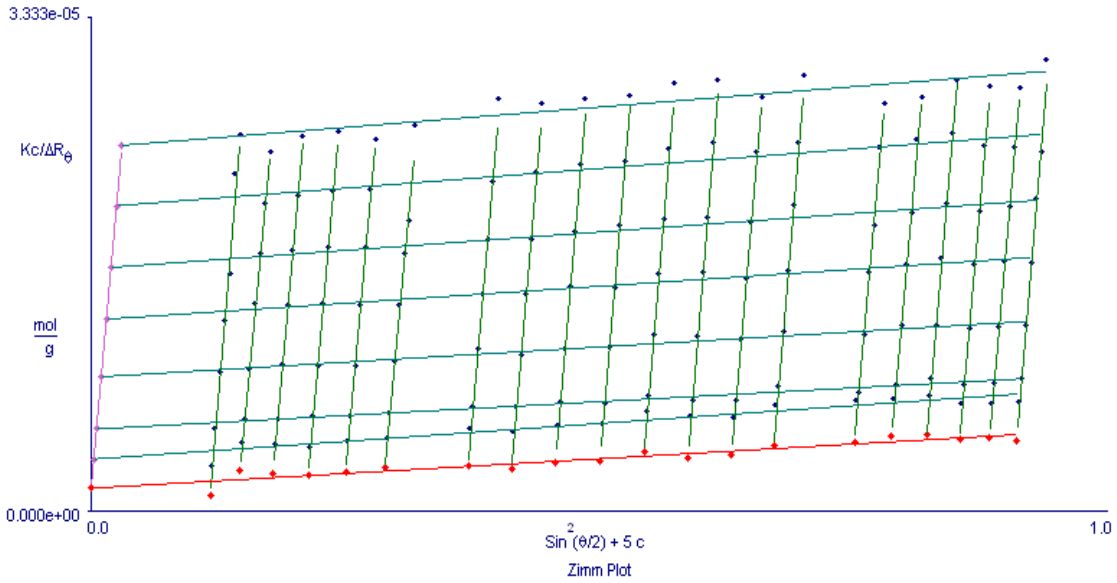


*Figure 112.* Zimm plot of JR400 in 0.5 wt. % NaCl aqueous solution at 25 °C.

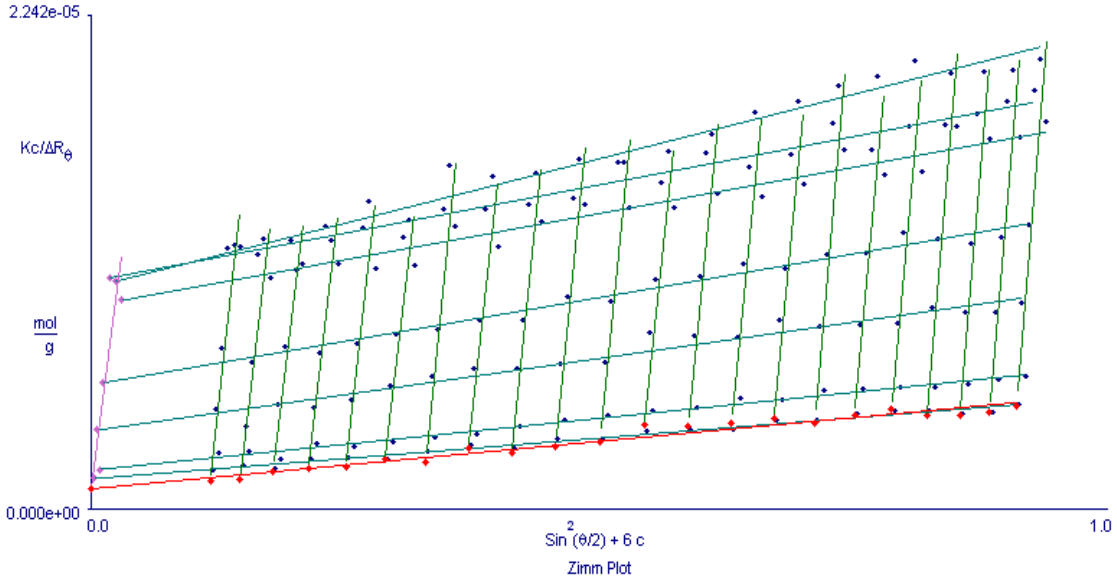


*Figure 113.* Zimm plot of JR30M in 0.5 wt. % NaCl aqueous solution at 25 °C.

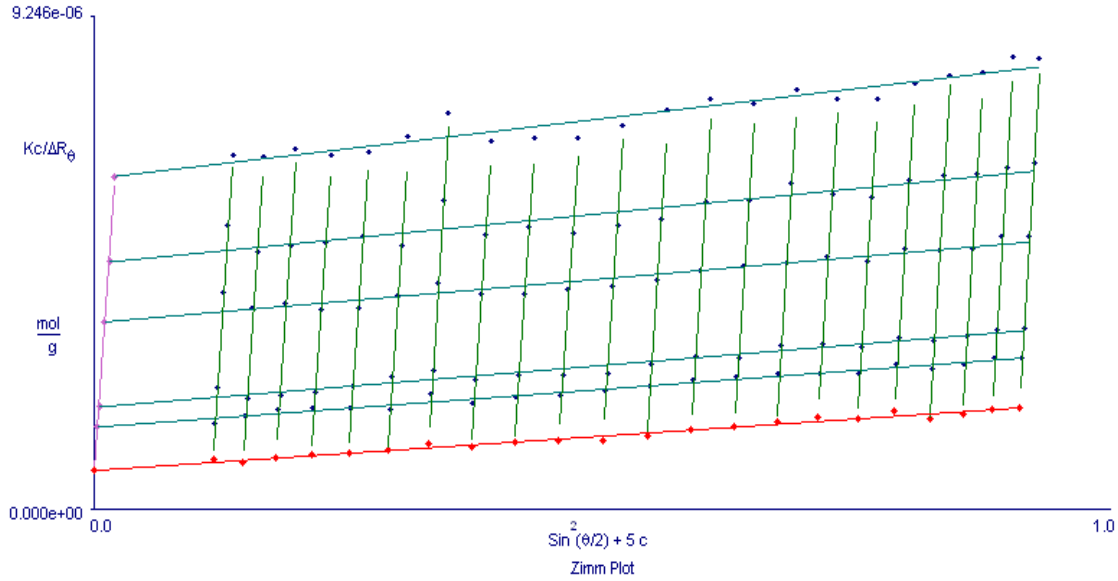


*Figure 114.* Zimm plot of MAPTAC in 0.5 wt. % NaCl aqueous solution at 25 °C.

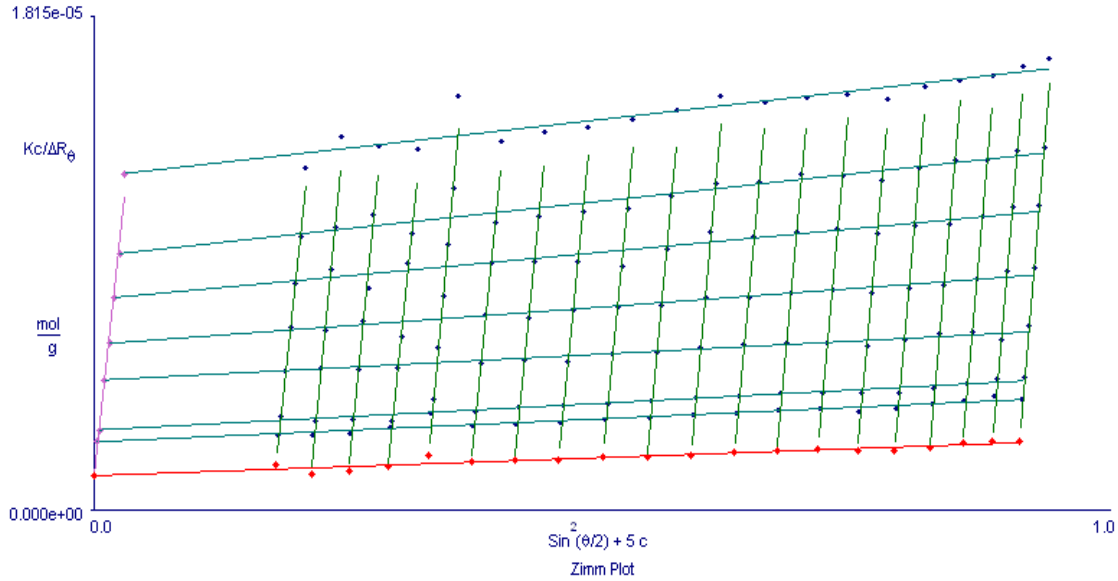


*Figure 115.* Zimm plot of polyquaternium 76 in 0.5 wt. % NaCl aqueous solution at 25 °C.

Table 6

*Molecular weight and radius of gyration of the cationic polymers.*

| Polymer | MW ($10^3$ g/mol) | Rg (nm) |
|---|---|---|
| JR 400 | 568 ± 66 | 105.1 ± 9.9 |
| JR 30M | 1080 ± 130 | 142 ± 12 |
| MAPTAC | 1316 ± 45 | 67.1 ± 4.5 |
| AMT | 849 ± 42 | 87.4 ± 2.8 |

*Nuclear Magnetic Resonance*

NMR analysis was used to determine the charge density of the cationic polymer used in this study. $^{13}$C NMR spectra were collected on the Varian UNITY-INOVA operating at 500 MHz. The charge density of the polymers was calculated by producing a $^{13}$C NMR spectra using Varian UNITY-INOVA 500 MHz spectrometer (Figure 116 to 119).

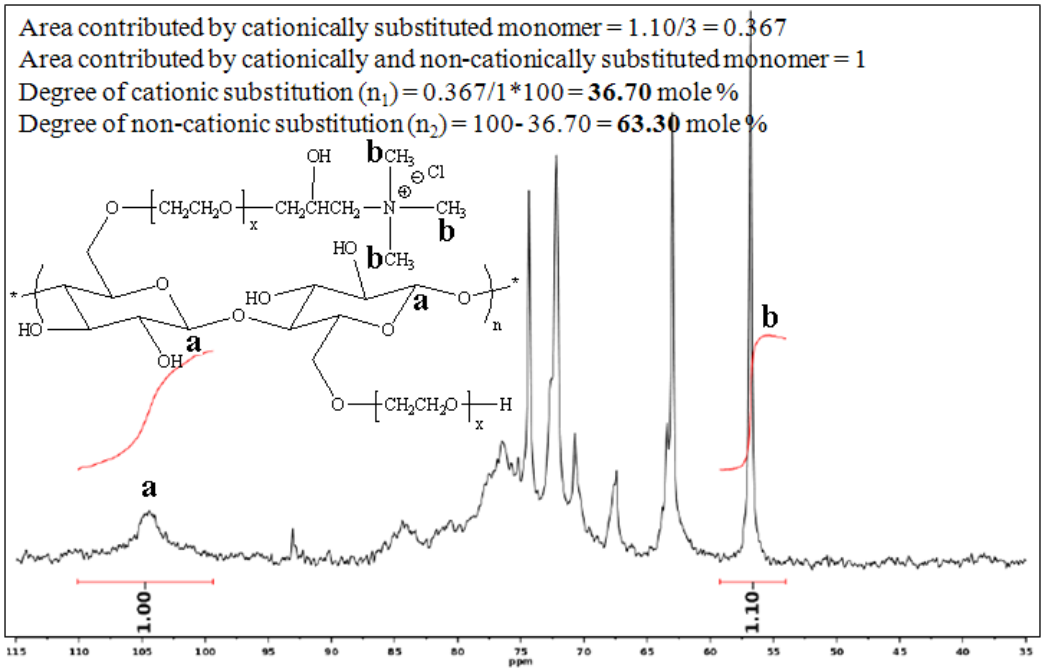


*Figure 116.* Structural analysis of JR400 by $^{13}$C NMR.

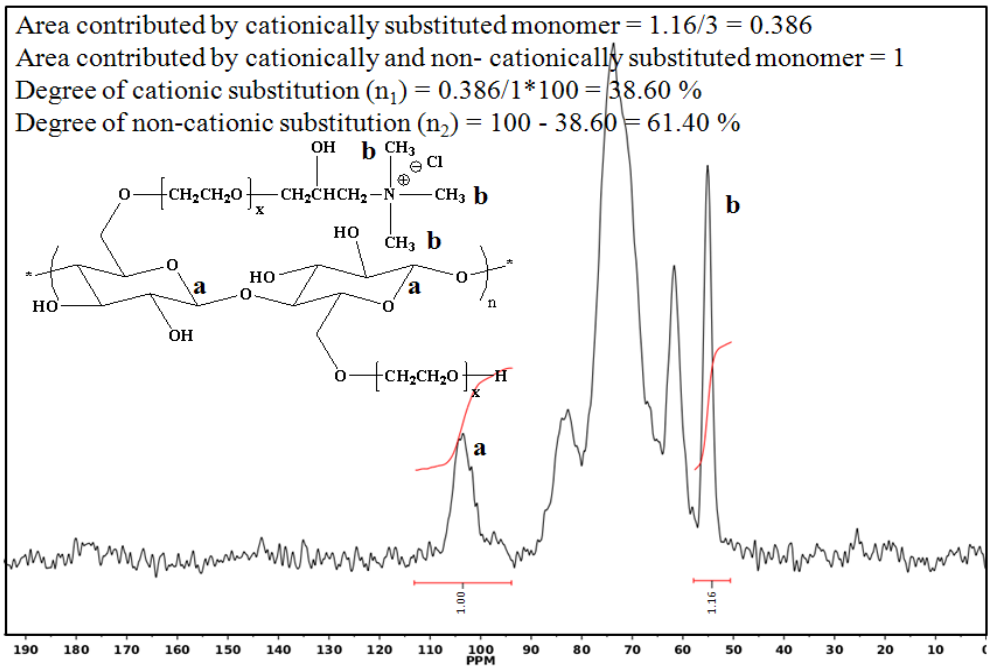


*Figure 117.* Structural analysis of JR30M by $^{13}$C NMR.

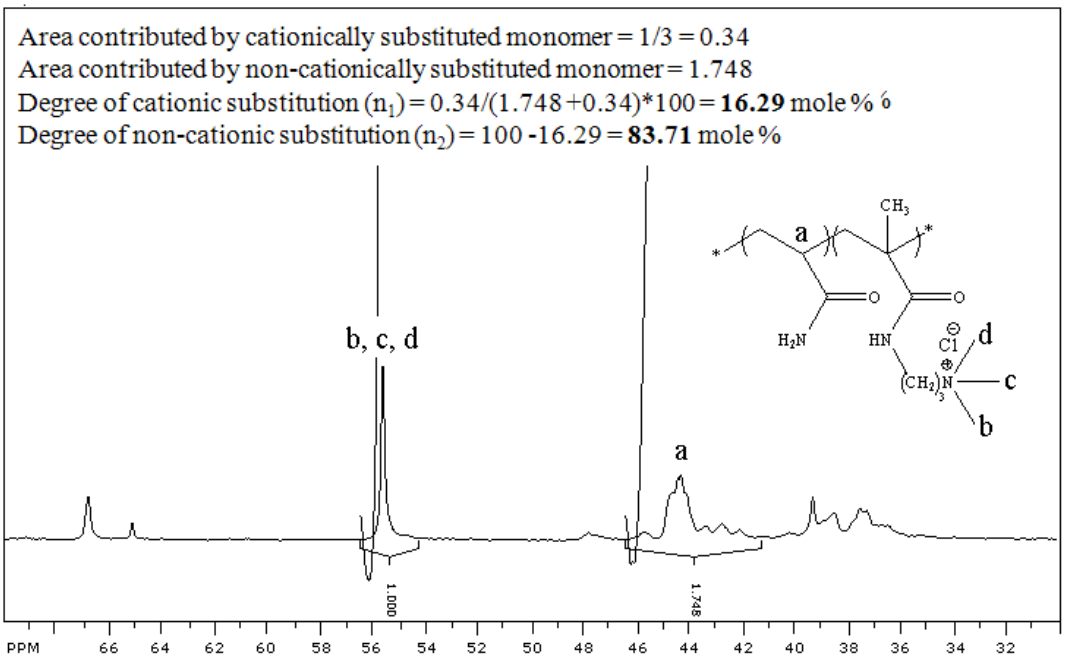


*Figure 118.* Structural analysis of MAPTAC by $^{13}$C NMR.

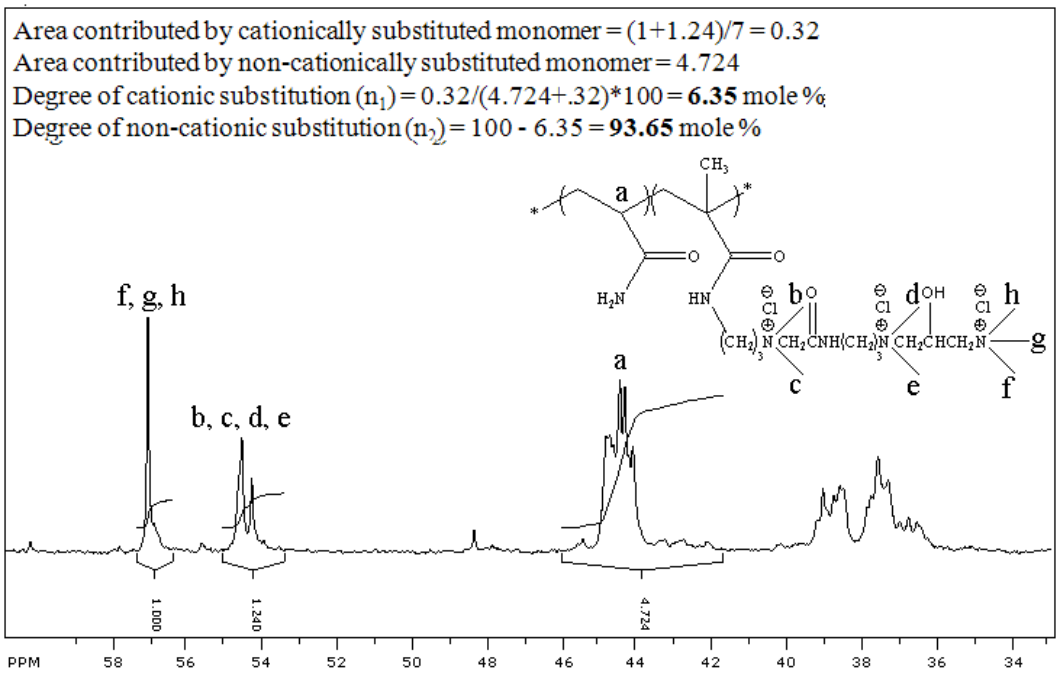


*Figure 119.* Structural analysis of polyquaternium 76 by $^{13}$C NMR.

Table 7

*Charge density of the cationic polymers.*

| Polymer | C.D. (mol %) | C.D. (meq/g) |
|---|---|---|
| JR 400 | 36.70 | 1.33 |
| JR 30M | 38.60 | 1.29 |
| MAPTAC | 16.29 | 1.7 |
| AMT | 6.35 | 1.89 |

*Surface Tension Measurements*

Surface tension measurements were performed on Krüss Processor Tensiometer K12 with Wilhelmy plate technique. In this technique, the interaction between the platinum plate and the surface of the solution being tested is measured in terms of force (F). The surface tension ($\gamma$) is related to force as;

$$\gamma = \frac{F}{l \cos \theta} \quad \text{Equation 25}$$

where, $l$ = is the perimeter of the Wilhelmy plate and $\theta$ = is the contact angle between the liquid phase and the plate and is assumed zero for complete wetting. For each test, the plate was dipped 2 mm inside the solution and the measurements were performed at 25 ± 0.5 $^{o}$C. The surface tension of DI water was found to be 72.05 mN/m. The plate was cleaned in between the runs by heating it, using a pencil flame propane torch before the measurements. The surface tension values were recorded when the standard deviation was below 0.1 mN/m, assuming equilibrium. In two phase region,

measurements were performed on the supernatant which was separated from the coacervate using the centrifugation process.

*Rheological Measurements*

The rheological measurements were performed on AR G2 rheometer (TA instruments) using double wall standard-size double concentric cylinder geometry with a set gap size (500 μm), at 25 ± 0.1 $^{o}$C. The steady state flow measurements were recorded in the 0.01 to 1000$s^{-1}$ shear rate region. The viscosity in the linear visco-elastic region was selected to compare the results. The dynamic rheological measurements such as elastic modulus (G'), loss modulus (G"), and complex viscosity (η*), were recorded in the 0.01 to 10Hz range at constant oscillation stress. This value was selected from a linear visco-elastic modulus region from a plot of elastic modulus vs. oscillation stress ($10^{-4}$ Pa to 1 Pa) at a constant frequency (1Hz).

In the two phase region, the rheological measurements were performed on coacervate using cone and plate geometry, at 25 ± 0.1$^{o}$C. The coacervate was separated using centrifugation process at 3000 rpm for 30 min. The steady state flow measurements were recorded in the 0.01 to 1000$s^{-1}$ shear rate region. The dynamic rheological measurements such as elastic modulus (G'), loss modulus (G"), and complex viscosity (η*), were recorded in the 0.01 to 10 Hz range at constant oscillation stress.

*Fluorescence Measurements*

The fluorescence spectra for polymer/surfactant mixtures were recorded on Infinite® M1000 (Tecan Group Ltd.) using pyrene as the fluorescence probe. The samples were loaded in a 96 well plate with glass wells. In the two phase region, only supernatant was analyzed. The emission scans of the polymer/surfactant mixtures were

recorded from 350 to 500 nm at constant excitation wavelength of 334 nm, excitation bandwidth of 5 nm, emission bandwidth of 15 nm, step size of 1 nm, and integration time of 1000 μs. These measurements were used to determine the critical aggregation concentration (CAC), micro-polarity and aggregation number of the polymer/surfactant mixtures.

# CHAPTER III

## EFFECT OF POLYMER CONCENTRATION AND MOLECULAR WEIGHT

In this chapter, the relation between the adsorption behavior and bulk complexation were explored in the low molecular weight JR400 and high molecular weight JR30M polymer with SDS, over a broad range of polymer concentration. The adsorption profile of this system was monitored using surface tension measurements, whereas, the bulk complexation was studied using rheological and fluorescence measurements.

### Polymer Solution Viscosity

For a polyelectrolyte solution, the concentration is divided into different regimes based upon the relationship between the solution specific viscosity and the polyelectrolyte concentration (Figure 120).[191,192] In the very dilute regime the specific viscosity increases as the polymer concentration decreases.[193] This inverse relationship is known as the 'polyelectrolyte effect'.

- In the dilute concentration regime, the viscosity increases with concentration and follows a $\eta \sim C$ relation.
- In the unentangled semi-dilute concentration regime, the viscosity gradually increases with concentration and follows a $\eta \sim C^{1/2}$ relation.
- In the entangled semi-dilute concentration regime, viscosity considerably increases with concentration and follows a $\eta \sim C^{3/2}$ relation.

These regimes are observed at very low, low and high polyelectrolyte concentrations, respectively. The concentration corresponding to the switch from dilute to unentangled semi-dilute concentration regime is defined as the critical overlap

concentration (C*), whereas, the switch from unentangled to entangled semi-dilute concentration regime is defined as the critical entanglement concentration ($C_e$). In the unentangled semi-dilute concentration regime, the polyelectrolyte chains overlap but do not entangle, while in the entangled semi-dilute concentration regime, the polyelectrolyte chains entangle.

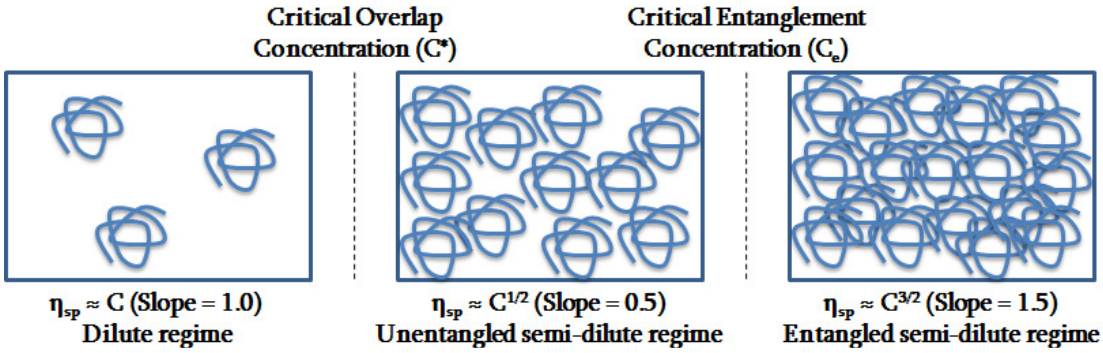


*Figure 120.* Different concentration regimes of a polyelectrolyte.

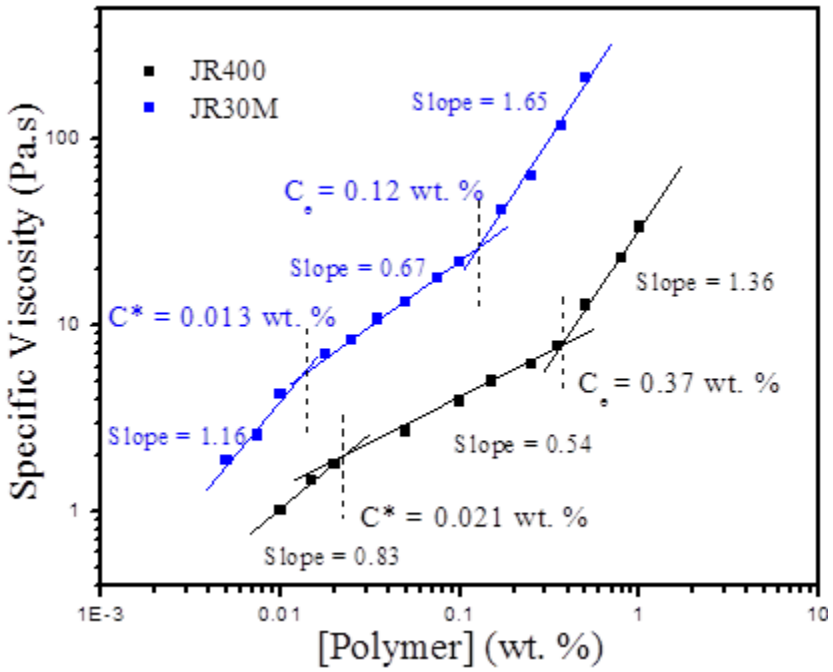


*Figure 121.* Critical overlap concentration (C*) and critical entanglement concentration ($C_e$) of JR400 and JR30M.

One of the aims of this research is to attempt to understand the mechanisms of polyelectrolyte/surfactant interaction by analyzing the adsorption behavior and bulk complexation of polyelectrolyte/SDS systems over this broad range of polyelectrolyte concentrations. In order to select the appropriate polyelectrolyte concentrations, initially, the concentration regimes were located by measuring the specific viscosity of the polyelectrolyte solution at different polyelectrolyte concentrations. The specific viscosity vs. concentration plot showed three defined slopes for JR400 and JR30M (Figure 121). This indicates that the specific viscosity and concentration relation follows the scaling theory of polyelectrolytes. Hence, for the low molecular weight JR400 the dilute regime lies below 0.021 wt. %, the unentangled semi-dilute regime is between 0.021 and 0.37 wt. % and the entangled semi-dilute regime is above 0.37 wt. %. For JR400, the critical overlap concentration is at 0.021 wt. % and the critical entanglement concentration is at 0.37 wt. %. Similarly, for the high molecular weight JR30M, the dilute regime lies below 0.013 wt. %, the unentangled semi-dilute regime between 0.013 and 0.12 wt. %, and the entangled semi-dilute regime above 0.12 wt. %. For JR30M, the critical overlap concentration is at 0.013 wt. % and the critical entanglement concentration is at 0.12 wt. %.

Table 8

*Selected JR400 and JR30M concentrations for this study.*

| Concentration Regime | [JR400] (wt. %) | [JR30M] (wt. %) | Cr = Cp/Ce |
|---|---|---|---|
| | 0.10 | 0.032 | ~ 0.27 |
| Unentangled | 0.15 | 0.05 | ~ 0.40 |
| Semi Dilute | 0.25 | 0.08 | ~ 0.70 |
| Entangled | 0.50 | 0.16 | ~ 1.35 |
| Semi Dilute | 0.80 | 0.26 | ~ 2.16 |

Our preliminary experiments showed that the surface tension of JR400/SDS and JR30M/SDS system showed an unexpected increase in surface tension at polymer concentrations above 0.1 wt % and 0.032 wt %, respectively (see details in Figure 122 below). Therefore, for this study, we have the selected rest of the concentrations above these concentrations which lie in the unentangled to entangled semi-dilute regime (Table 8).In the following discussion, these concentrations are expressed in terms of $C_r$, which is a ratio of polyelectrolyte concentration ($C_p$) to critical entanglement concentration ($C_e$).

Surface Tension Measurements

Surface tension ($\gamma$) measurements of aqueous solutions of SDS with and without JR400 and JR30M are shown in Figure 122 and 123, as a function of SDS concentration. In these measurements, the polymer concentration in the JR400/SDS and JR30M/SDS system was varied to encompass the unentangled to entangled semi-dilute regimes. The surface tension was measured directly on the solution in the single phase region. For the

two-phase region, the surface tension was measured on the supernatant which was separated from the coacervate by centrifugation.

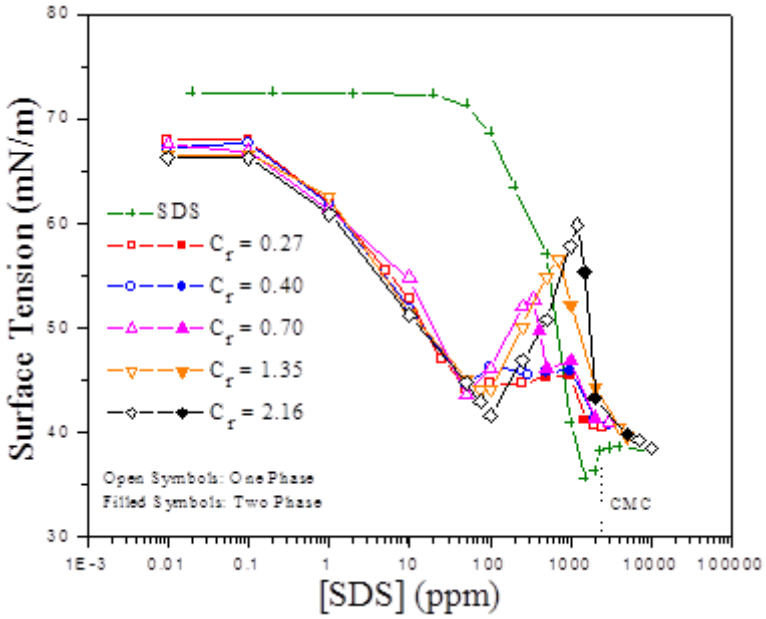


*Figure 122.* Surface tension curves of JR400/SDS system at different $C_r$, as a function of [SDS]. Empty symbols correspond to the one phase region and filled symbols correspond to the two phase region.

In the surfactant system, a decrease in the surface tension indicates adsorption of the surfactant molecules at the interface. However, at a certain surfactant concentration, the surface tension hardly changes with additional surfactant concentration. This corresponds to the surfactant concentration at which micelles form: the critical micelle concentration (CMC).[176] For the SDS system, the CMC value was found to be 2300 ppm i.e. 7.98 mM. This is close to the published value(8 mM).[190] The dip in the surface tension curve around 2000 ppm can be assigned to the impurities present in SDS. This is usually attributed to the long chain alkanols that are formed from hydrolysis of SDS in an aqueous environment.

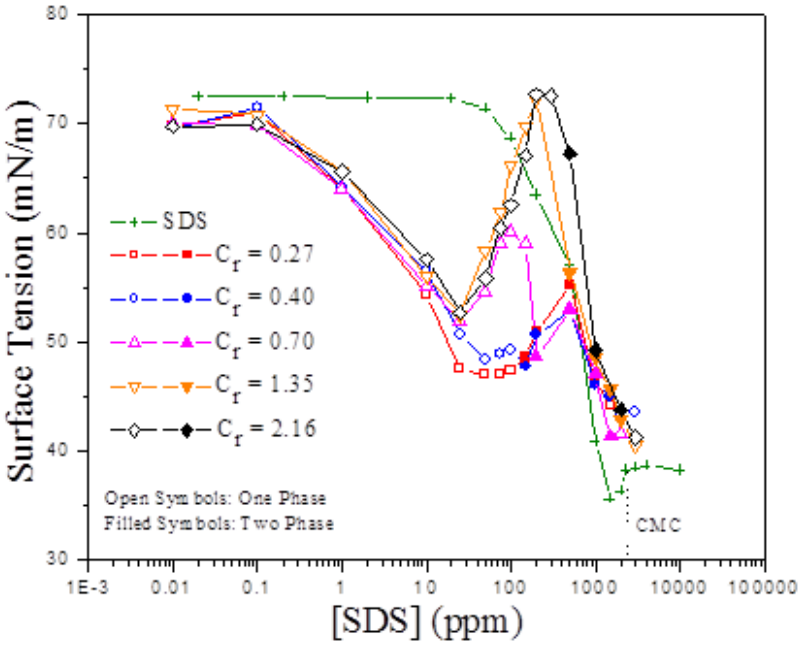


*Figure 123.* Surface tension curves of JR30M/SDS system at different $C_r$, as a function of [SDS]. Empty symbols correspond to the one phase region and filled symbols correspond to the two phase region.

In the presence of SDS, for all values of $C_r$ that were investigated, the surface tension of the JR400/SDS and JR30M/SDS system was considerably lower than SDS alone at concentrations that corresponded to the two-dimensional gaseous state for SDS. This measurably lower surface tension has been attributed to the formation of surface active polymer/surfactant complexes.[81,162,194-197] The enhanced surface activity of the complex is attributed to the enhanced hydrophobicity of the complex, which arises due to the adsorption of surfactant on the polymer. The first break point noticed on the polymer-surfactant surface tension curve is referred to as the critical aggregation concentration (CAC) of the polymer/SDS system.[162] Above this concentration, the surfactant forms micellar aggregates on the polymer.

In the JR400/SDS system, for $C_r \leq 0.40$, the surface tension decreased to a constant value at the CAC, and then, gradually decreased in the two phase region. This

signifies strong absorption of the JR400/SDS complex at the air-water interface. Similar surface tension behavior was observed in other polymer/surfactant systems.[102,170] On the other hand, with increase $C_r$ ($\geq$ 0.70 wt. %) the surface tension significantly increased as a function of SDS concentration in the one phase region above the CAC. As soon as the system entered the two phase region, the surface tension drastically decreased. Thus, a peak is observed on the surface tension curve. This behavior has been reported for other polymer/surfactant systems.[103-105,173,198-201] But in these instances, this peak appeared only in the two phase region.

Similar to the JR400/SDS system, in the JR30M/SDS system, for $C_r \leq 0.40$ the surface tension stayed constant in one phase region above the CAC. However, the surface tension increased in the two phase region. A similar increase in the surface tension was observed in the two phase region in other systems and was attributed to loss of polyelectrolyte and surfactant from the interface due to precipitation.[103-105] However, for $C_r \geq 0.70$ wt. %, the surface tension considerably increased in the one phase region above the CAC, and then drastically decreased in the two phase region.

In addition, in our system, with increase in the $C_r$ and molecular weight, the peak height increased and the surface tension peak apex moved to right (crossing the pure [SDS] surface tension curve). This suggests strong desorption from the interface, and it intensified with increase in the $C_r$.

Steady state flow measurements

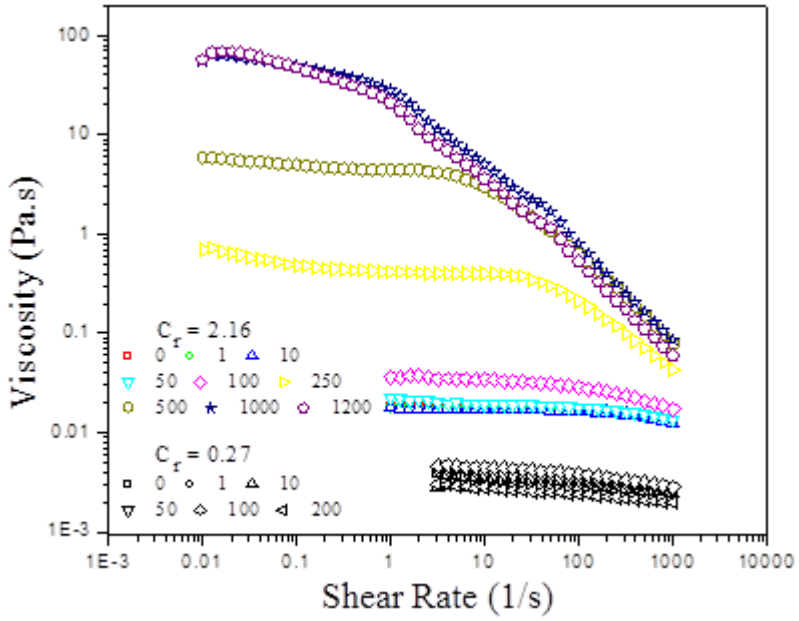


*Figure 124.* Viscosity of the JR400/SDS system at $C_r$ = 0.27 and 2.16, at different [SDS] in one phase region, as a function of shear rate. Legend: [SDS] in ppm.

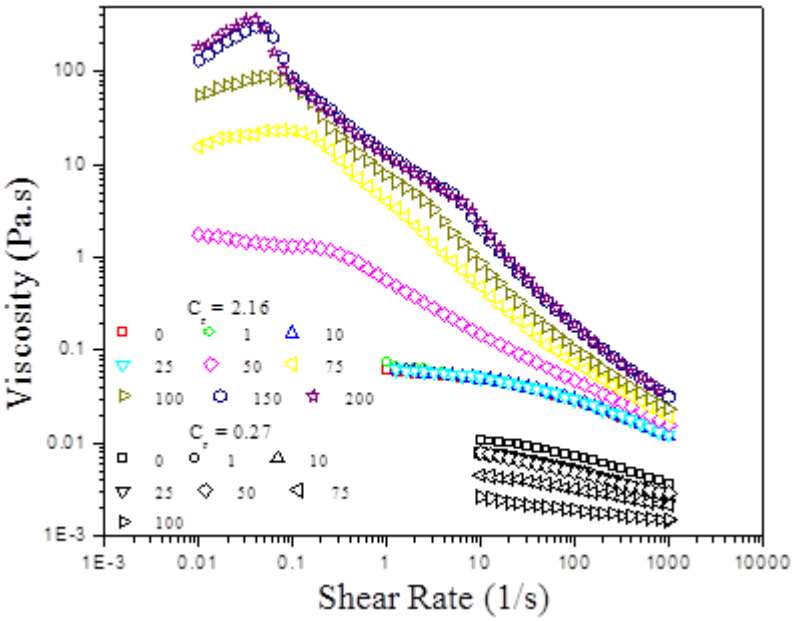


*Figure 125.* Viscosity of the JR30M/SDS system at $C_r$ = 0.27 and 2.16, at different [SDS] in one phase region, as a function of shear rate. Legend: [SDS] in ppm.

Figure 124 and 125 show the viscosities of the JR400/SDS and JR30M/SDS system at $C_r$ = 0.27 and 2.16 at different [SDS] in the one phase region, as a function of the shear rate. In the JR400/SDS system at $C_r$ = 2.16, the viscosity increased gradually up to the CAC (100 ppm SDS) of the system. However, above the CAC, the viscosity increased significantly. In addition, shear thinning behavior was also observed in this system above the CAC. This indicates a stronger association between the polymer and surfactant due to crosslinking of polymer chains by the surfactant aggregates developed on the chain,[202-205] leading to the formation of a gelled polymer network.[150,202] In contrast, at $C_r$ = 0.27, a small variation in viscosity is observed and shear thinning is absent, throughout the studied [SDS]. This indicates that crosslinking of polymer chains is unlikely. Likewise, in the JR30M/SDS system at $C_r$ = 2.16, strong gels were formed above the CAC (25 ppm SDS), whereas, at $C_r$ = 0.27, weak gels were formed throughout the studied [SDS] range.

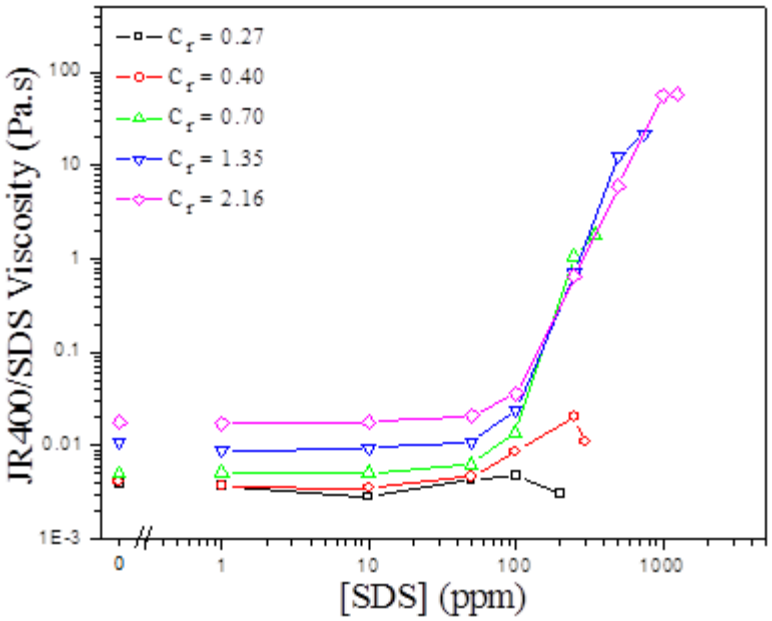


*Figure 126.* Viscosity of the JR400/SDS system at different polymer concentration, as a function of [SDS].

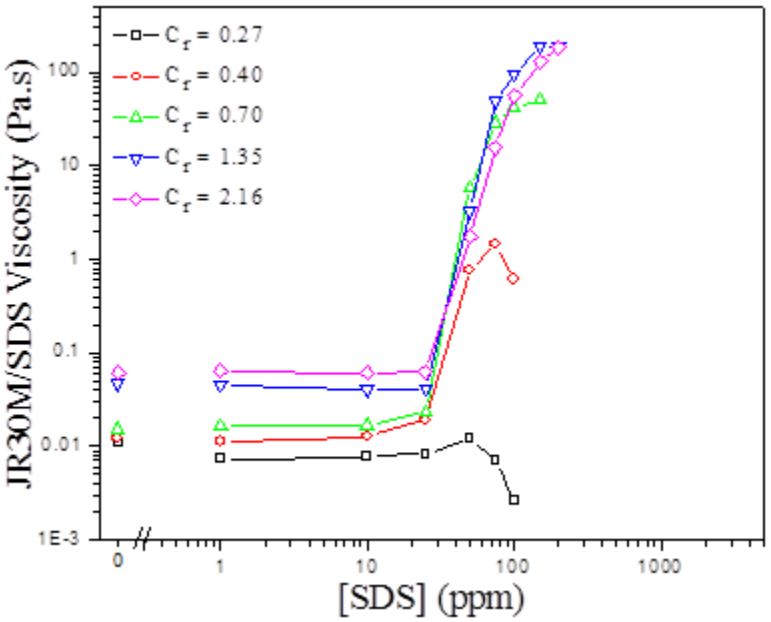


*Figure 127.* Viscosity of the JR30M/SDS system at different polymer concentration, as a function of [SDS].

In order to compare the viscosity results within the JR400/SDS and JR30M/SDS systems at different polymer concentration, viscosity versus SDS concentration plots were produced (Figure 126 and 127). These plots show clearly that the viscosity is highly

dependent on both the polymer and SDS concentration, and there are indications of critical concentrations for each of these components.

Below the CAC, at $C_r = 0.27$, the viscosity of JR400 and JR30M system decreased slightly on addition of SDS. This could be attributed to the added surfactant screening the polymer charge and reduction of the size of the polymer chain and possibly intramolecular hydrophobic interaction causing further reduction of the polymer's hydrodynamic volume.[203,206] However, the viscosity slightly increased around the CAC. This is attributed to the association between the polymer chains through surfactant micelles.[206] On the other hand, with increase in the polymer concentration, the viscosity is affected slightly below CAC. This indicates that the size of the polymer chain stayed unaltered in that region.

In contrast, above the CAC, the viscosity strongly depends on the polymer concentration in the JR400/SDS and JR30M/SDS systems. At $C_r = 0.27$, the viscosity of the system falls below the viscosity of the polymer solution without SDS. This kind of behavior was accredited to shrinking of the polymer.[162,203,206] However, as the polymer concentration increased ($C_r \geq 0.40$), the viscosity increased significantly, which as described earlier could be attributed to crosslinking of polymer chains by the surfactant aggregates. The maximum viscosity ($V_{max}$) attained by the polymer/SDS system increased with the polymer and surfactant concentration as well as the polymer molecular weight. From the viscosity results, it is seen that the fluctuations in the viscosity are noticeable above the CAC of the system. This is because the CAC marks the onset of the bulk complexation.

Furthermore, above the CAC, the viscosity of the system scaled more excessively with polymer concentration in the order $C_r = 0.70 > 1.35 > 2.16$ in both JR400/SDS and JR30M/SDS systems. Wu and coworkers observed that the viscosity increase in the unentangled concentration regime depends on polymer charge density for the poly(acrylic acid) (PAA), and cationic surfactant, alkyltrimethylammoniumbromide ($C_nTAB$, n = 12 & 16) system.[207] Increase in the viscosity was more pronounced at lower PAA charge density compared to higher charge density. To further elaborate this relation in our system, we have calculated the relaxation time of the gelled polymer network from the viscosity verses shear rate plot (Figure 124 and 125). The start of the shear thinning region is considered as the relaxation time.[202] At a particular polymer concentration, the relaxation time increased with increase in [SDS]. This is because the amount of SDS molecules in the crosslink increased with increase in [SDS], resulting in further strengthening of the network. However, at a particular [SDS], the relaxation time initially increased and then later on decreased (as seen in the JR30M/SDS system) with decrease in the polymer concentration. With decrease in polymer concentration, the cationic charges in the system decreases. It is plausible to postulate that the amount SDS molecules in the aggregates increase, thereby, increasing the number of junction zones, strengthening the network and increasing relaxation time. However, with further decrease of cationic charges, stoichiometry dictates that the hemi-micellar aggregates saturate each chain, whereupon the chains experience mutual repulsion and the network is disrupted – thereby lowering the relaxation time. Moreover, the relaxation time increases as the molecular weight of the polymer increases. This is consistent that the high molecular

weight polymer forms a strong gelled polymer network with more entanglements and micellar crosslinks than the polymer of lower molecular weight.

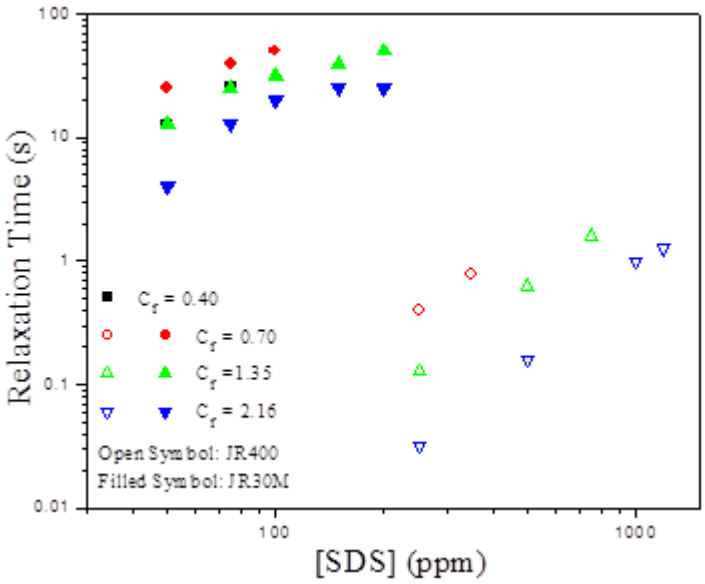


*Figure 128.* Relaxation time of gelled JR400/SDS and JR30M/SDS system at different polymer concentration, as a function of [SDS].

Dynamic rheological measurements

The dynamic rheological properties of the JR400/SDS and JR30M/SDS systems were measured at different polymer and SDS concentration, as a function of frequency (0.01 to 10 Hz) and at a constant oscillation stress value ($10^{-3}$ Pa). This stress value was chosen from the linear elastic modulus region on the elastic modulus verses oscillation stress ($10^{-4}$ to 1 Pa) plot. The dynamic rheological properties of the systems failing to show a linear elastic modulus region on the elastic modulus verses oscillation stress plot were not included in this analysis.

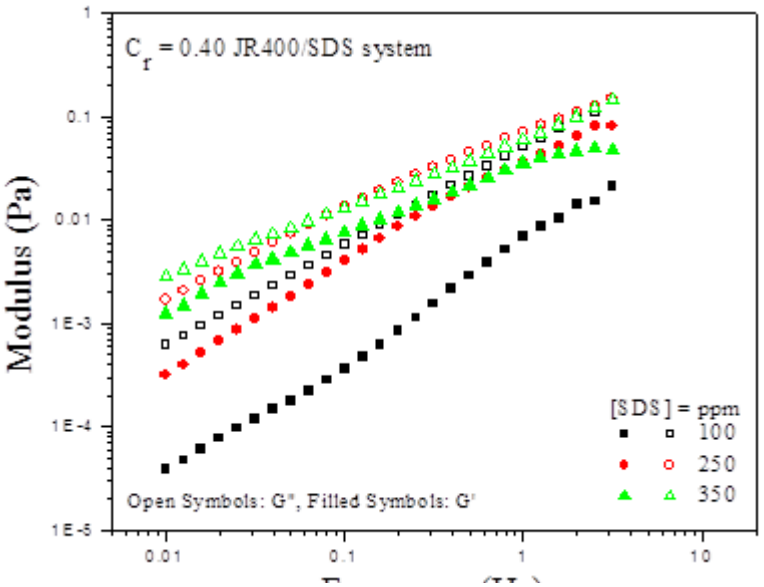


*Figure 129*. Elastic Modulus (filled symbols) and loss modulus (open symbols) of the JR400/SDS system at $C_r = 0.40$, as a function of frequency.

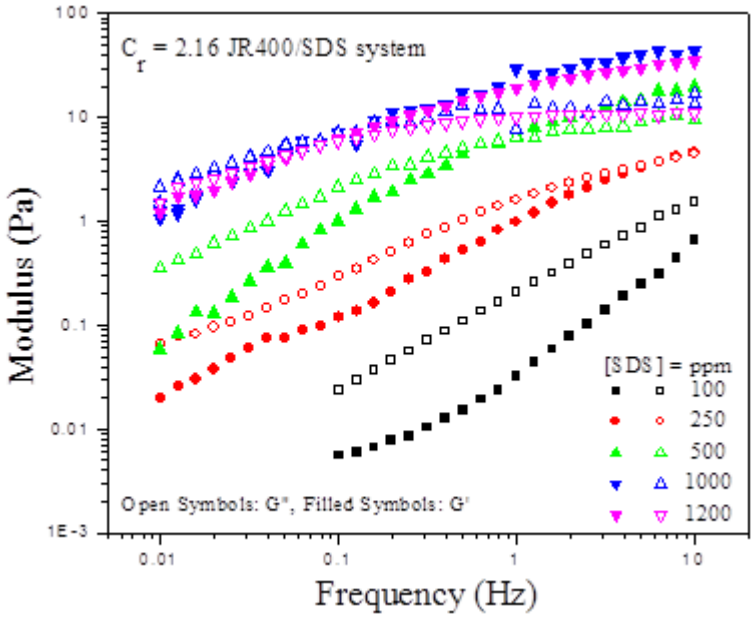


*Figure 130.* Elastic Modulus (filled symbols) and loss modulus (open symbols) of the JR400/SDS system at $C_r = 2.16$, as a function of frequency.

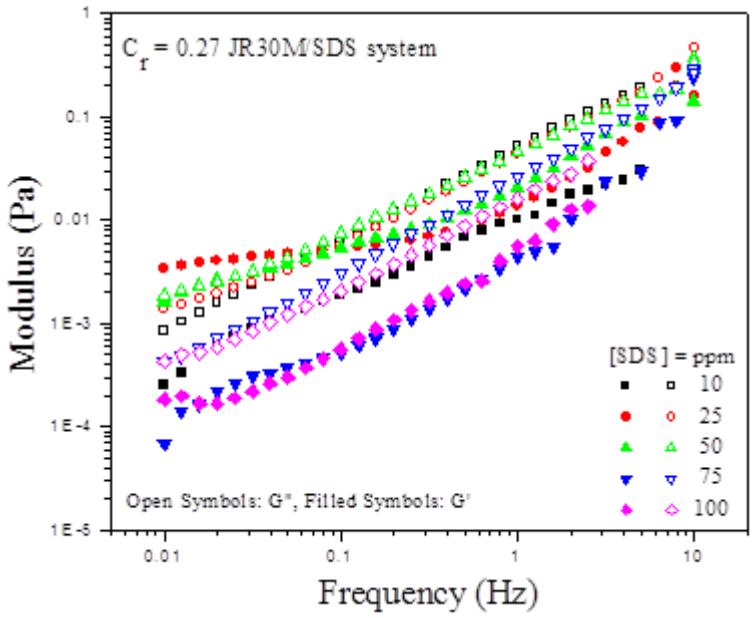


*Figure 131*. Elastic Modulus (filled symbols) and loss modulus (open symbols) of the JR30M/SDS system at $C_r = 0.27$, as a function of frequency.

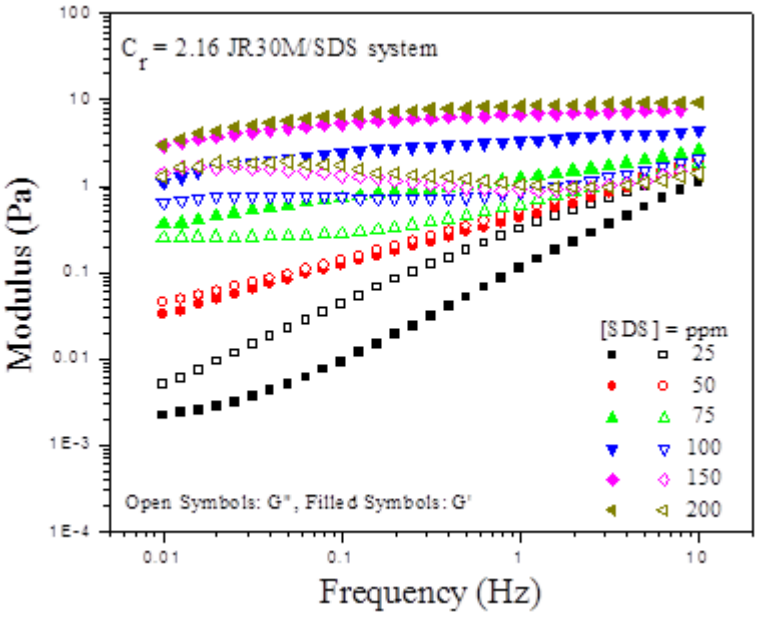


*Figure 132*. Elastic Modulus (filled symbols) and loss modulus (open symbols) of theJR30M/SDS system at $C_r = 2.16$, as a function of frequency.

Figures 129 to 132 show the modulus of the JR400/SDS and JR30M/SDS system at different $C_r$ and [SDS], as a function of frequency. At lower polymer concentration (lower $C_r$), the loss modulus is higher than the elastic modulus in both systems even though the [SDS] is above the CAC. This indicates the formation of weak gel at lower $C_r$.

On the other hand, at higher polymer concentration (higher $C_r$), the elastic modulus of the system is significantly higher than the loss modulus in both systems, with increase in the [SDS] beyond the CAC. This suggests formation of a strong polymer and SDS network through SDS crosslinks or micellar junction zones at higher $C_r$.

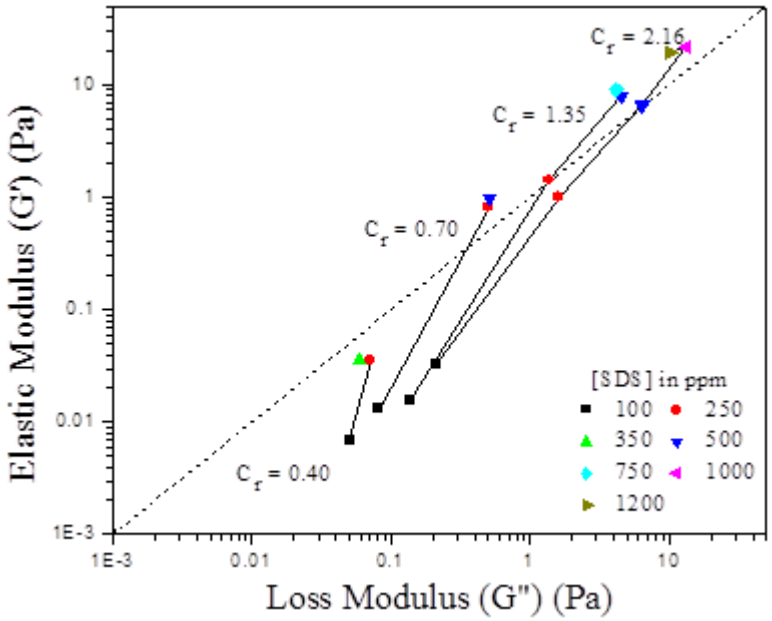


*Figure 133.* Elastic Modulus and loss modulus of the JR400/SDS system at 1 Hz and different $C_r$.

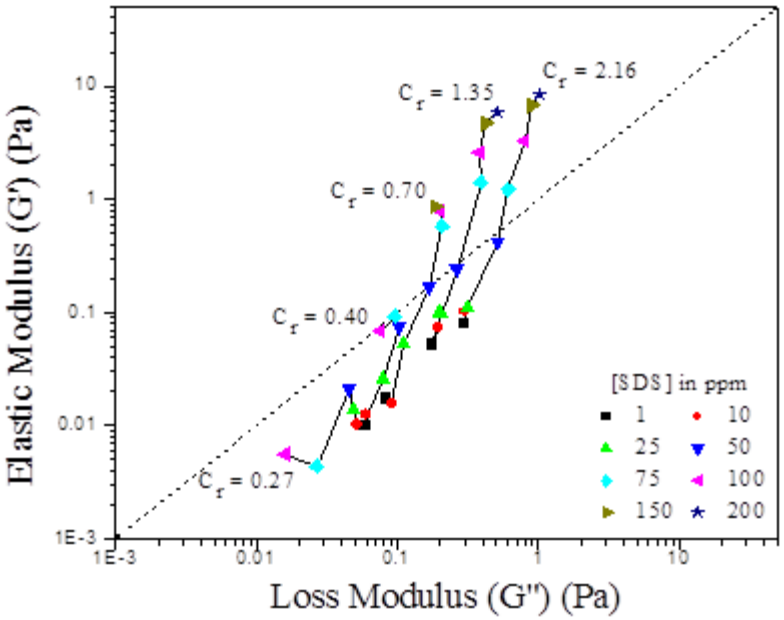


*Figure 134.* Elastic Modulus and loss modulus of the JR30M/SDS system at 1 Hz and different $C_r$.

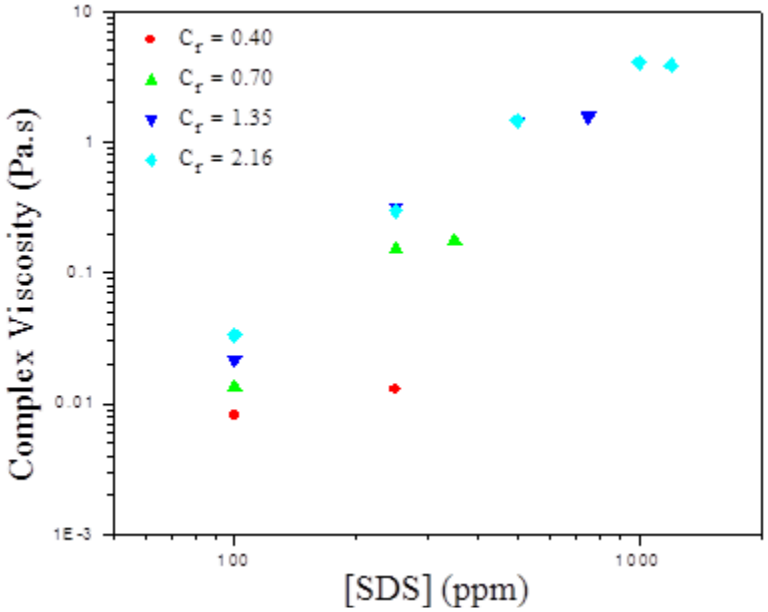


*Figure 135.* Complex viscosity of the JR400/SDS system at 1 Hz and different $C_r$.

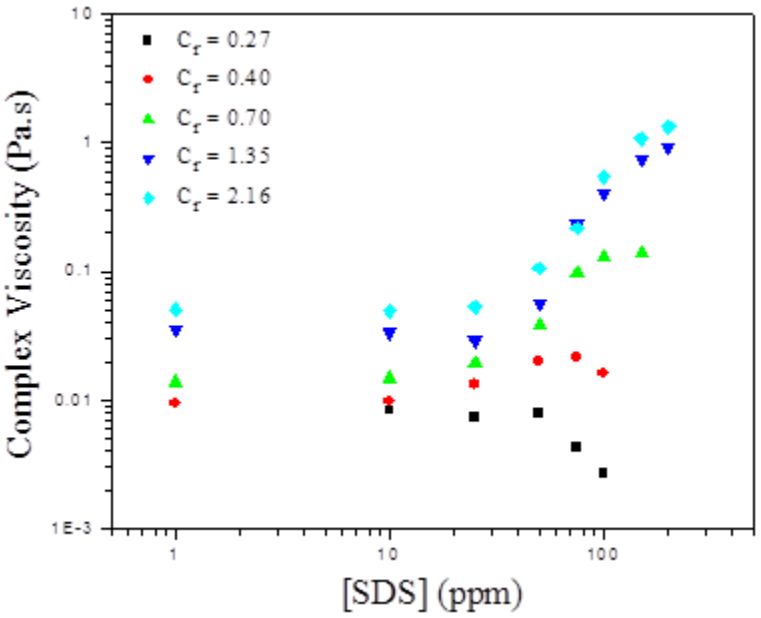


*Figure 136.* Complex viscosity of the JR30M/SDS system at 1 Hz and different $C_r$.

The elastic modulus and loss modulus of the JR400/SDS and JR30M/SDS system at 1 Hz frequency and at different $C_r$ are compared in Figure 133 and 134. Above the dotted line the elastic modulus is higher that the loss modulus. The elastic modulus further increases in absolute values as we move towards upper left corner of the plot. Conversely, below this line, the loss modulus is higher than the elastic modulus. Therefore, the dotted line represents the cross over between the two moduli. In this Figure, it is seen that, for both systems, if $C_r$ is higher than 0.40 the formation of strong polymer/SDS network is indicated. Additionally, the complex viscosity data also supports this (Figure 135 and 136). Moreover, the data points of the JR30M/SDS system, above the dotted line, lie close to the upper left corner than the JR400/SDS. Therefore, the high molecular weight JR30M/SDS system forms a stronger gel network than the low molecular weight JR400/SDS system. Chronakis and Alexandridis have attributed this to stronger association in the JR300/surfactant system as there are more crosslinks per chain for the high molecular weight JR30M.[150]

## Discussion

In this research, the correlation between the absorption behavior and the bulk complexation was investigated between the low molecular weight JR400/SDS and high molecular weight JR30M/SDS systems, over a relatively broad range of polymer concentrations.

The adsorption behavior of the JR400/SDS and JR30M/SDS system was analyzed by surface tension measurements. These measurements suggested that the adsorption behavior is dependent on the polymer molecular weight and the polymer concentration and the adsorption/desorption of polymer/surfactant complexes depended on critical concentrations for both surfactant and polymer. Particularly, in the one phase region above CAC, at $C_r \leq 0.40$, the surface tension of the JR400/SDS and JR30M/SDS system in the one phase region above CAC remained constant. Goddard made similar observations on the surface tension plot of the 0.1 wt. % JR400/sodium lauryl sulfate (SLS) system.[81,208] Through his experiments, he inferred that the surface tension stayed constant due to the formation of surface active JR400/SLS complex. Likewise, Taylor and coworkers have also observed that the PSS/$C_n$TAB surface tension remained constant and have attributed this to the absorption of the thick PSS/$C_n$TAB layer at the interface through neutron reflectivity studies.[102,170]

In contrast, at $C_r \geq 0.70$, the surface tension of the JR400/SDS and JR30M/SDS system increased considerably, in the one phase region above the CAC. Some polymer-surfactant systems also have been reported to show increase in the surface tension.[79,104,173,199-201,209] However, this increase was observed only in the two phase region. Staples and coworkers[103] found that the surface tension of the

poly(dimethyldiallylammonium chloride) (PDMDAAC)/SDS system abruptly increased in the two phase region. With the help of neutron reflectivity, they found that the interfacial concentration of PDMDAAC and SDS decreased corresponding to the increase in the surface tension. This suggested desorption of the PDMDAAC/SDS complexes from the interface. Therefore, they concluded that the desorption of the complexes occurred in the two phase region as the formation of the phase separated bulk complexes were preferred over the interracially adsorbed complexes.[173] Campbell and coworkers further explored the PDMDAAC/SDS system and found that, in the two phase region, the surface tension increased with the precipitation i.e. loss of the PDMDAAC/SDS complexes from the supernatant. Thus, they concluded that precipitation caused desorption of the surface active PDMDAAC/SDS complexes resulting in the increase in surface tension. This explanation differed from the interplay between the complexes at the interface and in bulk postulated by Staples and coworkers.[104] In another study, Campbell and coworkers analyzed the composition of the surface active complexes by neutron reflectivity as well as measured the amount of PDMDAAC/SDS complexes in supernatant, throughout the two phase region.[209] They found that, in the precipitation zone, PDMDAAC and SDS concentration at the interface decreased corresponding to increase in the surface tension. These results further supported their previous conclusion.

From the above studies, it is clear that the loss of polymer and surfactant complex from the supernatant raises the surface tension in the two phase region. However, we have found that for JR400/SDS and JR30M/SDS system the increase in the surface tension occurs in the one phase region above CAC. Previous investigators have reported

that the surface tension stays constant in the one phase region due to strong absorption of the complexes at the interface. Thus, desorption of the JR400/SDS and JR30M/SDS complexes from the interface cannot be explained by phase separation of the complex, as is the case for the PDMDAAC/SDS system discussed earlier. Above the CAC, the JR/SDS complexation occurs in the bulk. I asked the question, "does this complexation facilitate desorption of the surface active complexes and increase the surface tension?"

To further investigate this possibility, the rheological behavior of the bulk solution was studied to analyze the JR400/SDS and JR30M/SDS interaction in the bulk. Similar to surface tension results, the rheological parameters varied with the polymer concentration and molecular weight and a critical polymer concentration was indicated. Thus, at lower $C_r$, steady state flow measurements showed that the viscosity of the system decreased as the system approached the two phase region. Whereas, above a threshold value of $C_r$, the viscosity of the system increased markedly as the system approached the two phase region. Similar behavior was observed by Goddard in the JR400/SDS system:[210] at 0.1wt % JR400, viscosity of the system decreased, while, at 1 wt % JR400, viscosity of the system increased. He attributed this behavior to the intramolecular association at lower [JR400] and intermolecular association at high [JR400]. Li and coworkers have also shown that with increase in the polymer concentration the interaction mechanism changes from intramolecular to intermolecular association for the PDMDAAC/SDS/TX-100 system.[94] Therefore, in the JR400/SDS and JR30M/SDS systems, intramolecular association occurs when $C_r \leq 0.40$, whereas, intermolecular association occurs when $C_r \geq 0.70$. Thus, in the dynamic rheological measurements, it is seen that the elastic modulus and complex viscosity increased significantly when $C_r \geq$

0.70 with [SDS], suggesting formation of a strong gel network through intermolecular associations which are absent when $C_r \leq 0.40$.

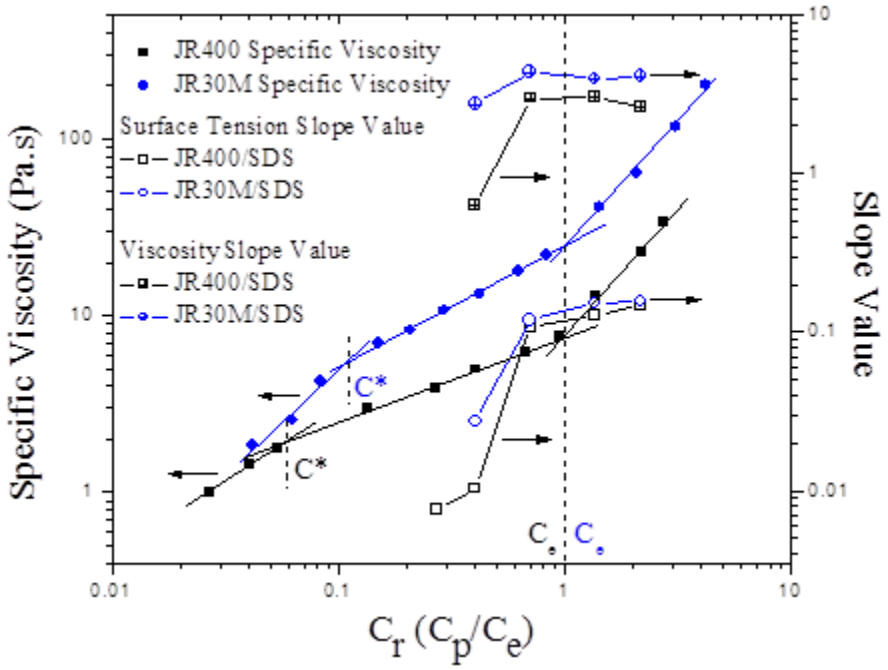


*Figure 137.* The specific viscosity, surface tension slope value curve and viscosity slope value curve for the JR400/SDS and JR30M/SDS system, as a function of $C_r$. The slopes values have been calculated in the one phase region above CAC. Negative slope values are not represented in the plot.

The surface tension and rheological results of the JR400/SDS and JR30M/SDS system are summarized in Figure 137, along with specific viscosity of JR400 and JR30M solutions, as a function of $C_r$. In this Figure, the surface tension and viscosity results have been represented as a slope value for each $C_r$, measured in one phase region above CAC region. The slope value suggests the rate of increase in a surface tension or viscosity with respect to [SDS]. $C_r = 1$ represent the critical entanglement concentration for both of the systems.

As seen in the previous sections, the surface tension and viscosity of the JR400/SDS and JR30M/SDS system pronounced increase at $C_r \geq 0.70$. Therefore, the slope value of the surface tension and viscosity reach a plateau value around at $C_r \geq 0.70$. The viscosity increase from $0.4 > Cr > 0.7$ can be attributed to a switch from intramolecular to intermolecular association in the bulk. Thus, this indicates that the changes taking place in the bulk complexation affect the adsorption at the interface. Therefore, the observed increase in the surface tension is also governed by the bulk association mechanism.

It is reasonable to conclude that the intermolecular association binds the complexes in the bulk through bound SDS crosslinking. With increase in $C_r$ ($\geq 0.70$) and [SDS], the association grows stronger and the binding takes place over a broader scale forming a strong gelled network. It is interesting that the bulk complex appears to desorb the surfactant from the interface. This indicates that the chemical potential of the surfactant is lower in the complex than at the surface and, therefore the surfactant is solubilized by the polymer/surfactant complex. The desorption increases with increase in JR concentration. In contrast, at $C_r \leq 0.40$, the intramolecular association causes the bulk complexes to collapse and therefore, networks are not formed. The surface tension remains constant in the one phase region above CAC (Figure 138). Therefore, these collapsed complexes are incapable of competing for the surfactant and polymer adsorbed at the interface.

(a) (b)

*Figure 138.* (a) Intramolecular association between polymer and SDS at $C_r \leq 0.40$ (b) intermolecular association between polymer and SDS at $C_r \geq 0.70$.

In the JR30M/SDS system, a strong gelled network is formed and the surface tension further increases compared to the JR400/SDS system. Therefore, increase in the polymer molecular weight enhances the intermolecular association.[94] Additionally, the Figure 138 also shows that the type of association is dependent on the concentration regime: intramolecular association occurs in the unentangled semi-dilute regime, whereas, intermolecular association occurs in the entangled semi-dilute regime. This indicates that for networks to form by polymer-surfactant interaction, the polymer chains must be close to or above the percolation threshold. Thus, the phenomenon depends upon a critical polymer threshold concentration. Although $C_r = 0.70$ lies in the unentangled regime, still this system shows intermolecular entanglement. This is probably because the addition of SDS induces association in between proximate chains through hydrophobic association.

# CHAPTER IV

## EFFECT OF POLYMER CONCENTRATION AND CHARGE LOCALIZATION

In this research, the relation between the adsorption behavior and bulk complexation has been explored for cationic MAPTAC and AMT polymers with SDS. The adsorption profile of this system is monitored using surface tension measurements, whereas, the bulk complexation is studied using rheological and fluorescence measurements. Moreover, the effect of charge localization and polymer concentration is also explored.

In literature, the effect of polymer charge density on polymer-surfactant interaction has been studied by selecting polymers with different charge densities. However, in the present study, the effect of charge localization - a different factor has been explored. In MAPTAC, the charge groups are linearly distributed along the backbone. In contrast, in AMT, the charges are more localized i.e., three charges are situated on a short branch chain on AMT backbone. The molecular weight, charge density, backbone flexibility, and hydrophobicity of these polymers are comparable.

Polymer Solution Viscosity

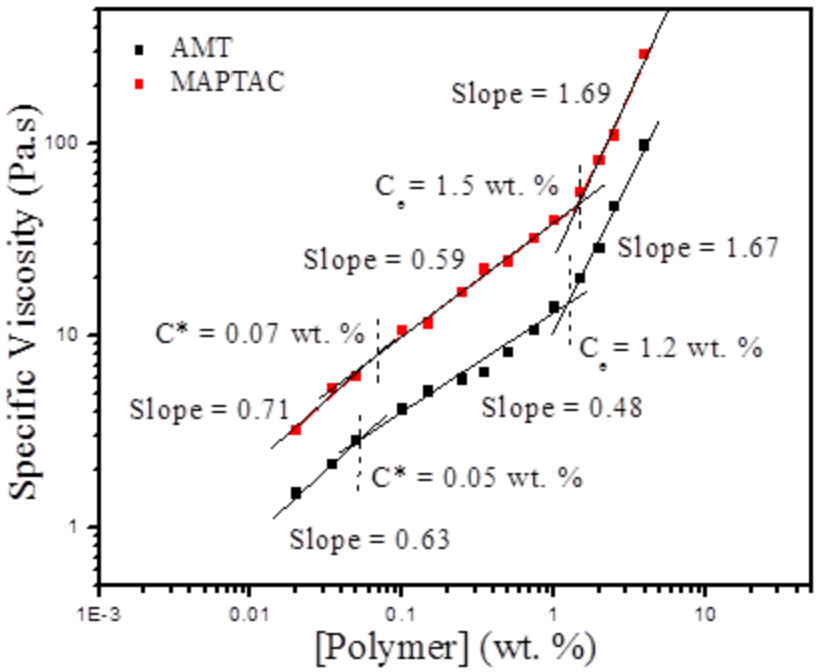


*Figure 139*. Critical overlap concentration (C*) and critical entanglement concentration ($C_e$) of MAPTAC and AMT polymers.

Similar to the previous chapter, we have considered a range of polymer concentration that encompasses the polymer concentration regime. The concentration regimes are located by measuring the specific viscosity of the polyelectrolyte solution at different polyelectrolyte concentrations, in order to select the appropriate polyelectrolyte concentrations (Figure 139). The specific viscosity and concentration relation follows the scaling theory of polyelectrolytes. Therefore, MAPTAC lies in the dilute regime below 0.07 wt. %; the unentangled semi-dilute regime between 0.07 and 0.15 wt. %; and the entangled semi-dilute regime above 0.15 wt. %. The critical overlap concentration for MAPTAC is at 0.07 wt. %, and the critical entanglement concentration is at 0.15 wt. %. AMT lies in the dilute regime below 0.05 wt. %; the unentangled semi-dilute regime between 0.05 and 1.2 wt. %; and the entangled semi-dilute regime above 1.2 wt. %. For

AMT, the critical overlap concentration is at 0.05 wt. % and the critical entanglement concentration is at 1.2 wt. %.

Initial experiments showed that the surface tension of AMT/SDS system showed varied below 0.25 wt % of AMT concentration, respectively. Therefore, for this study, we have selected the rest of the concentrations below these concentrations (Table 9). These concentrations are expressed in terms of $C_r$, which is a ratio of polyelectrolyte concentration ($C_p$) to critical entanglement concentration ($C_e$).

Table 9

*Selected MAPTAC and AMT concentrations for this study.*

| Concentration Regime | [MAPTAC] (wt. %) | [AMT] (wt. %) | $C_r = C_p/C_e$ |
|---|---|---|---|
| Dilute | 0.01 | 0.008 | ~ 0.006 |
| | 0.06 | 0.05 | ~ 0.04 |
| Unentangled Semi Dilute | 0.1 | 0.075 | ~ 0.06 |
| | 0.13 | 0.1 | ~ 0.085 |
| | 0.3 | 0.25 | ~ 0.2 |

## Surface Tension Measurements

Surface tension (γ) measurements of SDS systems with and without MAPTAC and AMT are shown in Figure 140 and 141, as a function of [SDS]. In these measurements, the polymer concentration in the MAPTAC/SDS and AMT/SDS system was varied from the dilute regime to the unentangled semi-dilute regime, and the surface tension was measured in the one phase, two phase and solubilized regions. In the two phase region, measurements were performed on the supernatant which was separated from the coacervate using a centrifugation process.

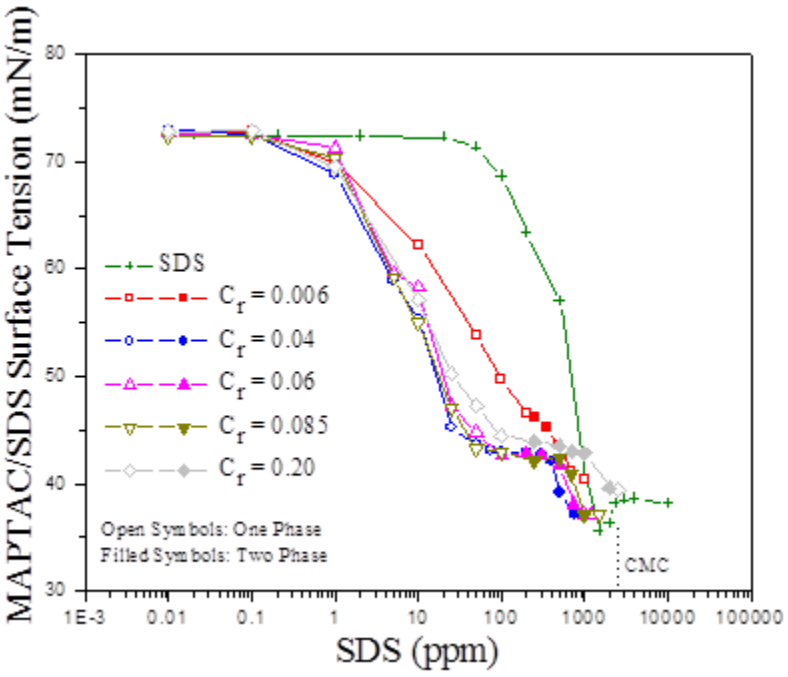


*Figure 140.* Surface tension curves of MAPTAC/SDS system at different $C_r$, as a function of [SDS]. Empty symbols correspond to the one phase region and filled symbols correspond to the two phase region.

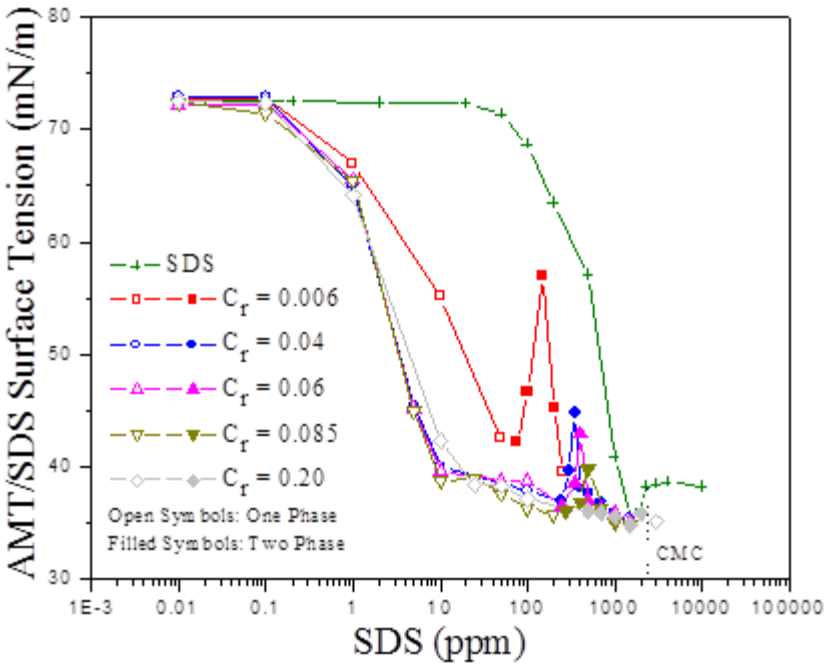


*Figure 141.* Surface tension curves of AMT/SDS system at different $C_r$, as a function of [SDS]. Empty symbols correspond to the one phase region and filled symbols correspond to the two phase region.

In the surfactant system, a decrease in the surface tension reflects adsorption of the surfactant molecules at the interface. However, above a certain surfactant concentration, a break point is observed on the surface tension curve. The surfactant concentration corresponding to this break point is known as the critical micelle concentration (CMC).[176] For the SDS system, the CMC value is found to be 2300 ppm i.e. 7.98 mM, which is close to the published value(8 mM).[190] The dip in the surface tension curve around 2000 ppm can be assigned to the impurities present in SDS. This is usually attributed to the long chain alkanols that are formed from the hydrolysis of SDS.

In the absence of SDS, the surface tension of MAPTAC and AMT was close to pure water (~ 72.5 mN/m). This indicates that both polymers are not surface active.

In the presence of SDS, for all $C_r$, the surface tension of the MAPTAC/SDS and AMT/SDS system dropped at a lower [SDS] (~ 0.1 ppm) than in the SDS system. This

early drop in the surface tension has been attributed to the formation of surface active polymer/surfactant complexes.[81,162,194-197] This surface activity of the complex is accredited to hydrophobicity of the complex which arises due to the adsorption of surfactant on the polymer. Moreover, the drop in the surface tension of the AMT/SDS system is steeper than the MAPTAC/SDS complex, which suggests that the AMT/SDS complex is quickly adsorbed at the interface. This indicates that the AMT/SDS complex is relatively more hydrophobic than the MAPTAC/SDS complex. This additional hydrophobicity may arise from increased adsorption of the SDS molecule on AMT due to its higher local charge density and/or due to the cationic charges on AMT being situated away from the backbone, which facilitates easy interaction with SDS than MAPTAC. Furthermore, the CAC value of the AMT/SDS systems is lower than the MAPTAC/SDS systems. This is again attributed to enhanced AMT and SDS interaction which promotes SDS micellization on the AMT at a lower [SDS] leading to significantly lower CAC values in AMT/SDS system than the MAPTAC/SDS system. Above the CAC, the surface tension of both the systems stays constant. However, the surface tension of the AMT/SDS system is lower than that the MAPTAC/SDS system. This indicates a higher adsorption of the AMT/SDS complex at the interface due to higher hydrophobicity.

In the two phase system, the surface tension of the MAPTAC/SDS stayed constant and decreased at a higher [SDS]. Similar surface tension behavior was observed in other polymer/surfactant systems[102,170] and was attributed to strong absorption of the polymer/surfactant complex at the air-water interface. However, the surface tension of the AMT/SDS system was found to be strongly dependent on $C_r$. At $C_r \leq 0.085$, the surface tension increased and then, decreased forming a peak on the surface tension

curve. The peak height increased with decrease in $C_r$. Similar surface tension peaks were observed in other polymer/surfactant systems.[103-105,173,198-201] This was attributed to desorption of the polymer and surfactant from the interface.[104,173,209] Therefore, in the AMT/SDS system, the desorption increased with decrease in AMT concentration. A similar relation has been observed for the poly(dimethyldiallylammonium chloride) (PDMDAAC)/SDS system.[173] On the other hand, at $C_r \geq 0.20$, the surface tension stayed constant.

Fluorescence Measurements

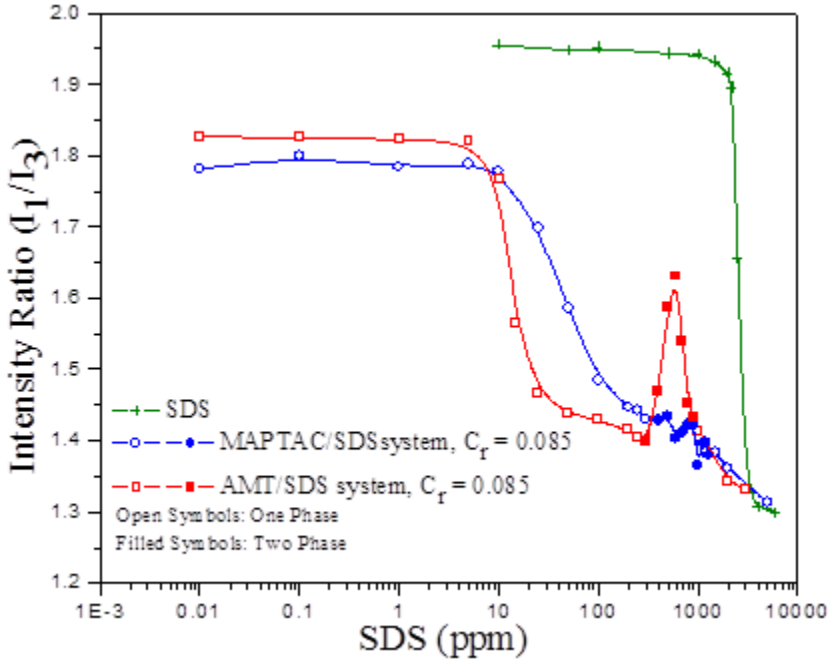


*Figure 142.* Intensity ratio SDS, MAPTAC/SDS and AMT/SDS systems in different regions, at different [SDS]. In coacervate phase, the measurements were recorded on the supernatant. Empty symbols correspond to one phase region and filled symbols correspond to two phase region.

The fluorescence technique is a simple and sensitive method to study the polymer-surfactant interaction. This technique uses a fluorescence probe which senses change in the micropolarity of the environment of the probe. For this study, pyrene is

used as a fluorescence probe to understand the formation of hydrophobic domains i.e., induction of hydrophobicity in the polymer/surfactant systems.[70,79,143]

When pyrene is excited at 335 nm, it produces emission spectra with five characteristic peaks. Between these peaks, the intensity ratio of peak I (at 373 nm) to peak III (at 384 nm) is very sensitive to the change in the polarity of the environment. The polarity dependence of pyrene arises due to loss of molecular geometry or distortion of the π-electron clouds. These physical changes occur as pyrene forms a complex with polar components of the system, leading to enhancement of peak III.[211,212] With increase in polarity, the intensity of the peak III ($I_3$) increases with the loss of intensity of peak I ($I_1$).[211,213] Therefore, the intensity ratio, $I_1/I_3$, determines the degree of polarity in the microenvironment. A high intensity ratio suggests a hydrophilic environment, whereas a low intensity ratio suggests a hydrophobic environment.

Intensity ratios for the SDS, MAPTAC/SDS and AMT/SDS systems are shown in Figure 142, as a function of SDS concentration. For polymer-surfactant systems, measurements were recorded in different phases. Empty symbols correspond to the one phase region, whereas, filled symbols correspond to the phase separated region. In the phase separated region, measurements were performed on the supernatant which was separated from the coacervate using a centrifugation process.

For the surfactant system, the intensity ratio abruptly changes in a narrow concentration region that corresponds to the CMC. This occurs due to solubilization of the pyrene in the hydrophobic domain formed by the SDS molecules. The break point, observed at higher intensity ratio, is defined as the CMC of the surfactant.[214] Similar to CMC, CAC is defined as the break point, observed at a higher intensity ratio in the

polymer-surfactant system. The CMC and CAC values measured using this technique were close to the values observed by the surface tension technique.

For the AMT/SDS system, the slope of the intensity ratio curve in the transition region ([SDS] ~ 10 ppm) is steeper compared to the MAPTAC/SDS system. A steeper slope indicates increased cooperative binding between polymer and surfactant. Moreover, it also suggests that the surfactant aggregates formed in both systems differ.[145] The intensity ratio of the AMT/SDS system is lower than the MAPTAC/SDS system in the one phase region. This indicates that the AMT/SDS complex is more hydrophobic than MAPTAC/SDS complex. In the two phase region, in contrast to the MAPTAC/SDS system, the intensity ratio of the AMT/SDS system increases which suggests loss of complexes in the AMT/SDS in the supernatant.

## Aggregation Number

The aggregation number of the MAPTAC/SDS and AMT/SDS complexes is found by steady-state fluorescence measurements using the following Equation:[215,216]

$$\ln\left(\frac{I_o}{I}\right) = \frac{n}{(C - C_{CAC})}[Q] \qquad \text{Equation 26}$$

where,

$I_0$ = emission light intensity without quencher at 373 nm

I = emission light intensity with quencher at 373 nm

n = aggregation number

C = total surfactant concentration

$C_{CAC}$ = critical aggregation concentration of the polymer/surfactant system

[Q] = quencher (cetylpyridinium bromide) concentration

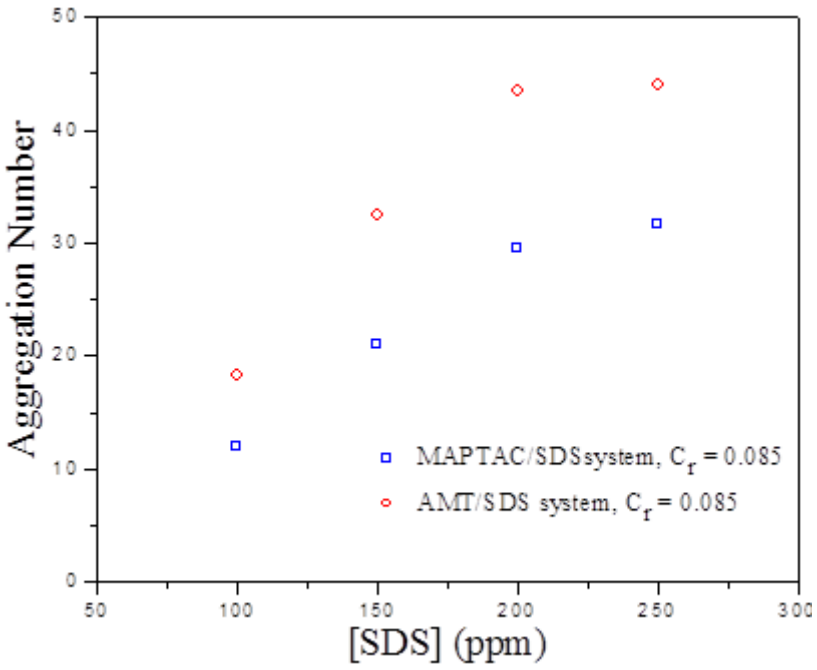


*Figure 143.* Aggregation number of the SDS in the MAPTAC/SDS and AMT/SDS complexes formed in the one phase region, at different SDS concentrations. The concentration of cationic polymer in the system was constant ($C_r$ = 0.085).

Figure 143 shows the aggregation number of the MAPTAC/SDS and AMT/SDS complexes in the one phase. The aggregation number of the two systems increased with increase in [SDS]. However, the aggregation number of the AMT/SDS complex was consistently larger than the MAPTAC/SDS complex. This indicates that the localized charges on the AMT absorb more number of SDS molecules in the micellar aggregates formed on AMT.

## Modulus of the Coacervate

Rheological measurements of the phase separated system were recorded to analyze the elastic modulus. The phase separated system was centrifuged to collect the coacervate at 3000 ppm for 30 min. In the two phase region, the modulus of the AMT/SDS system is higher than the MAPTAC/SDS system. This suggests that a stronger association between the phase separated AMT/SDS particles than the MAPTAC/SDS

coacervate particles. The modulus data was not collected for the rest of the systems as it was difficult to collect the phase separated particles using centrifugation as they formed a stable suspension in water.

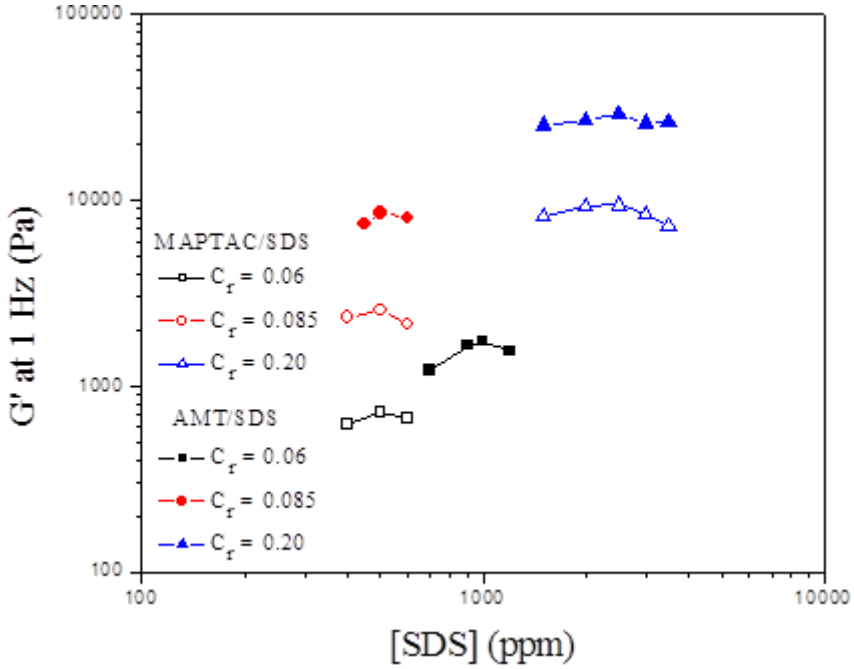


*Figure 144.* Modulus of MAPTAC/SDS and AMT/SDS coacervates, at different polymer and SDS concentrations.

## Discussion

In this research, the correlation between the adsorption behavior and the bulk complexation and the effect of charge localization was investigated between MAPTAC/SDS and AMT/SDS system, over a broad range of polymer concentrations that encompassed dilute and unentangled semi-dilute concentration regime. The charge location on MAPTAC and AMT vary: the charges are linearly distributed along the MAPTAC backbone, whereas, the charges are more localized in AMT.

The adsorption behavior of the MAPTAC/SDS and AMT/SDS system was analyzed by surface tension measurements. It was observed that the adsorption behavior

in the two phase region is dependent on the distribution of the charges on the polymer and the polymer concentration. The surface tension increases in the AMT/SDS system at $Cr \leq 0.085$. Staples and coworkers have seen similar increase in the surface tension in the two phase region in the poly(dimethyldiallylammonium chloride) (PDMDAAC)/SDS system and attributed it to desorption of the PDMDAAC/SDS complex from the interface, using neutron reflectivity.[173] Campbell and coworkers extended this understanding and concluded that desorption take place due to precipitation in the bulk.[104,209] On the other hand, the surface tension in the MAPTAC/SDS system stayed constant. Taylor and coworkers have also observed that the PSS/$C_n$TAB surface tension remained constant and have attributed this to the adsorption of the thick PSS/$C_n$TAB layer at the interface through neutron reflectivity studies.[102,170]

In the published literature, the reason behind two extreme adsorption behaviors at the interface in the polymer/surfactant system is disclosed. However, these behaviors are not linked to the polymer structural properties i.e., which polymer structural properties and how these structural properties affect adsorption or desorption. In our case, it is seen from Figure 140 and 141 the charge localization significantly affects the surface tension in the two phase region. To understand how it affects the surface tension, the MAPTAC/SDS and AMT/SDS systems are characterized using different techniques in the one and two phase region. Although, the adsorption differences are observed in the two phase region, investigation of the one phase region is important because the polymer/surfactant complex begins to form in the one phase region, which subsequently phase separates.

In the one phase region, the surface tension and fluorescence measurements indicate that AMT has higher affinity towards SDS and forms a more hydrophobic complex compared to MAPTAC. The three localized charges on AMT are situated on a short branch on the AMT backbone. This enhances the interaction between AMT and SDS compared to MAPTAC. Moreover, the aggregation number of SDS in the AMT/SDS complex is nearly 1.5 times more than the MAPTAC/SDS complex. This suggests that the localized charges increase the admicellar size in the polymer bound SDS aggregates. Thus, the AMT/SDS system is relatively more hydrophobic than MAPTAC/SDS system as seen in fluorescence measurements.

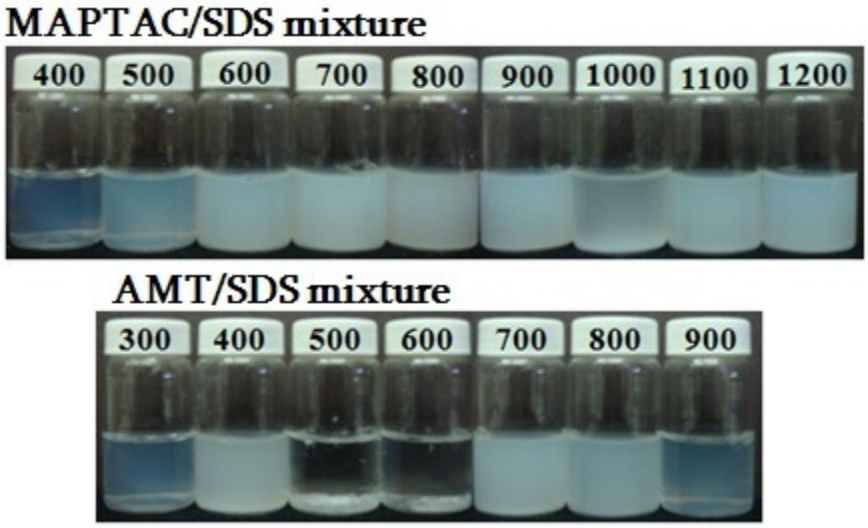


*Figure 145.* Photographic images of the (a) MAPTAC/SDS and (b)AMT/SDS systems in the two phase region. The concentration of cationic polymer in the system was constant ($C_r$ = 0.085). Numbers on the cap of the vials represent the [SDS] in ppm.

The appearance of the two phase region of the MAPTAC/SDS and AMT/SDS system at $C_r$ = 0.085 was recorded after magnetically stirring the systems for 24 hours (Figure 145). These photographic images were taken as soon as the vial was removed from the magnetic stirrer. As the SDS concentration increased, the turbidity of both the systems increased, and then, at a higher SDS concentration the turbidity decreased. This

indicates formation and solubilization of the two phase region.[4,70,76,79] However, in the AMT/SDS system, at intermediate SDS concentration, the phase separated particles flocculated and precipitated leaving behind a clear supernatant. In addition, some of the phase separated particles were deposited on the glass forming a ring on the vials. In the MAPTAC/SDS system, the precipitation is observed at intermediate SDS concentration ($900 \leq [SDS] \leq 1100$ ppm) only after keeping the sample undisturbed over 2 hours.

The phase separated complexes were characterized using rheological measurements. These measurements indicate that the association between the AMT/SDS phase separated particles is stronger than the MAPTAC/SDS phase separated particles. As seen in one phase region, the AMT/SDS complex is relatively hydrophobic than the MAPTAC/SDS complex. Thus, the hydrophobicity introduced in the AMT/SDS complex enhances the association of the phase separated AMT/SDS complex through SDS tail-tail hydrophobic interaction. Therefore, the AMT/SDS particles flocculate. Deposition of the phase separated particles on the glass also indicates that the particles are hydrophobic in nature.

Introduction of localized charges induces admicellar formation in the AMT/SDS system and therefore, increases the association between the AMT/SDS phase separated complexes at intermediate SDS concentration. The surface tension of the AMT/SDS system also increases in the same SDS concentration region. This indicates that the association between the phase separated particles in the bulk also extended to the AMT/SDS complexes adsorbed at the interface causing desorption. On the other hand, in more uniformly charged MAPTAC/SDS system, the extent of interaction is lower compared to AMT/SDS system. Therefore, association between the MAPTAC/SDS

phase separate particles is relatively low. As a result, the association between the bulk phase separated particles and the interfacially adsorbed complex is low. Therefore, precipitation does not affect the surface tension and does not increase in the two phase region.

# CHAPTER V

# EFFECT OF POLYMER CONCENTRATION AND BACKBONE RIGIDITY/HYDROPHOBICITY

The relation between the adsorption behavior and bulk complexation in the flexible MAPTAC and semi-flexible JR30M with SDS was studied at two concentrations polymer that comprised dilute and unentangled semi-dilute concentration regime. The adsorption profile of this system was monitored using surface tension measurements, whereas, the bulk complexation was studied using rheological measurements.

For this study, MAPTAC and JR30Mpolymers were selected which have comparable molecular weight and charge density but different backbone flexibility and hydrophobicity. MAPTAC is flexible and hydrophobic while JR30M is semi-rigid and hydrophilic. The polymer concentrations used in this study are as follows;

Table 10

*Selected MAPTAC and JR30M concentrations for this study.*

| Concentration Regime | [MAPTAC] (wt. %) | $C_r = C_p/C_e$ | [JR30M] (wt. %) | $C_r = C_p/C_e$ |
|---|---|---|---|---|
| Unentangled Semi Dilute | 0.30 | ~ 0.2 | 0.032 | ~ 0.27 |
| Entangled Semi Dilute | 2 | ~ 1.35 | 0.16 | ~ 1.35 |

Surface Tension Measurements

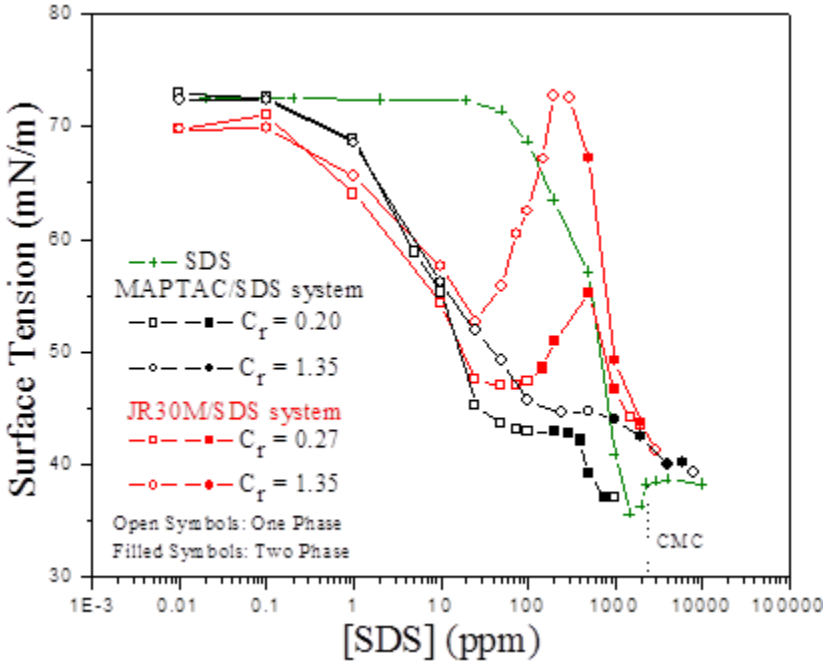


*Figure 146.* Surface tension curves of (a) MAPTAC/SDS and (b) JR30M/SDS system at different $C_r$, as a function of [SDS]. Empty symbols correspond to the one phase region and filled symbols correspond to the two phase region.

Surface tension (γ) measurements of SDS system with and without MAPTAC and JR30M are shown in Figure 146, as a function of [SDS]. In the two phase region, measurements were performed on the supernatant which was separated from the coacervate using a centrifugation process.

At $C_r = 0.27$, the surface tension of MAPTAC/SDS system stayed constant above the CAC in the one and two phase regions and then decreased at a higher SDS concentration. Similar surface tension behavior was observed in other polymer/surfactant systems[102,170] and was attributed to strong absorption of the polymer/surfactant complex at the air-water interface. However, at $C_r = 0.20$ the surface tension of the JR30M/SDS system increased in the two phase region. A similar surface tension peak was observed in

other polymer/surfactant systems.[103-105,173,198-201] This was attributed to desorption of the polymer and surfactant from the interface.[104,173,209]

The nature of the surface tension curve of MAPTAC/SDS system at $C_r$ = 1.35 was similar to that of $C_r$ = 0.27, suggesting strong absorption of the polymer/surfactant complex at the air-water interface. However, in the JR30M/SDS system at $C_r$ = 1.35, the surface tension increased in the one phase region above CAC.

Viscosity Measurements in One Phase

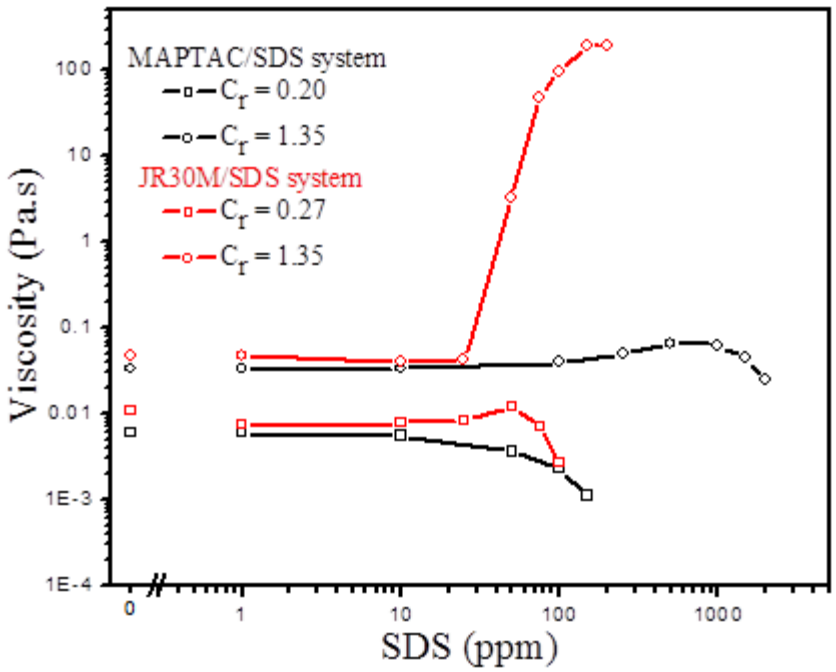


*Figure 147*. Viscosity of the (a) MAPTAC/SDS and (b) JR30M/SDS system at different polymer concentration, as a function of [SDS].

Figure 147 shows the viscosities of MAPTAC/SDS and JR30M/SDS at different polymer concentration, as a function of [SDS]. On addition of SDS, the viscosity of the MAPTAC/SDS system at $C_r$ = 0.20 & 1.35 and JR30M/SDS at $C_r$ = 0.27 decreases. This is accredited to shrinking of the polymer.[162,203,206] On the other hand, the viscosity of

JR30M/SDS at $C_r$ = 1.35 significantly increased. The increase in viscosity is attributed to crosslinking of polymer chains by the surfactant aggregates.[202-205]

## Discussion

Here, the correlation between the adsorption behavior and the bulk complexation and the effect of backbone hydrophobicity/rigidity was investigated between the MAPTAC/SDS and JR30M /SDS system, over a broad range of polymer concentration.

In the one phase region, the surface tension and viscosity markedly increases in the JR30M/SDS system at $C_r$ = 1.35 compared to the MAPTAC/SDS system at $C_r$ = 1.35. From the previous chapter, it is seen that the increase in JR30M/SDS system is due to the intermolecular association between the JR30M/SDS complexes to form a gelled network. At this level of JR30M concentration, the intermolecular association occurs as the polymer is semi-rigid and hydrophilic. On the other hand, for the MAPTAC/SDS system, the viscosity decreases on addition of SDS and this is attributed to the MAPTAC chain collapsing as it is flexible and hydrophobic in nature. This results in dissociation of the network and favors intramolecular association.

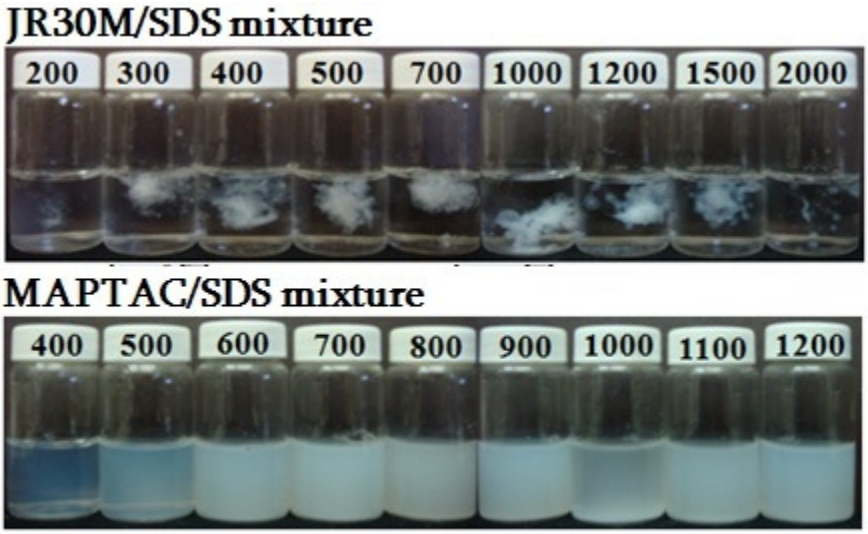


*Figure 148.* Photographic images of the (a) JR30M/SDS at $C_r$ = 0.27 and (b) MAPTAC/SDS at $C_r$ = 0.20 system in the two phase region. The concentration of cationic polymer in the system was constant ($C_r$ = 0.085). Numbers on the cap of the vials represent the [SDS] in ppm.

In the two phase region, the surface tension increases in the JR30M/SDS system at $C_r$ = 0.27, while, the surface tension of the MAPTAC/SDS system at $C_r$ = 0.20 stays constant. The appearance of the phase separated JR30M/SDS and MAPATC/SDS system is shown in Figure 140. The JR30M/SDS system appears to form a large phase separated particle through association as the JR30M backbone is semi-rigid and hydrophilic. Here, again the association causes desorption and thereby, increases the surface tension. On the other hand, the MAPTAC/SDS system forms tiny phase separated particles, introducing turbidity in the system. This can be explained by a MAPTAC collapse on interaction with SDS due to its flexible and hydrophobic backbone.

# CHAPTER VI

# CONCLUSIONS

In the studied polyelectrolyte/surfactant systems, the correlation between adsorption behavior of the complex at the interface and complexation in the bulk is explored. This correlation is analyzed with respect to polyelectrolyte concentration, molecular weight, charge localization, and backbone rigidity/hydrophobicity.

The molecular weight effect was studied between the low molecular weight JR400/SDS and high molecular weight JR30M/SDS system, in the unentangled (lower than $C_e$) and entangled (higher than $C_e$) semi-dilute concentration regimes. For concentrations lower than $C_e$, the JR/SDS systems showed strong adsorption at the interface and intramolecular association in the bulk, in the one phase region above the CAC. This association causes the complex to shrink. However, for concentrations close to and above $C_e$, the JR/SDS systems showed desorption from the interface and intermolecular association in the bulk, in the one phase region above the CAC. This association drives the surface active complexes in the bulk resulting in an increase in the surface tension. This indicates that the JR polymers chains should be close to entanglement condition in order to promote intermolecular association between the JR polymer and SDS in the bulk, and desorption of the complexes from the interface. Moreover, with an increase in molecular weight, the intermolecular association grows stronger and therefore, shows higher desorption.

The charge localization effect was studied between the linearly charged MAPTAC and locally charged AMT, in dilute (below C*) and unentangled semi-dilute (above C*) concentration regimes. Over the studied concentration range, the

MAPTAC/SDS system showed strong adsorption of the complex at the interface in the two phase region. However, the AMT/SDS system showed desorption of the complex from the interface in the two phase region. The hydrophobicity induced in the AMT/SDS complex due to charge localization increases the association between the interfacial and bulk phase separated complexes, resulting in desorption. As MAPTAC/SDS complexes lack this kind of association, this system shows adsorption at the interface.

The backbone rigidity/hydrophobicity effect was studied between the flexible/hydrophobic MAPTAC and semi rigid/hydrophilic JR30M, in dilute and unentangled semi-dilute concentration regimes. With increase in the concentration, theJR30M/SDS system showed desorption. This is because the semi rigid/hydrophilic JR30M polymer undergoes intermolecular association in the presence of SDS and drives the interfacial complex in the bulk. On the other hand, the MAPTAC/SDS system exhibits strong adsorption at the interface as the flexible/hydrophobic MAPTAC/SDS complex shrinks in size and therefore, the interfacial complex is not associated with the bulk complexation.

# REFERENCES


(1) Winnik, M. A.; Yekta, A. *Current Opinion in Colloid Interface Science.* **1997**, *2*, 424-436.

(2) Armstrong, R. W.; Strauss, U. P. *Encyclopedia of Polymer Science and Technology: Polyelectrolytes*; John Wiley & Sons: New York, NY, 1969; Vol. 10.

(3) Hara, M. *Polyelectrolytes: Science and Technology*; Marcel Dekker, Inc: New York, NY, 1992.

(4) Goddard, E. D.; Ananthapadmanabhan, K. P. *Interactions of Surfactants with Polymers and Proteins;* CRC Press: Boca Raton, FL, 1993.

(5) Patterson, G. *Physical Chemistry of Macromolecules*; CRC Press, Taylor & Francis: Boca Raton, FL, 2007.

(6) Schmidt, M. *Polyelectrolytes with Defined Molecular Architecture II*; Springer: New York, NY, 2004.

(7) Donnan, F. G. *Chem. Revs.* **1924**, *80*, 73-90.

(8) Everett, D. H. *Pure Appl. Chem.* **1972**, *31*, 619.

(9) Chapman, D. L. *Phil. Mag.* **1913**, *6*, 475.

(10) Gouy, G. *J. Phys.* **1910**, *4*, 475.

(11) Stern, O. Z. *Electrochem.* **1924**, *30*, 508.

(12) Wang, C.; Tam, K. C. *The Journal of Physical Chemistry B.* **2004**, *108*, 8976-8982.

(13) Anthony, O.; Zana, R. *Langmuir.* **1996**, *12*, 1967-1975.

(14) Hansson, P.; Almgren, M. *J. Phys. Chem.* **1996**, *100*, 9038.

(15) Reed, W. F.; Ghosh, S.; Medjahdi, G.; Francois, J. *Macromolecules.* **1991**, *24*, 6189-6198.

(16) Tanford, C. *Physical Chemistry of Macromolecules*; John Wiley & Sons, INC.: New York, 1967.

(17) Goddard, E. D. *Interactions of Surfactants with Polymers and Proteins.*; CRC Press: Boca Raton, FL, 1993.

(18) Wiggins, P. A.; Nelson, P. C. *Physical Review E.* **2006**, *73*, 031906.

(19) Berth, G.; Cölfen, H.; Dautzenberg, H. *Analytical Ultracentrifugation VI.* **2002**, 119, 50-57.

(20) Schatz, C.; Viton, C.; Delair, T.; Pichot, C.; Domard, A. *Biomacromolecules.* **2003**, *4*, 641-648.

(21) Liverpool, T. B. *Philosophical Transactions of the Royal Society A: Mathematical, Physical and Engineering Sciences.* **2006**, *364*, 3335-3355.

(22) Dobrynin, A. V. *Macromolecules.* **2005**, *38*, 9304-9314.

(23) Buhler, E.; Rinaudo, M. *Macromolecules.* **2000**, *33*, 2098-2106.

(24) Buhler, E.; Boué, F. *The European Physical Journal E: Soft Matter and Biological Physics.* **2003**, *10*, 89-92.

(25) Borochov, N.; Eisenberg, H. *Macromolecules.* **1994**, *27*, 1440-1445.

(26) Traube, J. *Justus Liebigs Annalen der Chemie.* **1891**, *265*, 27-55.

(27) Gibbs, J. W. *The collected works of J. Willard Gibbs*; Longmans: New York, NY, 1928.

(28) Langmuir, I. *Journal of the American Chemical Society.* **1917**, *39*, 1848-1906.

(29) McBain, J. W.; Salmon, C. S. *Journal of the American Chemical Society.* **1920**, *42*, 426-460.

(30) Hartley, G. S. *Aqueous Solutions of Paraffin-Chain Salts; A Study in Micelle Formation,*; Hermann & Cie: Paris, 1936.

(31) Tanford, C. *The Hydrophobic Effect: Formation of Micelles and Biological Membranes.*; John Wiley & Sons: New York, NY, 1980.

(32) Shinoda, K.; Yamaguchi, N.; Carlsson, A. *The Journal of Physical Chemistry.* **1989**, *93*, 7216-7218.

(33) Dubin, P. L. *J. Phys. Chem. B.* **2007**, *111*, 8468-8476.

(34) Swarbrick, J. *Encyclopedia of Pharmaceutical Technology*; 2 edition ed.; Marcel Dekker: Basel, Switzerland, 2004.

(35) Menger, F. M.; Seredyuk, V. A.; Apkarian, R. P.; Wright, E. R. *Journal of the American Chemical Society.* **2002**, *124*, 12408-12409.

(36) Tiebackx, F. W. *Z. Chem. Ind. Kolloide.* **1911**, *8*, 198.

(37) Bungenberg de Jong, H. G.; Kruyt, H. R. *Proc. Kinkl. Med. Akad. Wetershap.* **1929**, *32*, 849.

(38) Sanchez, C.; Mekhloufi, G.; Schmitt, C.; Renard, D.; Robert, P.; Lehr, C. M.; Lamprecht, A.; Hardy, J. *Langmuir.* **2002**, *18*, 10323-10333.

(39) Menger, F. M.; Peresypkin, A. V.; Caran, K. L.; Apkarian, R. P. *Langmuir*. **2000**, *16*, 9113-9116.

(40) Stover, H. *Macromolecules.* **2003**, *36*, 8773-8779.

(41) Burgess, D. J. *J. Coll. Interface Sci.* **1990**, *140*, 227-238.

(42) Ilekti, P.; Piculell, L.; Tournilhac, F.; Cabane, B. *J. Phys. Chem. B.* **1998**, *102*, 344.

(43) Zhang, K.; Karlstroem, G.; Lindman, B. *The Journal of Physical Chemistry.* **1994**, *98*, 4411-4421.

(44) Flory, P. J. *J. Chem. Phys.* **1941**, *9*, 660.

(45) Flory, P. J. *J. Chem. Phys.* **1942**, *10*, 51.

(46) Huggins, M. L. *J. Chem. Phys.* **1941**, *9*, 440.

(47) Huggins, M. L. *J. Am. Chem. Soc.* **1942**, *64*, 1712.

(48) Robeson, L. *Polymer Blends: 'A Comprehensive Review*; Hanser Gardner Publications: Cincinnati, OH, 2007.

(49) Teraoka, I. *Polymer Solutions: An Introduction to Physical Properties*; John Wiley & Sons, Inc.: New York, 2002.

(50) http://www.files.chem.vt.edu/chem-dept/marand/Lecture7.pdf **09/13/2012**.

(51) http://www.stanford.edu/class/cheme160/lectures/lecture10.pdf **09/13/2012**.

(52) http://polly.phys.msu.ru/ru/education/courses/polymer-intro/lecture7.pdf **09/13/2012**.

(53) http://sundoc.bibliothek.uni-halle.de/diss-online/04/04H140/t5.pdf **09/13/2012**.

(54) Thalberg, K.; Lindman, B.; Karlstrom, G. *J. Phys. Chem.* **1990**, *94*, 4289.

(55) Thalberg, K.; Lindman, B.; Karlstrom, G. *J. Phys. Chem.* **1991**, *95*, 3370.

(56) Mezei, A.; Ábrahám, Á.; Pojják, K.; Mészáros, R. *Langmuir.* **2009**, *25*, 7304.

(57) Pojják, K.; Bertalanits, E.; Mészáros, R. *Langmuir.* **2011**, *27*, 9139-9147.

(58) Hayakawa, K.; Kwak, J. C. T. *J. Phys. Chem.* **1982**, *86*, 3866.

(59) Wang, C.; Tam, K. C. *Langmuir.* **2002**, *18*, 6484-6490.

(60) Wang, C.; Tam, K. C.; Jenkins, R. D.; Tan, C. B. *J. Phys. Chem. B.* **2003**, *107*, 4667.

(61) Hayakawa, K.; Kwak, J. C. T. *J. Phys. Chem.* **1983**, *87*, 506.

(62) Voisin, D.; Vincent, B. *Adv. Colloid Interface Sci.* **2003**, *106*, 1.

(63) Wang, X.; Li, Y.; Li, J.; Wang, J.; Wang, Y.; Guo, Z.; Yan, H. *J. Phys. Chem B.* **2005**, *109*, 10807.

(64) Pi, Y.; Shang, Y.; Liu, H.; Hu, Y.; Jiang, J. *J. Colloid Interface Sci.* **2007**, *306*, 405.

(65) Matsuda, T.; Annaka, M. *Langmuir.* **2008**, *24*, 5707.

(66) Liu, J.; Zheng, L.; Sun, D.; Wei, X. *Colloids Surf., A.* **2010**, *358*, 93.

(67) Thalberg, K.; Lindman, B. *The Journal of Physical Chemistry.* **1989**, *93*, 1478-1483.

(68) Thalberg, K.; Lindman, B.; Karlstrom, G. *J. Phys. Chem.* **1991**, *95*, 6004.

(69) Lindman, B.; Khan, A.; Marques, E.; Graca da Miguel, M.; Piculell, L.; Thalberg, K. *Pure & Appl. Chem.* **1993**, *65*, 953-958.

(70) Goddard, E. D. G., J. V. *Principles of Polymer Science and Technology in Cosmetics and Personal Care*; Marcel Dekker Inc.: New York, 1999.

(71) Ulrich, S.; Seijo, M.; Stoll, S. *Curr. Opin. Colloid Interface Sci.* **2006**, *11*, 268–272.

(72) Langevin, D. *Adv. Colloid Interface Sci.* **2009**, *147–148*, 170–177.

(73) Iliopoulos, I.; Olsson, U. *The Journal of Physical Chemistry.* **1994**, *98*, 1500-1505.

(74) Sarrazin-Cartalas, A.; Iliopoulos, I.; Audebert, R.; Olsson, U. *Langmuir.* **1994**, *10*, 1421-1426.

(75) Deo, P.; Jockusch, S.; Ottaviani, M. F.; Moscatelli, A.; Turro, N.; Somasundaran, P. *Langmuir.* **2003**, *19*, 10747.

(76) Zhou, S.; Xu, C.; Wang, J.; Golas, P.; Batteas, J.; Kreeger, L. *Langmuir.* **2004**, *20*, 8482-8489.

(77) Deo, P.; Somasundaran, P. *Langmuir.* **2005**, *21*, 3950-3956.

(78) Deo, P.; Deo, N.; Somasundaran, P. *Langmuir.* **2005**, *21*, 9998-10003.

(79) Deo, P.; Deo, N.; Somasundaran, P.; Moscatelli, A.; Jockusch, S.; Turro, N. J.; Ananthapadmanabhan, K. P.; Ottaviani, M. F. *Langmuir.* **2007**, *23*, 5906-5913.

(80) Jones, M. N. *J. Colloid Interface Sci.* **1967**, *23*, 36.

(81) Goddard, E. D.; Phillips, B. B.; Hannan, R. B. *J. Soc. Cosmet. Chem.* **1975**, *26*, 461-475.

(82) Wang, Y.; Kimura, K.; Huang, Q.; Dubin, P. L.; Jaeger, W. *Macromolecules.* **1999**, *32*, 7128-7134.

(83) Dubin, P. L.; Oteri, R. *J. Colloid Interface Sci.* **1983**, *95*, 453.

(84) Dubin, P. L.; Davis, D. D. *Macromolecules.* **1984**, *17*, 1294.

(85) Dubin, P. L.; Davis, D. D. *Colloids Surf.* **1985**, *13*, 113.

(86) Dubin, P. L.; Rigsbee, D. R.; McQuigg, D. W. *J. Colloid Interface Sci.* **1985**, *105*, 509.

(87) Dubin, P. L.; Rigsbee, D. R.; Gan, L. M.; Fallon, M. A. *Macromolecules.* **1988**, *21*, 2555.

(88) Dubin, P. L.; Principi, J. M.; Smith, B. A.; Fallon, M. A. *J. Colloid Interface Sci.* **1989**, *127*, 558.

(89) Dubin, P. L.; Chew, C. H.; L.M., G. *J. Colloid Interface Sci.* **1989**, *128*, 566.

(90) Dubin, P. L.; The; S., S.; McQuigg, D. W.; Chew, C. H.; Gan, L. M. *Langmuir.* **1989**, *5*, 89.

(91) Dubin, P. L.; Vea, M. E.; Fallon, M. A.; The; S., S.; Rigsbee, D. R.; Gan, L. M. *Langmuir.* **1990**, *6*, 1422.

(92) Dubin, P. L.; The; S., S.; McQuigg, D. W.; Gan, L. M.; Chew, C. H. *Macromolecules.* **1990**, *23*, 2500.

(93) Xia, J.; Zhang, H.; Rigsbee, D. R.; Dubin, P. L.; Shaikh, T. *Macromolecules.* **1993**, *26*, 2759-2766.

(94) Li, Y.; Xia, J.; Dubin, P. L. *Macromolecules.* **1994**, *27*, 7049-7055.

(95) Li, Y.; Dubin, P. L.; Havel, H. A.; Edwards, S. L.; Dautzenberg, H. *Macromolecules.* **1995**, *28*, 3098-3102.

(96) Li, Y.; Dubin, P. L.; Havel, H. A.; Edwards, S. L.; Dautzenberg, H. *Langmuir.* **1995**, *11*, 2486-2492.

(97) Li, Y.; Dubin, P. L.; Dautzenberg, H.; Lueck, U.; Hartmann, J.; Tuzar, Z. *Macromolecules.* **1995**, *28*, 6795-6798.

(98) Swanson-Vethamuthu, M.; Dubin, P. L.; Almgren, M.; Li, Y. *Journal of Colloid and Interface Science.* **1997**, *186*, 414-419.

(99) Wang, Y.; Kimura, K.; Dubin, P. L.; Jaeger, W. *Macromolecules.* **2000**, *33*, 3324-3331.

(100) Mata, J. P. *J. Dispersion Sci. Technol.* **2006**, *27*, 49-54.

(101) Taylor, D. J. F.; Thomas, R. K.; Penfold, J. *Advances in Colloid and Interface Science.* **2007**, *132*, 69-110.

(102) Taylor, D. J. F.; Thomas, R. K.; Penfold, J. *Langmuir.* **2002**, *18*, 4748-4757.

(103) Staples, E.; Tucker, I.; Penfold, J.; Warren, N.; Thomas, R. K.; Taylor, D. J. F. *Langmuir.* **2002**, *18*, 5147-5153.

(104) Campbell, R. A.; Angus-Smyth, A.; Arteta, M. Y.; Tonigold, K.; Nylander, T.; Varga, I. *J. Phys. Chem. Lett.* **2010**, *1*, 3021.

(105) Campbell, R. A.; Yanez Arteta, M.; Angus-Smyth, A.; Nylander, T.; Varga, I. *The Journal of Physical Chemistry B.* **2011**, *115*, 15202-15213.

(106) Sakai, M.; Satoh, N.; Tsujii, K.; Zhang, Y.-Q.; Tanaka, T. *Langmuir.* **1995**, *11*, 2493-2495.

(107) Merta, J.; Torkkeli, M.; Ikonen, T.; Serimaa, R.; Stenius, P. *Macromolecules.* **2001**, *34*, 2937.

(108) Loyen, K.; Illiopoulos, I.; Audebert, R.; Ollsson, U. *Langmuir.* **1995**, *11*, 1053.

(109) Tam, K. C.; Farmer, M. L.; Jenkins, R. D.; Bassett, D. R. *Journal of Polymer Science Part B: Polymer Physics.* **1998**, *36*, 2275-2290.

(110) Petit-Agnely, F.; Iliopoulos, I.; Zana, R. *Langmuir.* **2000**, *16*, 9921-9927.

(111) Alami, E.; Almgren, M.; Brown, W. *Macromolecules.* **1996**, *29*, 5026-5035.

(112) Ma, S. X.; Cooper, S. L. *Journal of Rheology.* **2002**, *46*, 339-350.

(113) Elliott, P. T.; Xing, L.; Wetzel, W. H.; Glass, J. E. *Macromolecules.* **2003**, *36*, 8449-8460.

(114) Alexandridis, P. *Current Opinion in Colloid Interface Science.* **1996**, *1*, 490-501.

(115) Feng, Y.; Billon, L.; Grassl, B.; Khoukh, A.; François, J. *Polymer.* **2002**, *43*, 2055-2064.

(116) Bai, D.; Khin, C. C.; Chen, S. B.; Tsai, C.-C.; Chen, B.-H. *The Journal of Physical Chemistry B.* **2005**, *109*, 4909-4916.

(117) Ng, W. K.; Tam, K. C.; Jenkins, R. D. *Polymer.* **2001**, *42*, 249–259.

(118) English, R. J.; Raghavan, S. R.; Jenkins, R. D.; Khan, S. A. *J. Rheol.* **1999**, *43*, 1175–1194.

(119) Islam, M. F.; Jenkins, R. D.; Bassett, D. R.; Lau, W.; Ou-Yang, H. D. *Macromolecules.* **2000**, *33*, 2480-2485.

(120) Tirtaatmadja, V.; Tam, K. C.; Jenkins, R. D. *Macromolecules.* **1997**, *30*, 3271-3282.

(121) Tirtaatmadja, V.; Tam, K. C.; Jenkins, R. D. *Macromolecules.* **1997**, *30*, 1426-1433.

(122) Zhuang, D.; Ai-hua Da, J. C.; Zhang, Y.; Dieing, R.; Ma, L.; Haeussling, L. *Polymers for Advanced Technologies.* **2001**, *12*, 616-625.

(123) Dai, S.; Tam, K. C.; Jenkins, R. D.; Bassett, D. R. *Macromolecules.* **2000**, *33*, 7021-7028.

(124) Dai, S.; Chiu Tam, K.; Jenkins, R. D. *Journal of Polymer Science Part B: Polymer Physics.* **2005**, *43*, 3288-3298.

(125) Tam, K. C.; Ng, W. K.; Jenkins, R. D. *Polymer International.* **2007**, *56*, 569-575.

(126) Ng, W. K.; Tam, K. C.; Jenkins, R. D. *Eur. Polym. J.* **1999**, *35*, 1245-1252.

(127) English, R. J.; Gulati, H. S.; Jenkins, R. D.; Khan, S. A. *J. Rheol.* **1997**, *41*, 427–444.

(128) English, R. J.; Laurer, J. H.; Spontak, R. J.; Khan, S. A. *Eng. Chem. Res.* **2002**, *41*, 6425–6435.

(129) Tirtaatmadja, V.; Tam, K. C.; Jenkins, R. D. *Macromolecules.* **1997**, *30*, 3271–3282.

(130) Abdala, A. A.; Wu, W.; Olsen, K. R.; Jenkins, R. D.; Tonelli, A. E.; Khan, S. A. *J. Rheol.* **2004** *48* 979-994.

(131) Hoy, K. L.; Hoy, R. C.; Union Carbide Corporation, Danbury, Conn.: US, Jan 17, 1984.

(132) Barton, A. F. M. *Handbook of Solubility Parameters and Other Cohesion Parameters*; Second Edition ed.; CRC Press: Boca Raton, FL, 1991.

(133) Bai, G.; Nichifor, M.; Lopes, A.; Bastos, M. *The Journal of Physical Chemistry B.* **2005**, *109*, 21681-21689.

(134) Bai, G.; Catita, J. A. M.; Nichifor, M.; Bastos, M. *The Journal of Physical Chemistry B.* **2007**, *111*, 11453-11462.

(135) Bakeev, K. N.; Ponomarenko, E. A.; Shishkanova, T. V.; Tirrell, D. A.; Zezin, A. B.; Kabanov, V. A. *Macromolecules.* **1995**, *28*, 2886-2892.

(136) Kjøniksen, A.; Nilsson, S.; Thuresson, K.; Lindman, B.; Nyström, B. *Macromolecules.* **2000**, *33*, 877-886.

(137) Thuresson, K.; Soderman, O.; Hansson, P.; Wang, G. *The Journal of Physical Chemistry.* **1996**, *100*, 4909-4918.

(138) Smith, G. L.; McCormick, C. L. *Langmuir.* **2001**, *17*, 1719-1725.

(139) Bai, G.; Nichifor, M.; Lopes, A.; Bastos, M. *The Journal of Physical Chemistry B.* **2004**, *109*, 518-525.

(140) Burke, S. E.; Palepu, R. *Carbohydrate Polymers.* **2001**, *45*, 233-244.

(141) Goddard, E. D.; Leung, P. S. *Langmuir.* **1992**, *8*, 1499-1500.

(142) Iliopoulos, I.; Wang, T. K.; Audebert, R. *Langmuir.* **1991**, *7*, 617.

(143) Kwak, J. C. T. *Polymer-Surfactant Systems*; Marcel Dekker: New York 1998.

(144) Somasundaran, P.; Li, Y.; The Trustees of Columbia University in the City of New York: US, 2011.

(145) Magny, B.; Iliopoulos, I.; Zana, R.; Audebert, R. *Langmuir.* **1994**, *10*, 3180-3187.

(146) Halacheva, S. S.; Penfold, J.; Thomas, R. K.; Webster, J. R. P. *Langmuir.* **2012**, *28*, 14909-14916.

(147) Choi, L. S.; Kim, O. K. *Langmuir.* **1994**, *10*, 57-60.

(148) Shirahama, K.; Tashiro, M. *Bull. Chem. Soc. Jpn.* **1984**, *57*, 377.

(149) Chronakis, I. S.; Alexandridis, P. *Macromolecules.* **2001**, *34*, 5005.

(150) Chronakis, I. S.; Alexandridis, P. *Macromolecules.* **2001**, *34*, 5005-5018.

(151) Wallin, T.; Linse, P. *Langmuir.* **1996**, *12*, 305-314.

(152) Jonsson, M.; Linse, P. *J. Chem. Phys.* **2001**, *115*, 10975.

(153) Skepö, M.; Linse, P. *Physical Review E.* **2002**, *66*, 051807.

(154) Stoll, S.; Chodanowski, P. *Macromolecules.* **2002**, *35*, 9556-9562.

(155) Laguecir, A.; Stoll, S.; Kirton, G.; Dubin, P. L. *J. Phys. Chem. B.* **2003**, *107*, 8056-8065.

(156) Kayitmazer, A. B.; Seyrek, E.; Dubin, P. L.; Staggemeier, B. A. *J. Phys. Chem. B.* **2003**, *107*, 8158.

(157) Kayitmazer, A. B.; Shaw, D.; Dubin, P. L. *Macromolecules.* **2005**, *38*, 5198-5204.

(158) Cooper, C. L.; Goulding, A.; Kayitmazer, A. B.; Ulrich, S.; Stoll, S.; Turksen, S.; Yusa, S.-i.; Kumar, A.; Dubin, P. L. *Biomacromolecules.* **2006**, *7*, 1025-1035.

(159) Hayakawa, K.; Santere, J. P.; Kwak, J. C. T. *Macromolecules.* **1983**, *16*, 1642.

(160) Wang, H.; Wang, Y. *J. Phys. Chem. B.* **2010**, *114*, 10409–10416.

(161) Tricot, M. *Macromolecules.* **1984**, *17*, 1698-1704.

(162) Jain, N.; Trabelsi, S.; Guillot, S.; McLoughlin, D.; Langevin, D.; Letellier, P.; Turmine, M. *Langmuir.* **2004**, *20*, 8496-8503.

(163) Guillot, S.; McLoughlin, D.; Jain, N. J.; Delsanti, M.; Langevin, D. *Journal of Physics: Condensed Matter.* **2003**, *15*, S219.

(164) Bain, C. D.; Claesson, P. M.; Langevin, D.; Meszaros, R.; Nylander, T.; Stubenrauch, C.; Titmuss, S.; von Klitzing, R. *Advances in Colloid and Interface Science.* **2007**, *155*, 32-49.

(165) Kiefer, J. J.; Somasundaran, P.; Ananthapadmanabhan, K. P. *Langmuir.* **1993**, *9*, 1187.

(166) Mylonas, Y.; Staikos, G. *Langmuir.* **2001**, *17*, 3586-3591.

(167) Kogej, K.; Theunissen, E.; Reynaers, H. *Langmuir.* **2002**, *18*, 8799-8805.

(168) Kim, B.; Ishizawa, M.; Gong, J.; Osada, Y. *Journal of Polymer Science Part A: Polymer Chemistry.* **1999**, *37*, 635-644.

(169) Chen, L.; Yu, S.; Kagami, Y.; Gong, J.; Osada, Y. *Macromolecules.* **1998**, *31*, 787-794.

(170) Taylor, D. J. F.; Thomas, R. K.; Li, P. X.; Penfold, J. *Langmuir.* **2003**, *19*, 3712-3719.

(171) Penfold, J.; Tucker, I.; Thomas, R. K.; Taylor, D. J. F.; Zhang, X. L.; Bell, C.; Breward, C.; Howell, P. *Langmuir.* **2007**, *23*, 3128-3136.

(172) Lee, Y.; Dudek, A.; Ke, T.; Hsiao, F.; Chang, C. *Macromolecules.* **2008**, *41*, 5845-5853.

(173) Staples, E.; Tucker, I.; Penfold, J.; Warren, N.; Thomas, R. K. *Langmuir.* **2002**, *18*, 5139-5146.

(174) Monteux, C. C.; Williams, C. E.; Bergeron, V. *Langmuir.* **2004**, *20*, 5367-5374.

(175) Rosen, M. J.; Kunjappu, J. T. *Surfactants and Interfacial Phenomena*; Fourth Edition ed.; Wiley, John & Sons, Incorporated: Hoboken, New Jersey, 2012.

(176) Rosen, M. J. *Surfactants and Interfacial Phenomena* John Wiley & Sons, Inc.: New Jersey, 2004.

(177) Malovikova, A.; Hayakawa, K.; Kwak, J. C. T. *J. Phys. Chem.* **1984**, *88*, 1930.

(178) Ishiguro, M.; Koopal, L. K. *Colloids and Surfaces A: Physicochemical and Engineering Aspects.* **2009**, *347*, 69-75.

(179) Wesley, R. D.; Cosgrove, T.; Thompson, L.; Armes, S. P.; Baines, F. L. *Langmuir.* **2002**, *18*, 5704-5707.

(180) Sokolov, E.; Yeh, F.; Khokhlov, A.; Grinberg, V. Y.; Chu, B. *The Journal of Physical Chemistry B.* **1998**, *102*, 7091-7098.

(181) Cheng, Z.; Ren, B.; Gao, M.; Liu, X.; Tong, Z. *Macromolecules.* **2007**, *40*, 7638-7643.

(182) Nizri, G.; Makarsky, A.; Magdassi, S.; Talmon, Y. *Langmuir.* **2009**, *25*, 1980-1985.

(183) Liao, X.; Higgins, D. A. *Langmuir.* **2002**, *18*, 6259-6265.

(184) Zhou, S.; Burger, C.; Chu, B. *The Journal of Physical Chemistry B.* **2004**, *108*, 10819-10824.

(185) Kogej, K.; Evmenenko, G.; Theunissen, E.; Berghmans, H.; Reynaers, H. *Langmuir.* **2001**, *17*, 3175-3184.

(186) Zhou, S.; Hu, H.; Burger, C.; Chu, B. *Macromolecules.* **2001**, *34*, 1772-1778.

(187) Tomašić, V.; Tomašić, A.; Šmit, I.; Filipović-Vinceković, N. *Journal of Colloid and Interface Science.* **2005**, *285*, 342-350.

(188) Zhou, S.; Yeh, F.; Burger, C.; Chu, B. *The Journal of Physical Chemistry B.* **1999**, *103*, 2107-2112.

(189) Mezei, A.; Pojják, K.; Mészáros, R. *J. Phys. Chem. B.* **2008**, *112*, 9693.

(190) Mukerjee, P.; Mysels, K. J. *Critical micelle concentration of aqueous surfactant systems. National Standard Reference Data System* Washington, DC, 1971.

(191) Dobrynin, A. V.; Colby, R. H.; Rubinstein, M. *Macromolecules.* **1995**, *28*, 1859-1871.

(192) Boris, D. C.; Colby, R. H. *Macromolecules.* **1998**, *31*, 5746-5755.

(193) Eisenberg, H.; Pouyet, J. *Journal of Polymer Science.* **1954**, *13*, 85 - 91.

(194) Asnacios, A.; Langevin, D.; Argillier, J.-F. o. *Macromolecules.* **1996**, *29*, 7412-7417.

(195) Asnacios, A.; Langevin, D.; Argillier, J. F. *Eur. Phys. J. B.* **1998**, *5*, 905.

(196) Jain, N. J.; Albouy, P. A.; Langevin, D. *Langmuir.* **2003**, *19*, 5680.

(197) Jain, N. J.; Albouy, P.-A.; Langevin, D. *Langmuir.* **2003**, *19*, 8371-8379.

(198) Merta, J.; Stenius, P. *Colloid and Polymer Science.* **1995**, *273*, 974-983.

(199) Moglianetti, M.; Li, P.; Malet, F. L. G.; Armes, S. P.; Thomas, R. K.; Titmuss, S. *Langmuir.* **2008**, *24*, 12892-12898.

(200) Kristen, N.; Simulescu, V.; Vüllings, A.; Laschewsky, A.; Miller, R.; von Klitzing, R. *The Journal of Physical Chemistry B.* **2009**, *113*, 7986-7990.

(201) Bykov, A. G.; Lin, S.; Loglio, G.; Lyadinskaya, V. V.; Miller, R.; Noskov, B. A. *Colloids and Surfaces A: Physicochemical and Engineering Aspects.* **2010**, *354*, 382-389.

(202) Tsianou, M.; Alexandridis, P. *Langmuir.* **1999**, *15*, 8105-8112.

(203) Wu, Q.; Du, M.; Shangguan, Y.; Zhou, J.; Zheng, Q. *Colloids and Surfaces A: Physicochemical and Engineering Aspects.* **2009**, *332*, 13-18.

(204) Wu, Q.; Shangguan, Y.; Du, M.; Zhou, J.; Song, Y.; Zheng, Q. *Journal of Colloid and Interface Science.* **2009**, *339*, 236-242.

(205) Sardar, N.; Kamil, M.; Kabirud, D. *Colloids and Surfaces A: Physicochemical and Engineering Aspects.* **2012**, *415*, 413-420.

(206) Guillot, S.; Delsanti, M.; Désert, S.; Langevin, D. *Langmuir.* **2003**, *19*, 230-237.

(207) Wu, Q.; Du, M.; Ye, T.; Shangguan, Y.; Zhou, J.; Zheng, Q. *Colloid and Polymer Science.* **2009**, *287*, 911-918.

(208) Goddard, E. D.; Hannan, R. B. *Journal of Colloid and Interface Science.* **1976**, *55*, 73-79.

(209) Campbell, R. A.; Yanez Arteta, M.; Angus-Smyth, A.; Nylander, T.; Varga, I. *The Journal of Physical Chemistry B.* **2011**, *115*, 15202-15213.

(210) Goddard, E. D. *Colloids Surf.* **1986**, *19*, 301.

(211) Kalyanasundaram, K.; Thomas, J. K. *J. Am. Chem. Soc.* **1977**, *99*, 2039.

(212) Rosoff, M. *Vesicles*; Marcel Dekker, Inc: New York, 1996; Vol. 62.

(213) Onon, H. W.; Turley, W. D. *J.Phys. chem.* **1982**, *86*, 3501-3503.

(214) Goddard, E. D.; Turro, N. J.; Kuo, P. L.; Ananthapadmanabhan, K. P. *Langmuir.* **1985**, *1*, 352-355.

(215) Lee, J.; Moroi, Y. *Langmuir.* **2004**, *20*, 4376-4379.

(216) Dar, A. A.; Garai, A.; Das, A. R.; Ghosh, S. *The Journal of Physical Chemistry A.* **2010**, *114*, 5083-5091.